ANALYSIS OF CLIMATE CHANGE IMPACTS ON SURFACE ENERGY BALANCE OF LAKE HURON (ESTIMATION OF SURFACE ENERGY BALANCE COMPONENTS: REMOTE SENSING APPROACH FOR WATER – ATMOSPHERE PARAMETERIZATION)

By

PAKORN PETCHPRAYOON

B.Sc., Burapha University, l994

M.Sc., Mahidol University, 2001

M.A., University of Colorado, 2008

A thesis submitted to the

Faculty of the Graduate School of the

University of Colorado in partial fulfilment

of the requirement for the degree of

Doctor of Philosophy

Department of Geography

2015

This thesis entitled:

Analysis of Climate Change Impacts on the Surface Energy Balance of Lake Huron. (Estimation of Surface Energy Balance Components: Remote Sensing Approach for Water - Atmosphere Parameterizations)

written by Pakorn Petchprayoon
has been approved for the Department of Geography

_____
Dr. Peter D. Blanken

_____
Dr. Barbara P. Buttenfield

_____
Dr. Waleed Abdalati

Date_____

The final copy of this thesis has been examined by the signatories, and we find that both the content and the form meet acceptable presentation standards of scholarly work in the above mentioned discipline.

IRB protocol # _____

Pakorn Petchprayoon (Ph.D., Geography)

Analysis of Climate Change Impacts on the Surface Energy Balance of Lake Huron. (Estimation of Surface Energy Balance Components: Remote Sensing Approach for Water - Atmosphere Parameterizations)

Thesis directed by Professor Peter D. Blanken

Abstract

The purpose of this thesis was to investigate the physical processes of energy exchange between the water surface and atmosphere of Lake Huron in order to explain the processes behind such changes in long-term water levels and to monitor their spatial and temporal fluctuations. The lake surface water temperature and the four components of surface energy balance, including net radiation, latent heat, sensible heat, and heat storage, as well as evaporation rate, were estimated using the daily remotely sensed data from eleven years (2002-2012) with a multi-spatial resolution of 1 km to 5 km using the Moderate Resolution Imaging Spectroradiometer (MODIS) on board Terra satellite, together with in-situ measurements.

The regression analysis of the entire lake daily mean water surface temperature revealed a positive trend of 0.1 °C per year, indicating that the lake surface temperature increased by 1.1°C during the period 2002-2012. The warming rate was found to be greatest in the deepest areas of the lake, with a statistically-significant correlation between warming rate and depth. The four components of surface energy balance showed temporal and spatial heterogeneities. There were strong seasonal patterns for all of the components, which were very high in summer and low in

winter for net radiation and heat storage. In contrast, the latent heat and sensible heat were very high in the winter and very low in the summer.

Approximately 70% of the annual mean 30 min evaporation occurred during the fall and winter seasons, whereas the lowest evaporation rate occurred in March, which was only 3% of the annual mean of 30 min evaporation. There was an increase in the evaporation rate of approximately 1.4 mm m^{-2} over the 2005-2012 observation period, the water level decreased by 0.04 m during the period 2002-2012, and there was a decrease in total water storage by 1.18 cm during the entire study period (2004-2012). There was obviously a negative correlation between lake evaporation and lake water level and also total lake water storage. If the current evaporation trend continues, it can be assumed that the negative water level and total water storage trend will also continue.

ACKNOWLEDGEMENTS

A great many people have contributed to my academic career. I owe a debt of gratitude to all of those people that have made this dissertation possible.

Firstly, I would like to express my deepest gratitude to my advisor Prof. Peter Blanken for his continuous support of my Ph.D, study, for his incredible patience, excellent motivation, and immense knowledge. His guidance not only helped me throughout the research and writing of this dissertation, but also let me experience fieldwork and practical issues beyond the textbooks.

I would like to express my deepest appreciation to my first teacher in the U.S. Prof. Barbara Buttenfield, who introduced me to Geographic Information Science. As an international student, I really appreciate not only her excellent guidance, but also her kindness and understanding of the challenges that I faced in my new environment and in particular the cultural and language barriers.

I would also like to express my sincere appreciation to Prof. Waleed Abdalati, who continually and convincingly conveyed a spirit of adventure in regard to research and teaching in the field of remote sensing. I have benefited tremendously from his knowledge and experience.

I would like to express my deepest thanks to Prof. Konrad Stefen, who had always kindly provided clear guidance and constructive comments. I would also like to truly thank Prof. Hari Rajaram for being very supportive and encouraging during my research time at CU.

I would like to deeply thank Dr. Khalid Hussein; I am extremely grateful for his outstanding assistance, suggestions, and for always listening, giving me words of encouragement, and never letting me give up. He made me understand what a real friend is!

I am very thankful to my employer, GISTDA, and my supervisor, as well as my colleagues who played a crucial role in both my professional and academic career. I would like to thank the Thai students and people who live in Colorado, particularly the Hongpananond and Amornviwat families, who did not hesitate to devote their valuable time to me when it was most needed—it made my life easier during my study there. Also, I am grateful to Captain Dick, Uncle Mike, Terry, and Mark for their amazing support during my field work in the Great Lakes.

Finally I would like to thank my family, my parents, my sister, and my cousins for supporting me spiritually throughout my academic career and my life in general. Most importantly, I would like to thank my dear wife Jaruwan for her understanding, support, encouragement, patience, and unwavering love. Jaruwan is not only my wife, but my best friend, who has been with me all these years and has made them the best years of my life.

CONTENTS

CHAPTER

TABLES

Table

FIGURES

Figure

CHAPTER 1

INTRODUCTION

1.1 Statement of Problem

The North American Great Lakes contain one of the world's most important available freshwater. Containing approximately 23,000 km^3 of water, the lakes represent roughly 20% of the world's surface freshwater (Hartmann, 1990). Moreover, the lakes are one of highest demanding freshwater consumption systems in the world. The United States and Canada shared this water resource, which supports many significant uses, including, commercial navigation, commercial fishing, hydroelectric power, community water supplies, recreation, as well as fish and wildlife habitats (Assel *et al.*, 2004). Recently, decreasing water levels have been experienced in the Great Lakes (Lishawa *et al*., 2010). This current phenomenon is an issue because it is consistent with several climate change predictions, raising anxiety that the water level declines may continue (Sellinger *et al.*, 2008). Lake Huron is one of the Great Lakes experiencing this decrease in water levels (Sellinger *et al.*, 2008). The lake is not controlled for industrial hydropower or business navigation and is only nominally influenced by the inflow and outflow of the other lakes (Changnon, 2004). Thus, any changes in Lake Huron water levels are mainly due to climatic or other large-scale controls, including changes in surface water temperature, net radiation, and surface energy balance components.

Surface water temperature is one of the most importance variables in the physical processes determining atmospheric-water energy exchanges, which is vital for understanding the hydrological cycle and surface climate at local scales through global scales. A number of studies have found positive trends in the Great Lakes water temperature (e.g. Assel, 2005; Austin and

Colman, 2007; Dobiesz and Lester, 2009; Jones *et al*., 2006; Magnuson *et al*., 1997). However, to the present author's knowledge, the distribution of the increase of surface temperature for the entire lake and through the years spanning an entire decade (2002-2012) has never been explored before.

The surface net radiation is the great key component in understanding the surface energy balance and the heat flux interface with the atmosphere (Bisht *et al*. 2005; Sun *et al.,* 2013; Terjung *et al*., 1968), since it determines the energy available at the surface to heat water, thus driving the surface energy balance and ultimately determining the lake's surface temperature. The net radiation is one of the major determinants of the climate, since it integrates both major streams of radiation (shortwave and longwave) in both directions (incoming and outgoing). Over large areas, accurate information on the spatial and temporal variability of net radiation and its components (incoming shortwave, incoming longwave, reflected shortwave, and surface outgoing longwave radiation) is important for regional and global climate models (Dugual, 1994).

The net radiation received at the surface, when positive, represents a surplus of energy that must be partitioned as evaporation, sensible heat (convection), or heat storage, as expressed though the energy balance equation. Evaporation is one of the major components of the surface energy budget of large lakes and possibly the most complicated to estimate (Gianniou and Antonopolos, 2007). This term represents a major water loss and is an important factor in the lake's hydrology process (Derecki, 1981). Also, the evaporation rate can be linked to the changes in water level and water storage, which can be traced in observations of satellite altimetry and gravimetry.

Investigating, understanding, and unfolding the above physical processes of energy exchange between the water surface and the atmosphere is an essential pre-requisite to explaining the processes behind such changes in long-term water levels and monitoring their temporal and spatial fluctuations. However, the surface energy balance and its components are difficult and costly to measure, and accurate measurements of local surface energy balance components (particularly evaporation) generally make only at a limited number of suitable research sites possible (Granger and Bussieres, 2005). In addition, the measurements of a lake's energy balance are an extremely complex and time consuming procedure because the factors that determine the energy intensity vary both temporally and spatially. Furthermore, the exchange between the lake surface and atmosphere is typically measured at a few locations. Since the surface area of Lake Huron is so large that direct measurements of the complete surface energy balance involve all of the water surface, and continually yearlong, is not possible with currently available resources.

These problems can be addressed by using satellite remote sensing data, which provide a supplement to in-situ measurements by offering observations that are regularly, temporally, and spatially reliable. The quantities of lake-wide surface parameters can be measured without the under-sampling difficulty due to the insufficiency observation networks (Swenson and Wahr, 2009). Therefore, remote sensing measurements integrated with spatially-constant surface meteorological parameters and GIS processes will be used for assessing the magnitude of the surface energy balance of Lake Huron. This is necessary for the research community to better understand the changes in water level which have been encountered in recent years.

1.2 Study Area

Lake Huron (Figure 1.1) is the second largest of the Great Lakes by surface area with a surface area of 59,600 km^2, and the third largest freshwater lake on Earth. It is also the third largest by volume of water: 3,540 km^3. The mean surface height of Lake Huron is 176 m above sea level. The average depth of the lake is 59 m, whereas the maximum depth is 229 m. It has a length of 332 km and a greatest width of 245 km (Schertzer *et al*., 2008; Zimmermann, 2013). The Lake Huron coastline lengthens 6,157 km and is described by shallow, sandy beaches and the rocky shores of Georgian Bay (Schaetzl, 2005).

Spectacle Reef Lighthouse, located 17.22 km east of the eastern end of Bois Blanc Island at 45.7732 N and 84.1367 W, is the only station measuring year-round meteorological variables over the lake. The station uses the eddy covariance method to measure the turbulent heat fluxes (both sensible and latent heat), net radiation, air temperature, humidity, rain rate, and lake surface temperature. The lighthouse is the major platform providing year-round, continuous 30-min average meteorological and flux data for calculating and validating the parameters calculated from the satellite-based data for this study.

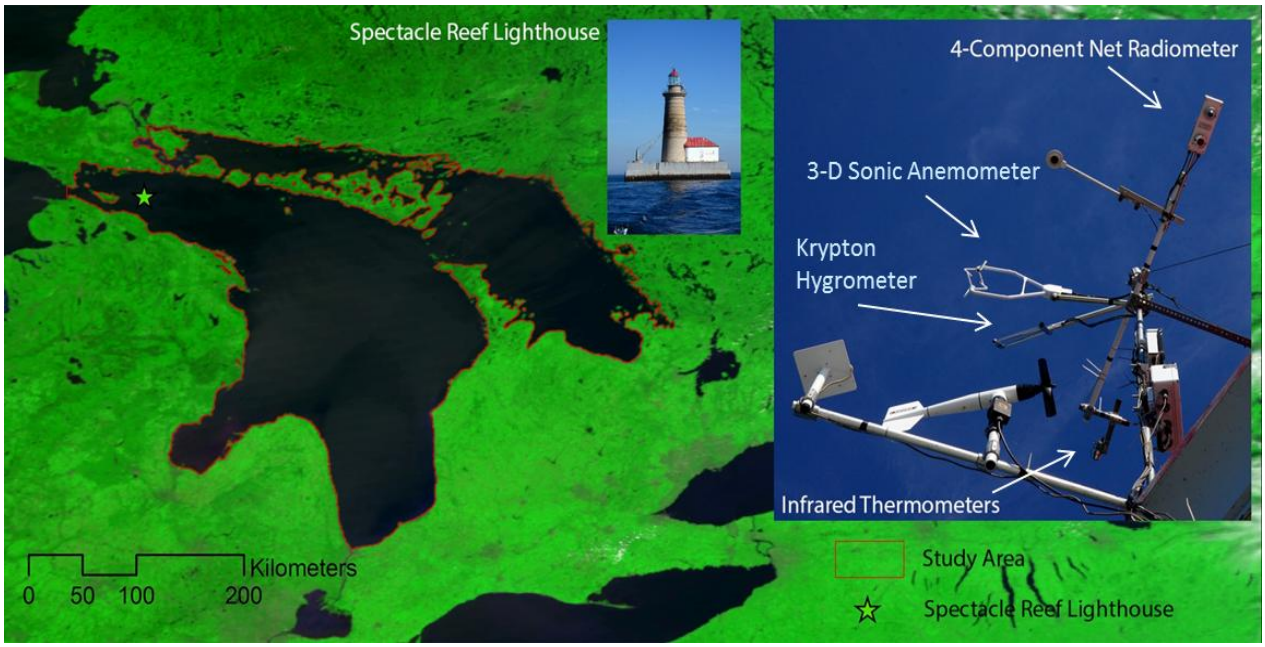

Figure 1.1 Satellite mosaic images from MODerate Resolution Imaging Spectroradiometer (MODIS) showing the study area and location of Spectacle Reef Lighthouse with the meteorological station located on the top

1.3 Objectives

1.3.1. *To assess the potential use of satellite sensors for estimating the energy balance components, particularly the latent heat flux (evaporation), and other variables required to estimate the evaporation across the lake: net radiation, surface temperature, air temperature, dew point temperature, and vapour pressure*.

The specific objective is to compute net radiation, surface temperature, air temperature, dew point temperature, and vapour pressure using passive remote sensing systems. This objective will address the potential of satellite data for measuring the continuous surface energy balance components over the lake.

1.3.2. *To determine a suitable method to estimate and predict a value for unmeasured areas due to cloud cover in order to continue the surface covering the whole lake area.*

While remote sensing data are ideal for measuring the continuous surfaces energy balance components, the major limitation in the use of satellite passive sensors is the occurrence of significant amounts of cloud cover. Therefore, the appropriate techniques will be used in order to fill in the missing data to continue surface covering the study area.

1.3.3. *To compare the surface energy balances calculated using satellite data with those estimated using existing meteorological data from direct measurement methods.*

The suitability of various energy balance component models will be examined to be applied directly to the parameters derived from the remote sensing data. Then, the surface energy balance and its components estimated from the satellites measurements will be compared with the results derived using eddy covariance method.

1.3.4. *To compute the energy balance for Lake Huron using existing and historical long-term satellite data records in order to observe changes in past energy budgets.*

A suitable model as identified in 1.3.3 will be applied using historical long-term satellite data records along with long-term meteorological data from surface station observations to estimate energy balance components. This will reveal the physical processes of energy exchange between the water surface and the atmosphere, which can explain the processes behind the changes in water level and make possible the monitoring of their spatial and temporal fluctuations.

1.4 Arrangement of Dissertation

This dissertation is arranged into six separated chapters. The present chapter includes a general introduction to statement of problem and the research objectives. It describes the study area and the location of Spectacle Reef Lighthouse with the meteorological station. The second

chapter, I apply thermal-infrared signal from MODIS on board the Terra satellite to assess surface temperature over the lake to improve our understanding of spatial and temporal variation, as well as, long-term changes in lake surface temperature driven by recent climate changes in the Great Lakes Region. In the third chapter, I estimate the spatial and temporal distribution, as well as, long-term changes in the lake surface net radiation and its four components under both clear and cloudy sky conditions using MODIS data without requiring additional data. The fourth chapter assesses the spatial and temporal variations, as well as long- term changes in the Lake Huron's surface energy balance using MODIS data. The main point is the emphasis on estimating the latent heat and sensible heat fluxes, but also presenting details on the correspondences between energy balance terms and meteorological variables, seasonal changes of these terms, and the water heat storage term. The fifth chapter estimates the changes in the lake evaporation using MODIS data together with the in-situ measurements. I link the evaporation rate to the changes in water level and water storage which can be traced in observations of satellite altimetry (Jason 1 and Jason2) and satellite gravimetry (Gravity Recovery And Climate Experiment, GRACE). The final chapter integrates and summarizes the key findings from all chapters, and conclusions the finding as well as discusses the possible future research topics.

1.5 Bibliography

Assel R.A. 2005. Classification of annual Great Lakes ice cycles: Winters of 1973-2002. *Journal of Climate*, 18, 4895-4904

Assel R.A., Quinn F H., Sellinger C.E. 2004. Hydroclimatic factors of the recent record drop in Laurentian Great Lakes water levels. *American Meteorological Society*, 85(8), 1143-1151

Austin J.A., Colman S.M. 2007. Lake Superior summer water temperatures are increasing more rapidly than regional air temperatures: A positive ice–albedo feedback. *Geophysical Research Letter,* 34, L06604, doi:10.1029/2006GL029021

Bisht G., Venturini V., Islam S., Jiang L. 2005. Estimation of the net radiation using MODIS (Moderate Resolution Imaging Spectroradiometer) data for clear sky days. *Remote Sensing of Environment*, 97, 52-67

Changnon S.A. 2004. Temporal behavior of levels of the Great Lakes and climate variability. *Journal of Great Lakes Research*, 30, 184–200

Derecki J.A. 1981. Stability effects on Great Lakes evaporation. *Journal of Great Lake Research*, 7(4), 357-362

Dobiesz N.E., Lester N.P. 2009. Changes in mid-summer water temperature and clarity across the Great Lakes between 1968 and 2002. *Journal of Great Lakes Research*, 35, 371-384

Dugual C.R. 1994. An approach to the estimation of surface net radiation in mountain area using remote sensing and digital terrain data. *Theoretical and Applied Climatology*, 55, 55-68

Gianniou S.K., Antonopoulos V.Z. 2007. Evaporation and energy budget in Lake Vegoritis, Greece. *Journal of Hydrology*, 345, 212-223

Granger R., Bussieres N. 2005. Evaporation/evapotranspiration estimates with remote sensing: *Remote Sensing in Northern Hydrology*. Dugua C.R., Pietroniro A. Eds. Washington, D C. American Geophysical Union

Hartmann H.C. 1990. Climate change impacts on laurentian great lakes levels. *Climatic Change*, 17, 49-67

Jones M.L., Shuter B.J., Zhao Y., Stockwell J.D. 2006. Forecasting effects of climate change on Great Lakes fisheries: Models that link habitat supply to population dynamic scan help. *Canadian Journal of Fisheries and Aquatic Sciences*, 63, 457-468

Lishawa S.C., Albert D.A., Tuchman N.C. 2010. Water level decline promotes Typha X glauca establishment and vegetation change in Great Lakes coastal wetlands. *Wetlands*, 30, 1085–1096

Magnuson J.J., Mortsch L.R., Schindler D.W., Quinn F.H., Webster K.E., Assel R.A., Bowser C.J., Dillon P.J., Eaton J.G., Evans H.E., Fee E.J., Hall R.I. 1997. Potential effects of climate changes on aquatic systems: Laurentian Great Lakes and precambrian shield region. *Hydrological Processes*, 11, 825-87

Schaetzl R.J. 2005. Watershed *of Lake Huron: Geography of Michigan and the Great Lakes Region*. Course Material of GEO 333 Geography of Michigan and the Great Lakes Region, Department of Geography, Michigan State University. Retrieved from http://web2.geo.msu.edu/geogmich/lakehuron.html

Schertzer W.M., Assel R.A., Beletsky D., Croley II, T.E., Lofgren B.M., Saylor J.H., Schwab D.J. 2008. Lake Huron climatology, inter-lake exchange and mean circulation. *Aquatic Ecosystem Health & Managemen*, 11, 144 - 152

Sellinger C.E., Stow C.A., Lamon E.C., Qian S.S. 2008. Recent water level declines in the lake Michigan-Huron system. *Environmental Science & Technology*, 42, 367-373

Sun Z., Gebremichael M., Wang Q., Wang J., Sammis T.W., Nickless A. 2013. Evaluation of clear-sky incoming radiation estimating equations typically used in remote sensing evapotranspiration algorithms. *Remote Sensing*, 5,4735-4752, doi:10.3390/rs5104735

Swenson S., Wahr J. 2009. Monitoring the water balance of Lake Victoria, East Africa, from space. *Journal of Hydrology*, 370, 163–176

Terjung W.T., Kickert R.K., Kochevar R.J., Mrowka J.P., Ojo S.O., Potter G.L., Tuller S.E. 1968. The annual March of the tropoclimatic spatial patterns of net radiation in Southern California. *Archives for Meteorology, Geophysics, and Bioclimatology, Series B*, 17, 21-50

Zimmermann K.A. 2013. *Great Facts about the Five Great Lakes.* Retrieved from http://www.livescience.com/32081-lake-huron.html

CHAPTER 2

A DECADE OF THE SPATIOTEMPORAL DISTRIBUTION OF SURFACE WATER TEMPERATURE ON LAKE HURON

2.1 Introduction

The North American Great Lakes are the largest freshwater resources in the world, and are of fundamental importance for the surrounding terrestrial life. Understanding the water-atmosphere interactions related to climate change requires various datasets of water surface variables, which involve energy exchanges between water and atmosphere. Surface water temperature is one of the most importance variables in the physical processes determining atmospheric-water energy exchanges, which is vital for understanding the hydrological cycle and surface climate at local through global scales. A number of studies have found positive trends in the Great Lakes water temperature (e.g. Assel, 2005; Austin and Colman, 2007; Dobiesz and Lester, 2009; Jones *et al*., 2006; Magnuson *et al*., 1997). However, to the present of author knowledge, the distribution of the increase of surface temperature for the entire lake and through the years spanning an entire decade (2002-2012) has never been explored before.

The change in the surface water temperature of the lake is very difficult to detect using traditional methods, such as near costal line meteorological measurements and shipboard observations due to spatial and temporal data gaps. Furthermore, changes in the lake surface temperature are typically measured at only a few locations. Since the surface area of Lake Huron is so large, direct measurements that cover all of the water surface are impossible with currently-available resources, especially during the winter season. These problems can be addressed using remote sensing data that offer a supplement to local measurements by providing comprehensive coverage of large areas, with data that are reliable and regularly updated. The surface

temperature can be measured using remote sensing instruments without the problem of inadequate samples inherent in date-sparse measurement networks (Swenson and Wahr, 2009).

For the measurement of surface water temperatures, a number of remote sensing satellites have been launched with spatial, temporal, spectral, and radiometric resolutions with comparative high accuracy (Steissberg *et al*., 2005). However, most of these satellites have low temporal resolution that obtain data every 16 days, such as Landsat and ASTER (Advanced Spaceborne Thermal Emission and Reflection Radiometer), at any particular area. Also, Landsat only acquire data during daytime in general. The MODerate Resolution Imaging Spectroradiometer (MODIS) and Advance Vary High Resolution Radiometer (AVHRR) overcomes these temporal resolution limitations and have played an important role in estimating surface temperature (Lu *et al.*, 2011) in providing daily coverage of the Earth's surface at a spatial resolution of 1×1 km^2 at large scan angles (Justice *et al*., 1998). The main limitation of these sensors is their incapability to penetrate clouds, which makes them available for only clear-sky conditions (Prigent *et al.*, 2003). Passive microwaves have been used to measure the surface temperature under all sky conditions because the microwave spectral region has the capability of penetrating clouds (Jensen, 2007; Howell *et al.*, 2009). However, this system has much coarser resolution (25×25 km^2) than that of thermal infrared sensors. At such a large pixel size, some pixels of surface temperature may be contaminated by the temperature of others surfaces and this is particularly true for the pixels in the satellite data of the near shorelines. Therefore, the datasets of this system were not applied in the present study.

This study applied thermal-infrared signals from MODIS on board the Terra satellite to assess the surface temperature of Lake Huron. This was necessary so that the research community can better understand how changes in the surface energy balance (e.g. evaporation)

that are affected by the water temperature influence the rapid changes in lake water level and ice cover. Moreover, remotely-sensed surface water temperature data that cover the entire lake at a high temporal resolution can be used to increase the accuracy of net radiation and surface energy budget models. The main objective of this study was to use MODIS thermal data for estimating the surface temperature over the lake in order to improve our understanding of spatial and temporal variation, as well as the long-term changes in lake surface temperature driven by recent climate changes in the Great Lakes region. The rest of this chapter is composed of the following sections: first is a description of the study site; second is a description of how accurate satellite surface temperature measurements are compared to direct temperature measurements; and third the spatial and temporal variations in the lake surface temperature are described. In the final section, conclusions are presented.

2.2 Study Area

Lake Huron is the second largest of the Great Lakes, with a surface area of 59,600 km^2. The lake contains a volume of 3,540 km^3, and a shoreline length of 6,157 km. The mean surface height of Lake Huron is 176 m above sea level. The lake's average depth is 59 m, while the maximum depth is 229 m. It has a length of 332 km and a greatest breadth of 245 km (Schertzer *et al.*, 2008). The Huron lakeshore extends 6,157 km and is characterized by shallow, sandy beaches and the rocky shores of Georgian Bay (Schaetzl, 2005). Because of these physical characteristics, Lake Huron is the second largest by surface area and the third largest fresh water lake on Earth. Additionally, this lake is the third largest by volume of water and has the longest shoreline of the Great Lakes (Zimmermann, 2013).

Lake Huron's thermal structure depends on the seasons due to the large annual variation of thermal cycle (Boyce *et al*., 1989) and the stratification of lake water caused by changes in water density due to changes in temperature. The convection overturning of Lake Huron occurs not only in the fall but also in the spring when the warm from the freezing temperature through 3.98 °C (Rao, 2012). The surface water temperature of the lake in the summer can reach 23 °C in August, which enables this lake to be a popular recreational spot in the summer, whereas low temperatures are at about 1 °C in the winter time (Zimmermann, 2013).

The Lake Huron watershed has a relatively low human population density, and is home for about 2.5 million people (USEPA, 2005). As a result, Lake Huron has retained much of its historic fish and wildlife habitat (USEPA, 2005). Based on the 2001 National Land Cover Dataset (Van and Meixner, 2006), the cropland in the Lake Huron Basin Watershed covers 52% of the land area and is the predominant land use, followed by forest area which covers 20% of the land area. Urban areas, wetlands, rangelands, and water constitute the remaining 28% of land cover. In the Lake Huron Basin, forest, wetland, and agriculture are dispersed throughout the northern area and agricultural land comprises the major part of the southern area. Residential area covers a small fraction of total land use in the Lake Huron region, and much developed area as well as major cities have occurred and grown along the shoreline (USEPA, 2005), as shown in Figure 2.1.

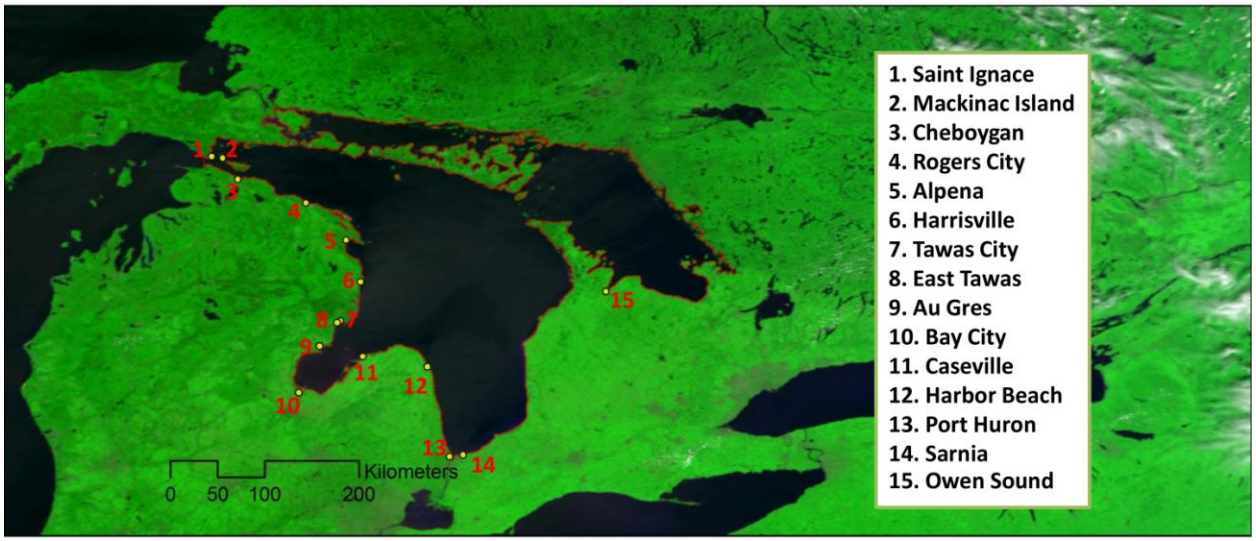

Figure 2.1 Location of major cities around Lake Huron

2.3 Objectives

In this chapter, the main goal is to estimate the surface temperature over the lake in order to expand our understanding of spatial and temporal variation, as well as long-term change in lake surface temperature. To achieve this goal, the objectives of this study are:

i) To examine the spatiotemporal distribution of the surface water temperature over Lake Huron using remotely-sensed data.

ii) To determine the characteristics and long-term changes in the surface water temperature over a period of 11 years (2002-2012).

iii) To investigate the connection between the changing rate of surface water temperature and lake depth.

2.4 Data and Methodology

2.4.1 Data

Two kinds of data sets were used: satellite observations and direct measurements.

For the satellite observations, thermal data obtained from the MODIS sensor on board the Terra satellite were used for this study. The sensor has a large scan angle with a field of view of ± 55º off-nadir, which yields a spatial coverage of 2,330 × 2,330 km^2. MODIS is a whiskbroom scanning imaging which obtains a 12 bit high radiometric resolution of thermal emission with a spatial resolution of 1×1 km^2 (Jensen, 2007). The satellite overpass over Lake Huron is approximately 11:30 am local solar time.

For the direct measurements, the water surface temperature data were measured using the infrared thermometer Everest I.R. Surface Temperature Sensor model 4000.4GL. The radiometric surface temperature sensor with a 15 degree field of view at a zenith view angle of 45 degree was mounted on the top of Spectacle Reef Lighthouse at a height of 31 m above the mean water level (Figure 2.2) The sensor measured the temperature range between -40 °C and 100 °C with ± 0.5 deg °C accuracy. The sensor was sampled every 5 seconds and was set to an averaging interval of 30 minutes. The data were recorded using the data logger (model CR23X Micro logger, Campbell Scientific Inc.). The system was powered by four12-V batteries charged by two solar panels.

Spectacle Reef Lighthouse, located 17.22 km east of the eastern end of Bois Blanc Island at 45.7732 N and 84.1367 W, is the only platform measuring year-round surface water temperature over the lake for calculating and validating the satellite data. The height of the instruments is 31 m above the mean water level, and the nearest shore is located 17.22 km east of

the eastern end of Bois Blanc Island. The height of the instruments is 31 m above the mean water level.

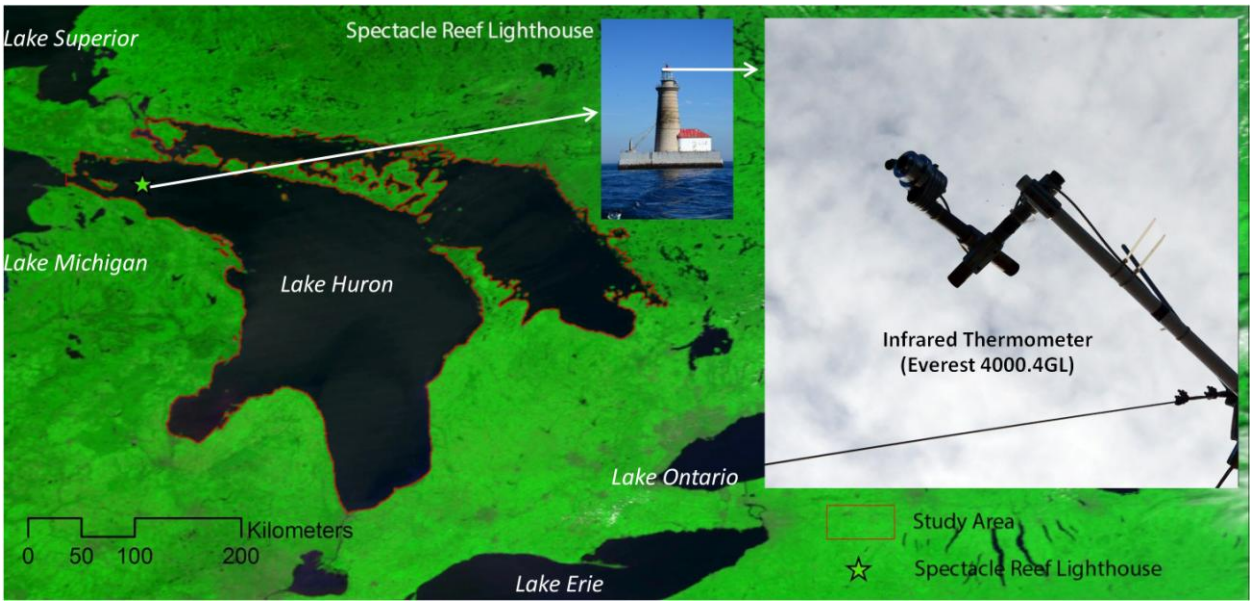

Figure 2.2 Location of Spectacle Reef Lighthouse with meteorological instruments, Everest I.R. surface temperature sensor model 4000.4GL)

2.4.2 Methodology

Figure 2.3 shows the conceptual framework for the data and methodology to estimate the lake surface temperature.

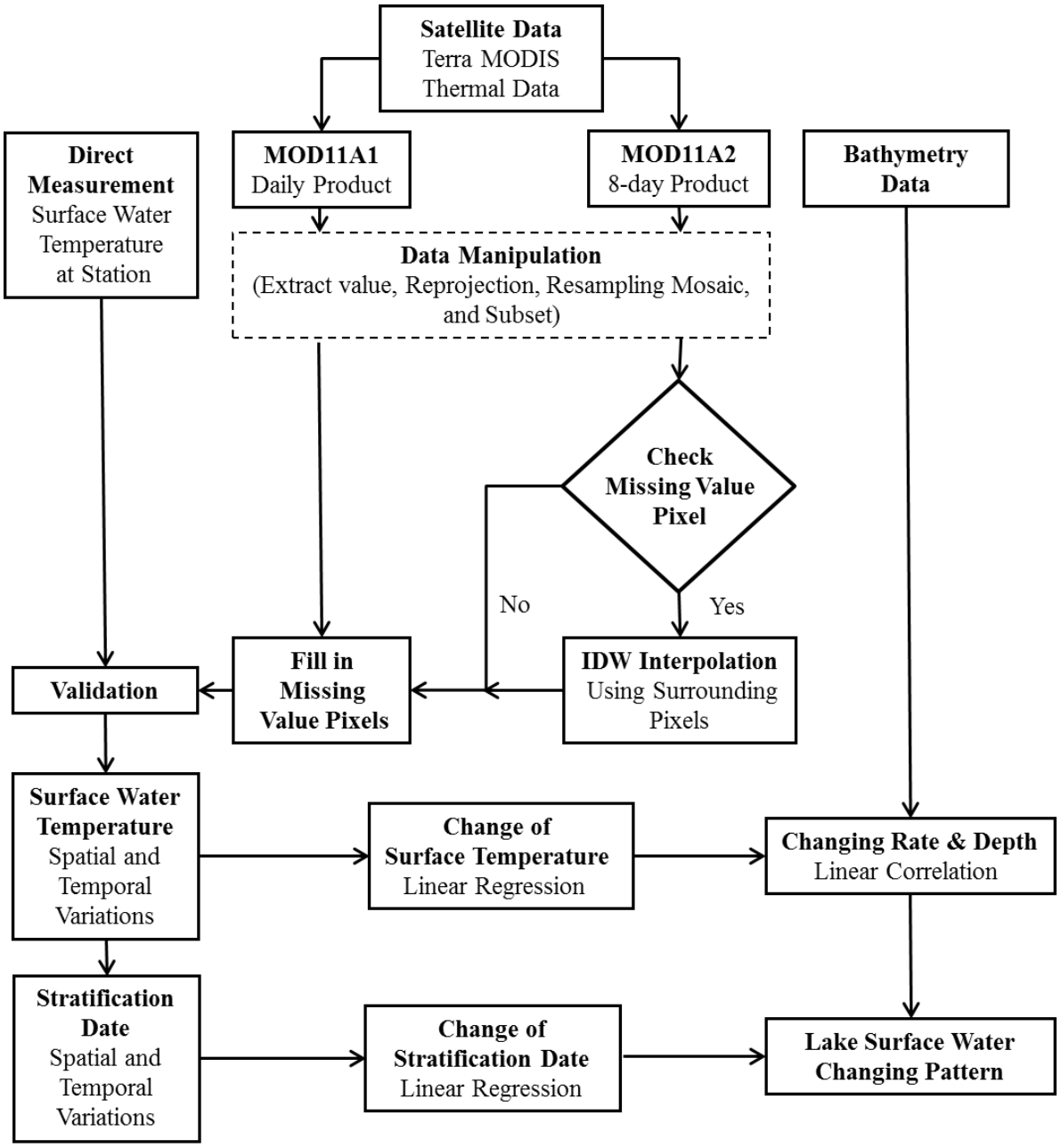

Figure 2.3 Schematic diagram shows the data and methodology for estimating the lake surface temperature and its change

2.4.2.1 Assessment of lake surface temperature

The surface temperature of Lake Huron between 2002- 2012 was derived from the MODIS sensor on board the TERRA sun synchronous orbit satellite; a total of 7984 images were used. The MODIS land-surface temperature (LST) level 2, 1×1 km^2 spatial resolution with geo-referenced product (MOD11A1 and MOD11A2), was acquired from the National Aeronautics and Space Administration Land Processes Distributed Active Archive Center. All of these data were in Hierarchical Data Format - Earth Observing System (HDF-EOS) format, which contained 22 object files including surface temperature, and time of surface temperature observation. The thermal images were extracted mosaicked using the MODIS Reprojection Tool (MRT, 2011). The nearest neighbor resampling was used for all transformation processes in this research because it preserves the original pixel brightness (Richards and Jia, 2006).

The split window method, the most validated and widely-used technique, was employed to calculate the surface temperature via a linear combination of the brightness temperatures measured from the satellite in two spectral channels in the thermal infrared region. For the MODIS data, thermal channels 31 (10.780-11.280 μm) and 32 (11.770-12.270 μm) are particularly suited to estimate surface temperature (Wan, 1999). The thermal radiances as observed by the sensor were converted to blackbody temperatures using the inversion of the Planck function, and the emitted spectral intensity of a black body is related to its temperature. Since these two channels are were close together, the atmospheric contribution to the measured radiances was the same and the transmittance differences between the two channels were only due to differences in the influence of atmospheric conditions (Kaleita and Kumar, 2000). The MODIS surface water temperature data have been widely validated for inland waters and

therefore are widely accepted as accurate (Crosman and Horel, 2009; Oesch *et al*., 2005; Oesch *et al*., 2008; Reinart and Reinhold, 2008).

As mentioned earlier, the major limitation in the use of thermal infrared from multi-spectral sensors is the occurrence of a significant amount of cloud cover, which prevents the passage of shortwave electromagnetic radiation. The cloud cover (derived from MODIS cloud mask product) ranged from 20 to 90 percent of the actual day-to-day weather (Figure 2.4) over Lake Huron. The figure illustrates the seasonal cycle with maximum cloud cover during wintertime and minimum during summertime (Ackerman *et al.,* 2013). The winter season has the highest amounts of cloud cover because of the great heat and moisture fluxes from the lake to the atmosphere. Cloud cover significantly modifies the surface energy balance (Jin, 2000), and therefore it is very important to retrieve the surface temperature under overcast skies. The biggest challenge in retrieving the surface temperature is to eliminate cloud contamination. MODIS's cloud-free data composite image (MOD11A2, 8 days composite product) was employed to fill in these missing value pixels (20-90 percent). However, it was found that throughout the winter season, there were several areas where new thermal imagery was not obtainable for more than 10 days because of cloud cover (Schwab *et al*., 1999). To overcome this problem of missing data in both MOD11A1 and MOD11A2, the Inverse Distance Weighted (IDW) spatial interpolation technique was used to calculate the missing pixel values of MOD11A2. Then the values of MOD11A2 were used to fill in the missing values in the daily MOD11A1 (middle of the chart of Figure 2.3). However, using MOD11A2 to fill in the missing data pixels in MOD11A1 could introduce uncertainty because the composite MOD11A2 data may be collected at different view angles, on different dates, and under different atmospheric conditions. Thus, it was necessary to validate the data before use.

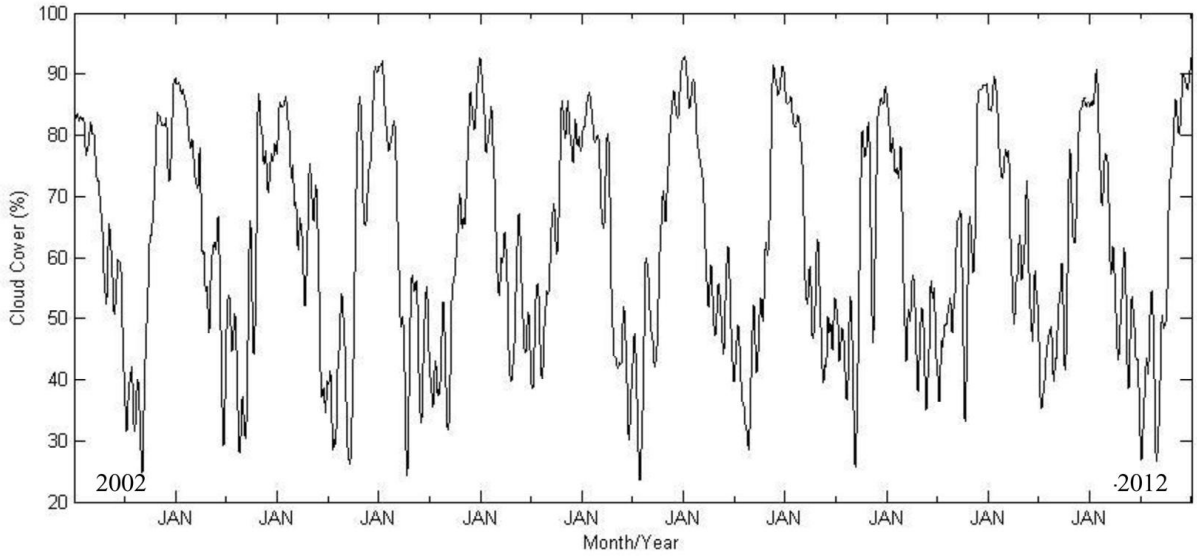

Figure 2.4 Percent of daily cloud cover over Lake Huron during 2002-2012 (cloud cover data derived from MODIS cloud mask product)

2.4.2.2. Surface temperature data validation

Validation is the procedure of evaluating the uncertainty of data obtained from satellite sensors. The data obtained from remote sensing system cannot be used with confidence without a validation process (Li *et al*., 2013). Moreover, the accurate estimates of the surface energy balance components, including surface temperature, is important for understanding the various physical processes of large lakes interact with their surrounding atmosphere (Lofgren and Zhu, 2000). This study applied the temperature-based method (T-based) to validate the surface temperature values. T-based is a ground-based technique that directly evaluates the satellite-derived surface temperature with in-situ direct measurements at the satellite overpass. This method has been applied to the validation of satellite data over different land cover and land use including large lakes, grasslands, and agricultural areas (Coll *et al*., 2005). The data of the

meteorological station on the top of Spectacle Reef Lighthouse, which is located 17.22 km east of the eastern end of Bois Blanc Island, were ideal for validation of the satellite data because the station is far from land and covers a large homogenous water surface area. The in-situ measurements were plotted (scatter plot) against the remotely-sensed data in order to explore the relationship and to correct the bias between in situ temperature and satellite surface water temperature of Lake Huron.

2.4.2.3. Spatial and temporal variations in lake surface temperature

After validation of the signature of the remote sensing temperature data, daily surface temperature maps of Lake Huron were created with a 1×1 km^2 grid resolution in order to examine the spatial distribution of the surface temperature in different seasons. All of the remote sensing estimates of the lake-wide temperatures were calculated using ERDAS IMAGINE 9.2 and ArcMap version 10.1 with the Python programming language.

In order to calculate the change in surface temperature, least squares linear regression was applied for each pixel with a daily temporal resolution over 11 years for the summer seasons. The slope of each regression line represented the surface temperature change (summer temperature change) during the study period.

2.5 Results and Discussion

2.5.1. Comparison of daily water temperature from satellite to temperature measured at Spectacle Reef.

The plot of the MODIS surface temperatures versus the direct surface temperature measurements from the meteorological station showed good agreement (Figure 2.5). However, it presented a bias of 0.57 °C (the measured temperature from the satellite was higher than the measurement from in situ station by 0.57 °C) for clear sky conditions, and -0.30 °C for cloudy-sky conditions. The bias during the clear sky conditions might have been due to the limitations in the processing of the MOD11L2 product, mainly the effective surface emissivity. For cloudy sky conditions, the bias may have resulted from atmospheric attenuation as a result of cloud cover, water vapor, and other atmospheric gases (Jensen, 2007), or the effect of data interpolations. If the thermal data are partially contaminated by clouds, the surface temperature will have a negative bias because the temperatures of clouds are lower than the lake water surface.

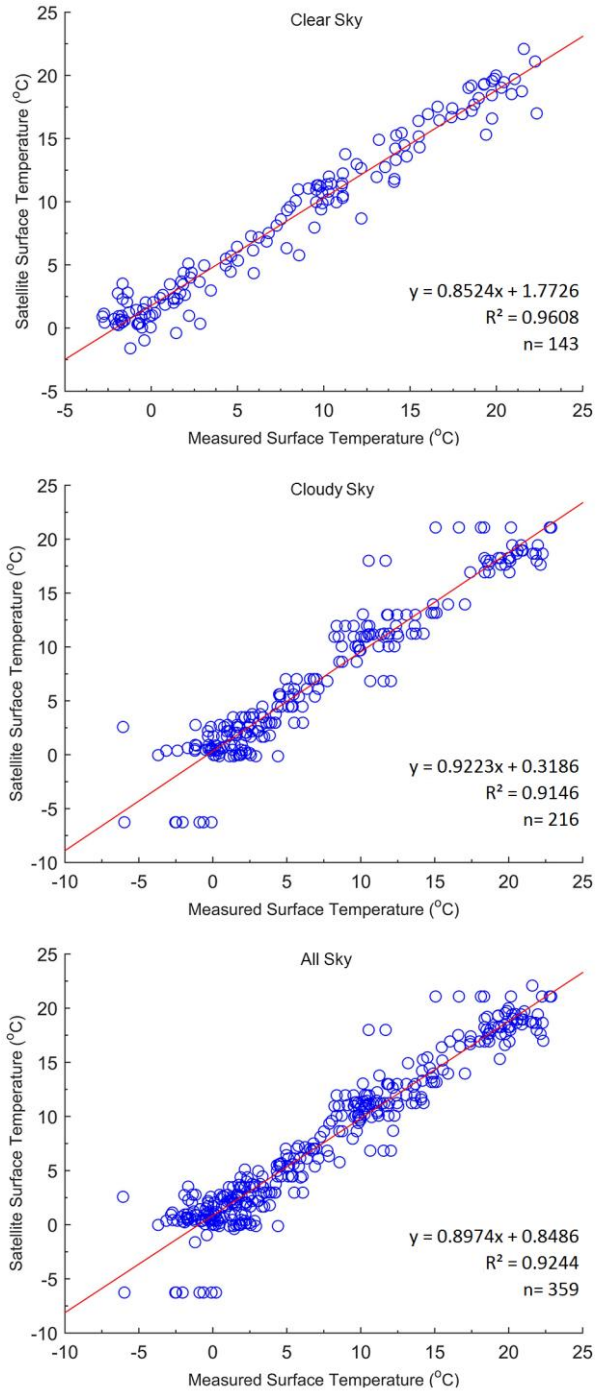

Figure 2.5 Scatter plots for the MODIS surface water temperature (°C) versus direct measurements (30 min average) in Lake Huron for the period 2002-2012

2.5.2. Spatial and temporal variations in lake surface temperatures

The average spatial distributions of seasonal (monthly) surface temperature conditions across the entire lake, including the descriptive statistics obtained from the remote sensing temperature data between 2002 and 2012, are shown in Figures 2.6 and 2.7. The monthly lake average temperature varied from -2.00 °C in February to 29.00°C in July and the standard deviation ranged from 0.95 °C in October to 3.13 °C in May. The spatial and temporal variations in lake surface temperature are described in detail below.

In winter (December – Mid-March), ice first is formed in the bays and other areas along the lake perimeter where the water is shallow. Thus, the spatial distribution patterns in the wintertime showed that the lake surface temperature was lower near shoreline than in the mid-lake region. The month of February exhibited the lowest mean surface temperature (-2.00 °C). The high spatial variability during the month of January (sigma = 2.98 °C) revealed the occurrence of stronger seasonal cooling.

In the spring (April-May), the solar energy increases over the lake surface because of more direct sun light and increased day length. Ice still covers some portions of the lake but some areas are melting. The patterns of spatial temperature distribution were opposite to the wintertime patterns. As the spring season progressed the water near the shorelines warmed rapidly whereas the mid-lake (the deeper section) temperature slowly increased. The month of May had the highest spatial variability, which is evidence of the strongest warming, particularly when certain parts of the lake reach thermal stratification (3.98 °C).

During the summer (June -August), the water surface was completely clear of ice. The distribution of the surface temperature of the lake surface tended to be zonal (especially in June and August), i.e. independent of the depth. The warmest water was near the shoreline, and the

coldest water was near the middle of the lake where the depth was greatest. The month of August had the highest mean surface temperature (29.00 °C), particularly in the southern part of the lake. During June there was high spatial variability mainly due to strong surface warming and thermal stratification.

In the fall (September - November), after maximum heat storage, the lake begins to lose heat, and the lake's surface temperature begins to decrease, starting from the north-west region. The range of the surface temperatures across the lake area was small compared to other seasons.

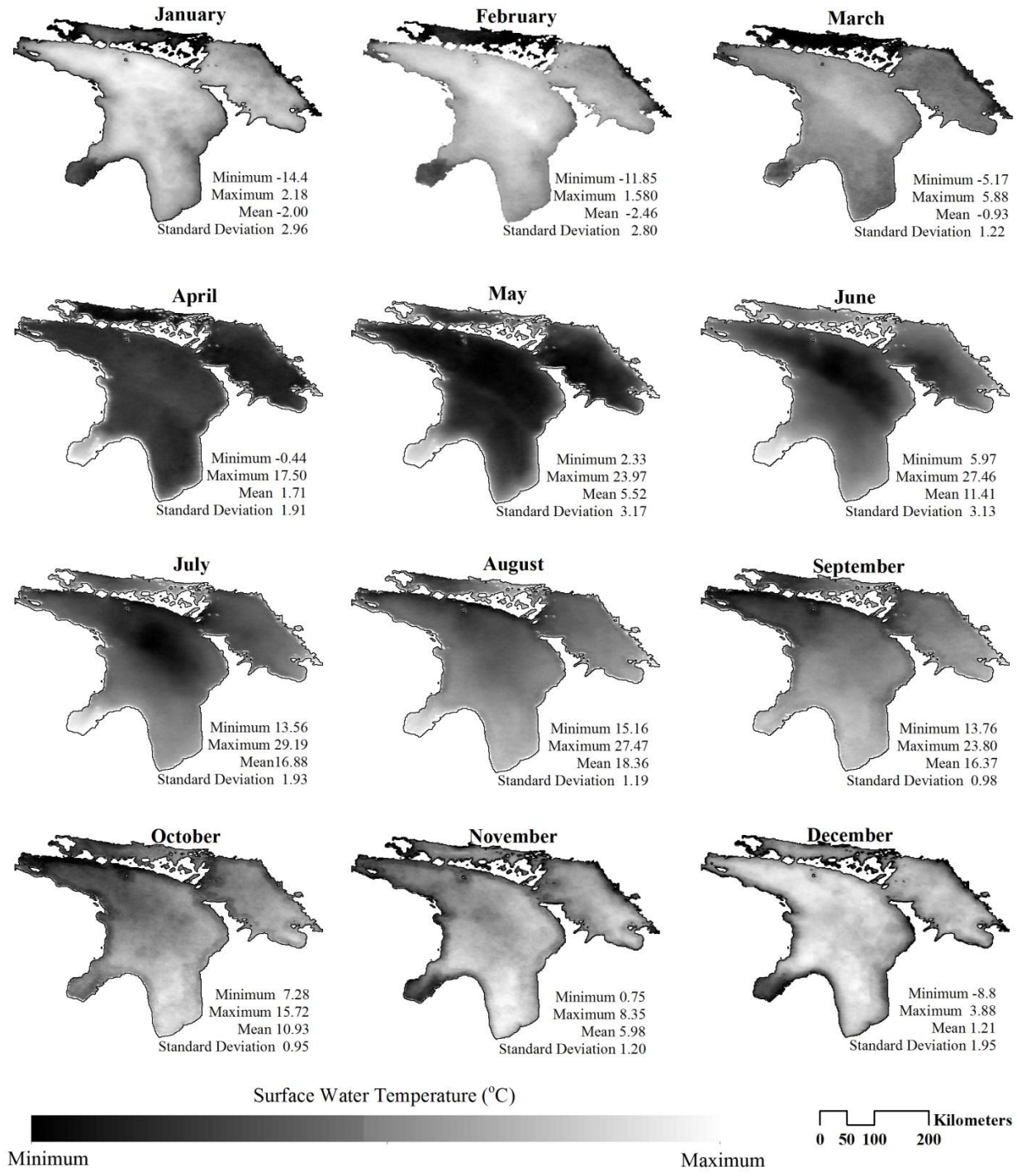

Figure 2.6 The spatial distribution of monthly surface temperature (°C) over Lake Huron averaged over the period 2002-2012. The gray scale displays the surface temperature variability for each month

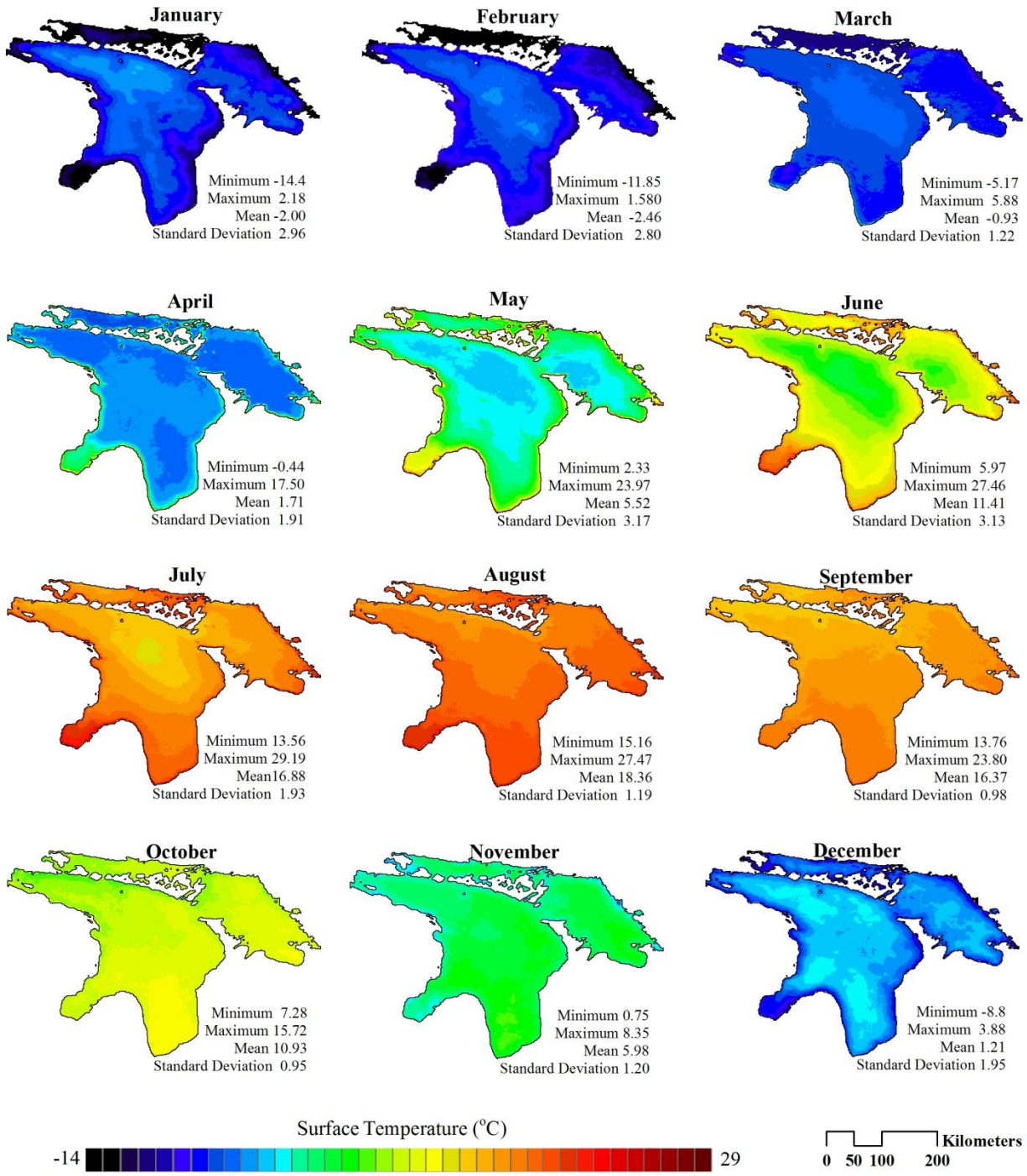

Figure 2.7 The spatial distribution of monthly surface temperature (°C) over Lake Huron averaged over the period 2002-2012. The colors scheme displays the annual surface temperature variability

2.5.3. Long-term changes in lake surface temperature

The regression analysis of the mean for the daily water surface temperature of the entire lake revealed a positive trend of 0.1 °C per year (Figure 2.8), indicating that the lake surface temperature increased by 1.1°C during the period 2002-2012. This positive trend is in agreement with Schneider and Hook (2010), who found that the surface of large lakes between mid and high northern latitudes have warming average of 1.0 °C per decade during the 15-year period studied (1985-1999).

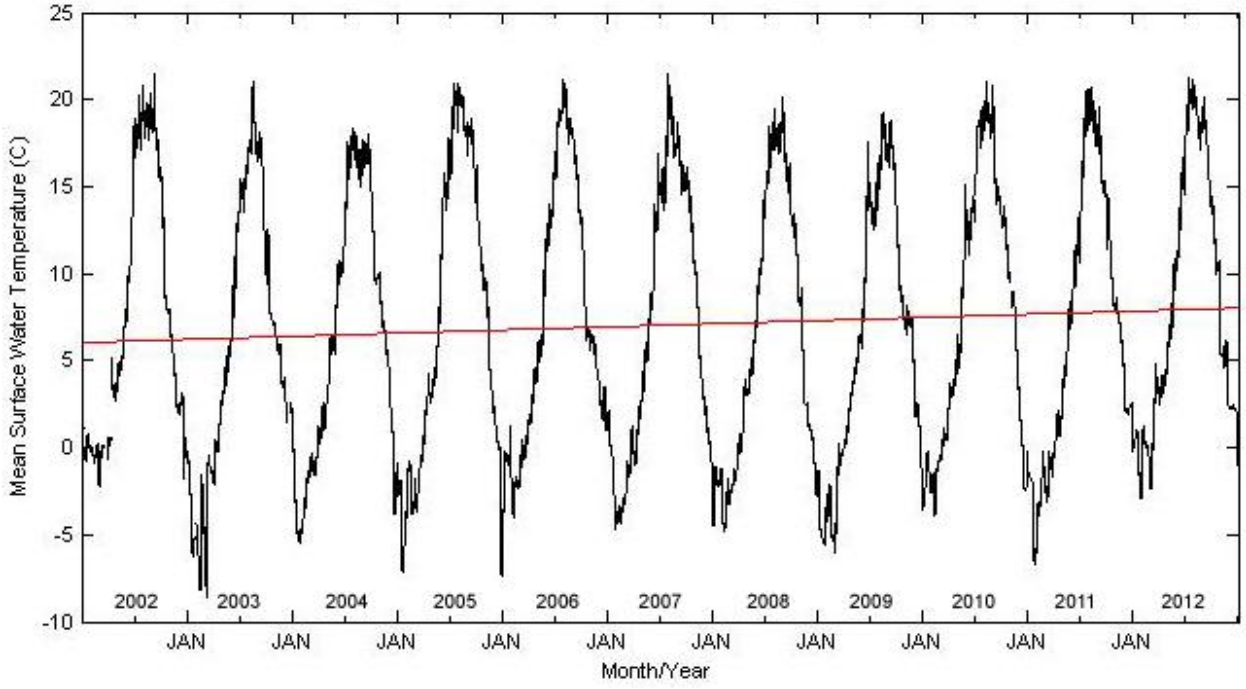

Figure 2.8 Surface water temperatures in Lake Huron during the period 2002-2012

Figure 2.9 shows the time series of the mean seasonal surface temperature and the trend line for the 11-year (2002–2012) period. The trend of the seasonal surface temperature exhibited an increase in winter, spring, and summer seasons, whereas it slightly declined during the fall season. However, the trend was not statistically significant for all of the seasons.

One of the important factors that influence the long-term changes in the water surface temperature of the lake is the onset of the summer stratification date, and the phenomenon of the warming trend is mostly due to the early onset of summer stratification in the lake. The present study showed that the starting date of summer stratification had been arriving earlier at the rate of approximately 1.4 days per year during the study period of 2002-2012 (Figure 2.10). This is greater than the rate formerly reported by Austin and Colman (2007), who stated that there was an increase in the onset of the stratification date of roughly 0.8 days per year in Lake Huron and of about 1.1 days per year in Lake Superior using the temperature data from the National Data Buoy Center (measure water temperature at 1m depth) from 1979-2006. The difference in the numbers of this study and theirs is probably due to the difference in the depth of measurement (skin temperature vs. 1 m). Despite different study periods, datasets, and methods, the results of both studies were consistent in detecting a rapid increase in lake temperature.

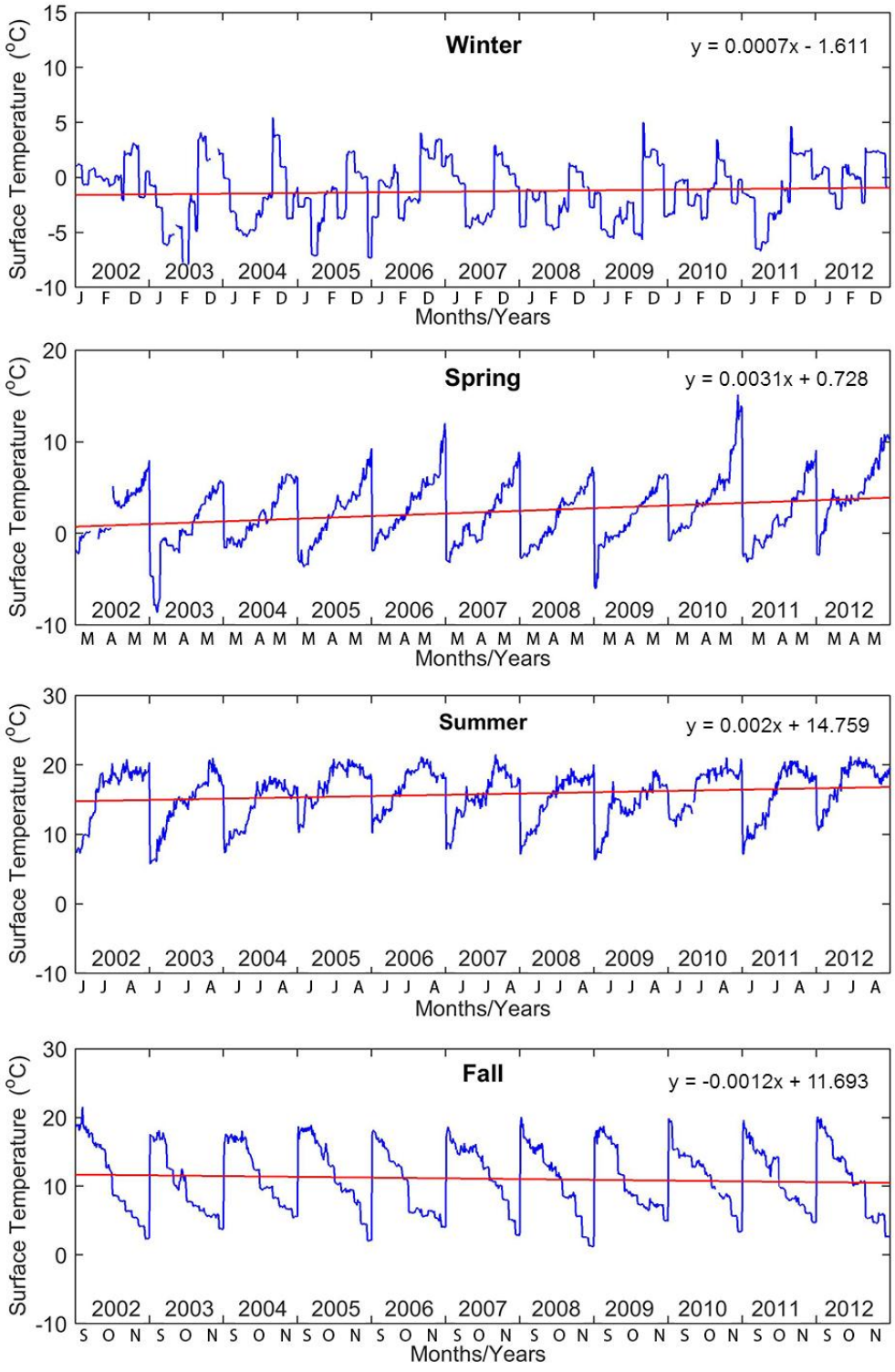

Figure 2.9 Time series of seasonal surface water temperature and the trend line for the 11-year (2002-2012) period

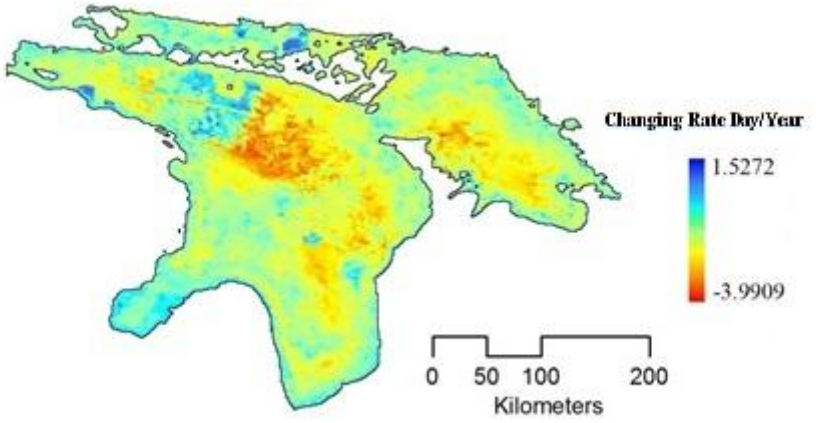

Figure 2.10 Spatial variations of surface temperature change rate of summer stratification date between 2002 and 2012

In the summer, the warming rate obviously varies with depth. The trend values from the surface water temperature during the warmest period of the year revealed interesting spatial variability patterns. The changing trends were more prominent in the deeper areas of the lake. The deepest area (224 m) also had the highest warming rate (0.0039 °C per day), whereas the lowest warming rate of nearly 0.0 °C per day was located in the shallower areas of the lake (Figure 2.11). These variations of changing temperature rates showed a statistically-significant correlation ($p < 0.05$) with the lake bathymetry. This phenomenon was due to the early summer stratification date, which allows for a longer time of solar radiation to warm the water. Another possible cause was the difference in the gaining heat between the shallow (warmer) and deeper portions (colder) of the lake. The lake's deeper areas have greater thermal memory which requires a longer time to heat until the temperature reaches 3.98 °C. Therefore, the colder surface water in the middle lake generally gains heat at a higher rate than the surface water near the shore, which is already warm during the spring season.

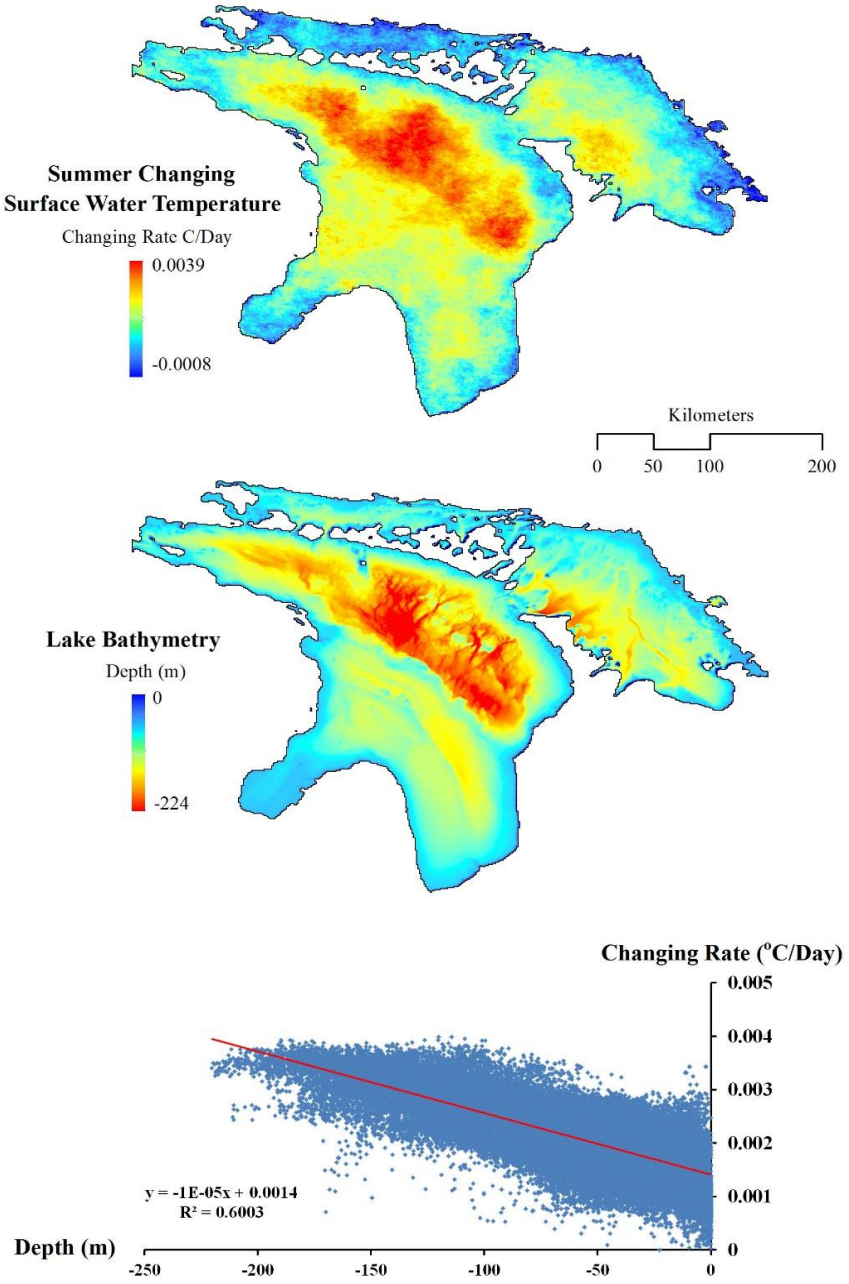

Figure 2.11 Spatial distribution of warming surface water temperatures in Lake Huron during the period 2002-2012 (Top), lake bathymetry (middle), and the scatter plot of warming rate during the period 2002-2012 and depth (bottom) (Bathymetry Data Source: NOAA National Geophysical Data Center)

2.6 Conclusion

This chapter examined the spatiotemporal distribution of the surface water temperature over Lake Huron using remotely-sensed data. Eleven (2002-2012) years of 1 x 1 km^2 surface temperature data were analyzed using images from the Moderate Resolution Imaging Spectroradiometer (MODIS) on board NASA's Terra satellite. Comparison of the MODIS-derived surface temperature with in situ point observations from Lake Huron yielded satellite minus in-situ differences of 0.57 °C for clear-sky conditions, and -0.30 °C for cloudy-sky conditions.

Having lower heat capacity, the shallow portion of the lake may experience earlier warming and cooling than the deep parts, resulting in spatial variability of the lake surface water temperature. For instance, the near-shore surface temperature was 20°C warmer than at the deepest region during the late spring and early summer. The lowest (and highest) surface temperature of Lake Huron was observed during the winter (and summer). The monthly lake average temperature varied from -2.0 °C in February to 29.0 °C in July and the standard deviation ranged from 0.95 °C in October to 3.13 °C in May. The study showed that the starting date of the summer stratification was earlier at the rate of approximately 1.4 days per year. This shift towards an earlier onset of summer stratification may have been due to the milder winter tendency. Weaker winter results in decreasing duration and amount of ice cover and consequently more lake absorbed solar energy, and faster return to summer stratification. 11-year record of satellite data revealed upward trends of daily water surface temperatures and the warming rate was found to be greatest in the deepest areas of the lake, showing a statistically-significant correlation between warming rate and depth.

This warming is expected to impact the lake environment, particularly regarding ice cover, evaporation, and lake water level, and the warming will likely result in a decreased duration and amount of winter ice cover, leading to an increase in winter lake evaporation while summer evaporation will increase due to high surface water temperatures. This increasing evaporation will very likely lead to a decline in lake water level, and such a decline would create a significant concern for the communication and commercial sectors that rely on the lake water system (Rao, 2012). Shipping companies and hydro-electric power plants would suffer economic repercussions, and harbors and marinas would also be adversely affected; shore-line erosion could also result (Blanken *et al*., 2011).

Some environmental alterations caused by the warming surface water temperature have the potential to be beneficial for some fish environments and human activities. Warmer water temperatures possible will enhance ecosystem productivity, and possibly the available habitats for warm-water native fish (Trumpickas *et al*., 2009). Warming temperatures may also extend the travel season, particularly the expansion of the swimming season.

The lake surface temperature data from the remote sensing satellites are gaining attention as a supplement to meteorological station data because of their continuous field rather than point-recorded measurements. This technique is useful in estimating and studying surface water temperature as well as detecting changes in the spatial and temporal variations in the lake surface temperature. To the best of my knowledge, this is the first study to explore the correlations between warming rate and lake depth, and this is mainly due to the use of this remote sensing technique. However, a better understanding of the results obtained from the long-term monitoring of surface water temperature is still required, as well as a deeper analysis of the long-term changes in net surface radiation. The information provided in this study represents an

important parameter for input to the numerical model for assessing the changes in surface net radiation, which can be comprehensive explored the recent changes in the radiation balance over Lake Huron.

2.7 Bibliography

Ackerman S.A., Heidinger A., Foster M.J., Maddux B. 2013. Satellite regional cloud climatology over the Great Lakes. *Remote Sensing*, 5, 6223-6240

Assel R.A. 2005. Classification of annual Great Lakes ice cycles: Winters of 1973-2002. *Journal of Climate*, 18, 4895-4904

Austin J.A., Colman S.M. 2007. Lake Superior summer water temperatures are increasing more rapidly than regional air temperatures: A positive ice–albedo feedback. *Geophysical Research Letters*, 34, L06604. doi:10.1029/2006GL029021

Blanken P.D., Spence. C, Hedstrom N., Lenters J.D. 2011. Evaporation from Lake Superior: 1. Physical controls and processes. *Journal of Great Lake Research*, 37, 707-716

Boyce F.M., Donelan M.A., Hamblin, P.F., Murthy C.R., Simons T.A. 1989. Thermal structure and circulation in the Great Lakes. *Atmosphere-Ocean*, 27(4), 607-642. doi: 10.1080/07055900.1989.9649358

Coll C., Caselles V., Galve J. M., Valor E., Niclòs R., Sanchez J.M., Viras R. 2005. Ground measurements for the validation of land surface temperatures derived from AATSR and MODIS data. *Remote Sensing of Environment*, 97, 288–300

Crosman E.T., Horel J.D. 2009. MODIS-derived surface temperature of the Great Salt Lake. *Remote Sensing of Environment*, 113, 73−81

Dobiesz N.E., Lester N.P. 2009. Changes in mid-summer water temperature and clarity across the Great Lakes between 1968 and 2002. *Journal of Great Lakes Research*, 35, 371-384

Howell E.L., Brown, L.C., Kang K., Duguay C.R. 2009. Variability in ice phenology on Great Bear Lake and Great Slave Lake, Northwest Territories, Canada, from SeaWinds/QuikSCAT: 2000-2006. *Remote Sensing of Environment*,113, 816 – 834

Jensen J.R. 2007. *Remote Sensing of the Environment*. 2nd ed. Upper Saddle River, New Jersey Prentice Hall

Jin M. 2000. Interpolation of surface radiative temperature measured from polar orbiting satellites to a diurnal cycle 2. Cloudy-pixel treatment. *Journal of Geophysical Research*, 105, 4061-4076

Jones M.L., Shuter B.J., Zhao Y., Stockwell J.D. 2006. Forecasting effects of climate change on Great Lakes fisheries: Models that link habitat supply to population dynamic scan help. *Canadian Journal of Fisheries and Aquatic Sciences*, 63, 457-468

Justice C.O., Vermote E., Townshend J.R.G., DeFries R., Roy D.P., Hall D.P., Salomonson V.V., Privette J.L., Riggs G., Strahler A., Lucht W., Myneni R., Knyazikhin Y., Running, S.W., Nemani R.R., Wan Z., Huete A., Leeuwen W., Wolfe R.E., Giglio L., Muller J.P., Lewis P., Barnsley M.J. 1998. The moderate resolution imaging spectroradiometer

(MODIS): land remote sensing for global change research. *IEEE Transactions on Geoscience and Remote Sensing,* 36, 1228-1249

Kaleita A.L., Kumar P. 2000. AVHRR estimates of surface temperature during the Southern Great Plains 1997 Experiment. *Journal of Geophysical Research,*105, 20791-20801

Lofgren B.M., Zhu, Y. 2000. Surface energy fluxes on the great lakes based on satellite observed surface temperatures 1992 to 1995. *Journal of Great Lakes Research,* 26, 305 – 314

Lu L., Venus V., Skidmore A., wang T., Luo G. 2011. Estimating land-surface temperature under clouds using MSG/SEVIRI observations. *International Journal of Applied Earth Observation and Geoinformation,* 13, 265-276

Magnuson J.J., Mortsch L.R., Schindler D.W., Quinn F.H., Webster K.E., Assel R.A., Bowser C.J., Dillon P.J., Eaton J.G., Evans H.E., Fee E.J., Hall R.I. 1997. Potential effects of climate changes on aquatic systems: Laurentian Great Lakes and precambrian shield region. *Hydrological Processes*, 11, 825-87

MRT (MODIS Reprojection Tool). 2011. User's Manual. Release 4.1. Land Processes DAAC. USGS Earth Resources Observation and Science (EROS) Center. 69 p

Oesch D., Jaquet J.M., Hauser A. Wunderle S. 2005. Lake surface water temperature retrieval using advanced very high resolution radiometer and moderate resolution imaging spectroradiometer data: Validation and feasibility study. *Journal of Geophysical Research*, 10(C12014), 1−17

Oesch D., Jaquet J.M., Klaus R., Schenker P. 2008. Multi-scale thermal pattern monitoring of a large lake (Lake Geneva) using a multi-sensor approach. *International Journal of Remote Sensing*. 29, 5785−5808

Prigent C., Aires F., Rossow W.R. 2003. Land surface skin temperatures from a combined analysis of microwave and infrared satellite observations for an all-weather evaluation of the differences between air and skin temperatures. *Journal of Geophysical Research*, 108, NO. D10, 4310. doi:10.1029/2002JD002301

Rao Y.R., 2012. Great Lake Processes: Thermal structure, circulation and turbulent diffusion processes. Encyclopedia of Lakes and Reservoirs. Bengtsson L., Herschy R.W. Fairbridge R.W. Eds. 298-303. doi: 10.1007/978-1-4020-4410-6_266

Reinart A., Reinhold M. 2008. Mapping surface temperature in large lakes with MODIS data. *Remote Sensing of Environment*. 112, 603−611

Richards J. A., Jia X. 2006. *Remote Sensing Digital Image Analysis: An Introduction*. 4th ed. Springer. 439 p

Schaetzl R.J. 2005. Watershed of Lake Huron: Geography of Michigan and the Great Lakes Region. Course Material of GEO 333 Geography of Michigan and the Great Lakes Region, Department of Geography, Michigan State University. Retrieved from http://web2.geo.msu.edu/geogmich/lakehuron.html

Schertzer W.M., Assel R.A., Beletsky D., Croley II T.E., Lofgren B. M., Saylor J.H., Schwab, D.J. 2008. Lake Huron climatology, inter-lake exchange and mean circulation. *Aquatic Ecosystem Health & Managemen*, 11, 144 - 152

Schneider P., Hook S. J. 2010. Space observations of inland water bodies show rapid surface warming since 1985. *Geophysical Research Letter*, 37, L22405

Schwab D.J., Leshkevich G.A., & Muhr, G.C. 1999. Automated mapping of surface water temperature in the Great Lakes. *Journal of Great Lakes Research,* 25, 468 - 481

Steissberg T.E., Hook, S.J., Schladow S.G. 2005. Characterizing partial upwellings and surface circulation at Lake Tahoe, California–Nevada, USA with thermal infrared images. *Remote Sensing of Environment*, 99: 2−15.

Swenson S., Wahr J. 2009. Monitoring the water balance of Lake Victoria, East Africa, from space. *Journal of Hydrology,* 370, 163–176

Trumpickas J., Shuter B.J., Minns C.K., 2009. Forecasting impacts of climate change on Great Lakes surface water temperatures. *Journal of Great Lakes Research,* 35, 454 - 463

USEPA (U.S. Environmental Protection Agency). 2005. *State of The Great Lake 2005, What Are The Current Pressures Impacting Lake Huron?* Retrieved from http://www.epa.gov/solec/indicator_sheets/huron.pdf

Van G.A., Meixner T. 2006. A global sensitivity analysis tool for the parameters of multi-variable catchment models. *Journal of Hydrology,* 324, 10-23

Wan Z. 1999. *MODIS Land Surface Temperature Algorithm Theoretical Basis Document.* Retrieve from http://modis.gsfc.nasa.gov/data/atbd/atbd_mod11.pdf

Zimmermann K. A. 2013. *Great Facts about the Five Great Lakes.* Retrieved from http://www.livescience.com/32081-lake-huron.html

CHAPTER 3

TEMPORAL AND SPATIAL VARIATIONS IN THE SURFACE RADIATION BALANCE OF LAKE HURON

3.1. Introduction

Understanding of the spatial distribution of net radiation is one of the main requirements for a physically-based model (Parlow, 2000). The surface net radiation (Q^*) is the algebraic sum of the four radiation components (Federer, 1968) including i) the incoming, downward, shortwave radiation from Sun and sky ($K\downarrow$), ii) the outgoing, upward, shortwave radiation of reflected solar radiation ($K\uparrow$), iii) the incoming longwave, thermal, radiation from the atmosphere ($L\downarrow$), and iv) the outgoing longwave radiation from the surface ($L\uparrow$). Therefore net radiation can be express as:

$$Q^* = K\downarrow - K\uparrow + L\downarrow - L\uparrow$$

On the basis of atmospheric research filed, short wavelengths usually referring to the part of the electromagnetic spectrum which is dominated by incoming radiation from the Sun typically extend from ultraviolet to near infrared (0.15 to 3 μm). Longwave radiation typically corresponding to the part of the spectrum dominated by radiation emitted by the Earth's surface and atmosphere extend from around 3.0 to 100 μm (Oke, 1996).

Net radiation is the great key component in understanding the surface energy balance and heat flux interface the atmosphere (Bisht *et al*. 2005; Sun *et al*., 2013; Terjung *et al*., 1968). This flux interface is the one of the major determinants of the climate. Over large areas, accurate information of the spatial and temporal variability of net radiation and its components (incoming shortwave, incoming longwave, outgoing shortwave and surface outgoing longwave radiation) are important for regional and global climate models (Dugual, 1994).

Point measurements of the net radiation and its components can be acquired from meteorological stations. In the Great Lakes region, in particular, there are few offshore meteorological stations which regularly measure the net radiation (Blanken, 2014; Lenters *et al*., 2013). However, typical tower footprints (upwind sampling area) for the measurement of the turbulent latent and sensible heat fluxes have length scales of 100–2000 m (Schmid, 1994) and 9000 m for the meteorological station on the Spectacle Reef lighthouse (Blanken, 2014). Because there are few observation stations and limitations on their footprint, there will never be sufficient flux towers or field measurements network to adequately characterize large areas of the Great Lakes under all conditions. Moreover, in the temporal scale, none such regular long-term instrumental observations exist on the water surface of Great Lakes because of winter severity and a lack of secure research instrument bases (Mckay *et. al*., 2011; Oyserman *et al*., 2012). Most available long-term net radiation measurement stations located on or near shore where signals are contaminated by surrounding non-water surfaces. Therefore, with far too sparse and period of off-shore observations, it is impossible to provide a realistic, thorough picture of net radiation that meet the requirement of climate research community.

Apart from actual direct measurement of radiation components, estimation can be approached using multi-spectral satellite data. Remote sensing satellites are the only technology that can efficiently and economically (although the satellite technology is expensive, but the data is free to the public) provide over-lake direct observations or lake-representative data for critically required inputs for estimating of surface radiation components. Clouds and the Earth's Radiant Energy System (CERES) on board Terra and Aqua satellites is the specific sensor that provides a comprehensive earth radiation budget (Geier *et al*., 2003), however, its approximately 1°× 1° spatial resolution is too coarse for this study.

Several studies have attempted to modulate the spatial resolution satellite data to assess net radiation by combining remote sensing satellite measurements with in-situ data (i.e. Santos *et at*., 2011; Wang and Liang, 2009). Some studies have used solely satellite data to estimate net radiation (Bisht and Bras, 2010; Jin *et. al*., 2011) or some of its components such as net surface shortwave radiation (e.g. Kim and Liang, 2010), net surface longwave radiation (e.g. Tang and Li, 2008). All these analyses were focused on a short term (1or 2 years) over land surface. To the present author's knowledge, this study is the first time to apply exclusively remote sensing data to study long-term surface net radiation under all sky conditions over a large lake.

The purpose of this chapter is to estimate the spatial and temporal distribution, as well as, long-term changes in the lake surface net radiation and its four components under both clear and cloudy sky conditions using MODIS data without requiring additional data. The results of this study will be significant and beneficial in helping to understand the spatial and temporal distribution of net radiation over a large lake that will contribute to the climate research community both at regional and global scales. Furthermore, the success of this method will prove that exclusive use of satellite data could effectively estimate net surface radiation worldwide.

This chapter composed of the following sections: the first is description of the study site, followed by a description of the study methods. Next, an assessment of the accuracy of satellite parameter measurements compared to the direct measurements is discussed. Next, the spatial and temporal variations (seasonally from 2002-2012) in the lake's surface net radiation is discussed. In the final section, conclusions are presented.

3. 2 Study Area

Lake Huron is the second largest of the Great Lakes, with a freshwater surface area of 59,600 km^2 and 3,540 km^3 of freshwater volume (Schertzer *et al.*, 2008). Lake Huron is on the U.S. – Canadian border and the lake is located between the eastern coast of Michigan and Ontario, Canada. Lake Huron is linked to Lake Michigan through the Straits of Mackinac. Hydrological, these two lakes are considering single lake.

Spectacle Reef Lighthouse, located 17.22 km of the eastern end of Bois Blanc Island at 45.7732 N and 84.1367 W, is the only station measuring year-round, continuous 30-min average net radiation and its four components for validating satellite data (Figure 3.1).

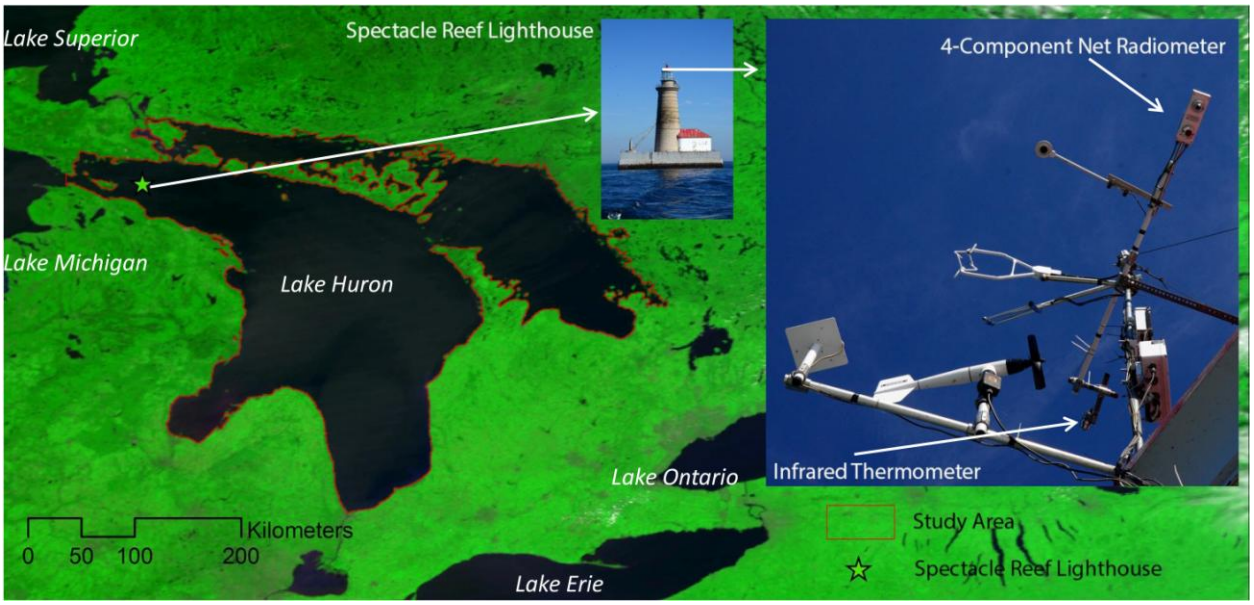

Figure 3.1 Study area and the location of Spectacle Reef Lighthouse with meteorological instruments (4-Component Net Radiometer, Infrared thermometer)

3. 3 Objectives

In this chapter, the intent is to explore the pattern of spatial and temporal distribution, as well as the long-term changes in the lake surface net radiation and its four components under both clear and cloudy sky conditions using satellite data. The specific objectives of this study are to:

i) Examine spatiotemporal distribution of surface net radiation and its four components over Lake Huron using remotely-sensed data.

ii) Determine the characteristic and long-term change of surface net radiation and its four components over a period of 11 years (2002-2012).

iii) Provide the important parameter for input to the numerical model for assessing the changes in the surface energy balance which can be comprehensively explore the recent changes in water level of Lake Huron.

3.4 Data and Methodology

3.4.1. Data

Two kinds of datasets were used: satellite observations and direct surface-based measurements.

3.4.4.1. Satellite Data

Measurement of net radiation and its components were obtained throughout the period between 2002 and 2012. Four data products from MODIS including MOD03 (Geological product), MOD06 (Cloud product), MOD07 (Atmospheric profile product), and MOD11 (Land surface temperature product) were used. These data are in the Hierarchical Data Format-Earth Observing System (HDF-EOS), which contains multi-object files, and were obtained from the

National Aeronautics and Space Administration MODIS Adaptive Processing System (MODAPS). The data are available at http://modaps.nascom.nasa.gov/services/. All products except MOD11 were extracted and mosaicked using the MODIS Conversion Toolkit (MCTK). For MOD11, the thermal images were extracted, reprojected, and mosaicked using the MODIS Reprojection Tool (MRT, 2011). The nearest neighbour resampling was applied for all of the data in order to preserve the original pixel brightness value (Richards, 2013). The following are the characteristic of each product.

The MOD03 product consists of geo-location field data calculated for each 1×1 km^2 spatial resolution. The MOD03 contains latitude, longitude, surface height, solar zenith and azimuth angles, and satellite zenith and azimuth angles.

The MOD06 cloud product provides cloud information, including cloud optical thickness, cloud top temperature, cloud emissivity, and cloud fraction at spatial resolution of 5×5 km^2.

The MODIS atmospheric profile product MOD07 provides air and dew point temperature profiles at a spatial resolution of 5× 5 km^2 at 20 levels of vertical atmospheric pressure.

MOD11 contains surface temperature at spatial resolutions of 1×1 and 5×5 km^2, respectively for clear sky days. (MOD11 data already calculated in Chapter 2).

3.4.1.2. In-situ Measurement

Ground data from the meteorological station located on the top of Spectacle Reef lighthouse were used for satellite data validation. The station provides 30 minute averages of a number of net radiation and its four components observation and data is recorded by Campbell Scientific CR23X micrologger.

The 4-Component Net Radiometer (Model CNR4 Campbell Scientific, Logan, UT) is used to measure the net radiation. The instrument has accuracy in daily total ranging from 5 to 15 %. The DC power supplied by four 12-V 115-Ah marine batteries charged by two 80-W solar panels. The datalogger and batteries were located in a dry location inside the lighthouse. Post-processing of these data, including quality control, was performed following Blanken *et al*., (2011).

3.4.2 Methodology

All surfaces obtain shortwave radiation during the day time and always exchange longwave radiation with the atmosphere. Because this exchange plays an important role in the regional surface energy balance, considerable research efforts has been made to better understand changes in the surface energy exchange, and to support spatial and temporal models that can predict energy fluxes across the lake and over time. For this study, net radiation at the water surface can be stated in terms of its components as:

$$Q^* = (1 - \alpha)K\downarrow + L\downarrow - L\uparrow \qquad (3.1)$$

where :

Q^* is the net radiation (0.15 -100 µm)

α is the surface albedo (no unit)

$K\downarrow$ is the incoming shortwave radiation flux density (0.15 – 3.0 µm)

$L\downarrow$ is the incoming longwave radiation flux density (3.0 – 100.0 µm)

$L\uparrow$ is the outgoing longwave radiation flux density (3.0 – 100.0 µm)

3.4.2.1 Surface Albedo

In a clear sky, in the absence of diffuse radiation, the reflectivity of the lake's surface can be estimated using solar zenith angle which is derived from MOD03 Geological product. Fresnel reflection for unpolarized radiation (Nunez *et al*. 1972) was applied. The equation can be written as:

$$\alpha\,(\theta,n) = \frac{1}{2}\left[\frac{sin^2(\theta-n)}{sin^2(\theta+n)} + \frac{tan^2(\theta-n)}{tan^2(\theta+n)}\right] \quad (3.2)$$

where :

θ is solar zenith angle

n is the angle of refraction for the medium

For water

$$\sin n = sin\frac{\theta}{m} \quad (3.3)$$

where:

m is the index of fraction equal to 1.33 for the visible spectrum region

Under cloudy sky conditions, albedo values were calculated from field data collected over Great Slave Lake (Blanken *et al.*, 2000). The author did not estimate albedo values directly

from Lake Huron in-situ measurements because the albedo signal was contaminated by the lighthouse's concrete base, which lead to overestimation of albedo values.

3.4.2.2 Incoming Shortwave Radiation

The computation of incoming shortwave radiation for clear sky conditions (W m^{-2}) was carried out using two parameters, vapor pressure and solar zenith angle. The method developed by Zillman (1972) cited in Bisht and Bras (2010) is used and the equation can be written as:

$$K\downarrow_{\text{Clear}} = \frac{S_0 \cos^2 \theta}{1.085\cos(\theta) + e_o(2.7+\cos(\theta)) \times 10^{-3} + \beta} \quad (3.4)$$

where :

S_o is the solar constant 1376 Wm^{-2}

β is a constant value 0.1

e_o is vapor pressure (hPa)

Solar zenith angle is derived from MOD03 Geological product. Vapor pressure, e_o (hPa) was estimated from dew point temperature data using Clausius-Clapeyron method (Roger and Yau, 1989 cited in Bisht and Bras, 2010) as the following equation:

$$e_o = 6.11 \exp\left[\frac{L_v}{R_v}\left(\frac{1}{273.15} - \frac{1}{T_d}\right)\right] \quad (3.5)$$

where :

L_v is the latent heat of vaporization (2.56 $\times 10^6 Jkg^{-1}$)

R_v is the constant of gas for water vapor (461 J kg^{-1} K^{-1})

T_d is dew point temperature (K)

Dew point temperature (T_d) was derived from MOD07 atmospheric profile product. Since the occurrence of overcast and cloudy-sky situation in the study area represent more than 50 percent of the actual day-to-day weather, shortwave radiation is attenuated through the cloud. Therefore, under cloudy sky conditions, I applied the method proposed by Slingo (1998), in which the incoming shortwave radiation (W m^{-2}) was calculated by weighting the shortwave radiation of clear sky using cloud fraction and cloud optical thickness. These two parameters were derived from MOD06 cloud product. The equation can be expressed as:

$$K\downarrow_{Cloudy} = K\downarrow_{\text{Clear}} \left[(1 - f_c) + f_c e^{-\tau_c / \cos(\theta)}\right] \quad (3.6)$$

where :

f_c is cloud fraction (no units)

τ_c is cloud optical thickness (no units)

3.4.2.3 Incoming Long-wave Radiation

Values for incoming longwave radiation (W m^{-2}) under clear-sky conditions were calculated using air temperature and air emissivity with the Stefan-Boltzman relationship.

$$L\downarrow = \sigma \varepsilon_a T_a^4 \quad (3.7)$$

where :

T_a is air temperature at the height of 31 m (^oK)

ε_a is effective air emissivity (no units)

σ is Stefan-Boltzman constant 5.67×10^{-8} W m^{-2} K^{-4}

Air temperature (T_a) was derived from MOD07 Atmospheric profile product. Effective air emissivity was estimated by Prata (1996) approach:

$$\varepsilon_a = 1 - (1 + \vartheta)\exp\left(\sqrt{1.2 + 3\vartheta}\right), \text{with } \vartheta = \left(\frac{46.5}{T_a}\right) e_0 \quad (3.8)$$

In the case of cloudy conditions, some pixels values of MOD07 were missing (between 40 – 85 % missing value during summer and winter season). Thus, MODIS's surface temperature from MOD06 cloud product was employed to fill in these missing values of dew point temperature and air temperature. According to Bisht and Bras (2010), the dew point temperature and air temperature were estimated by subtracting the offset of surface temperature obtained from MOD06. However, Bisht and Bras (2010) established a relationship between MOD06 (surface temperature) and MOD07 (dew temperature and air temperature for clear skies). In this study, the temperature offsets are the biases that are computed as the difference between the MOD06 surface temperatures and the in situ data from the Spectacle Reef meteorological station. The difference between surface water temperature and air temperature (dew point temperature also) was not constant year around. The offset was varied by season, particularly during winter, due to the different heat capacity of air and water. Thus, this study proposed calculating separate temperature offsets for winter and non-winter seasons.

Then, incoming long-wave radiation during all sky conditions was estimated as a combination of incoming longwave during clear sky condition and longwave emitted from clouds.

$$L\downarrow = \sigma\varepsilon_a T_a^4 + \sigma(1-\varepsilon_a)\varepsilon_c T_c^4 \quad (3.9)$$

where :

T_c is cloud temperature (K)

ε_c is cloud emissivity

Both cloud temperature and cloud emissivity were obtained from MOD06 cloud product.

3.4.2.4 Outgoing Longwave Radiation

Outgoing longwave radiation (W m^{-2}) was calculated using MODIS thermal surface temperature for all sky conditions as described in Chapter 2. The emitted longwave radiation was computed using the Stefan-Boltzman relationship which can be written as:

$$L\uparrow = \sigma\varepsilon_s T_s^4 \quad (3.10)$$

where :

T_s is water surface temperature (K)

ε_s is emissivity of water surface

3.4.3 Data Validation

Net radiation and its components were calculated using estimations of water surface and atmospheric parameters from remotely-sensed data. Therefore, the accuracy of these components must be validated with information acquired by the meteorological towers. Satellite data and field measurements gathered during the year of 2010 was used for validation. The ground-based technique that directly evaluates the satellite – derived surface net radiation variable with in-situ direct measurements at the satellite overpass. This method has been applied to validate

satellite data over different land cover and land use including large lakes, grasslands, and agricultural fields (Coll *et al*., 2005). The data of the meteorological station on the top of Spectacle Reef Lighthouse, which is positioned far from shoreline, is ideal data for validation of the satellite data, because the station is far from land and sited over a large homogenous water surface area. The in-situ measurements were plotted (scatter plot) against remotely sensed data in order to explore the relationship and to correct bias between in situ data and satellite variable of Lake Huron.

3.4.4 Spatial and Temporal Variations in Lake Net Radiation and Its Components

After validation of the signature of remote sensing data, maps of daily instantaneous net radiation and its components for Lake Huron were created over a period from 2002 to 2012 with 5×5 km grid resolution to examine the temporal and spatial distribution of net radiation in different seasons.

To calculate the change of net radiation and its four components, least squares linear regression was applied for each pixel with daily temporal resolution over 11 years. The slope of each regression line represents the change or trend in net radiation during the study period.

3.5 Results and Discussions

3.5.1 Comparison of daily satellite net radiation components to the ground-based observations

3.5.1.1 Comparison of daily satellite incoming shortwave radiation to the ground-based observations

The plot of MODIS incoming surface solar radiation versus direct measurements from pyranometer shows a good agreement. The R^2 was 0.77, in clear-sky conditions (Figure 3.2), and the R^2 under cloudy-sky conditions was 0.61. This difference might be due to the effect of the difference in spatial scale between direct measurements and satellites observations. The direct measurement recorded a single point from the meteorological station, whereas each pixel of satellite data record information at a 25 km^2 spatial coverage.

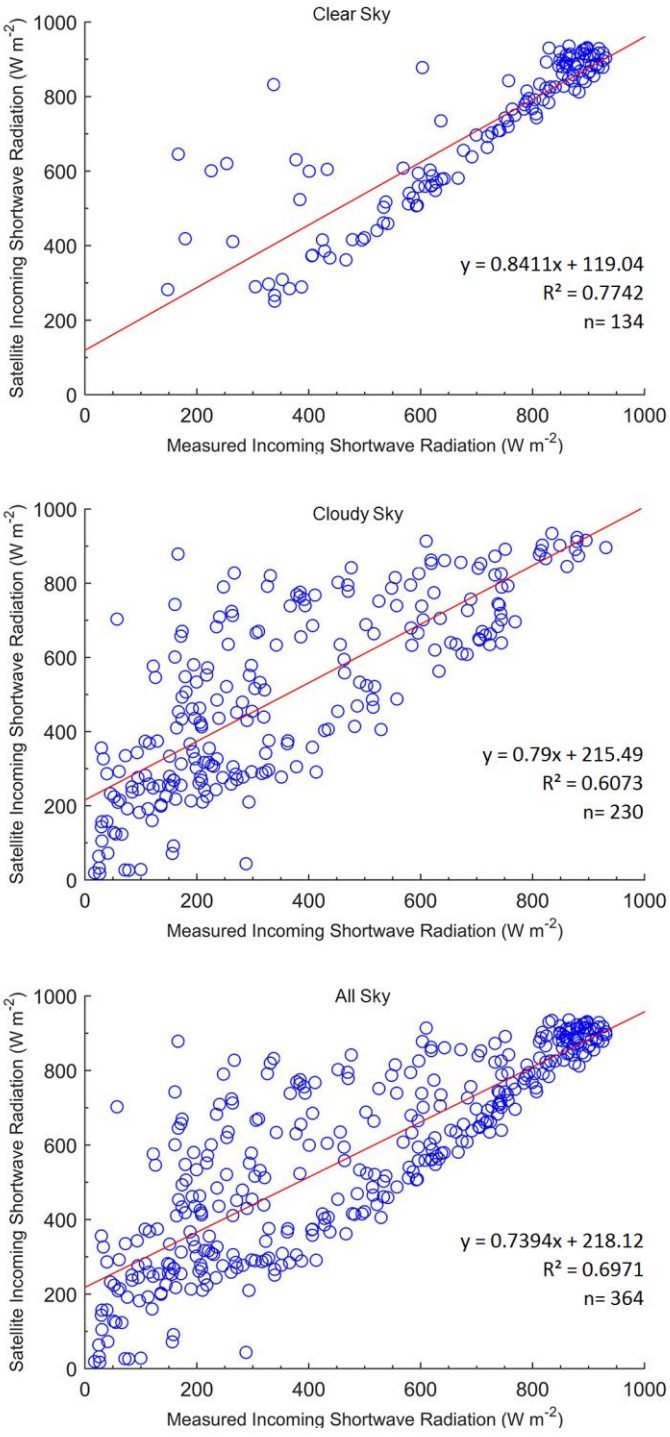

Figure 3.2 The comparison of satellite incoming shortwave radiation comparison to the data directly measurement under clear, cloudy, and all sky conditions (in Wm^{-2})

An important uncertainty associated with co-location of satellite and ground measurements are temporal and spatial sampling errors. Temporal sampling error arise from the fact that the surface measurement has 30 minute average incoming shortwave radiation calculated from measurements collected every 5 seconds, while satellite instantaneous capture signals with less than 1 second per pixel. Since, clouds change overtime, 30 minute different range of record time has a high potential to introduce different amount of incoming shortwave radiation. Spatial sampling error occurs because MODIS pixel aggregates the radiometric radiation signal from area of 5 x 5 km which is much greater than the pyranometer's field of view. A single small isolated cloud right over the meteorological station considerably reduces the shortwave incoming radiation reached at the pyranometer, whereas producing a small effect on the measurement from the satellite. In contrast, if there were overcast and cloud over almost of the satellite pixel except over the pyranometer, then the incoming shortwave radiation from surface measurement will higher than from the satellite observation. Moreover, if there are clouds nearby the station contributed diffuse radiation to the pyranometer surface, this would increase the difference in incoming radiation value measured from satellite and meteorological station (Figure 3.3).

Another uncertainty is the overestimation of incoming shortwave radiation under cloudy-sky conditions. Satellite cloud information seems to be brighter because satellite cloud transmits more shortwave to the lake surface than do the physical cloud. This is due to the under estimation of satellite cloud optical thickness (King *et. al*., 2013; Painemal and Zuidema, 2011) which is leading to the cloud observed from the satellite absorbing less shortwave radiation than the real clouds does. Satellite observed cloud properties are estimated under the assumption that observations for a given pixel have only one layer of cloud (Baum and Platnick, 2006).

Conversely, observations show that multi-layer of clouds are quite normal (e.g. Tian and Curry, 1989; Yi *et al*., 2008), particularly for the occurrence of semi-transparent thin cirrus cloud over lower-level clouds. In this circumstance, the assumption of an only one layer of cloud causes errors in the cloud information retrievals. The retrieved cloud optical thickness will have the smallest error if the highest cloud layer is opaque (Baum and Platnick, 2006).

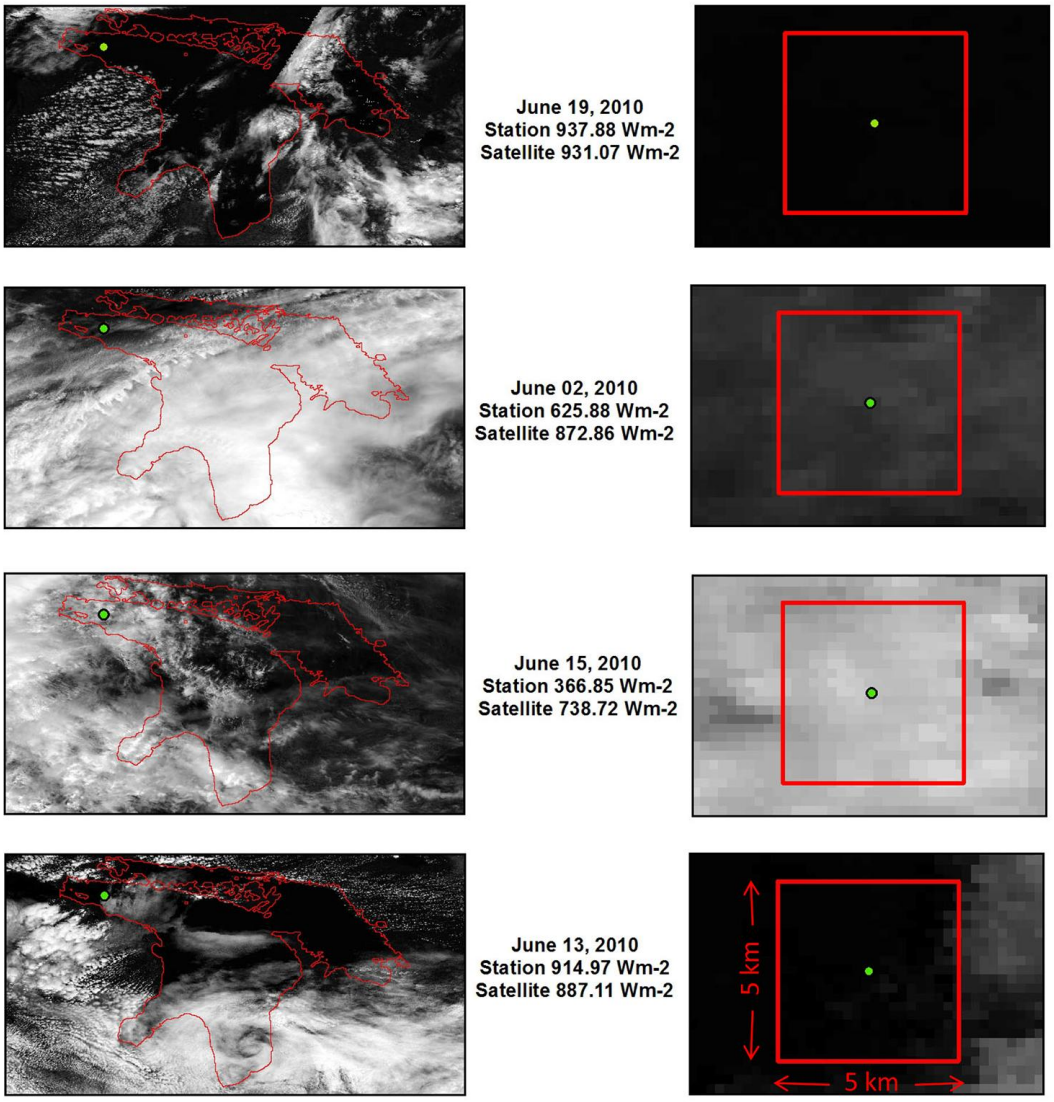

Figure 3.3 Satellite incoming shortwave radiation comparisons to the data directly measurement under difference cloudy sky conditions (in Wm^{-2})

3.5.1.2 Comparison of daily satellite outgoing shortwave radiation to the ground-based measurements.

Since the measurement of the reflected solar radiation was affect by the base of the lighthouse structure that could not be avoided, no validation was done for outgoing radiation. I understand that for satellite retrieved parameter that is lacking validation of data will introduce more uncertainty in study results, however, the reflected solar radiation was the smallest component of the net radiation (less than 5% of the net radiation).

3.5.1.3 Comparison of daily satellite incoming longwave to the ground-based measurements

Air and dew point temperatures are the important input parameters form satellite needed to compute downwelling longwave radiation. Figure 3.4 shows the comparison of satellite's air temperature and air temperature directly measured by meteorological station.

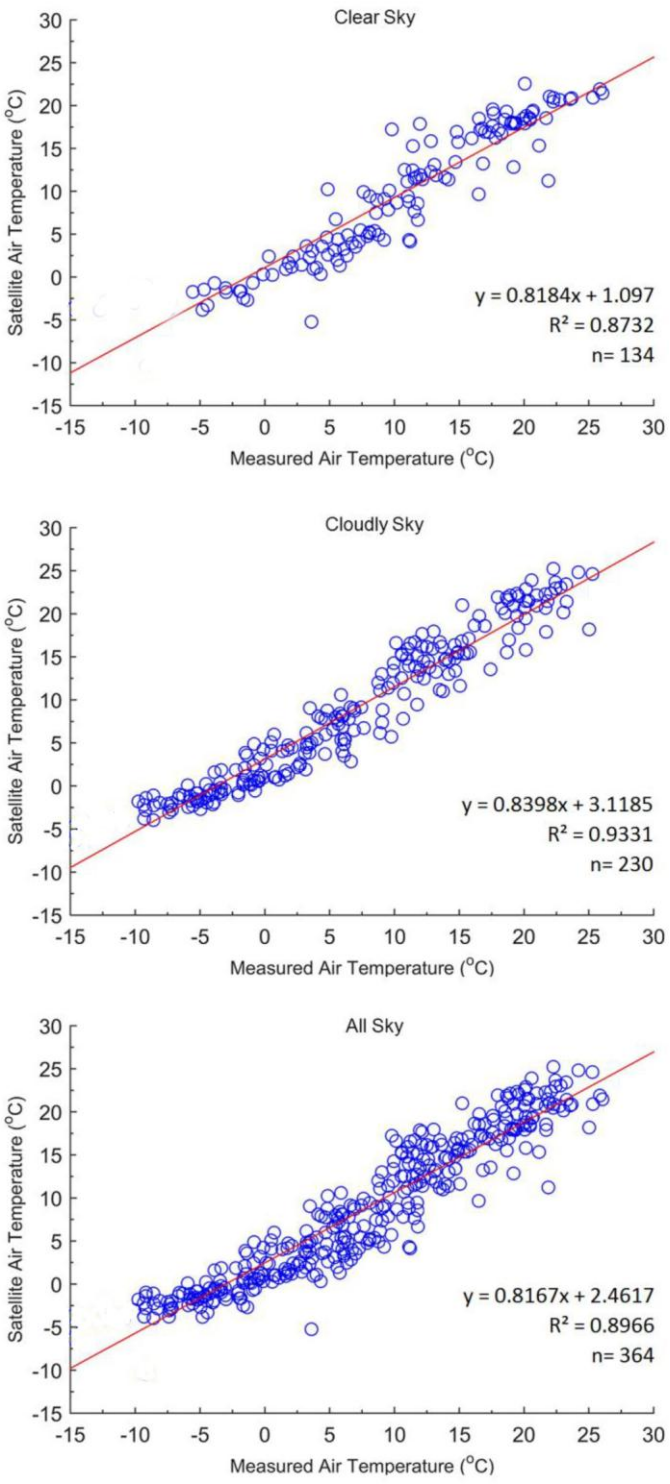

Figure 3.4 Scatter plot of satellite's air temperature versus the directly measured data (30 min average) under clear, cloudy, and all sky conditions for the year 2010

The comparison shows the strong relationship between air temperatures derived from direct measurement and satellite observed data with correlation coefficient (R^2) of 0.87, 0.93, and 0.90 for clear, cloudy, and all sky condition consecutively. The lower R^2 of air temperature on the clear sky condition can be caused by the outliers that occur in cloud contaminated pixel which typically have lower temperature (Rizzoli *et al*., 2007) and a large amount of the pixels with higher errors are located near cloud boundary (Czajkowski *et al*., 2000).

Air temperature derived from satellite tends to be higher than the temperature from direct measurement and the difference increases with decreasing temperature below -5 °C and the cause may due to the limitation in the processing of MOD07 product that comes from the signal error in the very dry air conditions common at these low temperatures.

This study applied dew point temperature to estimate vapor pressure (e_o) using the Clausius-Clapeyron method. Satellite estimated vapor pressure was then compared to the direct measurements of vapor pressure over the lake surface as shown in Figure 3.5. The vapor pressure scatter plots of satellite estimated versus directly measured illustrate a good agreement between these two data sources with R^2 0.87, 0.90, and 0.88 for clear, cloudy, and all sky condition respectively. The difference between the two measurements increases with the increase in vapor pressure. This may be due to introduced by different sources including the model and data.

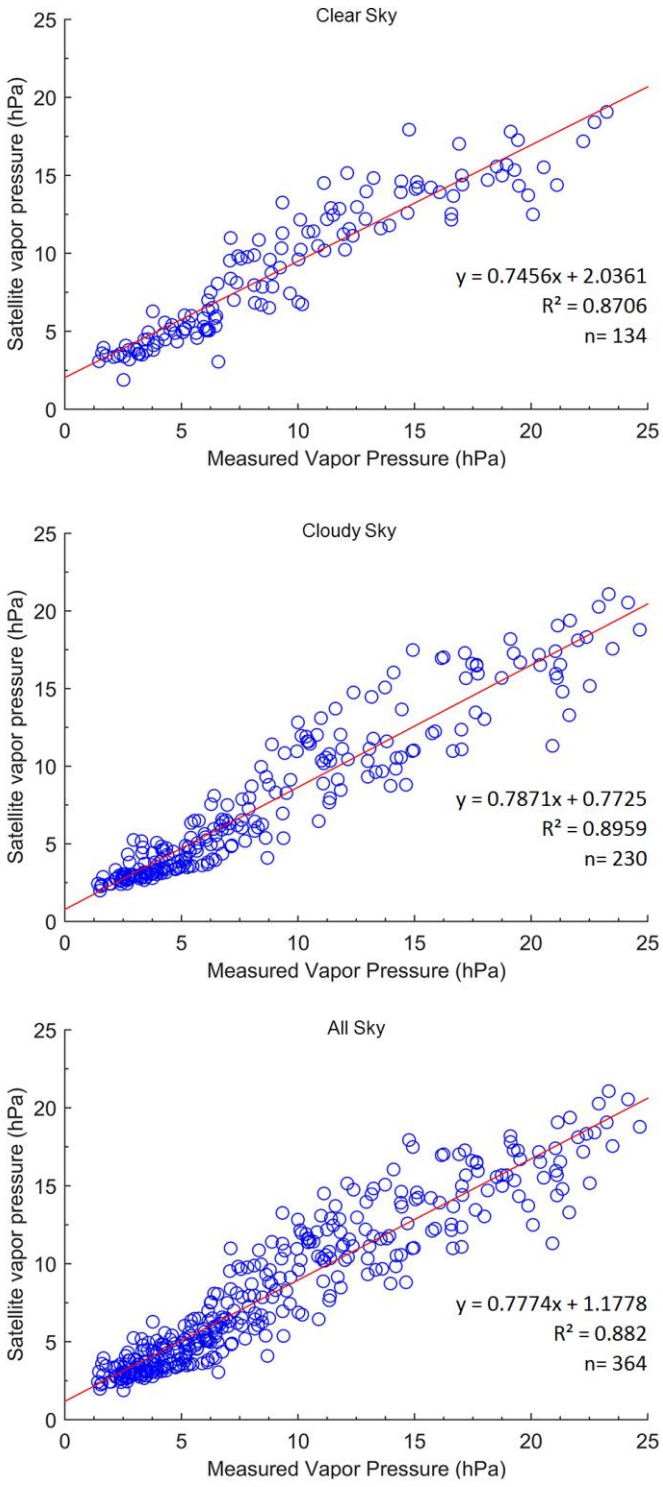

Figure 3.5 Scatter plot of satellite's vapor pressure versus the directly measured data (30 min average) under clear, cloudy, and all sky conditions for the year 2010.

Figure 3.6 shows the scatter plot of incoming longwave radiation calculated from satellite compared to the data retrieved from ground station. The correlation coefficient between these two data sources are 0.72, 0.60, and 0.64 for clear, cloudy, and all sky condition, respectively. These low coefficient value is mainly due to the effect of the difference in spatial scale observed and cloud cover impacts as discussed earlier in the section 3.5.1. Moreover, these low correlations may be caused by the error of retrieving cloud temperature. Since the satellite can only detect the temperature at the top of cloud, this may not represent the actual physical cloud base temperature.

3.5.1.4. Comparison of daily satellite outgoing longwave to the ground-based measurements

Direct measurements of outgoing longwave radiation were not available because of signal contamination from the lighthouse base, thus measurements of surface water temperature by infrared thermometer were converted to acquire observations of upwelling longwave using the Stefan-Boltzman relationship assuming constant surface water emissivity of 0.97. The scatter plot between outgoing longwave radiation calculated from satellite and from infrared thermometer is shown in Fig 3.7

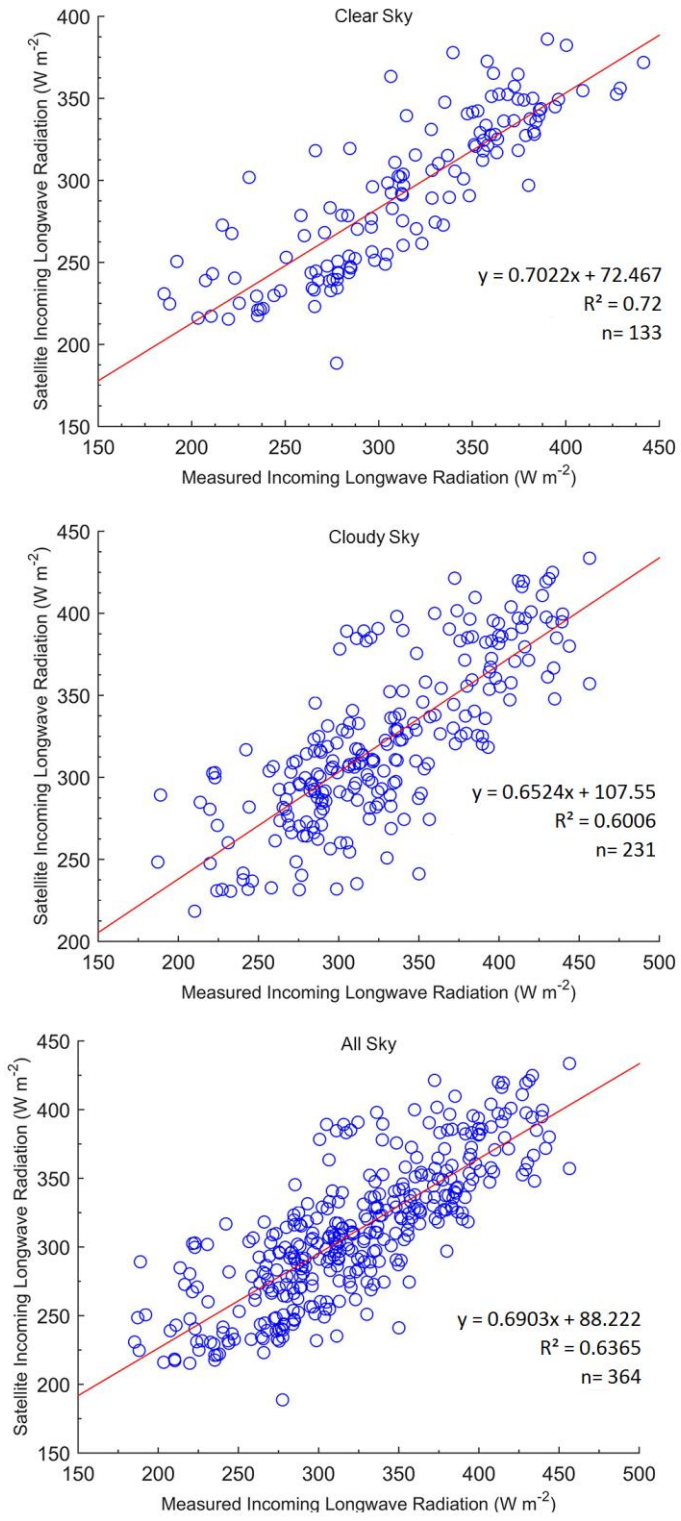

Figure 3.6 Scatter plot of satellite incoming longwave radiation versus the directly measured data (30 min average) under clear, cloudy, and all sky conditions for the year 2010

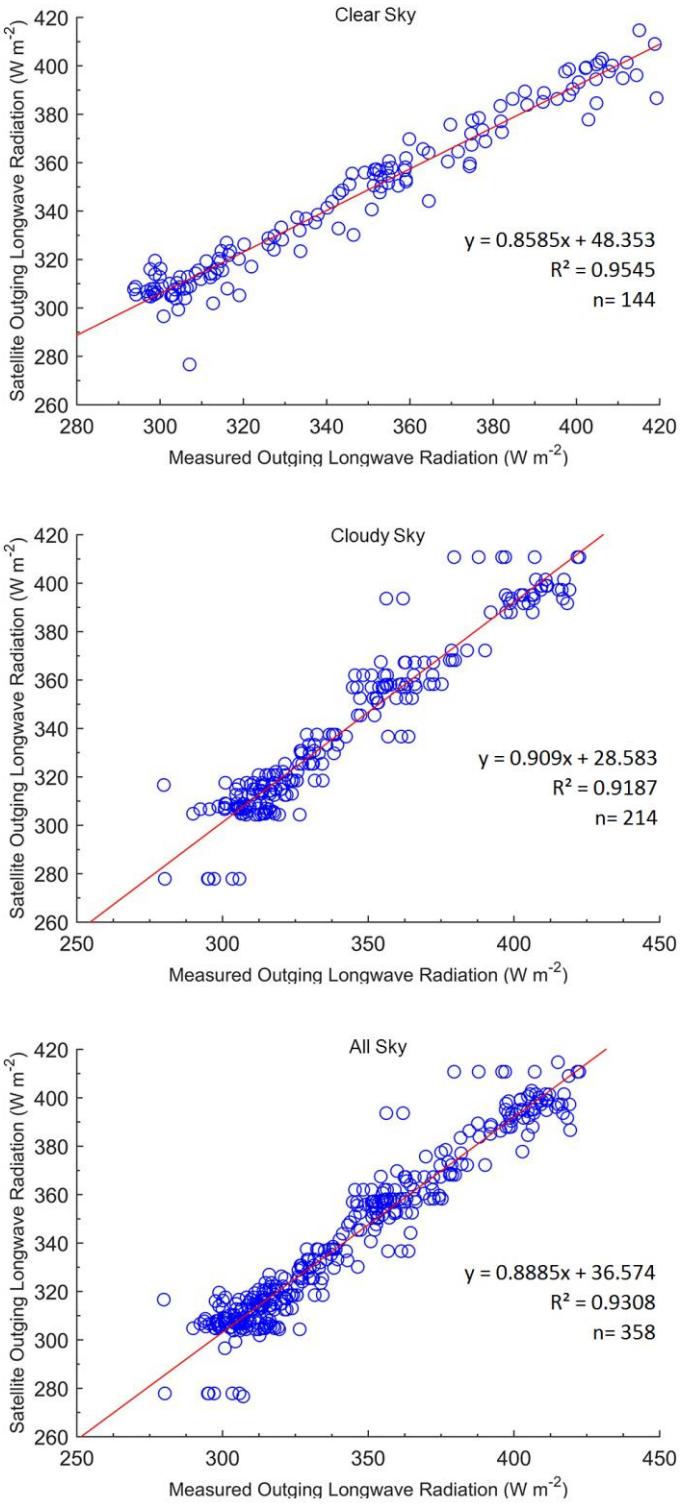

Figure 3.7 Scatter plot of Satellite outgoing longwave radiation versus the directly measured data (30 min average) under clear, cloudy, and all sky conditions for the year 2010

3.5.2 Spatial distribution of net radiation components

Spatial distributions of the average monthly and seasonal surface net radiation conditions and its components, including incoming shortwave, outgoing shortwave, incoming longwave, and outgoing longwave radiation of Lake Huron obtained from remote sensing satellite data between 2002 and 2012, were produced. Color (and gray scale) scheme illustrated monthly mean instantaneous radiation values, dark (cold tone color) areas represent lower values of radiation, while bright (warm tone color) areas mean higher intensities of the radiation. The following are the details of spatial distribution of net radiation and each component.

3.5.2.1 Incoming shortwave radiation

The annual distribution of incident radiation has an approximately regular latitudinal pattern (Figure 3.8 and 3.9) which is control by the solar zenith angle. At lower solar elevation angles in the wintertime, the solar beam travels a longer path toward the lake surface, and therefore the smallest value of incoming solar radiation was detected. The lowest monthly mean value (200.96 W m^{-2}) of incoming solar radiation flux density over the lake occurred in the month of December, and the lowest values of 173.48 W m^{-2} in the highest latitude locations of the lake, where the relative solar zenith angle were the smallest. Another factor that decreases the amount of incident surface solar radiation during the wintertime is the constant presence of clouds, which significantly attenuate the incoming shortwave by the processes of scattering and absorption.

During the summer, the sun is positioned highest in the sky and lowest percentage of cloud cover occurs. This result in smaller amount of solar radiation scattered and absorbed (average 36 % scattered and absorbed) during this time. The month of June has the highest mean

intensity of incoming shortwave radiation (864.97 W m^{-2}), particularly in the southern part of the lake where it received shortwave energy up to 885.70 W m^{-2}. After the summer solstice (June 21), the incident solar radiation decreases with the increase in solar zenith angle. The shortwave energy continues to decline until it reached the lowest intensity in December at the winter solstice and increased again in the spring season.

3.5.2.2 Outgoing shortwave radiation

Figure 3.10 and 3.11 show spatial distribution of outgoing shortwave radiation. Reflected (outgoing) short-wave radiation over the lake surface was the smallest with approximately less than 40 W m^{-2} relative to the other three terms of radiation budget components due to the very low albedo of water surface. The monthly mean of radiation fluxes ranking between winter and summer from 22.19 to 32.81 W m^{-2}.

Outgoing shortwave radiation is controlled by the independent variables incoming shortwave radiation and surface albedo which is particularly regulated by the angle at which the solar radiation arrives at the water surface (Oke, 1996), and also amount of cloud covers (under cloudy sky condition). The minimum values of reflected radiation were recorded in winter, presumably in low incident solar radiation and more cloud cover; and maximum values were recorded during the high incident solar radiation and cloudless in summer.

3.5.2.3 Incoming longwave radiation

Incoming longwave radiation to the lake surface is primarily controlled by the property of clouds, air temperature, and the amount of vapor pressure. As shown in Figure 3.12 and 3.13, spatial distribution patterns of wintertime show that incoming longwave energy was lower near the shoreline than in the mid-lake region. This is likely due to higher cloud concentration at the

mid-lake than the cloud concentration at near land surface (Figure 3.14), resulting in large variations in the down welling longwave radiation (sigma of about 9.5) during this season. Winter months appear to have slightly greater incoming longwave energy than early spring (March and April). This is possibly due to the influencing of longwave radiation emitted from clouds which is in surplus during the winter time. The lowest mean incoming long wave occurred in March (264.16 W m^{-2}).

Near the shore line, higher quantities of incoming longwave radiation were received, whereas lower fluxes is near the middle of the lake during late spring and early summer. Then the patterns were reversed from late summer and continue through fall. Areas offshore received more longwave radiation than that near lake boundary. The most apparent cause for the higher incoming longwave radiative fluxes at the middle of the lake during the late summertime is that the middle lake observed percent of cloud cover was higher than at near shoreline (Figure 3.14). The month of August had the highest mean incoming longwave energy of 365.70 W m^{-2}. After August, the incoming longwave radiation begins to weak and it reached the minimum values in winter and early spring.

3.5.2.4 Outgoing Long-wave Radiation

Longwave emission from the lake is controlled by lake surface water temperature (Chapter 2) an surface emissivity, thus the spatial and temporal distribution of outgoing radiation have similar patterns of that of the skin temperature (Stefan-Boltzmann Law) which had a higher magnitude in summer and lower magnitude in winter (Figure 3.15 and 3.16). In the winter, outgoing radiation was lower near shoreline than in mid-lake region. The month of February had the lowest mean emitted energy of 295.59 w m^{-2}.

In the spring, the month of May had the highest spatial variability implying that some areas were started to warm early and reached thermal stratification which lead to rapid warming. The lake surface reached the highest radiation emittance during the summertime, particularly in the southern part of the lake. The month of August has the highest mean surface thermal emittance of 397.12W m^{-2}, then declined through late fall and winter.

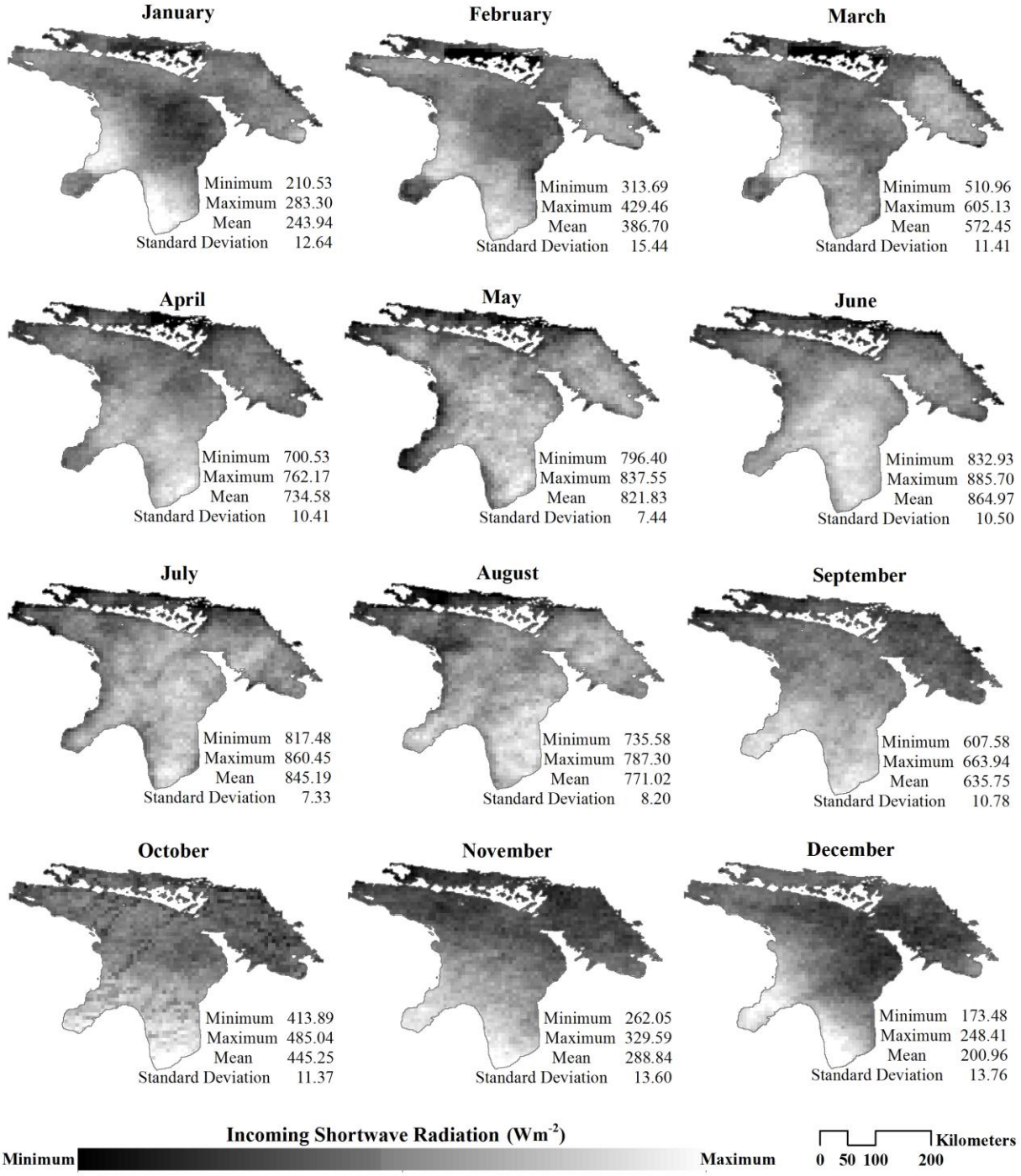

Figure 3.8 Spatial distribution of monthly average of incoming shortwave radiation (in W m^{-2}) from 2002 – 2012. The gray scale displays the incoming shortwave radiation variability of each month

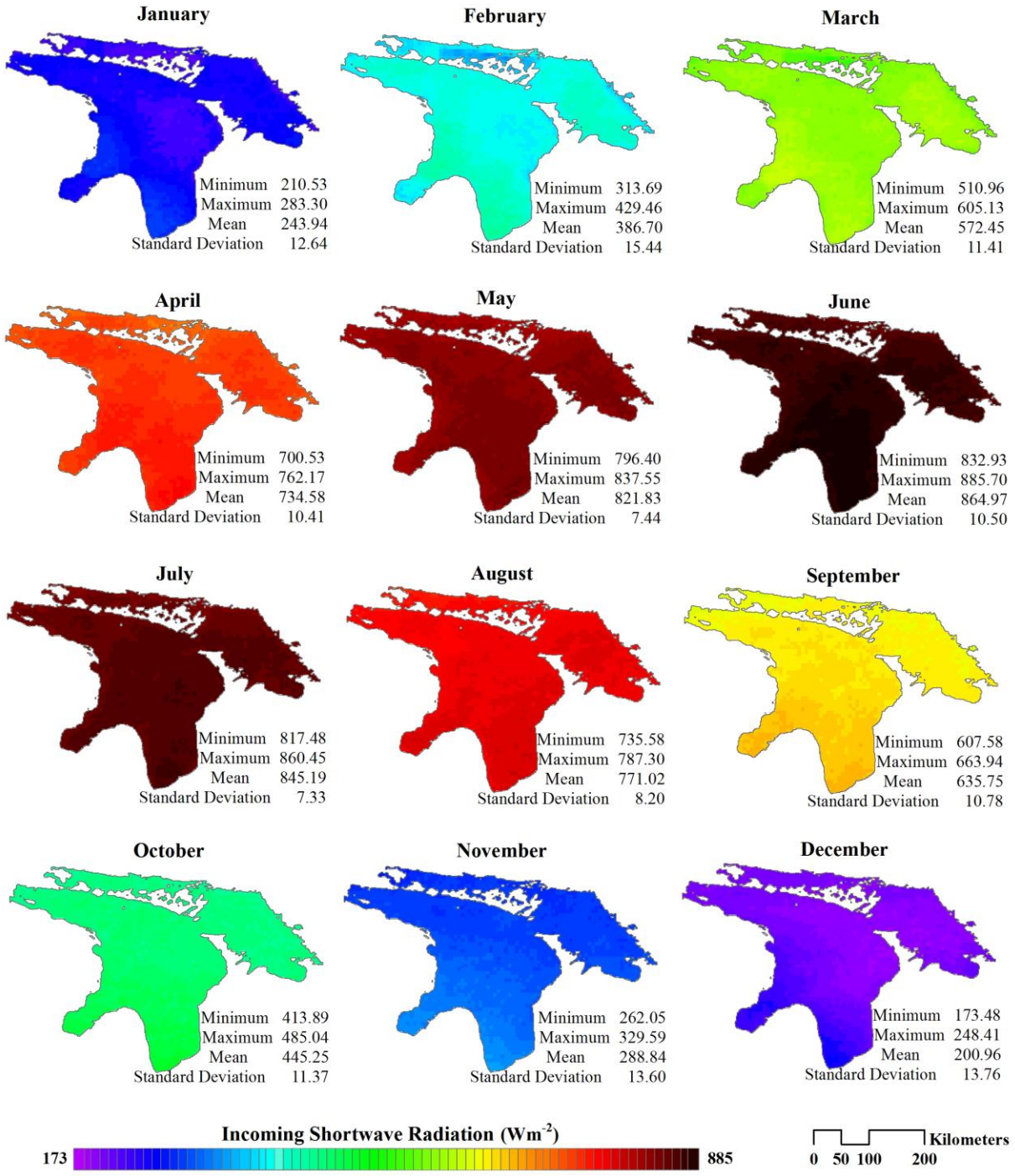

Figure 3.9 Spatial distribution of monthly average of incoming shortwave radiation (in W m^{-2}) from 2002 – 2012.The colors scheme displays the annual incoming shortwave radiation variability

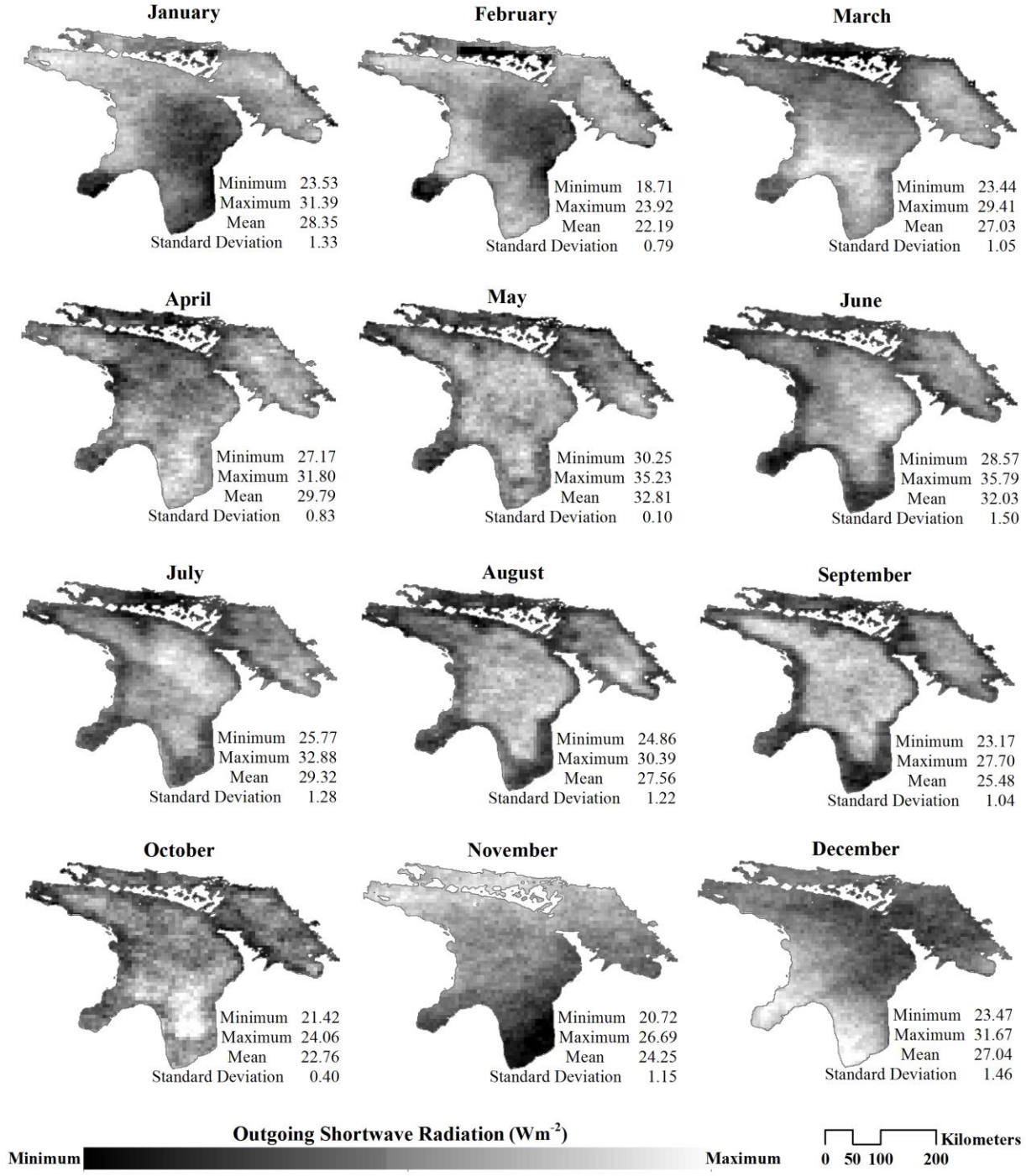

Figure 3.10 Spatial distribution of monthly average of outgoing shortwave radiation (in W m^{-2}) from 2002 – 2012. The gray scale displays the outgoing shortwave radiation variability of each month

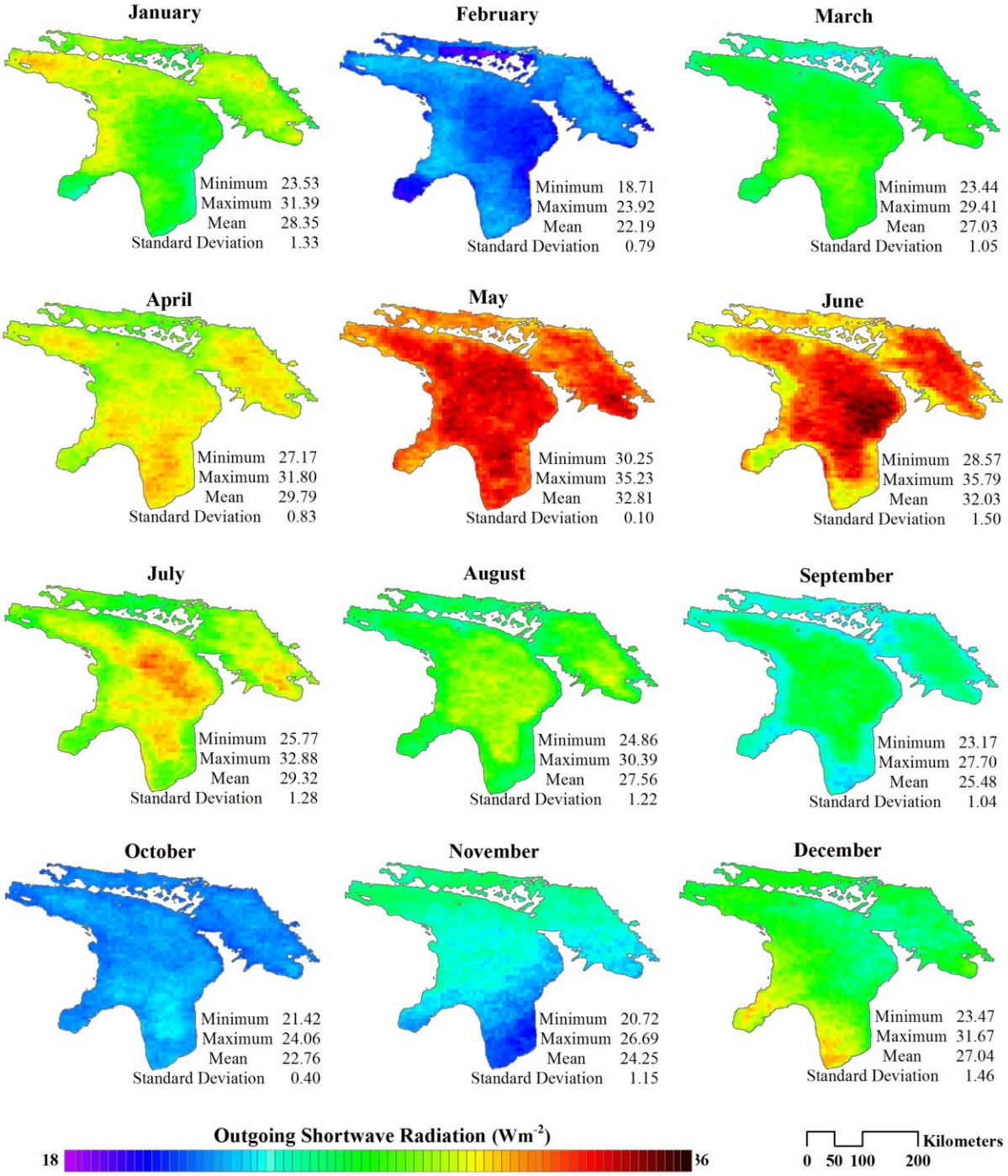

Figure 3.11 Spatial distribution of monthly average of outgoing shortwave radiation (in W m^{-2}) from 2002 – 2012. The colors scheme displays the annual outgoing shortwave radiation variability

.

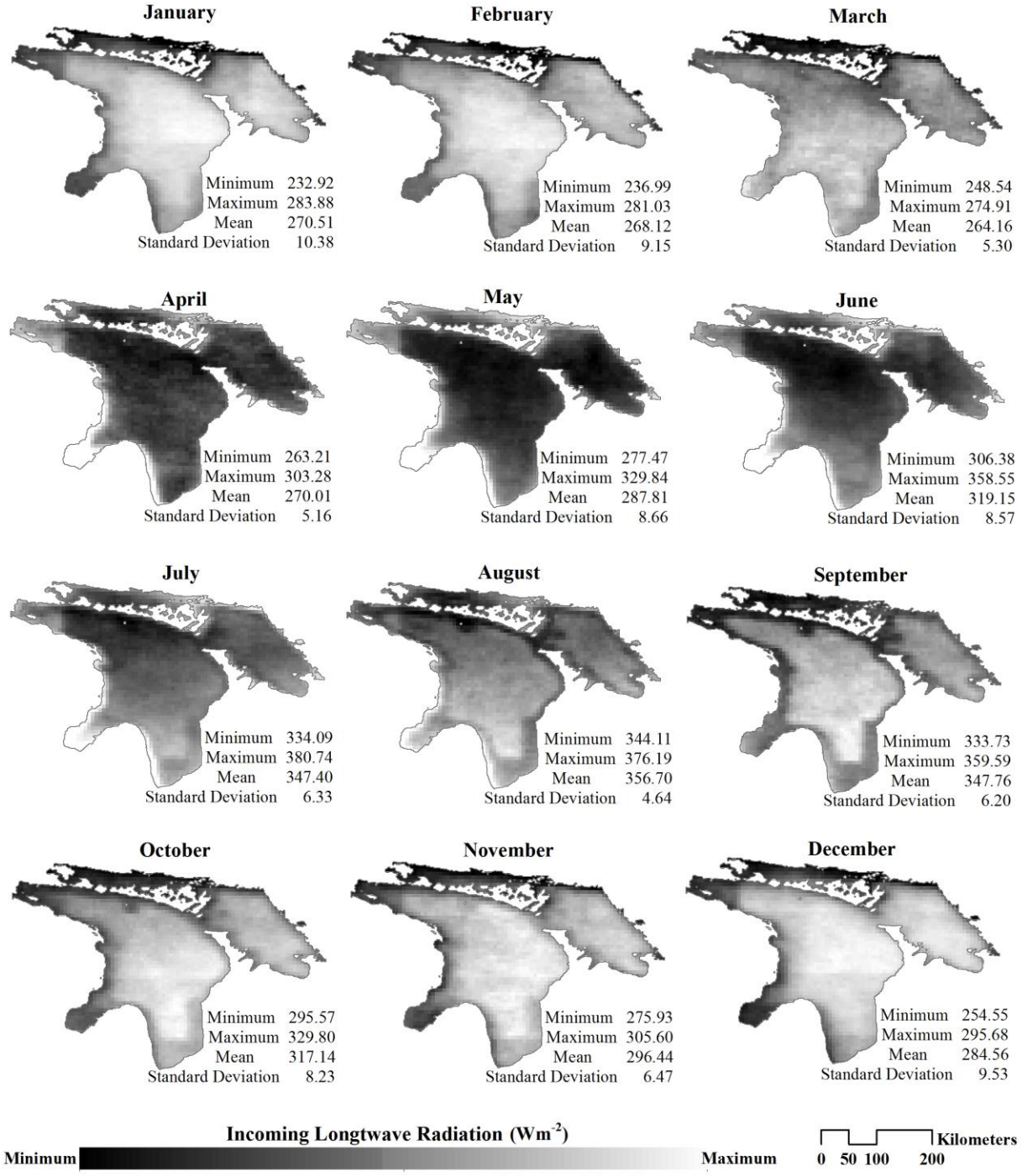

Figure 3.12 Spatial distribution of monthly average of incoming longwave radiation (in W m^{-2}) from 2002 – 2012.The gray scale displays the incoming longwave variability of each month.

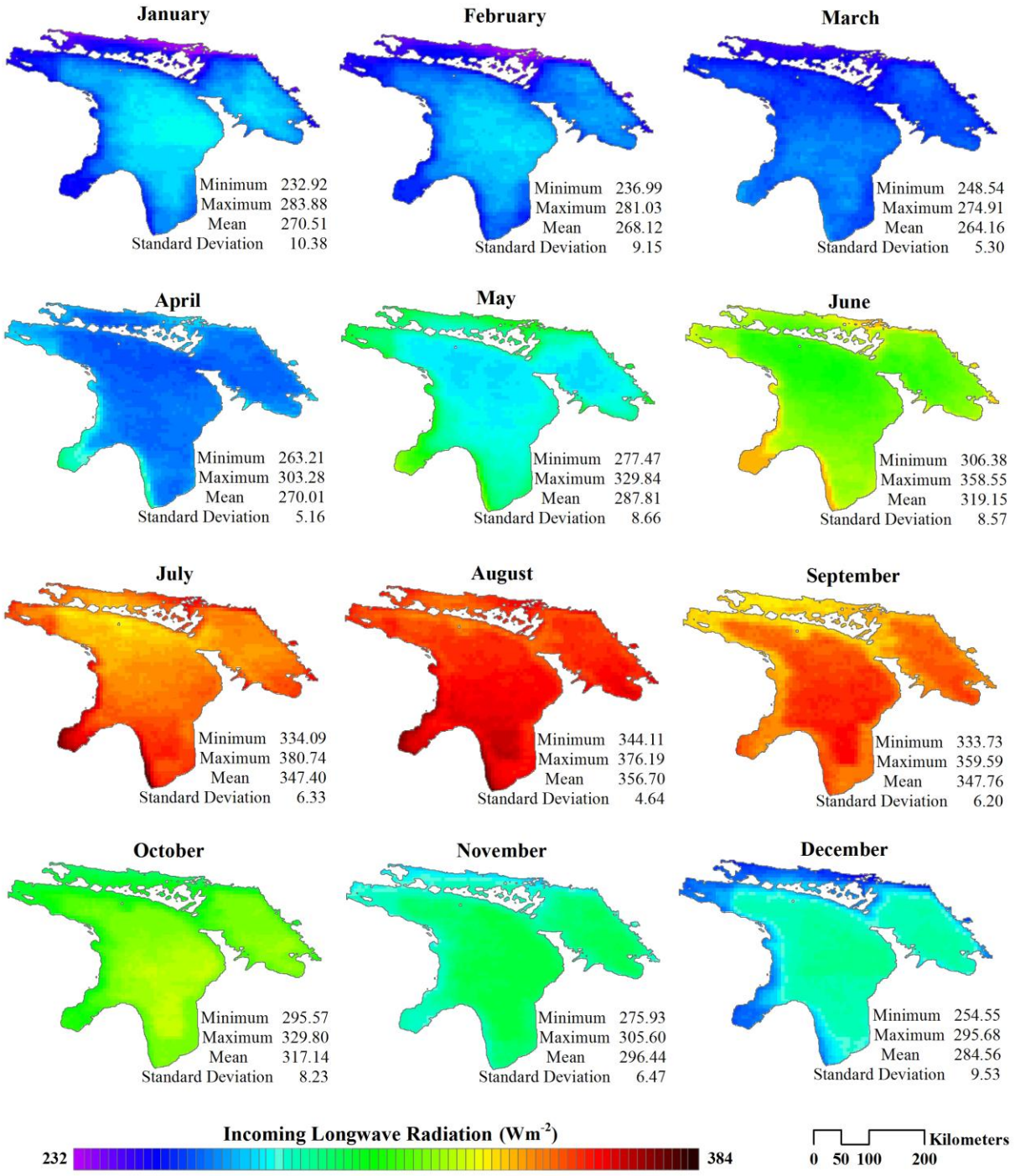

Figure 3.13 Spatial distribution of monthly average of incoming longwave radiation (in W m^{-2}) from 2002 – 2012. The colors scheme displays the annual incoming longwave radiation variability

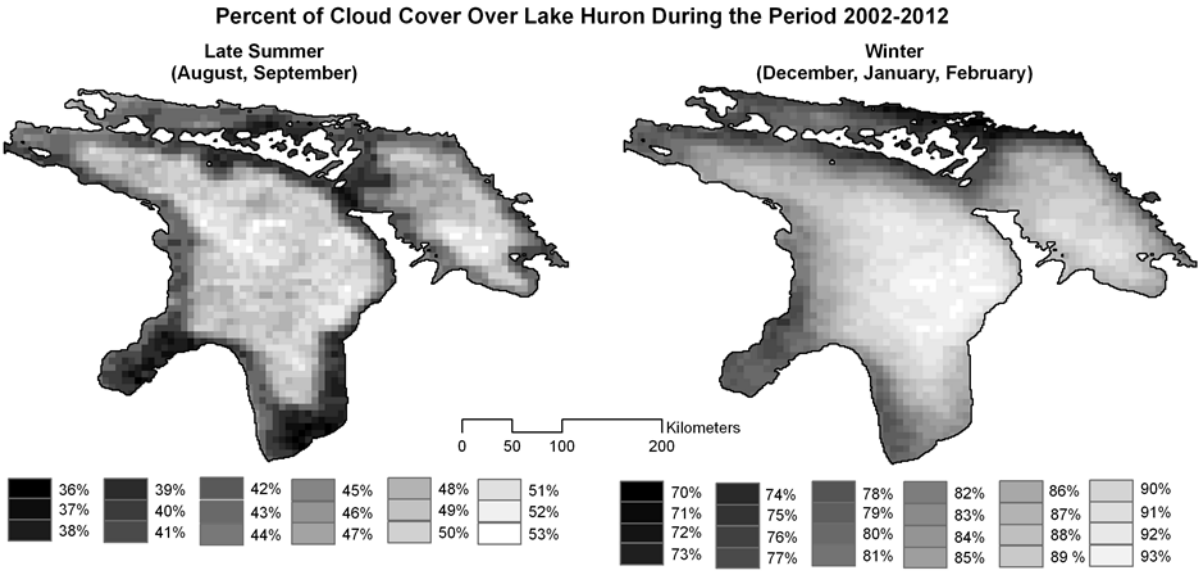

Figure 3.14 Percent of cloud cover over Lake Huron in winter and late summer seasons from 2002 -2012 (the data was calculated from MODIS cloud product)

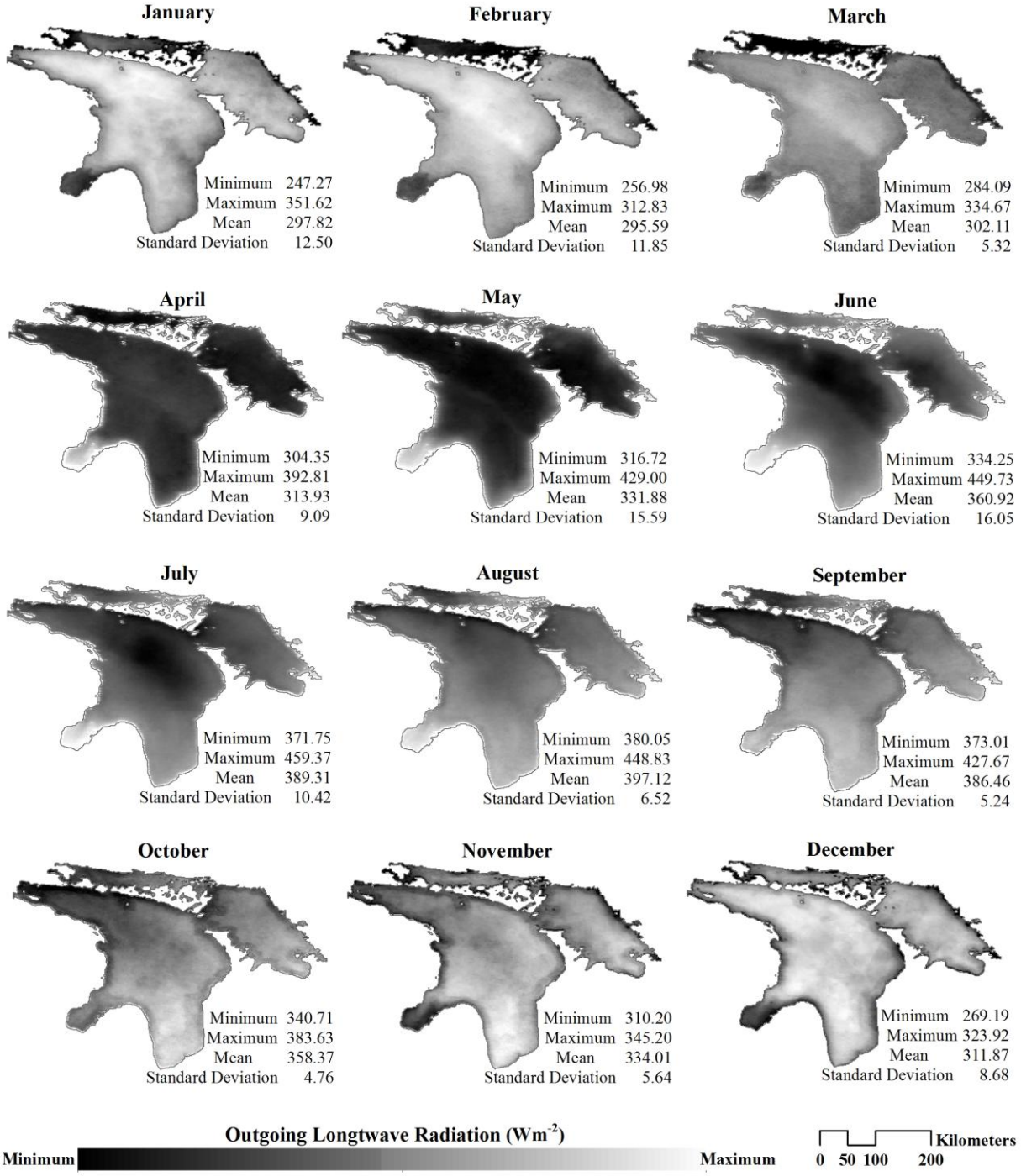

Figure 3.15 Spatial distribution of monthly average of outgoing longwave radiation (in W m^{-2}) from 2002 – 2012.The gray scale displays the outgoing longwave radiation variability of each month

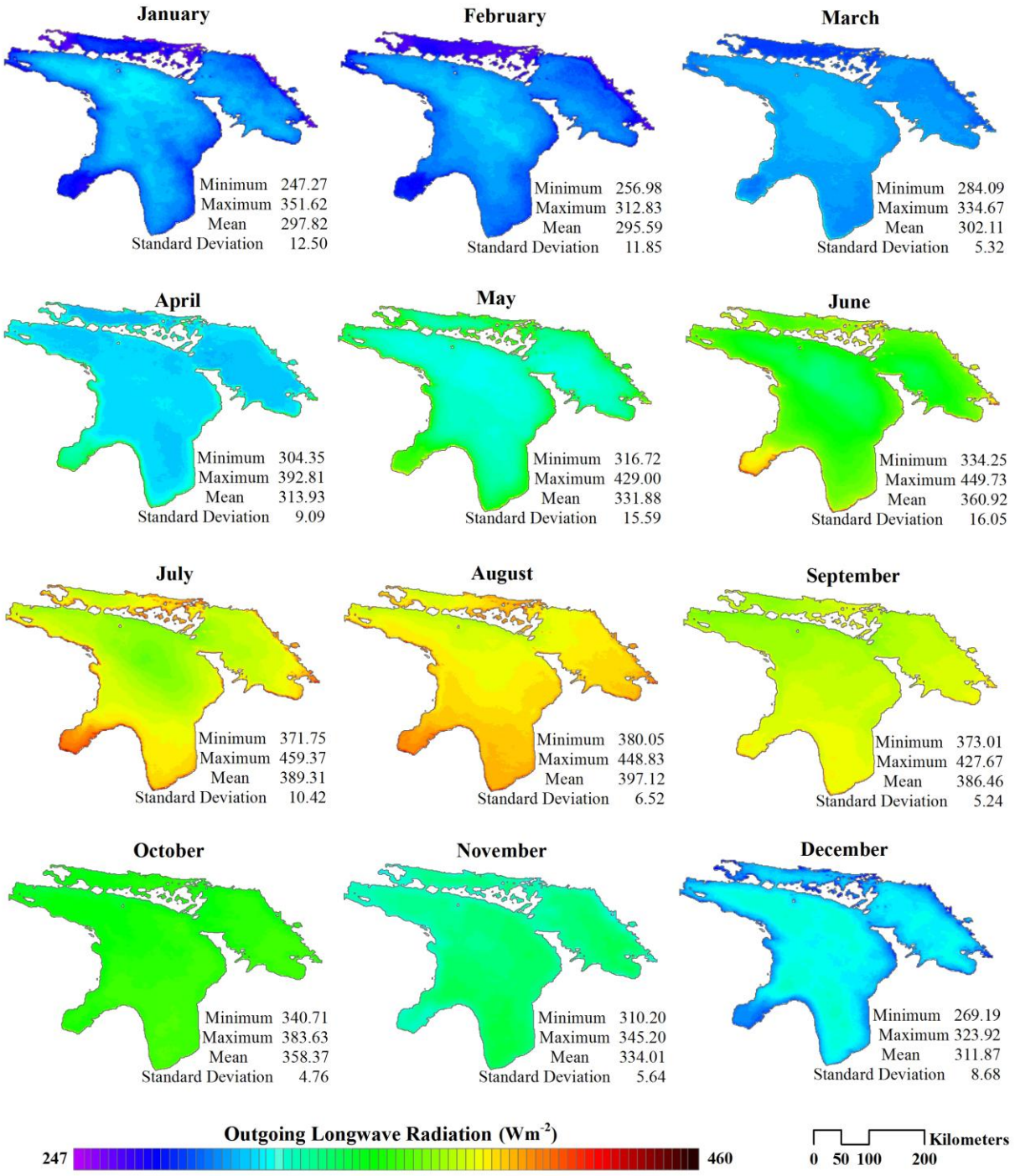

Figure 3.16 Spatial distribution of monthly average of outgoing longwave radiation (in W m^{-2}) from 2002 – 2012.The colors scheme displays the annual outgoing longwave radiation variability.

3.5.2.5 Net radiation

Figure 3.17 and 3.18 shows the annual variation and ratio of net radiation and each of its components during the period of 2002-2012. The instantaneous net radiation was dominated by incident shortwave radiation, indicated that daytime radiation budget was remarkable for its high energy absorption value of the lake. The ratio of net radiation and incoming shortwave radiation is nearly constant all year around, but the pattern is slightly greater during the wintertime. Outgoing shortwave flux has relatively small value due to the very low reflection coefficient of water.

For longwave radiation, the difference between upward and downward longwave radiation was also almost constant with positive values between 30 Wm^{-2} (winter) to 50 Wm^{-2} (summer) which was an indication that the water surface lost longwave radiation than it gained all year around. Longwave radiation (incoming and outgoing) also had less seasonal variation and much lower density than the incoming shortwave radiation, particularly in the summertime which present the lowest ratio of net radiation and longwave radiation. In winter, due to the high thermal inertia of lake water and high cloud cover, both downward and upward longwave radiation was greater than incident shortwave which had the lowest intensity due to the low solar angles and the frequent occurrence of clouds. These results the ratio of net radiation and longwave radiation are greater during the wintertime

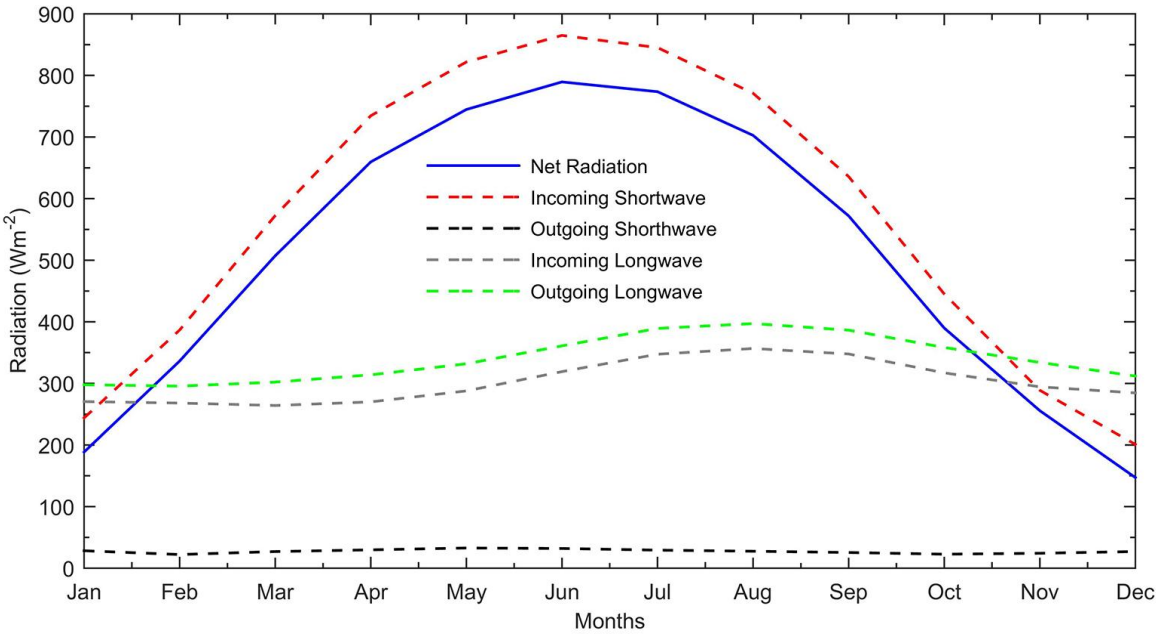

Figure 3.17 Annual change of net radiation and its components including incoming shortwave, outgoing shortwave, incoming longwave, and outgoing longwave over Lake Huron (in W m^{-2})

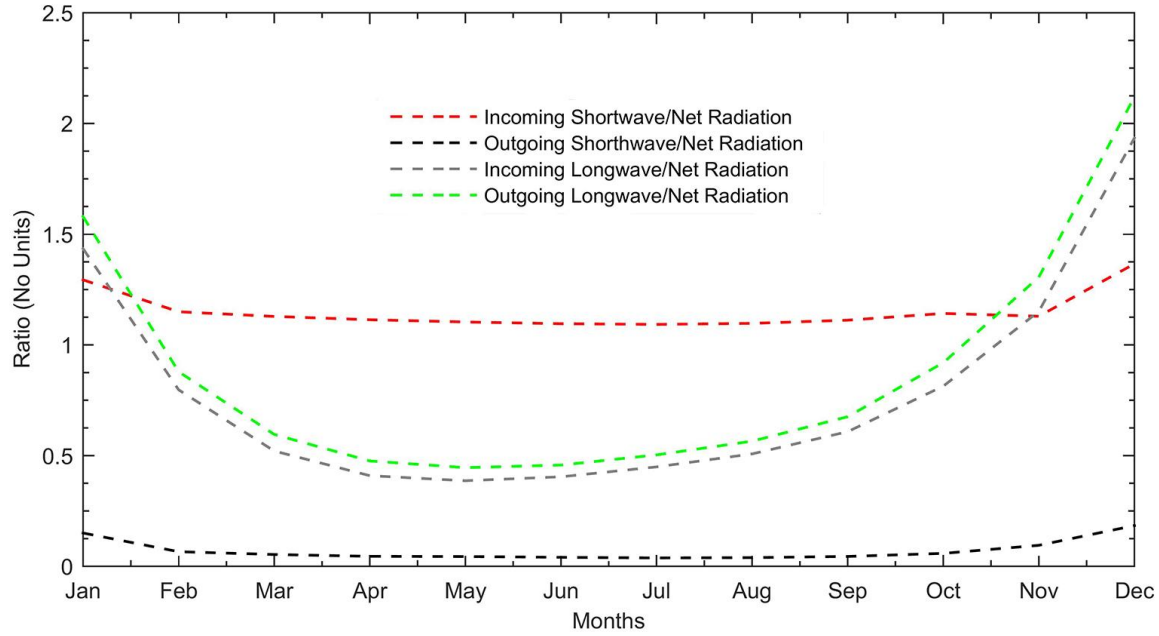

Figure 3.18 Ratio of the net radiation and each of its components during the period of 2001-2012

Figure 3.19 and 3.20 show the spatial distribution of yearly daytime instantaneous surface net radiation over Lake Huron. In January – April and October – December, the distribution of net radiation has an approximately regular latitudinal pattern which is controlled by solar zenith angle. In March, with the increase in solar elevation, the net radiation increased rapidly which is almost two times greater than the value of February. In April, the net radiation continued to increase but the variation with latitude was not obvious.

From May to September, the spatial distribution of net radiation over the lake did not show the variation with latitudinal. The variability of net radiation was related to lake's bathymetry and the presence or absence of cloud covers. June was the month of highest net radiation. After this month, the net radiation starts to decrease due to decreasing of solar elevation and still had high water surface temperature which meant greater emission on long-wave radiation. The latitudinal pattern of net radiation spatial distribution started to reconstruct in September and again reached regular latitudinal pattern.

Clouds influence the accuracy of the derived surface net radiation (Liang *et al*., 2012) and represent the main cause of uncertainty in climate change estimates (Solomon *et al.*, 2007). The intensity of surface shortwave radiation, longwave radiation, and resulting net radiation have been long recognized that are strongly affected by clouds. Low, thick clouds primarily reflect solar radiation which attenuates the incoming shortwave radiation. High, thin clouds mainly allow incoming solar radiation to reach the lake surface; and at the same time, they trap some of the outgoing thermal radiation emitted by the lake and radiate it back downward to the lake surface. Figure 3.21 shows yearly variation of cloudiness over the lake which has the greatest values during the period November – February (more than 75%) and lowest from July- August with cloud cover about 40%. At the transition from the summer regime to the winter regime,

especially from September-October, the cloud cover increase was dramatic primarily due to the large evaporation (latent heat flux) and sensible heat fluxes that occur in the winter from large lakes when they remain ice free (Blanken *et al*., 2000)

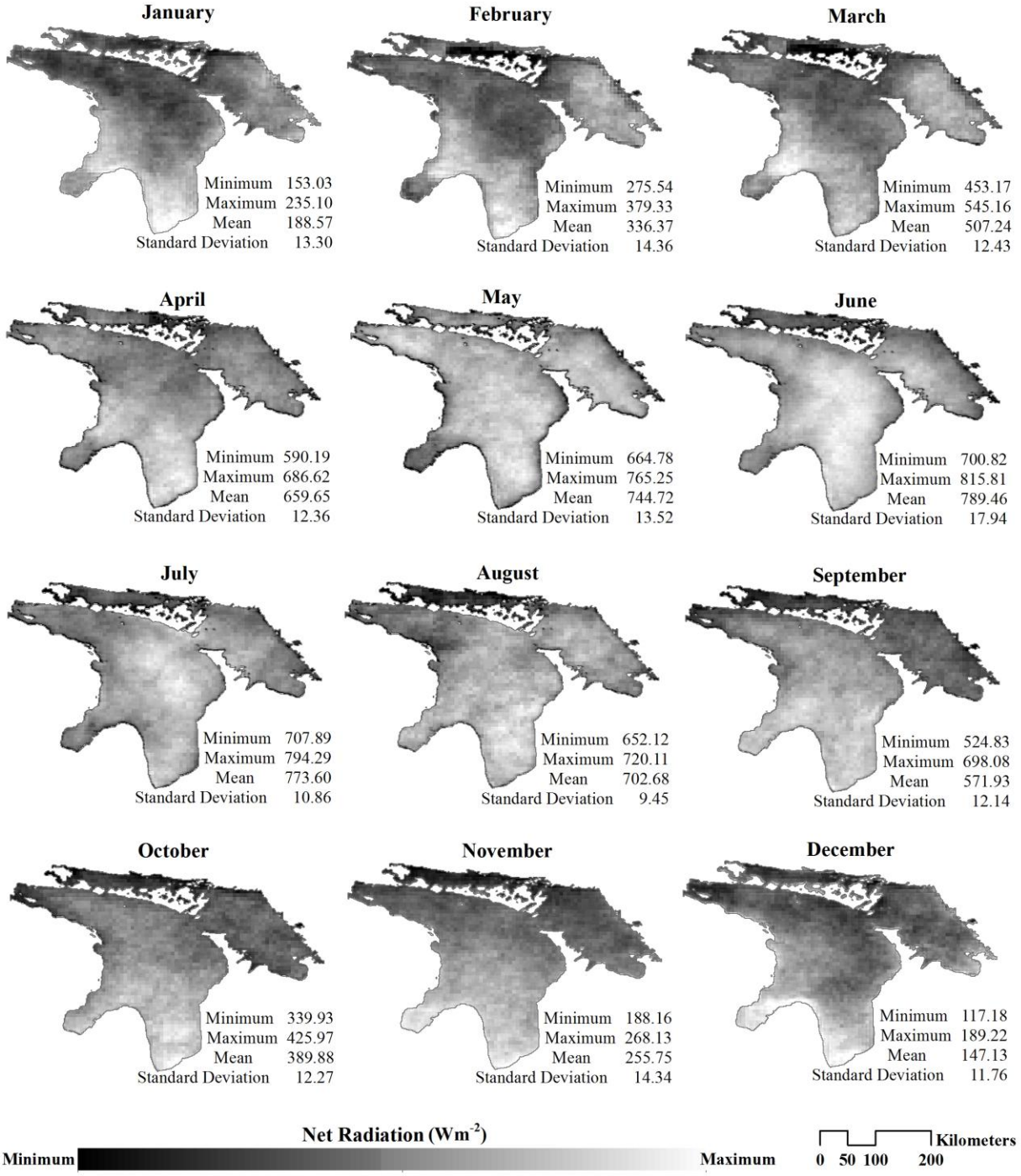

Figure 3.19 Spatial distribution of monthly average of net radiation (in W m^{-2}) from 2002 – 2012.The gray scale displays the net radiation variability of each month

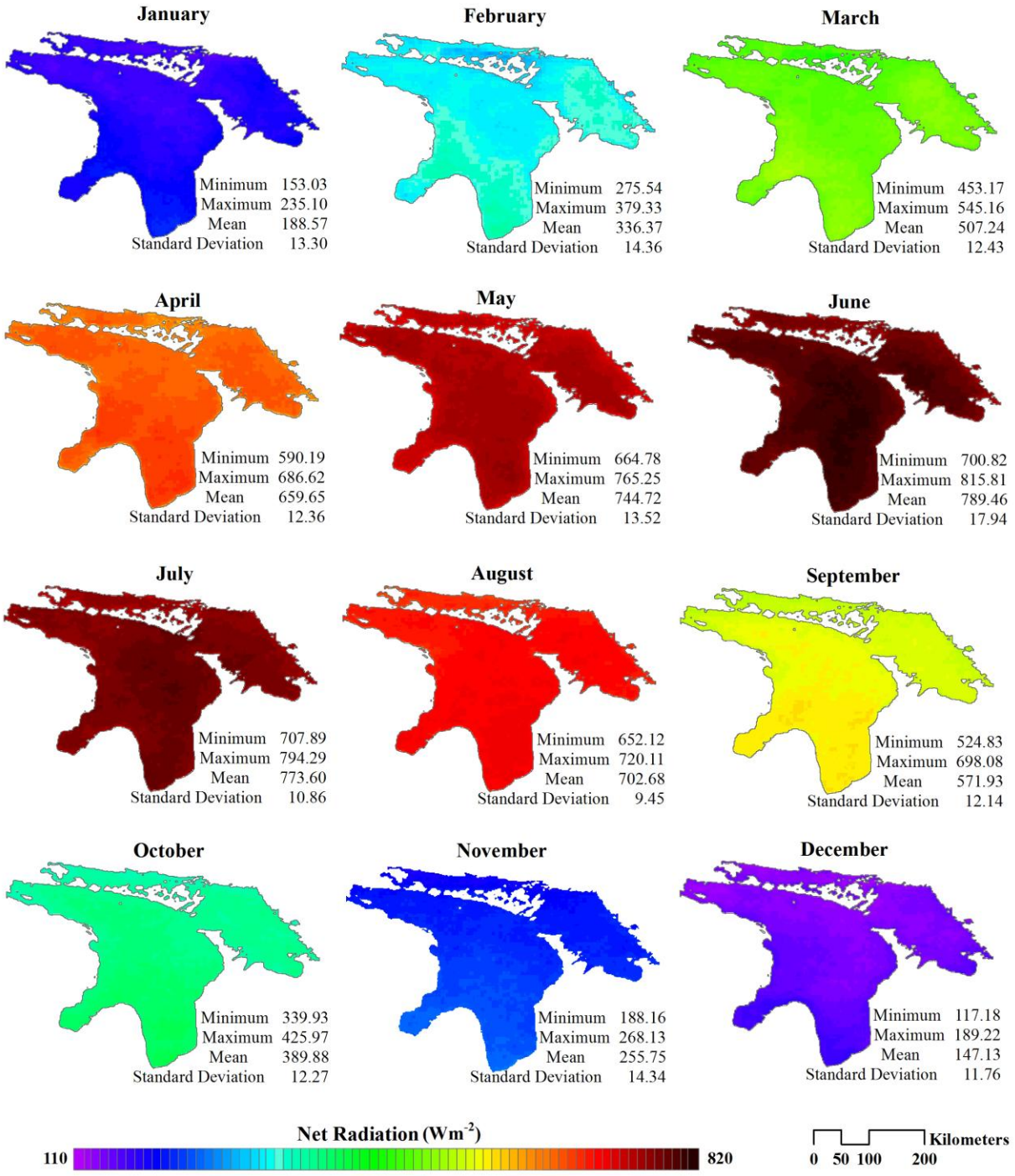

Figure 3.20 Spatial distribution of monthly average of net radiation (in W m^{-2}) from 2002 – 2012.The colors scheme displays the annual net radiation variability

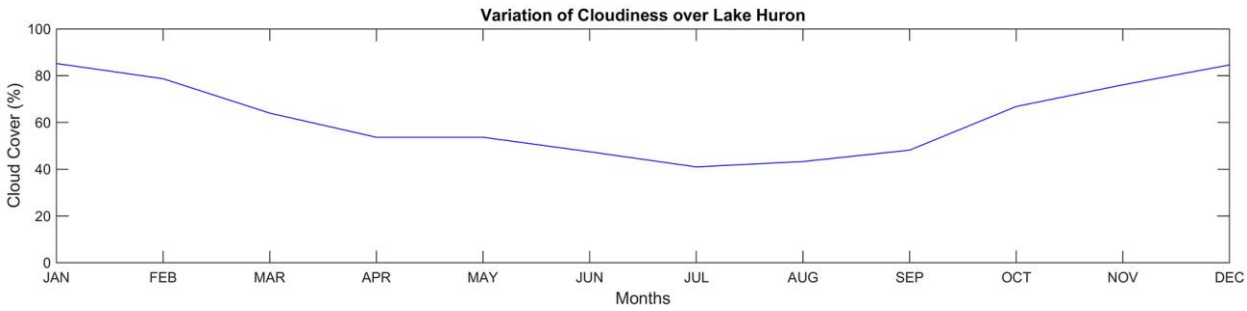

Figure 3.21 Annual variation of cloudiness over Lake Huron

3.5.3 Long-term changes in surface net radiation and its components over Lake Huron

Figure 3.22 – 3.25 show time series of mean instantaneous daily radiation at the lake's surface in W m^{-2} and the trend line for the 11-years (2002–2012) period. The trend exhibited a decline in incoming shortwave, increase in incoming longwave, outgoing longwave, and outgoing shortwave radiations. However, all of these components were not statistically significant.

Net radiation, according to changes of its four components, shows a decline of 1.09 Wm^{-2} per year corresponding to 12.04 W m^{-2} for the entire period 2002-2012 (Figure 3.26). The decrease in surface incident solar radiation followed by an increase in outgoing long wave radiation contributed to this observed trend. There was a slight increase in downwelling longwave radiation, which was relatively small compared to the decrease in incoming shortwave radiation. The following are details of the three net radiation components (incoming shortwave, incoming longwave, and outgoing longwave) that had an important contribution to the trends in net radiation.

Incoming solar radiation over the lake had a downward trend of 1.38 W m^{-2} per year corresponding to 15.25W $m^{-2}$for the entire period 2002-2012.This result agreement with Hinkelman *et al*. (2009) who observed a decline in solar surface radiation in North America

during the period 1998-2004 and similarly to Liepert (2002) who observed a reduction of 19 Wm^{-2} in surface solar radiation in the United States between the 1960s and the 1980s.

This study used 1367 W m^{-2} solar constant, therefore the variations in incidence solar radiation that reached the lake surface cannot be justified by changes in the sun luminosity. Therefore, the changes of incoming shortwave radiation had to be a result of variations in the atmosphere transparency, which controlled by the occurrence of cloud, aerosols, and water vapor. From our observation, there were slight decrease in cloud cover and its optical thickness over the lake, which would supposedly allow more incoming shortwave radiation to reach the surface. However, our results showed a decrease in the incoming solar radiation. Thus, in this case, a reduction in amount of cloud cover could not be accounted for as a factor lead to increase in surface shortwave radiation. This corresponds to the study of Qian *et al*. (2006) and Norris and Wild (2007) who reported that changes in cloud cover effect can be detected on an inter-annual basis, however, their influence to the long term trend of incoming solar radiation is not constantly noticeable.

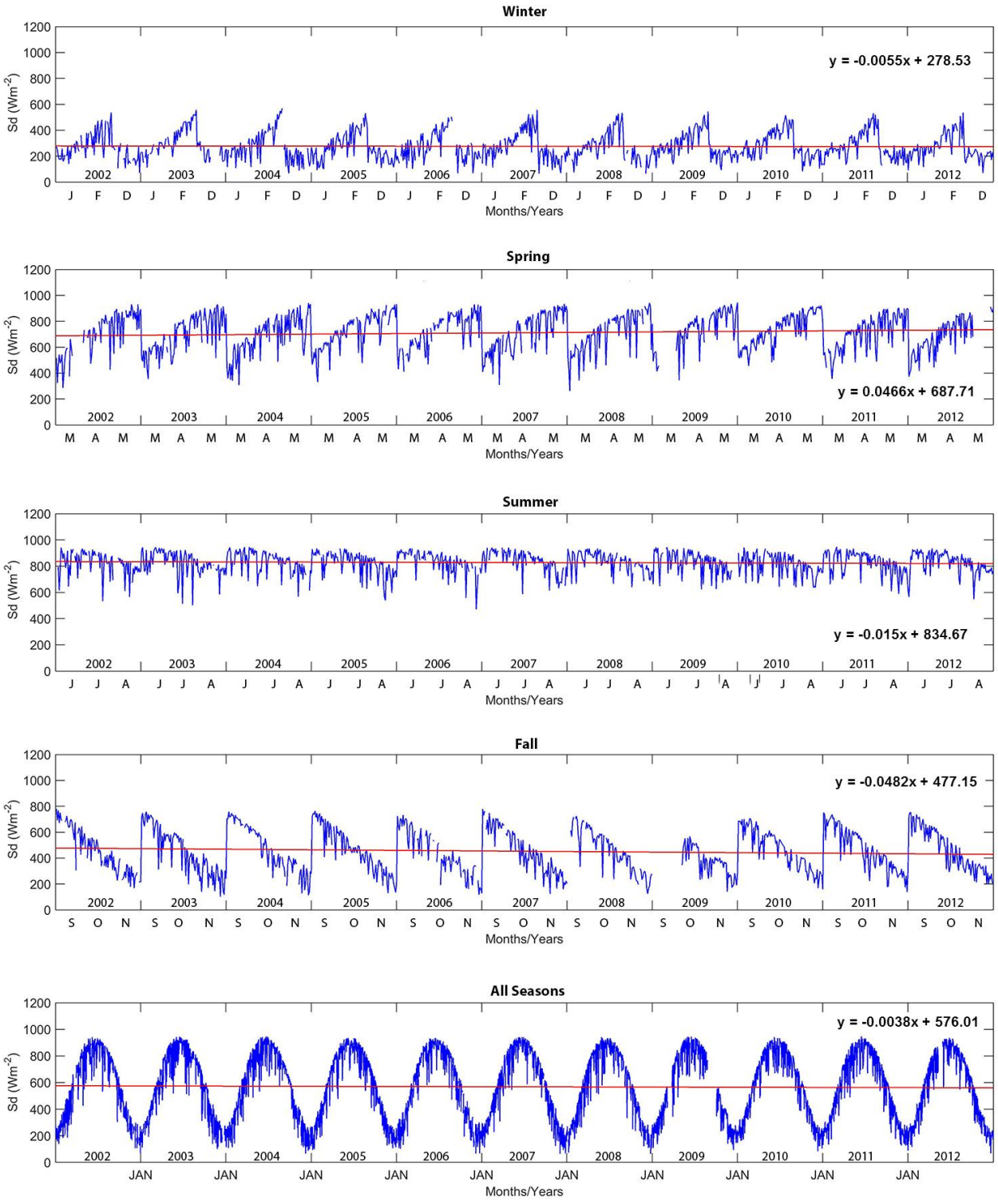

Figure 3.22 Time series of daily incoming shortwave radiation at the lake surface (in W m^{-2}): for the 11-years (2002–2012) of Lake Huron. The trend line of the radiation is also shown

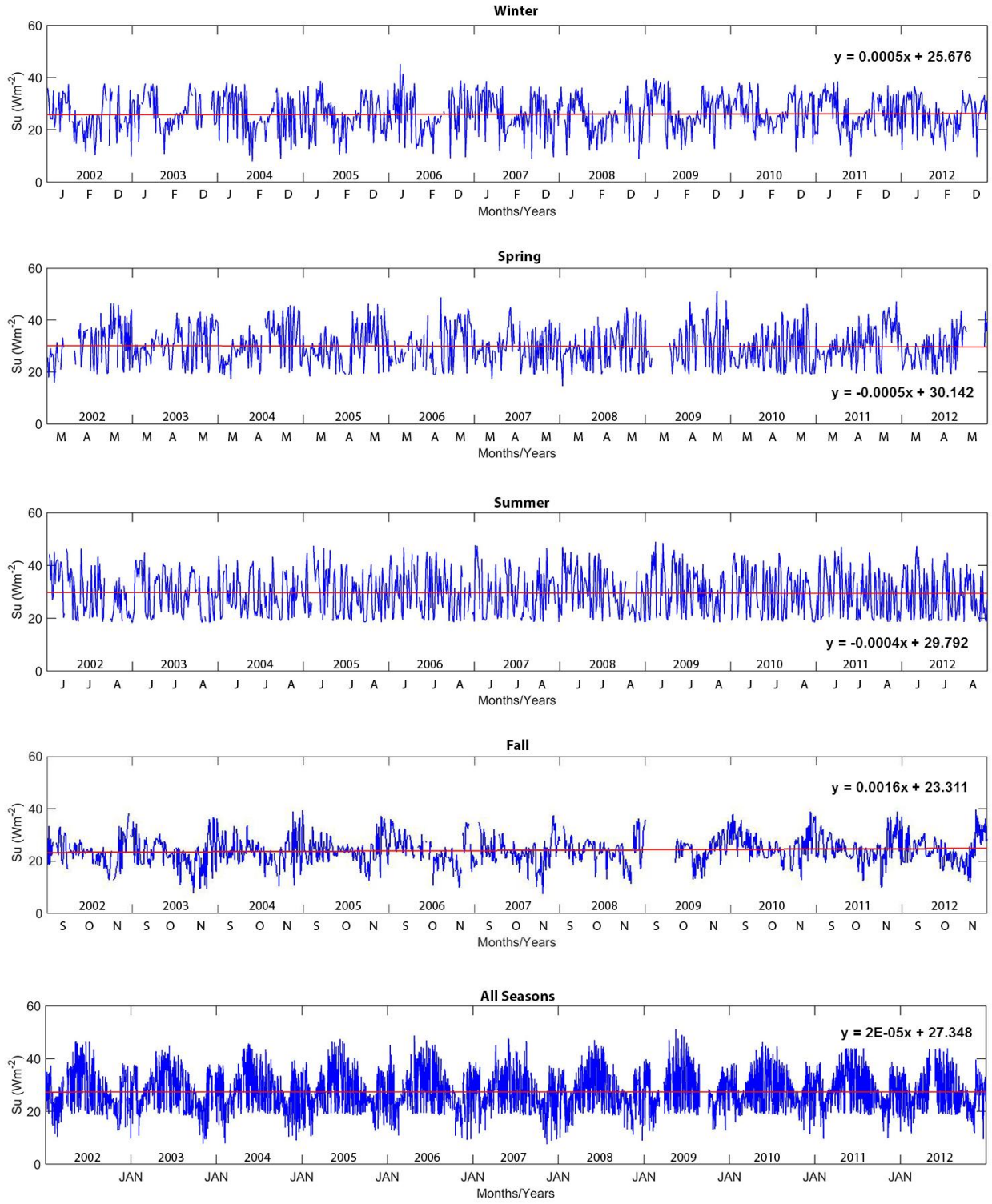

Figure 3.23 Time series of daily outgoing shortwave radiation at the lake surface (in W m^{-2}): for the 11-years (2002–2012) of Lake Huron. The trend line of the radiation is also shown

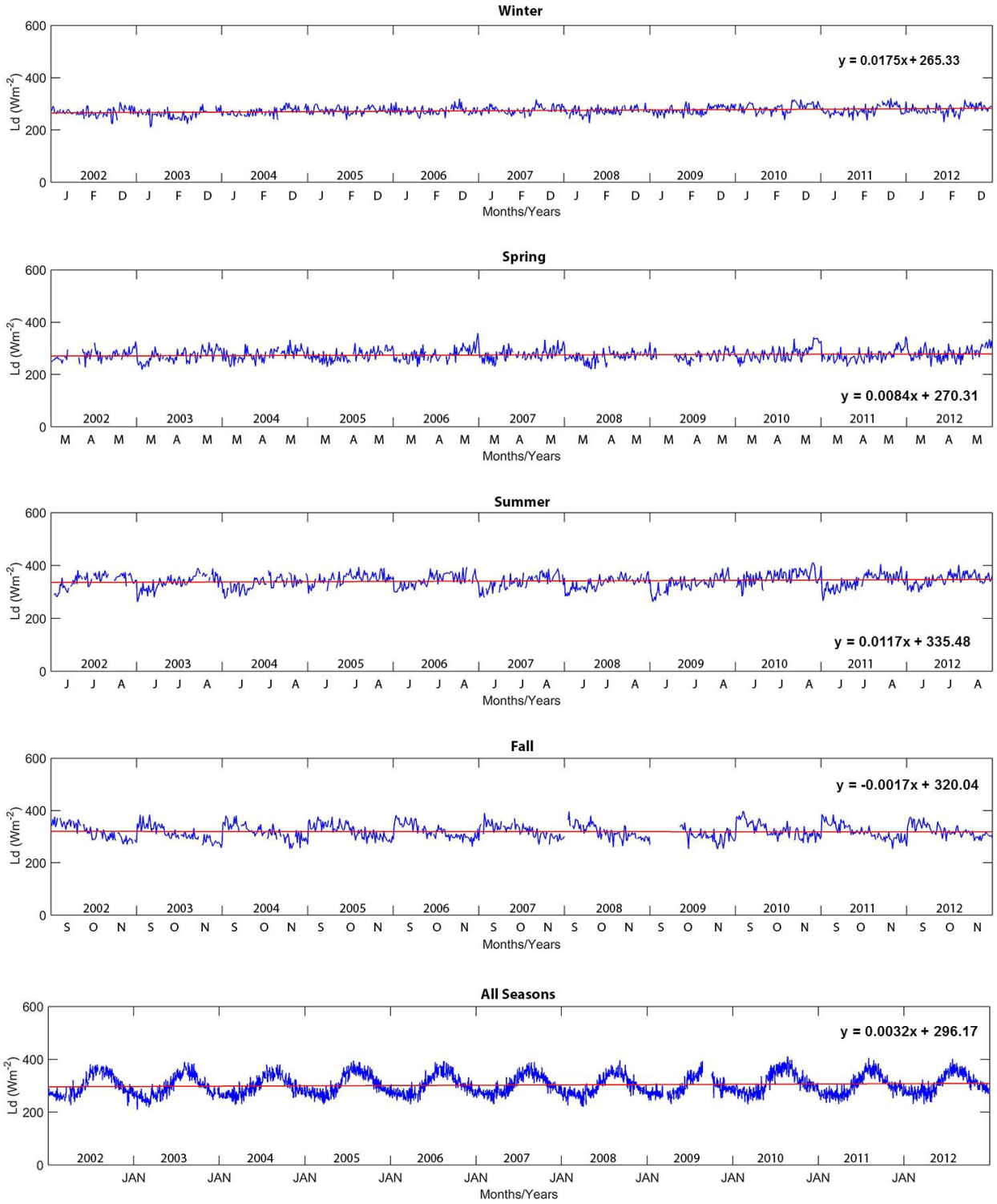

Figure 3.24 Time series of daily incoming longwave radiation at the lake surface (in W m^{-2}): for the 11-years (2002–2012) of Lake Huron. The trend line of the radiation is also shown

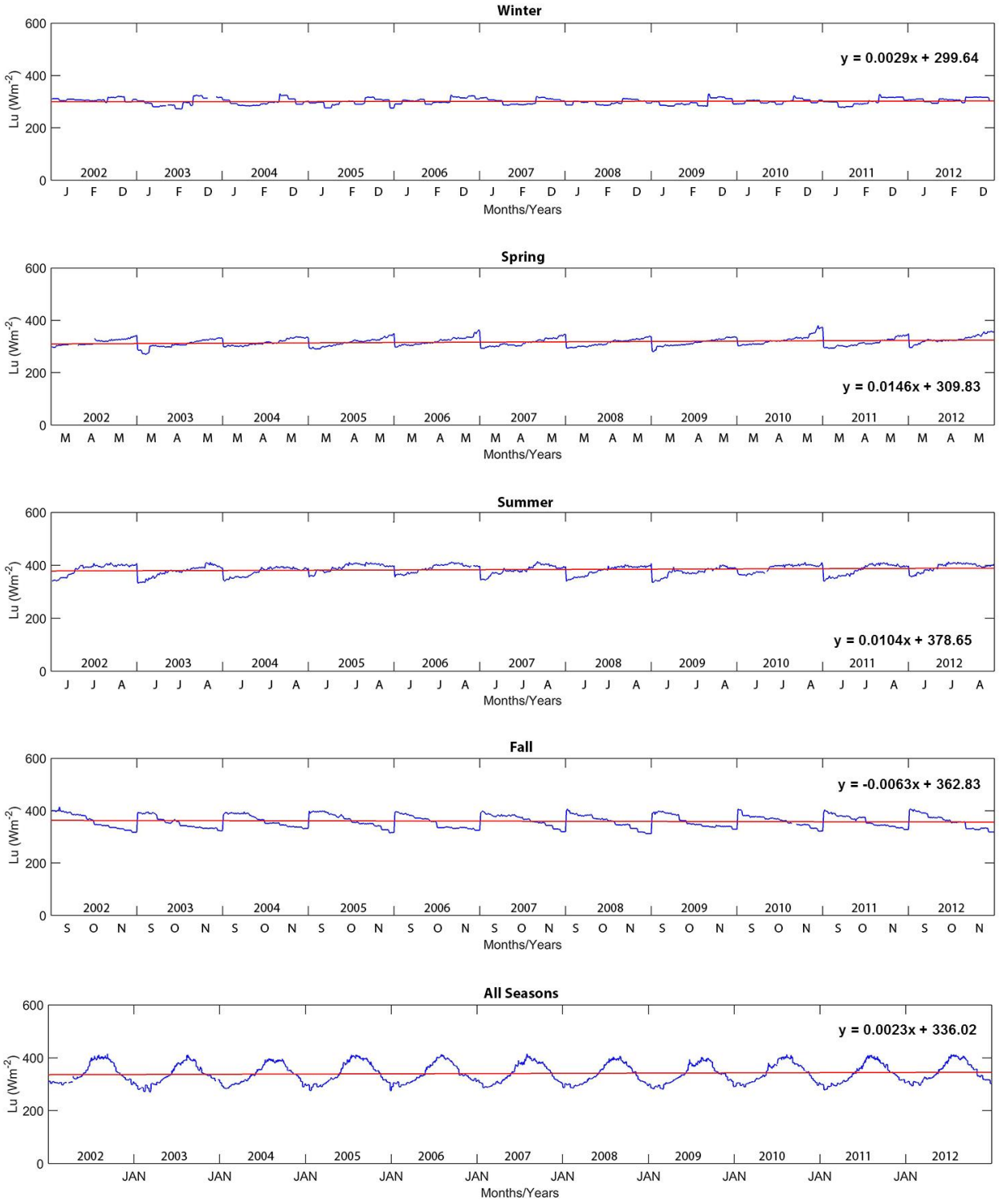

Figure 3.25 Time series of daily outgoing longwave radiation at the lake surface (in W m^{-2}): for the 11-years (2002–2012) of Lake Huron. The trend line of the radiation is also shown

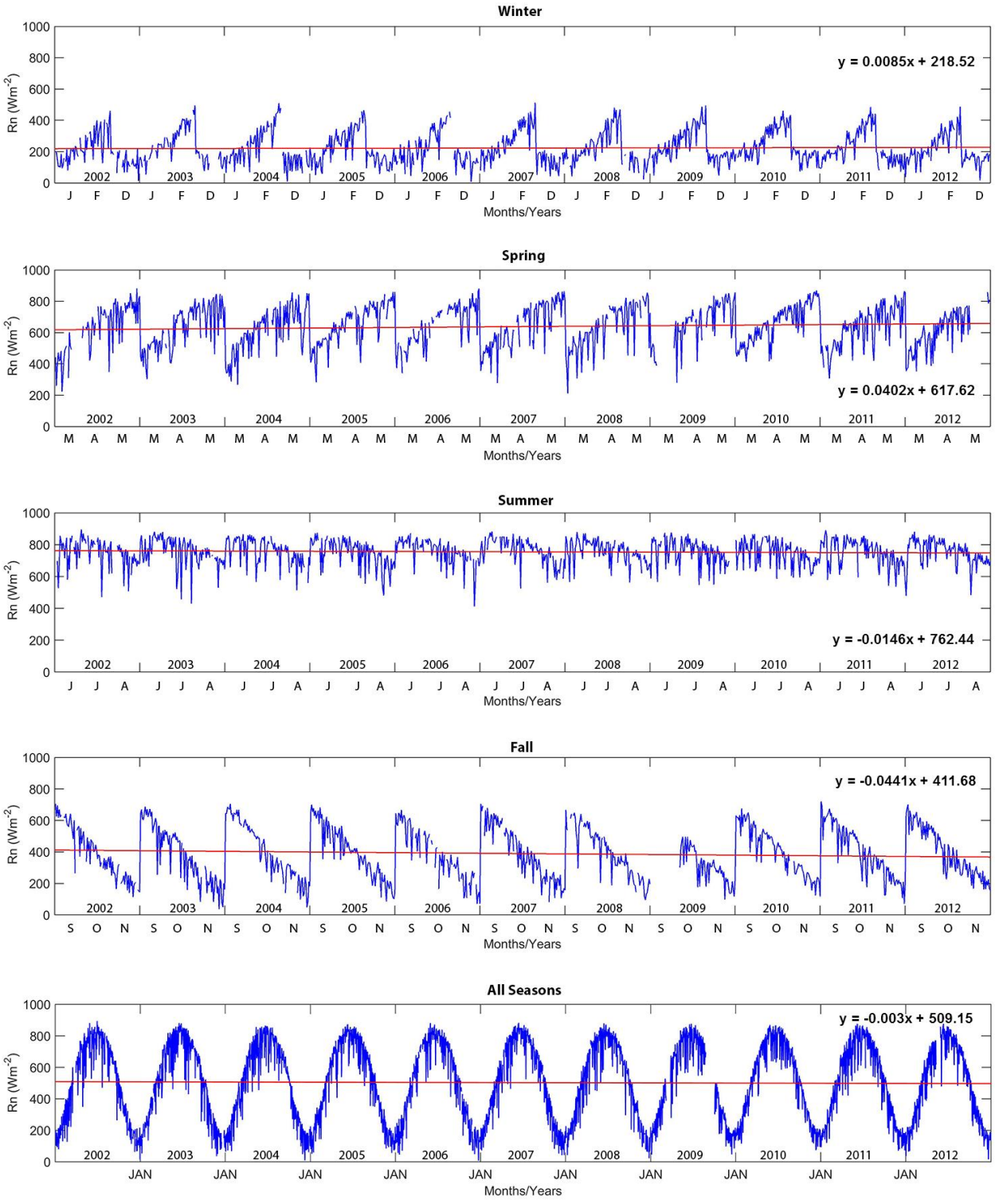

Figure 3.26 Time series of daily net-radiation at the lake's surface (in W m^{-2}): for the 11-years (2002–2012) of Lake Huron. The trend line of the radiation is also shown

The possible reason for the reduction in surface incoming shortwave radiation was the absorption of shortwave radiation by water vapor in the air. This study observed an increase in vapor pressure (Figure 3.27), which in-turn could result in a decrease in incident surface solar radiation. This is a reasonable explanation, because water vapor is the most absorbing gas in the atmosphere (Monteith and Unsworth, 2008) and it has a number of absorption bands in the shortwave spectral regions where the most intensive are the bands in ultraviolet and near infrared. Although the absorption band in visible ranges are very small, but are present (Liou, 2002) within the wavelength between 0.572-0.703 μm (Kondratyev, 1969). Our study results corresponded to the study of Arking, 1996 who claimed that water vapor is the most dominant factor in the atmospheric absorption. Braswell and Lindzen (1998) also found that water vapor in clear air absorbs significant amount of solar radiation.

The incoming longwave radiation had an increase of 1.13 W m^{-2} per year corresponding to about 12.45 Wm^{-2} for the 11 years. The change in incoming longwave is generally influenced by the change of temperature and humidity of the atmosphere and by the cloud covers (Sicart *et al*., 2010). As mentioned earlier, cloud cover and cloud optical thickness were slightly decreasing over the study period, thus the increase in incoming longwave radiation was driven by the long-term increase in vapor pressure (Figure 3.27) and air temperature. Outgoing longwave had also an upward trend of 0.84 Wm^{-2} per year corresponding to about 9.23 W m^{-2} for the entire study period (2002-2012). This increase was mainly due to the increase of lake surface water temperature (Chapter 2).

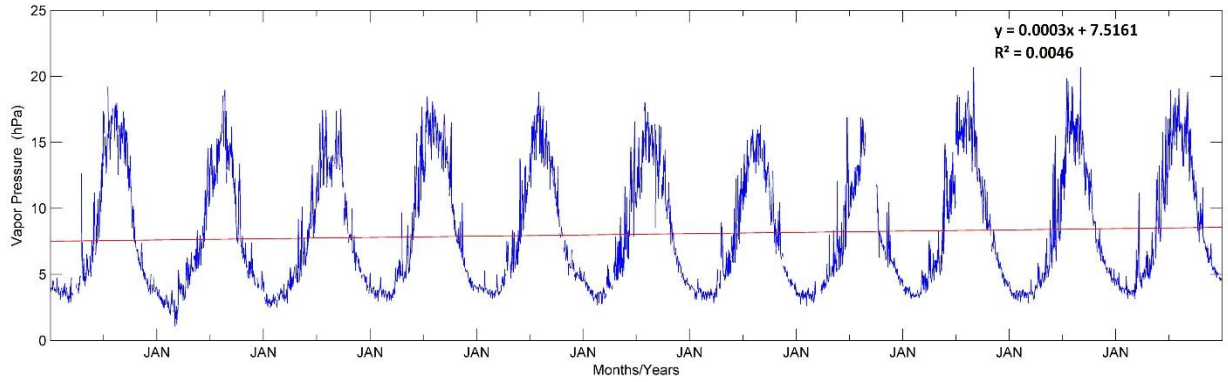

Figure 3.27 Time series of daily instantaneous vapor pressure over Lake Huron with its trends imposed

3.6 Conclusion

Inter-annual and long-term variability of surface net radiation was estimated from MODIS data using a four-component approach which depends on calculating incoming solar radiation and reflected shortwave radiation. The Stefan - Boltzmann law was applied to estimate upwelling and downwelling longwave radiations. A good correlation was found between the parameters calculated from satellite data and in situ observations. The correlation coefficient was higher than 0.90 for outgoing longwave radiation, whereas incoming radiation (both shortwave and longwave) had a correlation coefficient of approximately 0.60 due to the difference in spatial sampling between satellite and ground station. No validation was carried out for the outgoing shortwave radiation, because of the contamination of the outgoing signal from the lighthouse base and no other ground measurements were available.

The spatial distribution of the net radiation and its four components shows temporal and spatial heterogeneities, which followed the pattern of latitudinal location and lake surface temperature. The study found that the decrease in incoming shortwave radiation, increase in outgoing shortwave, incoming longwave, and outgoing longwave over the 11- years observation

period. The instantaneous net radiation is dominated by incident shortwave radiation, however, it declined by 1.09 W m^{-2} per year corresponding to about 12.04 W m^{-2} for the entire period (2002-2012). This is mainly due to the decrease in incoming shortwave radiation, followed by increase in outgoing longwave radiation. The positive trend of outgoing longwave radiation is obviously a result of the increase of surface water temperature (in Chapter 2). The possible reason of reducing surface incoming shortwave radiation is mainly due to the increase of energy absorption by water vapor in the atmosphere.

Use of satellite data for computing the net radiation parameters presented in this chapter will allow a better spatial distribution and improve spatial resolution, and analysis at wide areas. Some studies have used satellite data to estimate net radiation (Bisht and Bras, 2010) or particular component of net radiation (e.g. Tang and Li, 2008; Sun *et al*., 2013), although these analyses were focused in a particular year. This study is probably the first time remotely sensed data has been used to study long-term surface net radiation at all sky condition, and therefore it has a capability to assess surface radiation budget globally. Also the information provided in this study can be an important parameter for input to the numerical model for assessing the magnitude of surface energy balance that can explore the cause of recent water level changes phenomenon, as well as for climate models.

3.7 Bibliography

Arking A. 1996. Absorption of solar energy in the atmosphere: discrepancy between model and observations. *Science*. 273, 779-781

Baum B., Platnick S. 2006. Introduction to MODIS cloud products. In: *Earth science satellite remote sensing.* Vol. 1: Science and Instruments. p 74–91

Bisht G., Bras R.L. 2010. Estimation of net radiation from the MODIS data under all sky conditions: Southern Great Plains case study. *Remote Sensing of Environment*, 114, 1522-1534

Bisht G., Venturini V., Islam S., Jiang L. 2005. Estimation of the net radiation using MODIS (Moderate Resolution Imaging Spectroradiometer) data for clear sky days. *Remote Sensing of Environment*, 97, 52-67

Blanken P.D. 2014. *Footprint Analysis*. Unpublished manuscript

Blanken P.D. 2014. *The Value of Observations: The Great Lakes Evaporation Network*. Retrieved from http://www.ijc.org/en_/blog/2014/02/18/value_observations_great_ lakes_ evaporation_network/

Blanken P.D., Rouse W.R., Culf A.D., Spence C., Boudreau L.D., Jasper J.N., Kochtubajda B., Scertzer W.M., Marsh P., Verseghy D. 2000. Eddy covariance measurements of evaporation from Great Slave Lake, Northwest Territories, Canada. *Water Resources Research*, 36(4), 1069-1077

Blanken P.D., Spence. C, Hedstrom N, Lenters J.D. 2011. Evaporation from Lake Superior: 1. Physical controls and processes. *Journal of Great Lake Research*, 37, 707-716

Braswell W.D., Lindzen R.S. 1998. Anomalous short wave absorption and atmospheric tides. *Geophysical Research Letters*, 25, 1293-1296

Coll C., Caselles V., Galve J.M., Valor E., Niclòs R., Sanchez J.M., Viras R. 2005. Ground measurements for the validation of land surface temperatures derived from AATSR and MODIS data. *Remote Sensing of Environment*, 97, 288-300

Czajkowski K.P., Goward S.N., Stadler S., Walz A. 2000. Thermal remote sensing of near surface environmental variables: Application over the Oklahoma Mesonet. *The Professional Geographer*, 52(2), 345–357

Dugual C. R. 1994. An approach to the estimation of surface net radiation in mountain area using remote sensing and digital terrain data. *Theoretical and Applied Climatology*, 55, 55-68

Federer C.A. 1968. Spatial variation of net radiation, albedo and surface temperature of forests. *Journal of Applied Meteorology*, 7, 789-795

Geier E.R., Green R.N., Kratz D.P., Minnis P., Miller W.F., Nolan S.K., Franklin C.B. 2003. *CERES Data Management System Single Satellite Footprint TOA/Surface Fluxes and Clouds (SSF) Collection Document, Release 2 Version 1*. NASA Langley Research Center Hampton, VA. 243 p

Hinkelman L.M., Stackhouse P.W., Wielicki B.A., Zhang T.P., Wilson S.R. 2009. Surface insolation trends from satellite and ground measurements: Comparisons and challenges. *Journal of Geophysical Research*, 114, D00D20. doi:10.1029/2008JD011004

Jin Y., Randerson J.T., Goulden M.L. 2011. Continental-scale net radiation and evapotranspiration estimated using MODIS satellite observation. *Remote Sensing of Environment,* 115 (9), 2302-2319. doi: 10.1016/j.rse.2011.04.031

Kim H.Y., Liang S. 2010. Development of hybrid method for estimating land surface shortwave net radiation from MODIS. *Remote Sensing of Environment*, 114, 2393-2402

King N.J., Bower K.N., Crosier J., Crawford L. 2013. Evaluating MODIS cloud retrievals with in situ observations from VOCALS-Rex. *Atmospheric Chemistry and Physics*, 13, 191-209, doi:10.5194/acp-13-191-2013

Kondratyev K.V. 1969. *Radiation in the Atmosphere (International Geophysics Series, Volume 12)*. 1st ed. New York. Academic Press

Lenters J.D., Anderton J.B., Blanken P., Spence C., Suyker A. E., 2013 Assessing the Impacts of Climate Variability and Change on Great Lakes Evaporation. *2011 Project Reports.* Brown D., Bidwell D., Briley L. Eds. Available from the Great Lakes Integrated Sciences and Assessments (GLISA) Center. Retrieved from http://glisaclimate.org/media/GLISA_Lake_Evaporation.pdf

Liang S., Li X., Wang J. 2012. *Advance Remote Sensing: Terrestrial Information and Application*. Academic Press is an imprint of Elsevier. ISBN: 978-0-12-385954-9. 800 p

Liepert B.G., 2002. Observed reductions of surface solar radiation at sites in the United States and world wide from 1961 to 1990. *Geophysical Research Letter*, 29, 1421, 10.1029/2002GL014910

Liou K.N. 2002. *An Introduction to Atmospheric Radiation*, *Vol 84*. 2nd ed. Academic Press. 583 p

Mckay R.M.L., Beall B.F.N., Bullerjahn G.S., Woityra W.C. 2011. Winter limnology on the Great Lakes: The role of the U.S. Coast Guard. *Journal of Great lakes Research*, 37(1), 207-210

Monteith J.L., Unsworth M.H. 2008. Principles of Environmental Physics. 3rd ed. Amsterdam, Boston, Elsevier. 418 p

MRT (MODIS Reprojection Tool). 2011. *User's Manual. Release 4.1*. Land Processes DAAC.USGS Earth Resources Observation and Science (EROS) Center. 69 p

Nunez M., Davies J.A., Robison P.J., 1972. Suface albedo at a tower site in Lake Ontario. *Boundary-Layer Meteorology*, 3,77-86

Norris J.R., Wild M. 2007. Trends in aerosol radiative effects over Europe inferred from observed cloud cover, solar "dimming" and solar "brightening." *Journal of Geophycal Research*, 112, D08214, doi:10.1029/2006JD007794

Oke T.R. 1996. *Boundary Layer Climate*. 2nd Ed. Routledge. 435 p

Oyserman B.O., Woityra W.C., Bullerjahn G.S., Beall. B.F.N., Mckay R.M.L. 2012. Collecting winter data on U.S. Coast Guard ice breakers. *EOS, Transactions American Geophysical Union*, 93(10), 105-106, doi: 10.1029/2012EO100002

Painemal D., Zuidema P. 2011. Assessment of MODIS cloud effective radius and optical thickness retrievals over the Southeast Pacific with VOCALS-REx in situ measurements. *Journal of Geophycal Research*, 166, D24206, doi:10.1029/2011JD016155

Parlow E., 2000. Snow runoff models using remotely sensed data. *Remote Sensing for Environmental Data in Albania: A Strategy for Integrated Management*. Buchroithner M. F. Ed. Boston. Kluwer Academic Publishers

Prata A.J. 1996. A new long-wave formula for estimating downward clear sky radiation at the surface. *Quarterly Journal Royal Meteorological Society*, 122, 1127-1151

Qian Y., Kaiser D.P., Leung L.R., Xu M. 2006. More frequent cloud-free sky and less surface solar radiation in China from 1955 to 2000. *Geophysical Research Letters*, 33, L01812, doi:10.1029/2005GL024586

Richards J.A. 2013. *Remote Sensing Digital Image Analysis: An Introduction*. 5th ed. Springer, New York. 494 p

Rizzoli A., Neteler M., Rosà R., Versini W., Cristofolini A., Bregoli M., Buckley A., Gould E. A. 2007. Early detection of TBEv spatial distribution and activity in the Province of Trento assessed using serological and remotely-sensed climatic data. *Geospatial Health*, 1(2), 169–176

Roger R.R., Yau M.K. 1989. *A Short Course in Cloud Physics*. 3rd ed. New York. Pergamon Press. 227 p

Santos C.A., Nascimento R.L., Rao T.V., Manzi A.O. 2011. Net radiation estimation under pasture and forest in Rondônia, Brazil, with TM Landsat 5 images. *Atmosfera*, 24(4), 234-446

Schertzer W.M., Assel R.A., Beletsky D., Croley II T.E., Lofgren B.M., Saylor J.H., & Schwab D.J. 2008. Lake Huron climatology, inter-lake exchange and mean circulation. *Aquatic Ecosystem Health & Managemen*, 11, 144 – 152

Schmid H.P. 1994. Source areas for scalars and scalar fluxes. *Boundary Layer Meteorology*, 67(3), 293-318

Sicart J.E., Hoch R., Ribstein P., Chazarin J.P. 2010. Sky longwave radiation on tropical Andean glaciers: Parameterization and sensitivity to atmospheric variable. *Journal of Glaciology*, 56(199), 854-860, doi:10.3189/002214310794457182

Slingo A. 1989. A GCM parameterization for the shortwave radiative properties of water clouds. *Journal of Atmospheric Science*, 46, 1419-1427

Solomon S., Qin D., Manning M., Chen Z., Marquis M., Averyt K. B., Tignor M., Miller H. L. Eds. 2007. *Climate Change 2007*: *The Physical Science Basis*. New York, Cambridge University Press

Sun Z., Gebremichael M., Wang Q., Wang J., Sammis T. W., Nickless A. 2013. Evaluation of clear-sky incoming radiation estimating equations typically used in remote sensing evapotranspiration algorithms. *Remote Sensing*, 5, 4735-4752. doi:10.3390/rs5104735

Tang B., Li Z.L. 2008. Estimation of instantaneous net surface longwave radiation from MODIS cloud-free data. *Remote Sensing of Environment*, 112, 3482-3492.

Terjung W.T., Kickert R.K., Kochevar R.J., Mrowka J.P., Ojo S.O., Potter G.L., Tuller S.E. 1968. The annual March of the tropoclimatic spatial patterns of net radiation in Southern California. *Archives for meteorology, geophysics, and bioclimatology, Series B*, 17, 21-50

Tian L., Curry J.A. 1989. Cloud overlap statistics. *Journal of Geophycal Research*, 94, 9925-9935

Wang W., Liang S. 2009. Estimation of high-spatial resolution clear-sky longwave downward and net radiation over land surfaces from MODIS data. *Remote Sensing of Environment*. 113, 745-754

Yi Y., Minnis P., Huang J., Mack S., Chen Y., Ayers K. 2008. Validation of multi layered cloud properties using *A-Train Satellite measurements Geoscience and Remote Sensing Symposium, 2008. IGARSS 2008. IEEE International*. 574-577

CHAPTER 4

LAKE-WIDE ESTIMATES OF THE SURFACE ENERGY BALANCE OF LAKE HURON

4.1 Introduction

The Great Lakes are one of the highest intensively used freshwater systems on earth. The lakes contain approximately 23,000 km^3 of water, which correspond to roughly 20% of the world's surface freshwater (Hartmann, 1990). These interconnected freshwater lakes are shared between the United States and Canada and support many crucial uses (Assel *et al*., 2004). Recently, decreasing water levels have been experienced in the Great Lakes. This current phenomenon of water level variations is an important issue because it is constant with many climate change predictions, raising anxiety that the decreasing of Great Lakes water level possibly will continue (Sellinger *et al*., 2008). Lake Huron is one of the Great Lakes that has experienced a decrease in water levels. The lake is not controlled for hydroelectric power or business navigation and is simply minimally influenced by the inflow and outflow of the other lakes (Changnon, 2004). Thus, the changes of water levels in Lake Huron are mainly reacting to climatic or other large-degree powers, including the physical control of the surface energy balance, which provides clues to how these drivers are changing.

One of the major components of the surface energy balance of large lakes and possibly the most complicated to calculate is evaporation from the lake surface (Gianniou and Antonopolos, 2007). This term represents a major water loss and is an important factor in the lake's hydrology process (Derecki, 1981). The eddy correlation technique for directly measuring the surface energy balance is considered to be the best approach for assessing evaporation (Lenters *et al.*, 2005; Winter *et al.*, 2003). However, accurate measurements of the local energy

balance components, particularly evaporation, are commonly completed only at a small number of research sites (Granger and Bussieres, 2005). There are few studies estimating the surface energy balance and evaporation over large lakes using highly-accurate direct measurements such as the eddy covariance method (e.g. Blanken *et al*., 2000; Blanken *et al*., 2011; Rouse *et al*., 2005; Spence *et al*., 2011; Spence and Rouse, 2002).

Regarding the energy balance approach, in comparison to the water budget approach, there are also few studies conducted on the Great Lakes. Bolsenga (1975) determined the evaporation over Lake Huron using the energy balance method. His results have shown reasonable agreement with the evaporation calculated with the mass transfer method. Lofgren and Zhu (2000) applied the lake surface temperature derived from satellite data together with meteorological data to calculate the surface energy fluxes on the Great Lakes. Blanken *et al*. (2011) conducted the first direct measurement of the surface energy balance using the eddy covariance method over Lake Superior from June, 2008 to present. Spence *et al.* (2011) applied remote sensing data together with a climate model to examine the spatial distribution of evaporation across all of Lake Superior from the summer of 2008 to the fall of 2010. However, the long-term (i.e. several years) estimates of evaporation and surface energy balance over Lake Huron using both techniques have not been reported. The major difficulty in estimating lake evaporation using the energy balance method is the lack of meteorological measurements on the lake and there is no adequate technique to interpolate the meteorological data from sparse surface observations. Regarding the eddy covariance systems, there are difficulties associated with the direct measurements of lake evaporation because they involve major financial investment in terms of devices, station maintenances, and field works (Yao, 2009).

Long-term continuing observations and in-situ data are essential for understanding lake evaporation and evaluating the effects of evaporation change in water resources. The latent heat energy is one of the energy balance components that act as a connection between the energy and water budgets of the lake; thus changes in the energy of surface can make a significant change in water levels (Lofgren and Zhu, 2000). Measuring the lake's energy balance is a very complicated and time-consuming procedure, because the factors that determine the energy intensity differ both spatially and temporally. Also, exchanges between the lake surface and atmosphere require updated information measured directly at the location. Since the surface area of the lake is so large, direct measurement of elements year-round over the entire water surface is not possible with currently-available resources.

Satellite remote sensing is most likely the only capable and practical technique to supply regional to global observations of some meteorological variables that are relevant to the calculation of surface energy balance, including net radiation, and latent and sensible heat fluxes. Regionally and globally-averaged quantities can be calculated without the under-sampling problem due to a limited number of observation networks (Swenson and Wahr, 2009). Therefore, application of specially-equipped remote sensing combined with spatially-constant surface meteorological parameters and GIS is necessary for assessing the magnitude of the surface energy balance of large lakes such as Lake Huron. It is also very useful for the research community to better understand the changes in the water level phenomenon that has been encountered in recent years.

The purpose of this chapter is to estimate the spatial and temporal variations, as well as the long-term changes in the Lake Huron's surface energy balance using MODerate resolution Imaging Spectroradiometer (MODIS) data, calibrated and verified by surface meteorological

observations. The results of this study will be significant and beneficial in discovering the spatial and temporal distributions of the energy budget over large lakes. This will contribute to the research community studying climate both on regional and global scales. Furthermore, the results of this study will improve our understanding of the reasons behind the fluctuations in water levels.

This chapter focuses on estimating the latent heat and sensible heat fluxes, but also presents details on the connections, between energy balance components and meteorological variables, seasonal changes of these components, and the water heat storage component. The first section describes the study area, followed by a description of the data and study methods. Next, the 2010 surface energy balance estimated from satellite data compared to direct measurements is presented. Next, a discussion of the seasonal spatial and temporal variations from the period 2002-2012 is given. Finally, conclusions are presented.

4.2 Study Area

Lake Huron is the second largest surface fresh water of the Great Lakes, with the area of 59,600 km^2, and it is the third largest fresh water lake on earth. Lake Huron contains water volume of 3,540 km^3, and a shoreline length (including islands) of 6,157 km (MacDonagh-Dumler *et al.*, 2005). The lake has a length of 332 km and a greatest breadth of 245 km. (Schertzer *et al.*, 2008; Zimmermann, 2013). Lake Huron is connected to Lake Michigan, which lines at the similar surface elevation, by the narrow waterway Straits of Mackinac, assembly them geologically and hydrologically the single water body, which is known as Lake Michigan-Huron.

The Spectacle Reef Lighthouse, located 17.22 km east of the eastern end of Bois Blanc Island at 45.7732 N and 84.1367 W, is the only station measuring year-round meteorological variables over the lake. The station uses the eddy covariance method to measure the turbulent heat fluxes (both sensible and latent heat), net radiation, air temperature, humidity, rain rate, and lake surface temperature. The lighthouse is the major platform providing year-round, continuous 30-min average meteorological and fluxes data for estimating and validating the latent and sensible heat fluxes for this study.

4.3 Objectives

This chapter focuses on estimating the latent heat and sensible heat fluxes, but also presents heat storage and total heat fluxes into the lake surface by combining data from satellite and meteorological station data in order to discover the spatial and temporal distribution of the energy budget over Lake Huron. In order to achieve this goal, the objectives of this study are:

i) To examine the spatiotemporal variation of the latent heat and sensible heat fluxes as well as the surface energy balance using a combination of remotely-sensed data and field measurements

ii) To determine the characteristic and long-term change of the surface energy balance component over a period of 11 years (2002-2012)

4.4 Data and Methodology

4.4.1 Data

Two kinds of datasets were used: satellite observation and direct surface-based measurements.

4.4.1.1. Satellite data

Estimation of the latent heat flux, the sensible heat flux, and lake the surface energy balance were obtained throughout the period of 2002 –2012 at daily time intervals. Four data products from MODIS, including MOD03 (Geological product), MOD06 (Cloud product), MOD07 (Atmospheric profile product), and MOD11 (Land surface temperature product), were used. The characteristics of each product were already described in the previous chapters. All of the surface energy balance requirement input parameters from satellite were already calculated and validated in previous chapters (Chapter 2: surface water temperature; Chapter 3: net radiation, vapour pressure, and air temperature).

4.4.1.2. In-situ Measurement

There are three sources of in-situ data: the meteorological station installed on top of the Spectacle Reef Lighthouse (45.773 N, 84.136 W), the NOAA National Data Buoy Center (station 45003 located at 45.351 N, 82.840 W), and the NOAA meteorological station on the Alpena Harbor Light (45.0560 N, 83.424 W). The Spectacle Reef Lighthouse is the major platform providing meteorological and fluxes data for calculating and validating the latent and sensible heat fluxes. The height of the instruments is 31 m above the mean water level, and the nearest shore is located 17.22km east of the eastern end of Bois Blanc Island. The latent heat and sensible heat were calculated using the method described by Blanken *et al.*, (2011), over Lake Superior. The latent heat flux can be directly converted to mm of evaporated water by dividing by the latent heat of evaporation and the density of water. The vertical wind speed was measured using a 3-D sonic anemometer (Figure 4.1 A) (model CSAT-3, Campbell Scientific, Logan, UT), whereas water vapour density was measured using a highly-sensitive hygrometer (Figure 4.1B) (model KH20, Campbell Scientific, Logan, UT). The statistics (means and covariances) of the high-frequency sampled data were collected at 30-min intervals using a datalogger (model CR23X, Campbell Scientific, Logan, UT). The DC power was supplied by four 12-V 115-Ah marine batteries charged by two 80-W solar panels. The datalogger and batteries were located in a dry location inside the lighthouse. Post-processing of these data, including quality control, was performed following Blanken *et al*. (2011).

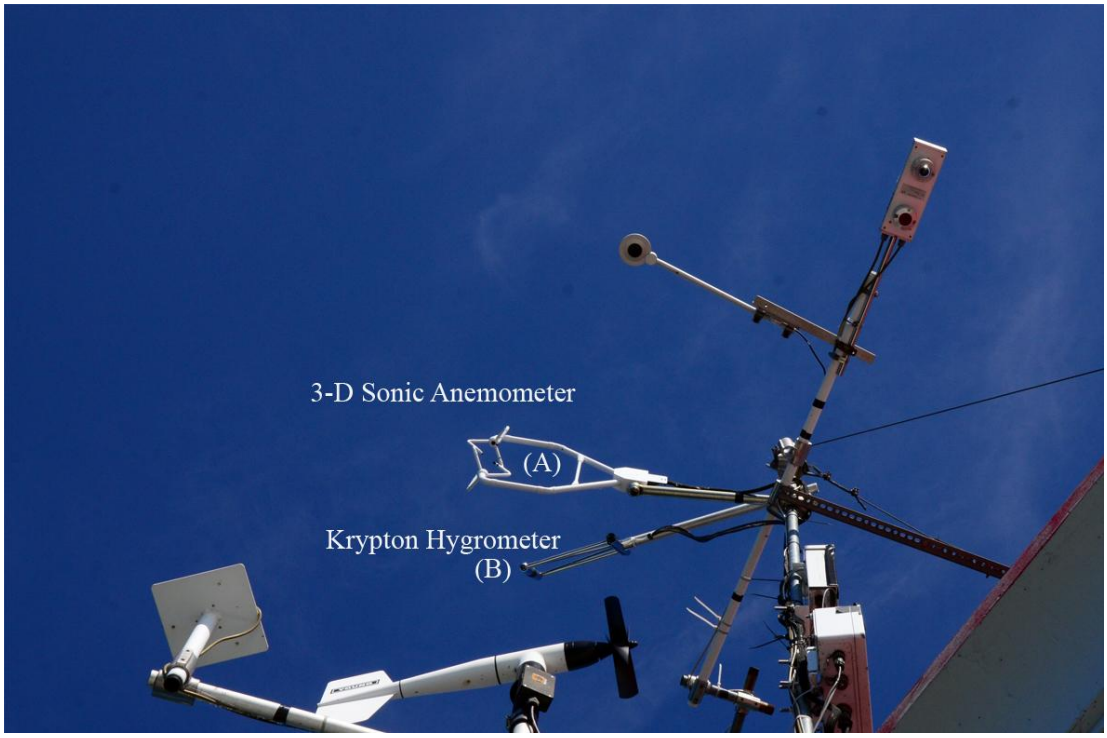

Figure 4.1 3-D sonic anemometer (A) and Krypton Hygrometer (B) located on the roof of Spectacle Reef Lighthouse. These are the major instruments providing meteorological and flux data for calculating and validating latent and sensible heat fluxes, September, 2014. Credit: Pakorn Petchprayoon

The two NOAA meteorological stations provided wind speed data which were recorded before September 2009 (before the Spectacle Reef Lighthouse station was operational). The National Data Buoy Center (buoy station 45003 located at latitude: 45.351, longitude: -82.840), provided long-term wind speed data except during the winter season (all buoys operate only during the April-October shipping season), while the Alpena Harbor Light Station (Latitude: 45.059722, Longitude: -83.423611) provided year-round long-term wind speed data. Therefore, the wind speed data from this station were used to calculate the turbulent heat fluxes and the buoy data were used when there were data gaps in the Alpena Station. If there were still missing wind speed data, the long-term mean value from the three meteorological stations (Alpena, Buoy, and Lighthouse) was applied.

The horizontal wind speed from the NOAA station 45003 was measured using an R.M. Young model 5103 wind sensor. The sensor was located 44 km from the shore, 3.2 m above the lake surface. The sampled data were collected at 5 second intervals and averaged every 10 minutes. For the Alpena Harbor Light Station, horizontal wind speed was also measured using R.M. Young model 5103 wind sensor. The sensor was located 12 m above the mean water surface, and was moved to 18 m above lake surface on October 27, 2005. The sampled data were collected at 5 second intervals and averaged every 5 minutes using a datalogger (model CR200, Campbell Scientific, Logan, UT). The system was AC-powered.

4.4.2. Methodology

The general surface energy balance equation of a water body surface can be expressed by

$$Q^* = Q_E + Q_H + Q_s + Q_{GL} \quad (4.1)$$

where:

Q^* is the net radiation (W m^{-2})

Q_E is the latent heat flux (evaporative heat flux)(W m^{-2})

Q_H is the sensible heat flux (W m^{-2})

Q_s is heat storage in the water (W m^{-2})

Q_{GL} is the heat conduction across the lake bottom (W m^{-2})

In large water bodies such as the Great Lakes, Q_{GL} is negligible because the heat loss through the lake bottom is presumably small compared to the surface radiative exchanges and the net advective components since solar radiation cannot penetrate to the lake bottom and all of the energy absorbed by the water volume (Oke 1996; Rouse *et al.*, 2005). Also, the advection of heat

from precipitation and the inflow and outflow in large, deep lakes are small compared to the radiation exchanges (Schertzer and Taylor, 2009). The resulting surface energy balance for a large water body can therefore be simplified as:

$$Q^* = Q_E + Q_H + Q_s \tag{4.2}$$

4.4.2.1 Net Radiation

The equation for estimating net radiation can be expressed as:

$$Q^* = (1 - \alpha)K\downarrow + L\downarrow - L\uparrow \tag{4.3}$$

where

α is the surface albedo (no units)

$K\downarrow$ is the incoming shortwave radiation flux density (W m^{-2})

$L\downarrow$ is the incoming longwave radiation flux density (W m^{-2})

$L\uparrow$ is the outgoing longwave radiation flux density (W m^{-2})

The estimation of the radiation balance was provided in Chapter 3; hence the results based on equation 4.3 will be used for estimating the lake surface energy balance in this chapter.

4.4.2.2 Latent heat flux

The evaporative (latent) Q_E heat flux term from the remote sensing estimates of lake-wide conditions was calculated using the bulk aerodynamic formulae. The latent heat flux was calculated as follows (Large *et al*., 1997):

$$Q_E = \rho_A L_V c_E |U| [e_{SAT}(T_S) - r e_{SAT}(T_A)] \frac{0.622}{p_A} \tag{4.4}$$

where

ρ_A is the air density (1.2 kg m^{-3})

L_V is the vaporization of latent heat(2.501×10^6 J kg^{-1})

c_E is a coefficient of turbulent exchange (no units)

U is the horizontal wind speed (m s^{-1})

e_{SAT} is the saturation vapour pressure(hPa)

T_S is the water surface temperature (^oC)

r is the relative humidity(no units)

T_A is the air temperature (^oC)

p_A is the atmospheric surface pressure (hPa)

Relative humidity r can be calculated using the equation:

$$r = \frac{e}{e_{SAT}} \times 100 \tag{4.5}$$

where

e is the ambient vapour pressure (hPa)

Saturation vapour pressure e_{SAT} was calculated using the Magnus-type equations (e.g. (Koutsoyiannis, 2012).

$$e_{SAT} = 6.1094 \exp\left(\frac{17.625T}{243.04+T}\right) \tag{4.6}$$

Complete long term in-situ measurements of wind speed, even from a single station, were not available. Thus, some constraints were imposed on the wind speed (U) and coefficient of turbulent exchange for the water vapour (c_E). Wind speed data were collected from three different meteorological station sites: Spectacle Reef Lighthouse (main station), NOAA's National Data Buoy Center (station 45003), and NOAA's meteorological station on the Alpena Harbor Light, because no single meteorological station was available for the entire study period. The wind field was considered homogeneous for the whole lake, since there were no multiple meteorological stations covering the entire lake. Therefore, this study used wind speed at the height of 12 m (before October 27, 2005) and at of 18 m (after October 27, 2005) because the wind speed sensor was moved to a higher position. Since all of the parameters and results from this study were compared to the in-situ based measurements at the height the observations at Spectacle Reef lighthouse (31 m), the wind speed was extrapolated at the NOAA station's measured height (12 m and 18 m) to a height of 31 m (Spectacle Reef Lighthouse) using the standard power law equation (Schertzer and Taylor, 2009). The increase of wind speed with height can be calculated by:

$$U_2 = U_1 \times \left(\frac{Z_2}{Z_1} \right)^{1/7} \tag{4.7}$$

where

U_1 is known horizontal wind velocity at level Z_1 (m s^{-1})

U_2 is the wind velocity to be calculated at height level Z_2 (m s^{-1})

Z_1 reference height where U_1 is known (m)

Z_2 is the height above lake level for velocity U_2 (m)

Due to a lack of spatial data representation over the Great Lakes, the above equation was applied without adjusting for stability (Schertzer and Taylor, 2009) since there were no direct measurements of the sensible heat flux and friction velocity during the time before September 2009 that were required to calculate the atmospheric stability using either the Richardson Number or Monin-Obukov Length. Thus, the stability condition over the lake could not be estimated and adjustment of wind speed at different height was done without reference to a stability correction.

After the wind speed was extrapolated to the height of the Spectacle Reef Lighthouse station, regression analysis was applied to determine the relationship between the wind speed measured at the lighthouse station and each of the other two stations for four seasons. Then the regression equations (Table 4.1) were used to adjust the wind speed.

Table 4.1 Seasonal regression equations for wind speed adjustment

Station	Winter (DJF)	Spring (MAM)	Summer (JJA)	Fall (SON)
Alpena	y = 0.1421x + 5.0903	y = -0.0007x + 7.0372	y = 0.6664x + 2.1318	y = 1.1846x + 0.2327
Buoy			y = 0.421x + 2.9036	y = 0.1421x + 5.0903

The coefficients of the turbulent exchange of the latent heat flux (c_E) were also considered to have similar spatial value for the whole lake. Alcantara *et al.* (2010) assumed that c_E had a constant value of 1.1×10^{-3} for both temporal and spatial coverage in the study of heat fluxes over the Itumbiara Reservoir in Brazil. Also, Derecki (1981) and Quinn (1979) assumed that the c_E and c_H were equal for a study of Great Lakes evaporation. This study proposed to calculate the coefficients of turbulent exchange c_E and c_H for Lake Huron using latent heat, wind speed, surface temperature, air temperature, and vapour pressure gradient data observed

from the meteorological station at the Spectacle Reef Lighthouse from 2010-2011. The coefficient of turbulent exchange for the latent heat was estimated as (adjusted from Alcantara *et al*., 2010):

$$c_E = \frac{Q_E P_A}{0.622 \times \rho_A L_V |U| \left[e_{SAT}(T_S) - r e_{SAT}(T_A) \right]} \quad (4.8)$$

4.4.2.3 Sensible heat flux

The sensible Q_H heat flux term was estimated using Equation 4.9 (Large *et al*., 1997):

$$Q_H = \rho_A c_p c_H |U| (T_S - T_A) \quad (4.9)$$

where

c_p is the specific heat capacity of air (1.005×10^3 kg m^{-3})

c_H is a coefficient of turbulent exchange (no units)

The same assumptions used for estimation of c_E were applied for the calculation of the coefficient of turbulent exchange for sensible heat (c_H). The c_H was estimated using the following equation: (adjusted from Alcantara *et al*., 2010)

$$c_H = \frac{Q_H}{r_A c_p |U| (T_S - T_A)} \quad (4.10)$$

The odd values of c_E and c_H were removed using the standard deviation (sigma) specific to each year. The coefficient values greater than the value of two sigma above the mean value and lower than the value of two sigma below the mean value were eliminated.

4.4.2.4 Heat storage

The heat storage term was estimated as a residual of the surface energy balance:

$$Q_S = Q^* - Q_E - Q_H \quad (4.11)$$

4.4.3 Comparison of latent heat and sensible heat to the ground-based observations

For the comparison, latent and sensible heat fluxes calculated for 2010 were used. The latent heat and sensible heat fluxes calculated from satellite parameters, together with wind speed data and the coefficients of turbulent exchange from meteorological stations, were compared to the heat fluxes derived using the eddy correlation method, which is a direct measurement technique. For validation of the results of heat fluxes, the coefficients of 2011 were used instead of mean value to compute the heat fluxes of 2010, and this mainly to reduce any dependency of the data, since the mean was calculated from 2010 and 2011 data.

4.4.4 Spatial and temporal variations in lake surface energy balance

Maps of the daily surface energy balance components of Lake Huron were created with a 5×5 km^2 grid resolution in order to examine the temporal and spatial distribution of the surface energy balance components in different seasons. All of the remote sensing estimates of lake-wide conditions were calculated using ERDAS IMAGINE 9.2 and ArcMap version 10.1 using the Python programming language

To calculate the change of surface energy balance components, least squares linear regression was applied for each pixel with daily temporal resolution over 11 years. The slope of each regression line represents the net radiation change during the study period.

4.5 Results and Discussion

4.5.1 Coefficient of turbulent exchange

The transfer coefficients for the latent heat and sensible heat calculated at the Spectacle Reef Lighthouse for the period of 2010-2011 are shown in Figures 4.2 and 4.3. Both coefficients of turbulent exchange displayed strong seasonal patterns. The values of the two coefficients were higher during winter than the summer and other seasons. Table 4.2 and Table 4.3 show the seasonal median of transfer coefficient for the years 2010 and 2011, as well as the mean of the two years that were used to calculate the latent heat and sensible heat fluxes.

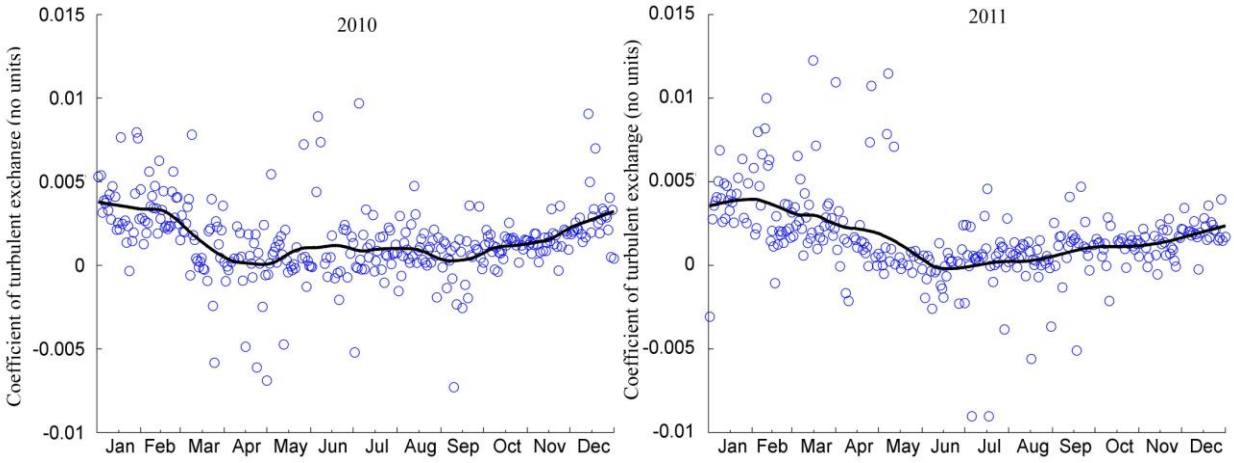

Figure 4.2 Daily coefficient of turbulent exchange value for the latent heat fluxes calculated using data observed from the meteorological station at the Spectacle Reef Lighthouse for the years 2010 and 2011. The solid black line displayed the seasonal variation

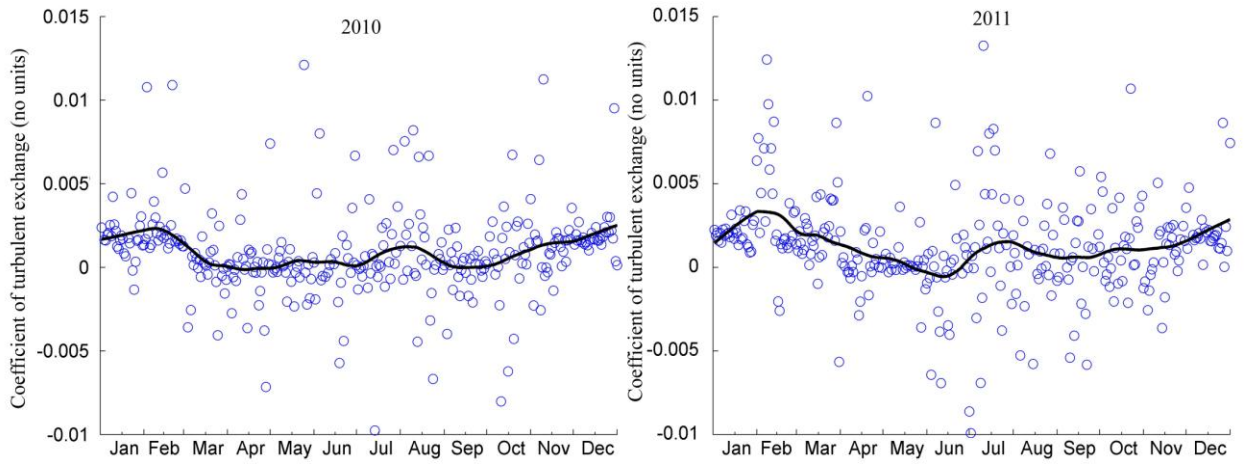

Figure 4.3 Daily coefficient of turbulent exchange value for the sensible heat fluxes calculated using data observed from the meteorological station at the Spectacle Reef Lighthouse for the years 2010 and 2011. The solid black line displayed the seasonal variation

Table 4.2 Seasonal median of the transfer coefficient for the latent heat flux of Lake Huron (no units)

	Winter (DJF)	Spring (MAM)	Summer (JJA)	Fall (SON)
2010	2.81×10^{-3}	0.43×10^{-3}	0.73×10^{-3}	1.19×10^{-3}
2011	2.61×10^{-3}	1.51×10^{-3}	0.34×10^{-3}	1.29×10^{-3}
Mean	2.71×10^{-3}	0.97×10^{-3}	0.54×10^{-3}	1.24×10^{-3}

Table 4.3 Seasonal median of the transfer coefficient for the sensible heat flux of Lake Huron (no units)

	Winter (DJF)	Spring (MAM)	Summer (JJA)	Fall (SON)
2010	1.72×10^{-3}	0.07×10^{-3}	0.17×10^{-3}	0.63×10^{-3}
2011	1.94×10^{-3}	0.48×10^{-3}	0.69×10^{-3}	0.89×10^{-3}
Mean	1.83×10^{-3}	0.21×10^{-3}	0.43×10^{-3}	0.76×10^{-3}

Several studies indicate that the transfer coefficient is proportional to the wind speed, whereas others have found no such relationship (Smedman *et al.,* 2007). For this study, the transfer coefficient of latent heat and sensible heat were plotted against wind speed in Figure 4.4. The results show that most of the frequencies of transfer coefficient were not sensitive to the wind speed, except during the wintertime.

In winter, the observation showed that when the wind speed exceeds a value of approximately 3 m s^{-1}, the transfer coefficients do not increase with the wind speed but either decrease or are constant as wind speed increases further. However, the transfer coefficients were increased again for strong winds (14 m s^{-1}).

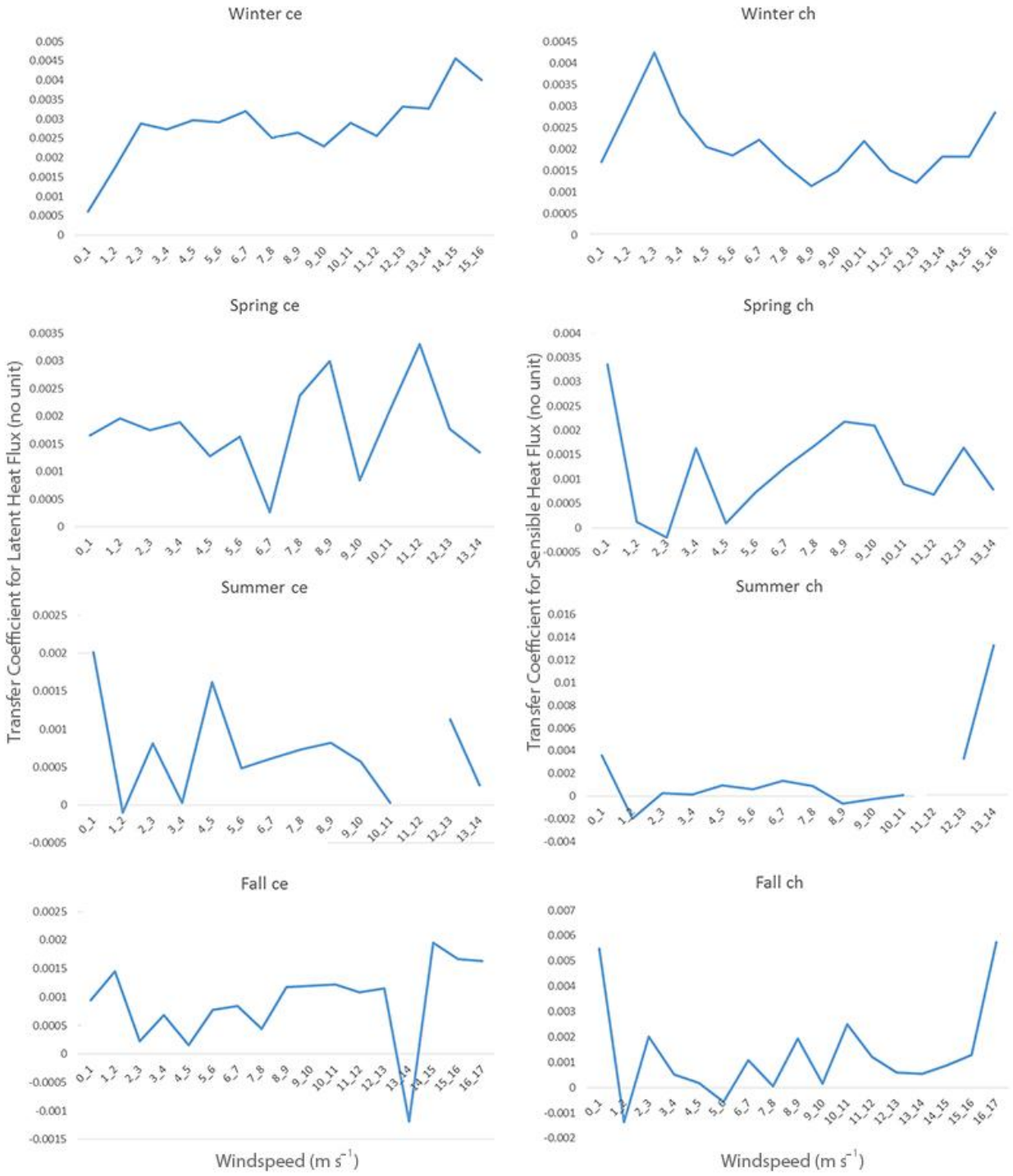

Figure 4.4 Transfer coefficient for latent heat (left) and sensible heat (right) (no unit) plotted against wind speed (m s^{-1})

4.5.2 Comparison of satellite latent and sensible heat fluxes to the ground-based observations

4.5.2.1 Latent heat flux

The plot of latent heat flux calculated from the satellite parameters together with data from the meteorological stations versus the latent heat derived from the eddy correlation method shows an agreement with an R^2 of 0.56, slope 0.49, offset 25.27, and n = 340 (Figure 4.5). Figure 4.6 shows that the satellite-derived latent heat fluxes corresponded well with the values from the eddy correlation method. However, the satellite-derived latent heat fluxes were underestimated by 50% compared to the eddy correlation method. This large difference was mainly due to the fact that the latent heat measurements from the eddy correlation method were high (~200 W m^{-2}), whereas the value of the satellite-derived latent heat fluxes were low (near zero W m^{-2}), in particular during the summer (JJA). Although there was a difference between the daily latent heat flux values calculated from satellite data and those from the eddy correlation method, the annual latent flux obtained by the two methods was very close (Figure 4.7).

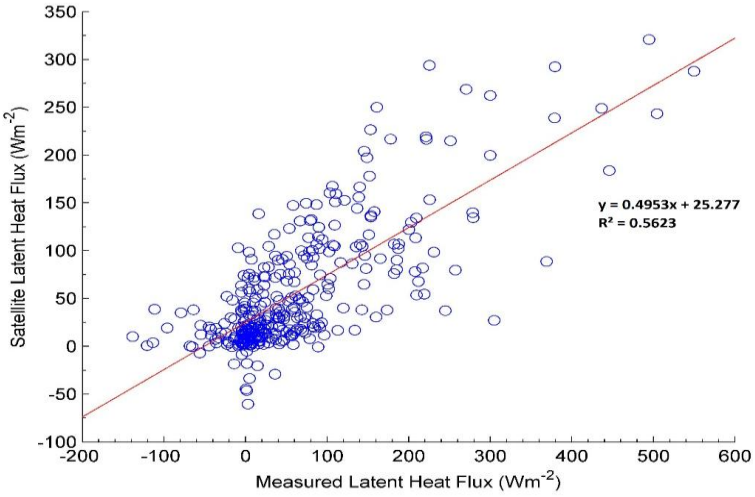

Figure 4.5 Scatter plot of satellite latent heat fluxes versus observed latent heat fluxes (30 min average) from the meteorological station at the Spectacle Reef Lighthouse for the year 2010

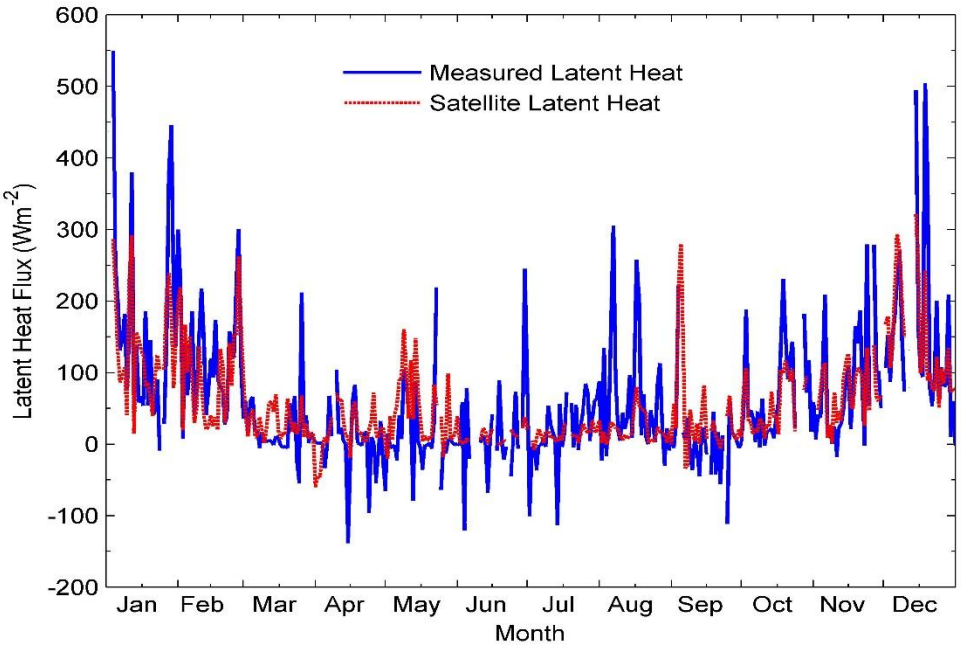

Figure 4.6 Comparison of satellite latent heat fluxes (red line) and observed latent heat fluxes (30 min average) from the meteorological station (blue line) at the Spectacle Reef Lighthouse for the year 2010

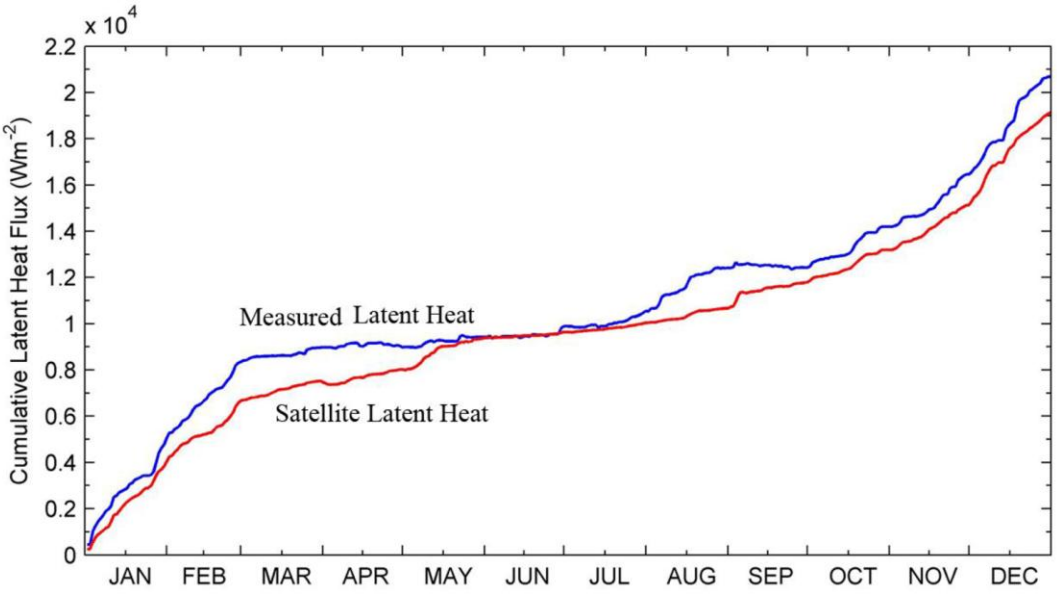

Figure 4.7 Cumulative satellite latent heat fluxes (red line) and cumulative observed latent heat fluxes (30 min average) from the meteorological station (blue line) at the Spectacle Reef Lighthouse for the year 2010

4.5.2.2 Sensible heat flux

The plot of sensible heat calculated from the satellite parameters together with data from the meteorological stations versus the latent heat derived from the eddy correlation method shows an agreement with an R^2 0.59, slope 0.48, offset 14.95, and n = 340 (Figure 4.8). Figure 4.9 shows that the satellite-based sensible heat fluxes were lower than those from the eddy correlation method, particularly in the spring and winter (~ 52% underestimation) period. Also, the cumulative values of the satellite sensible heat were very low compared to the eddy correlation values (Figure 4. 10).

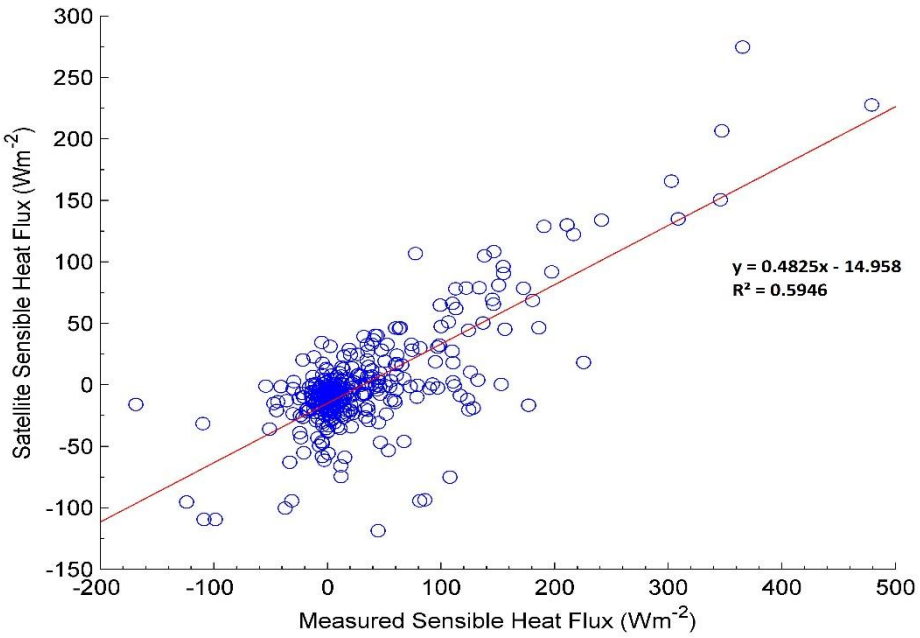

Figure 4.8 Scatter plot of satellite sensible heat fluxes versus observed sensible heat fluxes (30 min average) from the meteorological station at the Spectacle Reef Lighthouse for the year 2010

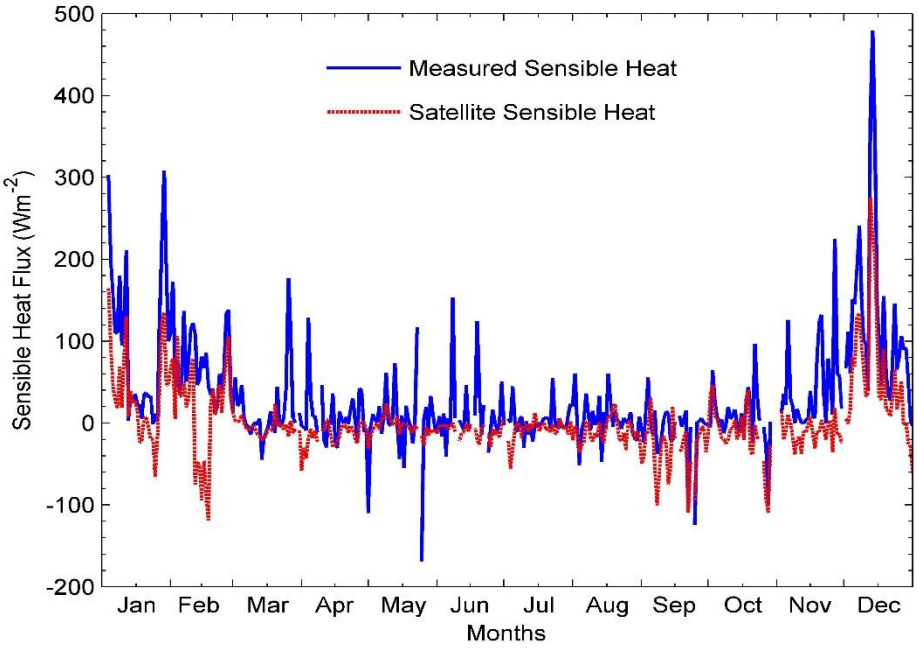

Figure 4.9 Comparison of satellite sensible heat fluxes (red line) and observed sensible heat fluxes (30 min average) from the meteorological station (blue line) at the Spectacle Reef Lighthouse for the year 2010

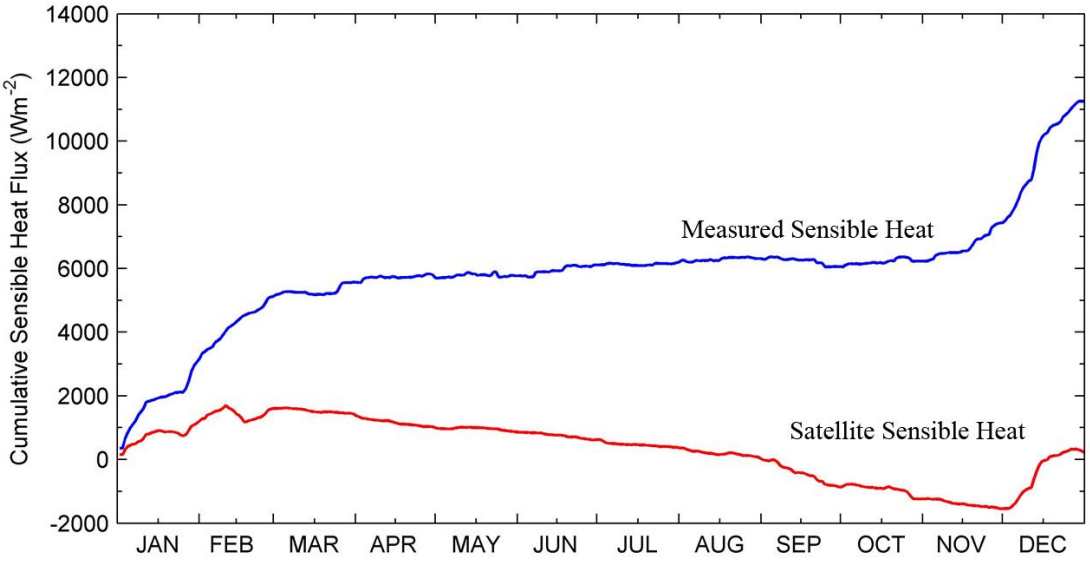

Figure 4.10 Cumulative satellite sensible heat fluxes (red line) and cumulative observed sensible heat fluxes (30 min average) from the meteorological station (blue line) at the Spectacle Reef Lighthouse for the year 2010

4.5.2.3 Comparison of the entire lake fluxes with the heat fluxes at the lighthouse location

Figures 4.11 and 4.12 show the individual pixel value of heat fluxes at the area of 25 km^2 surrounding Spectacle Reef Lighthouse compared to the whole lake mean flux values. For the latent heat flux, both values generally had the same trend over the study period, but they had different magnitudes. The lighthouse pixel values had higher amplitude than the values for the whole lake mean flux, particularly in the winter season. Negative latent heat fluxes indicated the condensation of water on the lake surface.

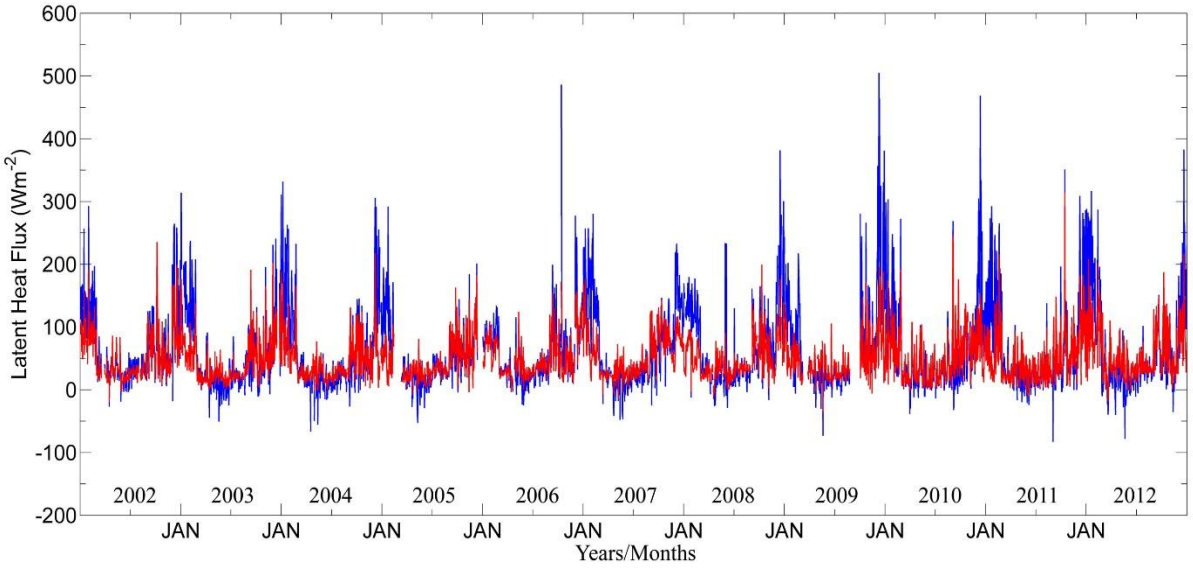

Figure 4.11 The individual pixel value of latent heat fluxes at the area of Spectacle Reef Lighthouse (blue line) compared to the whole lake mean latent heat fluxes (red line) for the period 2002-2012

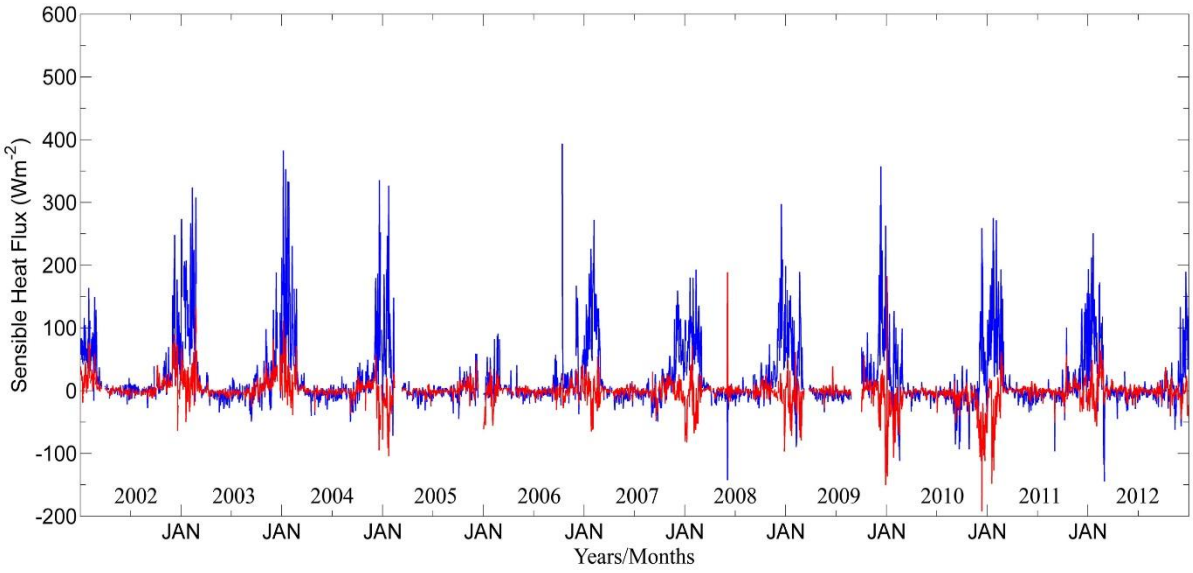

Figure 4.12 The individual pixel value of sensible heat fluxes at the area of Spectacle Reef Lighthouse (blue line) compared to the whole lake mean sensible heat fluxes (red line) for the period 2002-2012

The transfer of the sensible heat flux between the lake water surface and air normally follows the same temporal variation pattern as the latent heat flux. The results revealed similar patterns when the single pixel flux values over the Spectacle Reef Lighthouse were examined. However, when the mean sensible heat over the whole lake area was considered, there were negative values in the winter season of the years 2004-2005, 2005-2006, 2006-2007, 2007-2008, 2008-2009, 2009-2010, and 2010-2011. This indicated that the air temperature was higher than the temperature of the water surface, and that the sensible heat was transferred from the air to the lake surface, which is incorrect. According to the observations, this situation did not occur during the winter season when the water surface temperature was higher than the air temperature.

This situation might have been due to the over-estimation of the air temperature during the winter time from the MOD07 atmospheric profile product, particularly in the mid-lake region, and/or because of the spatial heterogeneity of the air temperature, which was lower near

the shore (and also in the northern lake region) and higher in the middle of the lake in the winter time. Figure 4.13 shows the mean water surface temperature and air temperature during the winter season. The surface water temperature was higher than the air over the lighthouse, which was located near the shoreline. Thus the sensible heat flux followed the known trend (i.e. the sensible heat flux was transferred from the surface to the atmosphere). In contrast, in the mid-lake region, the air temperature was higher than the water surface temperature, and thus the sensible heat flux was negative. There were no in-situ data available for the air temperature in the mid-region of the lake in the winter season. Therefore, the validations for the air temperature in those areas were not possible.

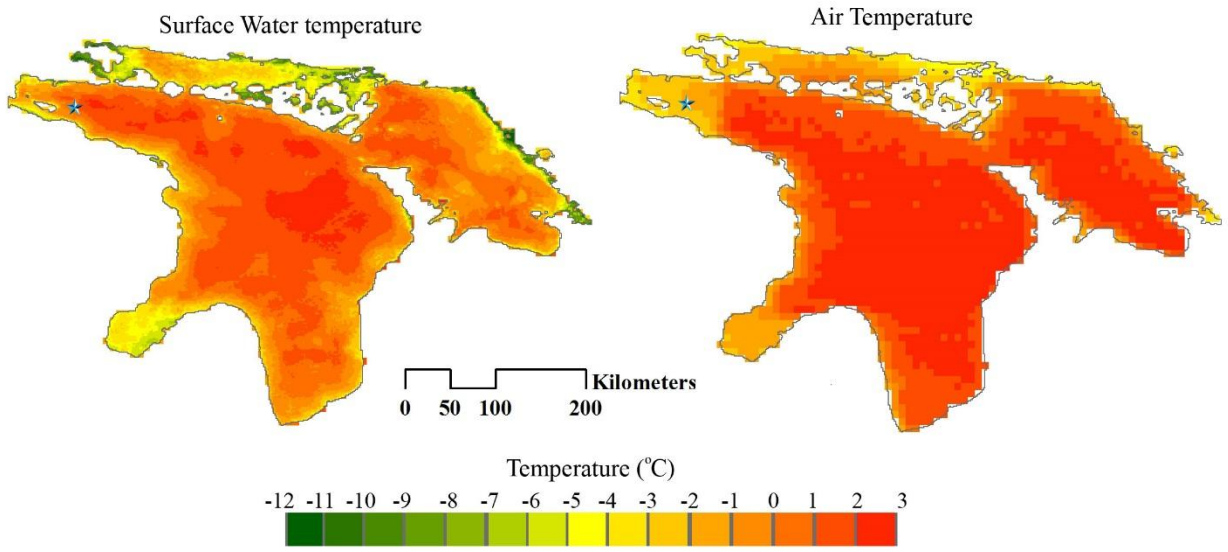

Figure 4.13. Mean surface (left) and air (right) temperature over Lake Huron during the winter season of 2003/2004. The blue star presents the location of Spectacle Reef Lighthouse.

The latent heat flux was also affected by MODIS overestimation of air temperature; however, it was less affected compared to the sensible heat flux estimation. This was because the calculation of latent heat flux depends on the vapour pressure gradient (Eq. 4.4), whereas the sensible heat flux depends mainly on surface and air temperatures (Eq. 4.9).

The MODIS data compared well with the in-situ data and a reasonable air temperature at the location of the lighthouse was obtained during the wintertime. The higher values of air temperature compared to the water surface temperature in the mid-lake region could be explained by two aspects. First, by nature a large lake may have a higher air temperature than situ surface temperature in the mid-region. Second, different atmospheric conditions near situ shoreline and the middle of the lake may exist, and thus the magnitude of attenuation to the satellite signal varies between the two areas. Currently, these two possible reasons could not be proven due to a lack of surface-based measurements in the middle of the lake during the winter season.

As mentioned earlier, the mean sensible heat over the whole lake area was underestimated (negative value) during the winter season for the years 2004-2005, 2005-2006, 2006-2007, 2007-2008, 2008-2009, 2009-2010, and 2010-2011. Those years had negative sensible heat values, because the estimation of the sensible heat was affected by overestimation of the air temperature. Therefore, these years were not used to study the spatial distribution of all energy balance components.

4.5.3 Energy balance components and their spatial distribution

In this chapter, the energy balance components for the years 2002-2004 and 2012, which were less affected by errors in the sensible heat flux calculation due to the uncertainty in air

temperature, are presented. The mean seasonal instantaneous surface energy balance components with spatial standard deviation values are presented in Table 4.4. Net radiation and heat storage reached their highest values in the summer season (months JJA) and the lowest values were in the winter season (months DJF). In contrast, the latent and sensible heat fluxes reached their seasonal maximum in the winter periods and their minimum intensity during the spring and summer periods.

Table 4.4 Seasonal mean heat fluxes (W m^{-2}) average over Lake Huron, with spatial standard deviation in parentheses. The value was based on the heat fluxes of 2002 to 2004 and 2012

Season	Latent heat flux	Sensible heat flux	Net radiative flux	Heat storage
Winter (DJF)	84.04 (27.27)	14.94 (33.18)	224.57 (14.69)	125.59 (67.44)
Spring (MAM)	29.49 (36.01)	0.28 (3.35)	620.80 (14.78)	591.03 (30.82)
Summer(JJA)	26.15 (11.69)	-2.45 (4.25)	755.56 (13.27)	731.86 (27.12)
Fall (MAM)	59.82 (7.73)	3.52 (3.72)	394.46 (13.47)	331.11 (19.15)

The spatial distributions of the average seasonal surface energy balance components, including net radiation, latent heat flux, sensible heat flux, and the heat storage term for Lake Huron obtained from the remote sensing satellite and meteorological data between 2002 to 2004 and 2012, were produced. The color (and gray scale) schemes illustrated seasonal mean instantaneous (i.e. during the satellite overpass) radiation and heat flux values, and the dark (cold tone color) areas represented the lower values of heat fluxes and radiation, while the bright (warm tone color) areas meant higher intensities of heat fluxes and radiation fluxes. The following are details of the spatial distribution for each surface energy balance component.

4.5.3.1. Net radiation

The daily instantaneous net radiation calculated from the previous chapter was reproduced to a seasonal average as shown in Figure 4.14. The net radiation was mainly controlled by incident solar radiation, adjusted by cloud cover, and surface albedo. It was also influenced by the incoming long-wave radiation as a function of air temperature, vapour pressure, and cloud cover, and by outgoing long-wave radiation, depending on the lake surface water temperature.

In the winter (DJF), the spatial distribution of the net radiation had an approximately regular latitudinal pattern, which was primary controlled by the solar zenith angle. The winter presented the lowest mean radiation value of 224.57 W m^{-2} (Table 4.4). During spring (MAM), with the increase of solar elevation, the net radiation increased to almost three times the mean winter value, but the latitudinal character was not obvious.

In the summer (JJA), the spatial distribution of net radiation over the lake did not show a latitudinal trend. The variability of net radiation was related to the lake's surface temperature and the presence or absence of cloud cover. In the fall (SON), the net radiation decreased and it was almost two times less than the mean net radiation for the summer. This was primarily due to the decrease in solar elevation.

4.5.3.2 Latent heat flux

The transfer of latent heat from the lake surface was mainly controlled by wind speed, water temperature, air temperature, and amount of vapour pressure. There were large latent heat fluxes in the wintertime and much smaller values in spring and summer (Table 4.4). The seasonal mean spatial variability of the latent heat fluxes is presented in Figure 4.15. The winter

period exhibited the greatest latent heat flux over the lake-wide area, particularly in the middle and northern part of the lake. This was because of the low humidity of the cold air covering the lake surface and the high surface water temperature (compared to the air temperature), which introduced high humidity on the lake water surface.

In the spring, the air was warm, whereas the lake surface water temperature was relatively cool. The latent heat had noticeably weaker intensity during this time and continued through early summer. Small values of latent heat flux were present in most areas of the lake except for the southern shore line. Almost all of the net radiation that reached the lake between spring and summer period was used to heat the water (increase the heat storage, Table 4.4).

In the summer, the area of small active latent heat extended from the lake shorelines, especially in the southern part, toward the deeper area at the mid-region of the lake. During the fall, most of the lake had a large latent heat flux because the high heat capacity of the lake resulted in continued high water temperatures (thus high saturation vapour pressures) and in the meantime the air temperature and humidity decreased and the rate of their decrease was greater than the decrease in the surface water temperature. This aspect lead to a further increase in the magnitude of latent heat flux in the fall and this increase of latent heat flux continued through the winter season. Since these turbulent heat fluxes were estimated on the basis of an ice-free surface condition, the received fluxes for January through March might have been overestimated because the fluxes could have been transferred between the water surface and atmosphere freely.

The seasonal cycle of latent heat flux from the present study was compared with other studies of the Great Lakes. Lofgren and Zhu (2000) for example calculated turbulent heat (under the assumption of an ice-free surface) using the satellite water surface temperature and other meteorological data during the period 1992-1995. Similar to the present study's results, they

obtained high values of latent heat flux during the winter and smaller values in the summer. This result is also similar to the study of Blanken *et al.* (2011) and Spence *et al.* (2011), who found a strong seasonal pattern of evaporation over Lake Superior, with a peak in December and January and very low evaporation in August and March.

Although the present results were agreement with previous studies, the turbulent heat fluxes were calculated on the assumption of a homogeneous wind speed for the entire lake, because there were no multiple meteorological stations covering the entire lake. Therefore, this may have led to uncertainty concerning the resulting fluxes because of the spatial variability in the wind speed.

4.5.3.3 Sensible heat flux

The transfer of the sensible heat flux between the lake water surface and air usually follows the same temporal variation pattern as the latent heat flux. The sensible heat flux demonstrates high intensity in winter and much less intensity in spring and summer (table 4.4). In the winter season for the years 2004-2005, 2005-2006, 2006-2007, 2007-2008, 2008-2009, 2009-2010, and 2010-2011, as mentioned earlier, the sensible heat over the whole lake area was negative (i.e. heat was transferred from the air to the lake surface) due to the overestimation of the MODIS air temperature in the mid-region of the lake. Therefore, spatial distributions of the average seasonal latent heat between 2002 to 2004 and 2012 were produced. However, even for these years, the effects from the overestimated air temperature were still apparent in the winter season, especially in the mid-region of the lake.

The seasonal mean spatial variability of the sensible heat fluxes is presented in Figure 4.16. Winter had the highest sensible heat flux over most of the area, particularly in the northern

- western part of the lake (though the middle part of the lake showed lower values because of the effect of the overestimated air temperature). The high average sensible heat in the winter was due to the fact that the surface water was warmer than the overlying air.

The magnitude of the sensible heat flux in the spring and summer time was similar, much lesser than that in the winter time. This indicated that the lake water surface was cooler than the overlying air during both seasons. However, the spatial distribution characteristics were different. In the spring, the sensible heat was lower near the shoreline than in the mid-lake region. In contrast, during the summertime, the lake area near the shoreline had relatively higher sensible heat than in the mid-lake region. In the fall, the lake still had a high temperature compared to the air, whereas the air temperature declined. For this season, the sensible heat began to increase.

Similar to the latent heat flux, the results for the sensible heat flux spatial estimates were compared with the study of Lofgren and Zhu (2000). There was good agreement between the present study's results and theirs, except during the winter, when in the present study the sensible heat flux tended to be larger in the northern part of the lake than in other lake areas, whereas their study showed a great intensity of sensible heat in the mid-lake region. This was mainly due to the MODIS air temperature over estimation in the middle part of the lake during the wintertime, which resulted in an underestimation of the sensible heat flux in those regions.

4.5.3.4 Heat storage

Energy stored or released from the lake is one of the most difficult terms to estimate when water temperature profiles are not available. For this study, the heat storage term was

estimated as a residual of the energy balance (Eq. 4.11). The heat stored or released from the lake followed the same temporal variation pattern (but opposite sign) of the net radiation.

The heat storage in the winter presented the lowest mean values due to the decrease of net radiation, while the lake released heat in the form of latent and sensible heat. Figure 4.17 shows that the lower lake heat storage occurred in the north-western area, whereas higher intensity was seen in the southern part of the lake.

During the spring and summer, with the increase in net radiation and a decrease in latent and sensible heat, the heat storage increased and reached maximum intensity in the summer. This indicated that most of the energy was used to warm the water. The highest values of the stored heat were in the middle (deep water) of the lake and lowest values near the lake shoreline.

The heat storage began to decrease during the fall and early winter because of the decrease in net radiation and also because of the loss of energy due to the transfer of latent and sensible heat flux to the atmosphere. During this period the temperature of lake water surface was higher than the overlying air.

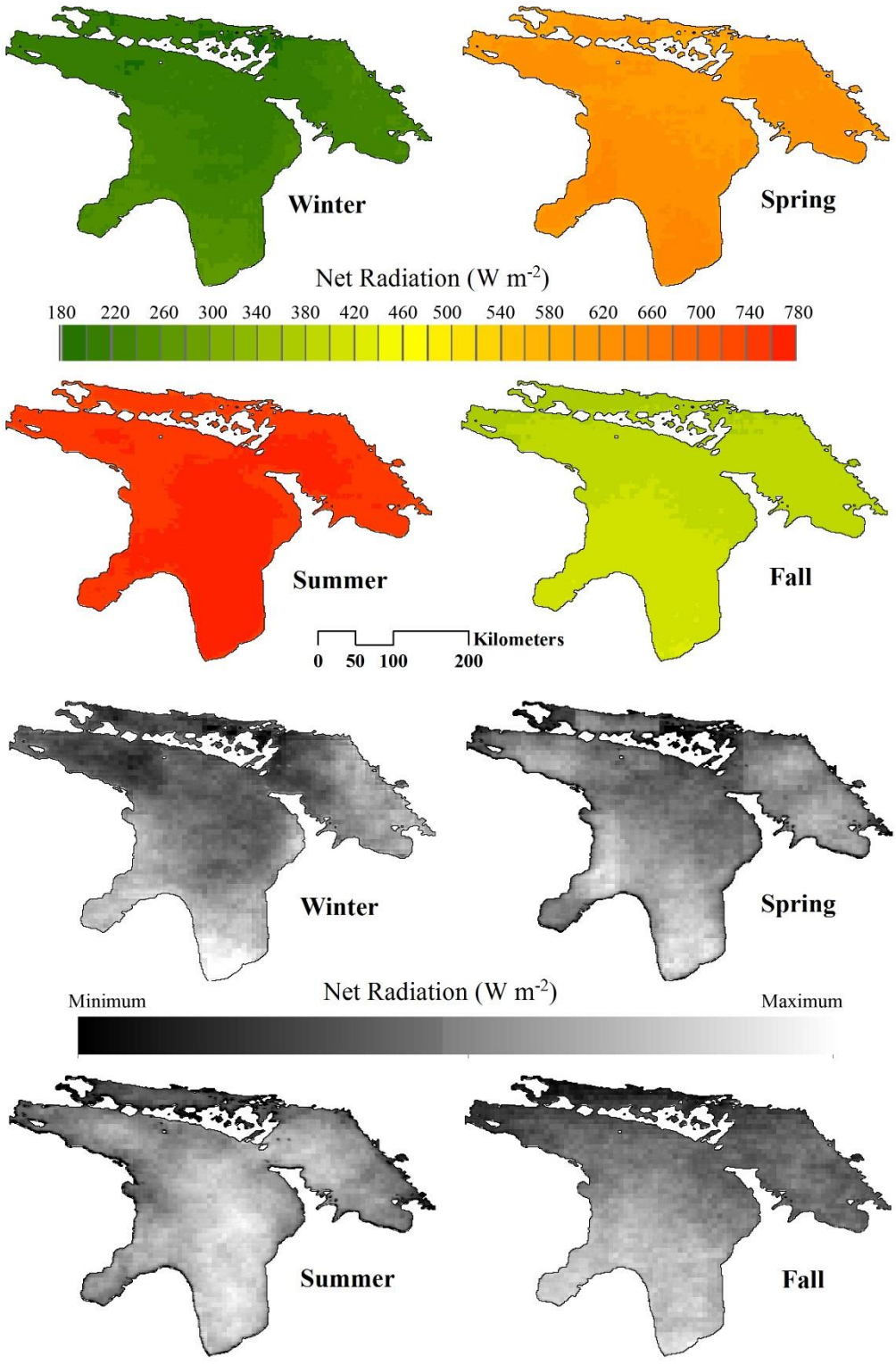

Figure 4.14 Seasonal average spatial distribution of net radiation (in W m^{-2}) for the years 2002-2004 and 2012. The gray scale in the lower part shows the radiation variability of each season

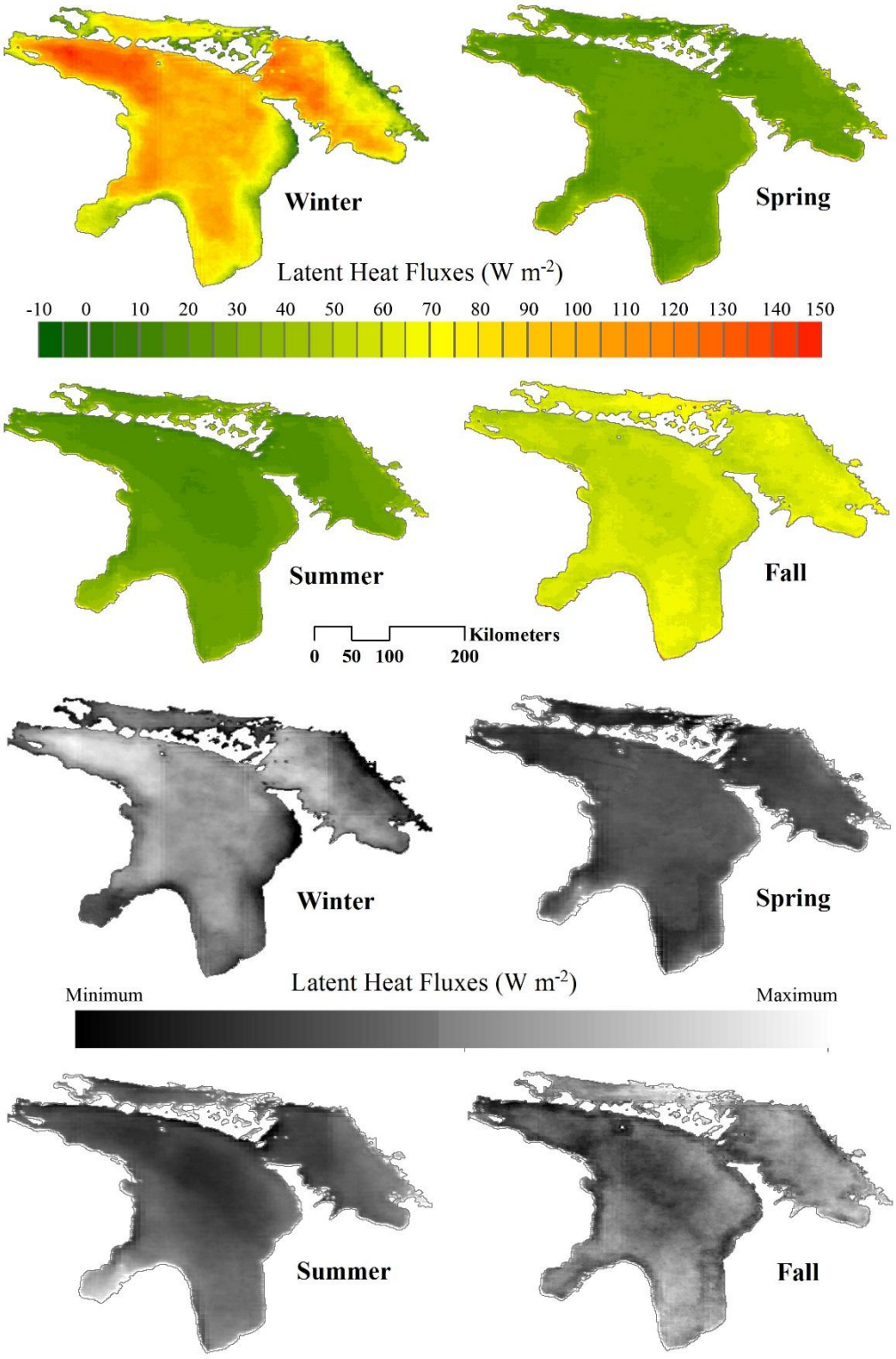

Figure 4.15 Seasonal average spatial distribution of latent heat flux (in W m^{-2}) for the years 2002-2004 and 2012. The gray scale in the lower part shows the radiation variability of each season.

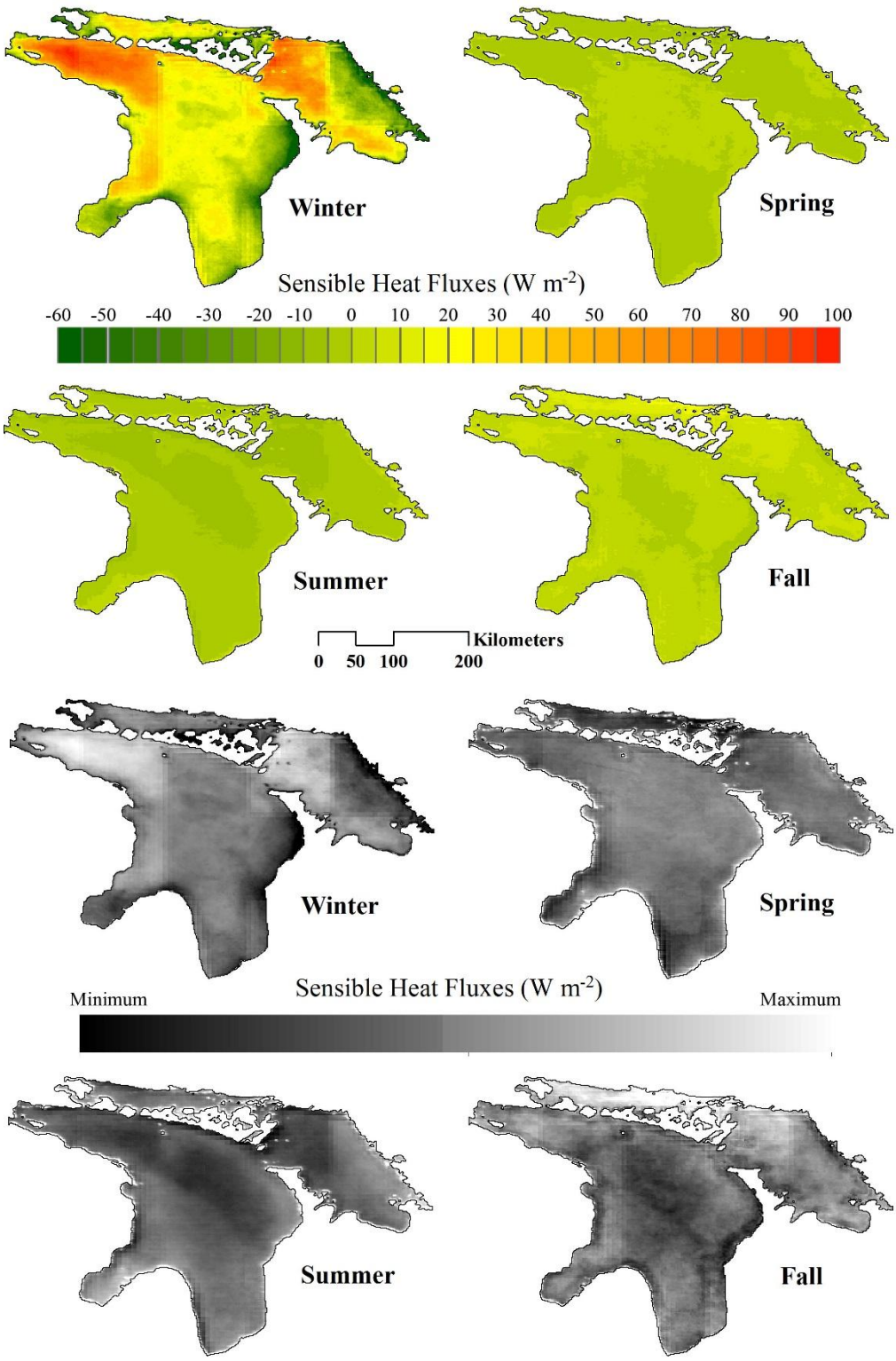

Figure 4.16 Seasonal average spatial distribution of sensible heat flux (in W m^{-2}) for the years 2002-2004 and 2012. The gray scale in the lower part shows the radiation variability of each season.

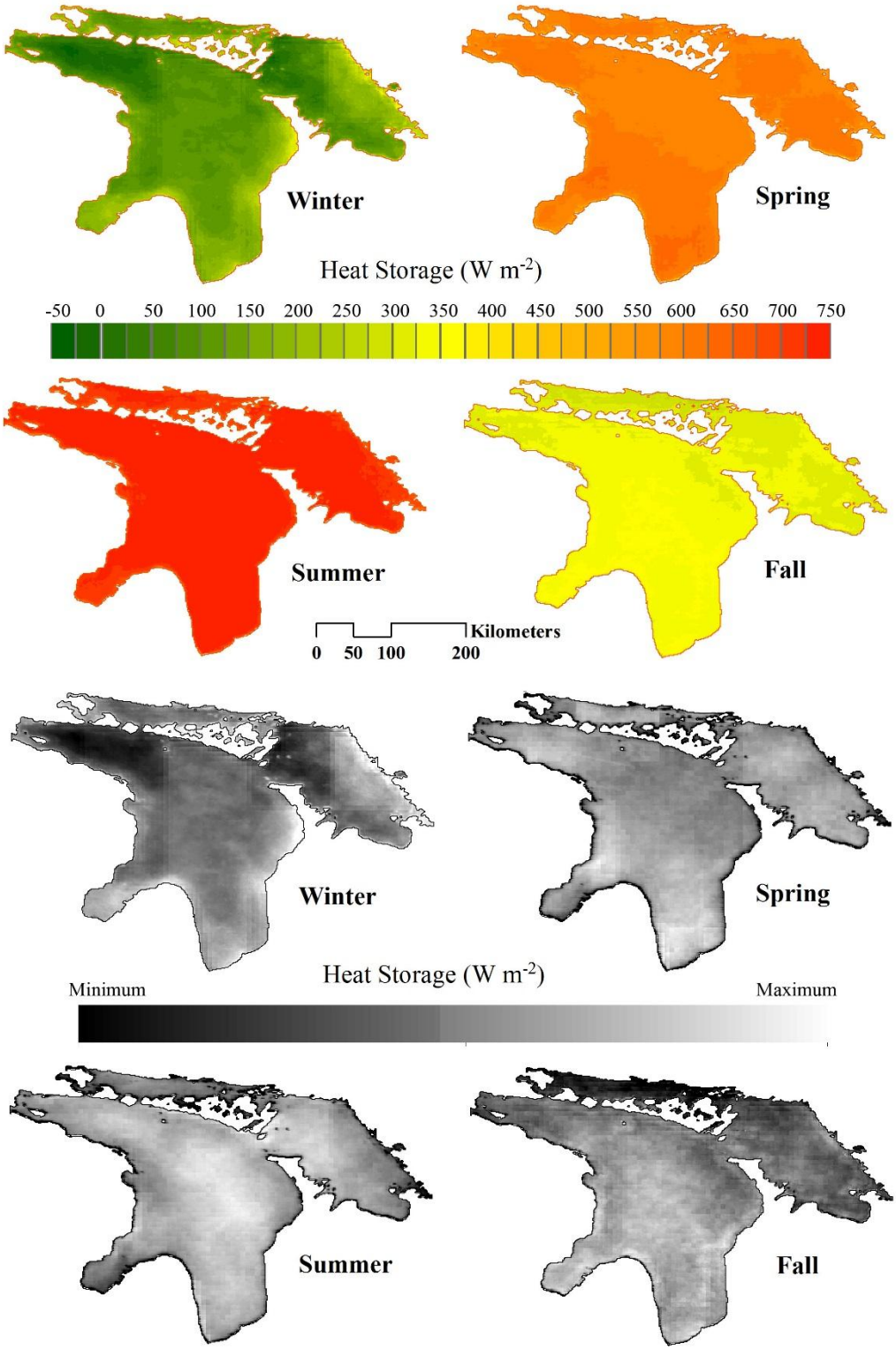

Figure 4.17 Seasonal average spatial distribution of heat storage (in W m^{-2}) for the years 2002-2004 and 2012. The gray scale in the lower part shows the radiation variability of each season.

4.5.4 Change in the surface energy balance

Due to the underestimation of the sensible heat flux in the mid-lake regions in the wintertime, the study of the long-term changes in the surface energy balance was investigated in the area surrounding the Spectacle Reef Lighthouse. Figure 4.18 shows the seasonal surface energy balance components for the study period. The seasonal latent heat estimated from the satellite for the period of 2010-2011 was very close to the estimates of the eddy correlation method (R^2 = 0.95). The maximum net radiation was received during the summer when it reached a value greater than 700 Wm^{-2} and the minimum was in the winter (~200 W m^{-2}). Almost all of the net radiation was stored as heat in the lake. In the fall, the net radiation began to decrease and the lake started to release the stored energy into the atmosphere through sensible and latent heat fluxes by releasing all of the stored heat. The latent and sensible heat fluxes reached their maximum in the winter. The spatial ice cover data were not accounted for in the estimation of the heat fluxes and thus the results of the turbulent heat fluxes presented in this study during the winter season might have been overestimated, particularly during exceptionally cold years (2003 and 2009, Figure 4.19). This is because the turbulent heat fluxes could have been greatly reduced by the formation of ice (Blanken *et al*., 2011).

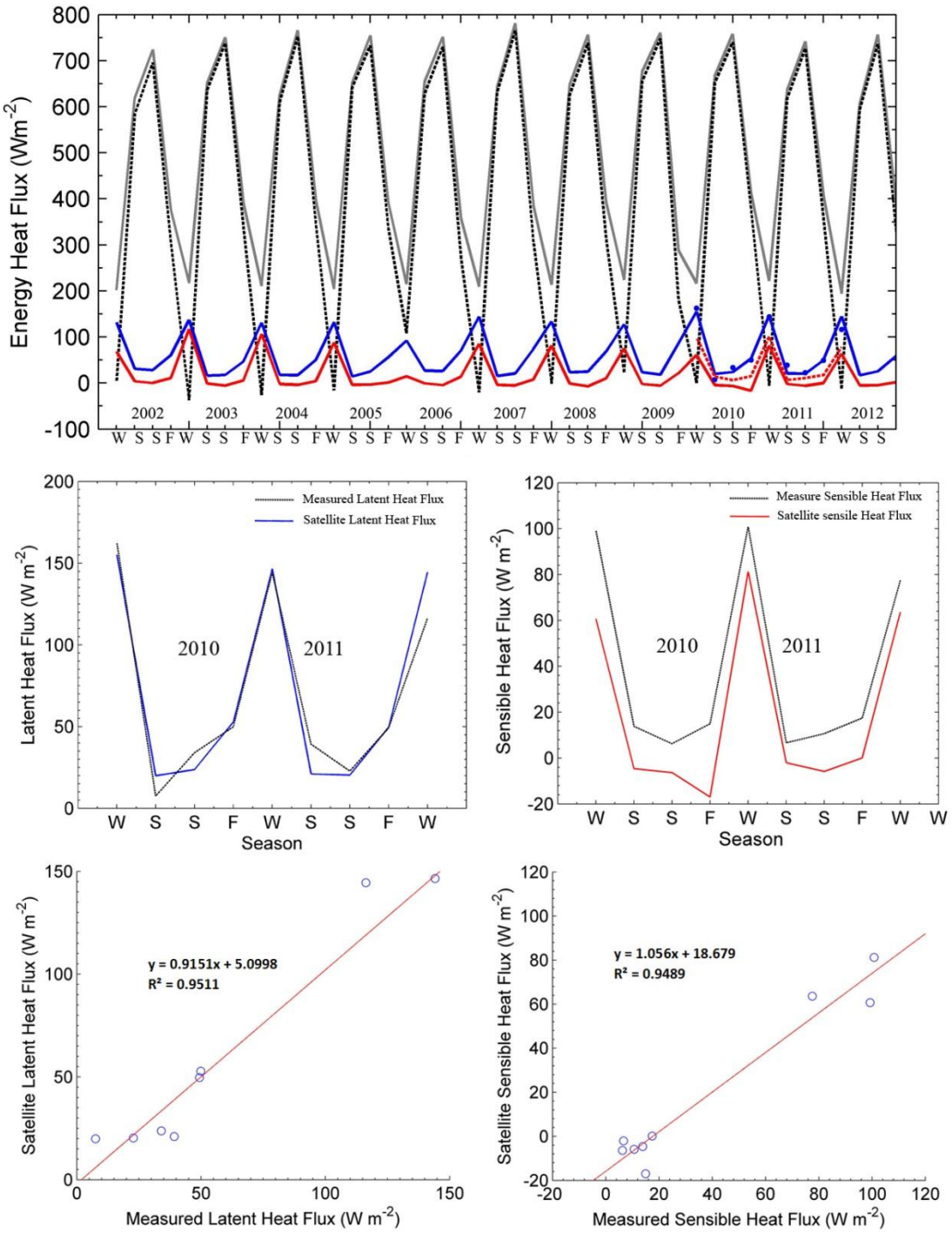

Figure 4.18 (Top Panel) Seasonal surface energy balance components for the period 2002-2012. Net radiation is the grey dotted line, the gray color is heat storage, and the blue and red represent latent and sensible heat fluxes, respectively. The blue and red dotted line (year 2010-2011) show the latent (blue) and sensible (red) heat derived using the eddy covariance method. The middle and lower panel present a comparison and scatter plot of the seasonal satellite turbulent heat fluxes derived using the eddy covariance method.

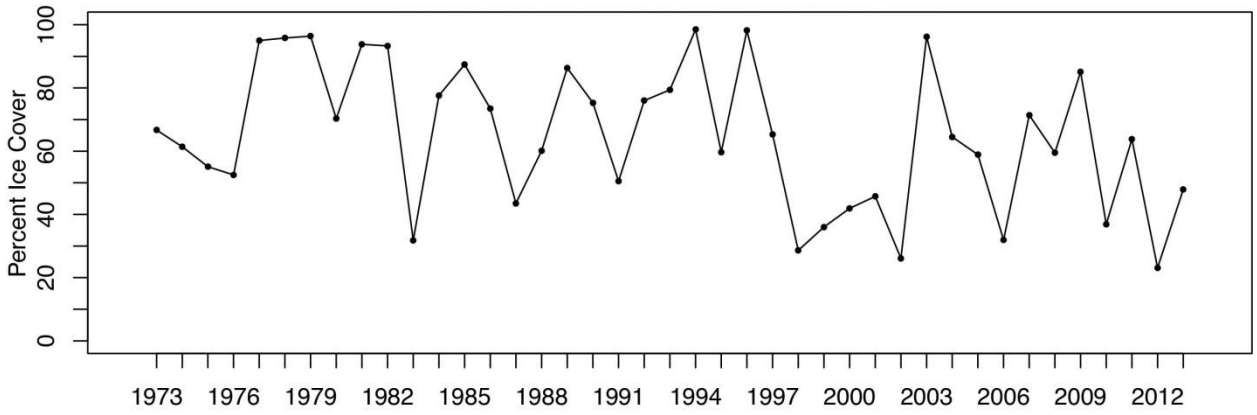

Figure 4.19 Lake Huron annual maximum ice cover during the period 1972-2013. Data Source: Great Lakes Environmental Research Laboratory, National Oceanic and Atmospheric Administration. http://www.glerl.noaa.gov/data/ice/

Figure 4.20 - 4.23 shows the time series for the mean seasonal surface energy balance on the lake's surface and the trend line for the 11-year period (2002–2012). In the winter, the seasonal trend exhibited an increase in net radiation, latent heat, and heat storage, whereas the sensible heat declined. In the spring, the net radiation and heat storage had the same trend as during the winter (i.e. increased), while the turbulent heat fluxes exhibited a negative trend. In the summer, there was a decrease in net radiation and sensible heat; however, the heat storage and latent heat flux increased. For the fall season, only the latent heat exhibited a positive trend. However, for none of the components was the trend statistically significant, except for the sensible heat flux. This indicated no seasonal long-term changes in the energy balance components. The statistically-significant, negative sensible heat trend was partly due to errors in estimating the air temperature.

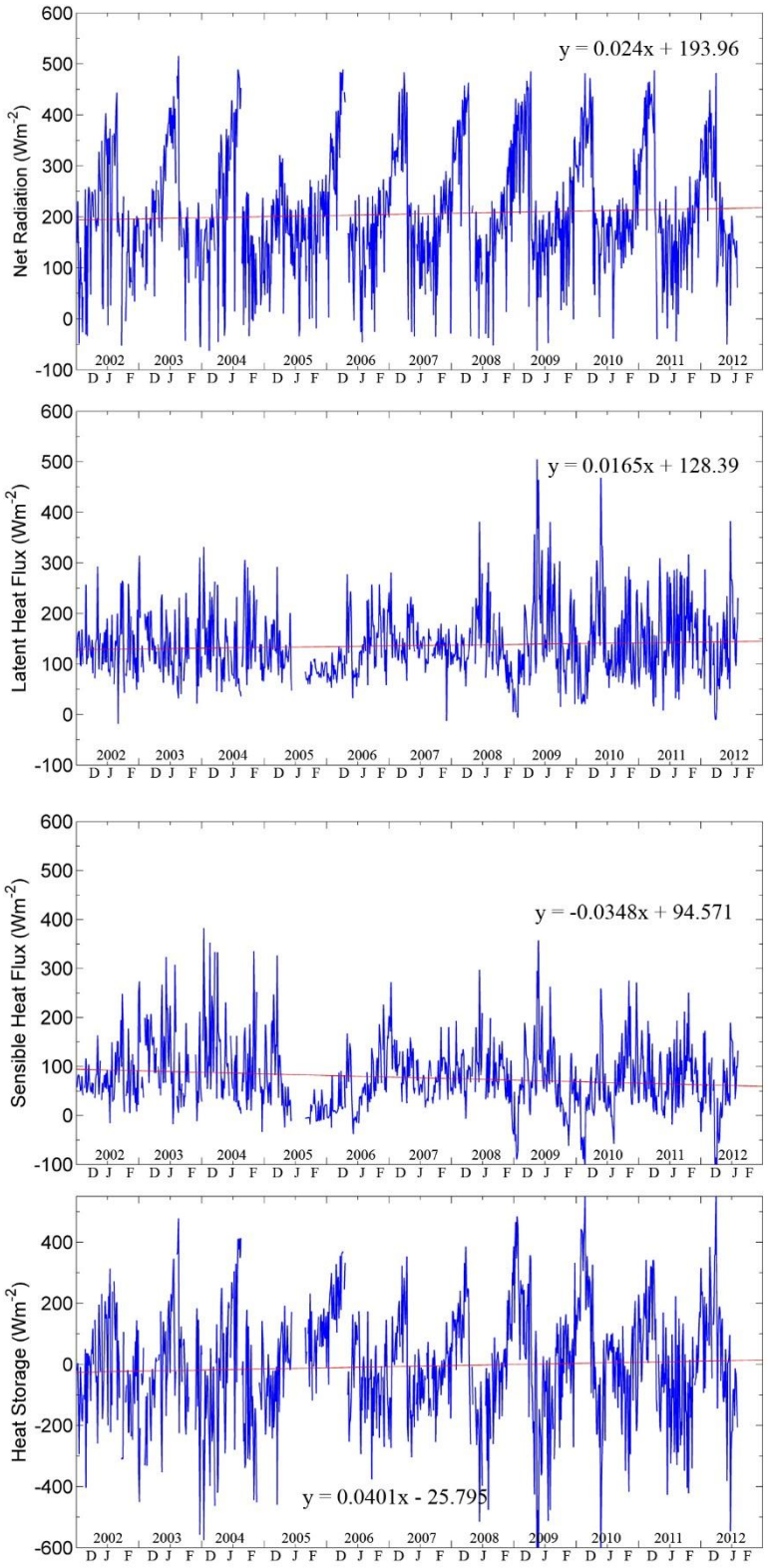

Figure 4.20 Time series for the daily surface energy balance components during the winter season (DJF) and the trend line for the 11-year period (2002-2012)

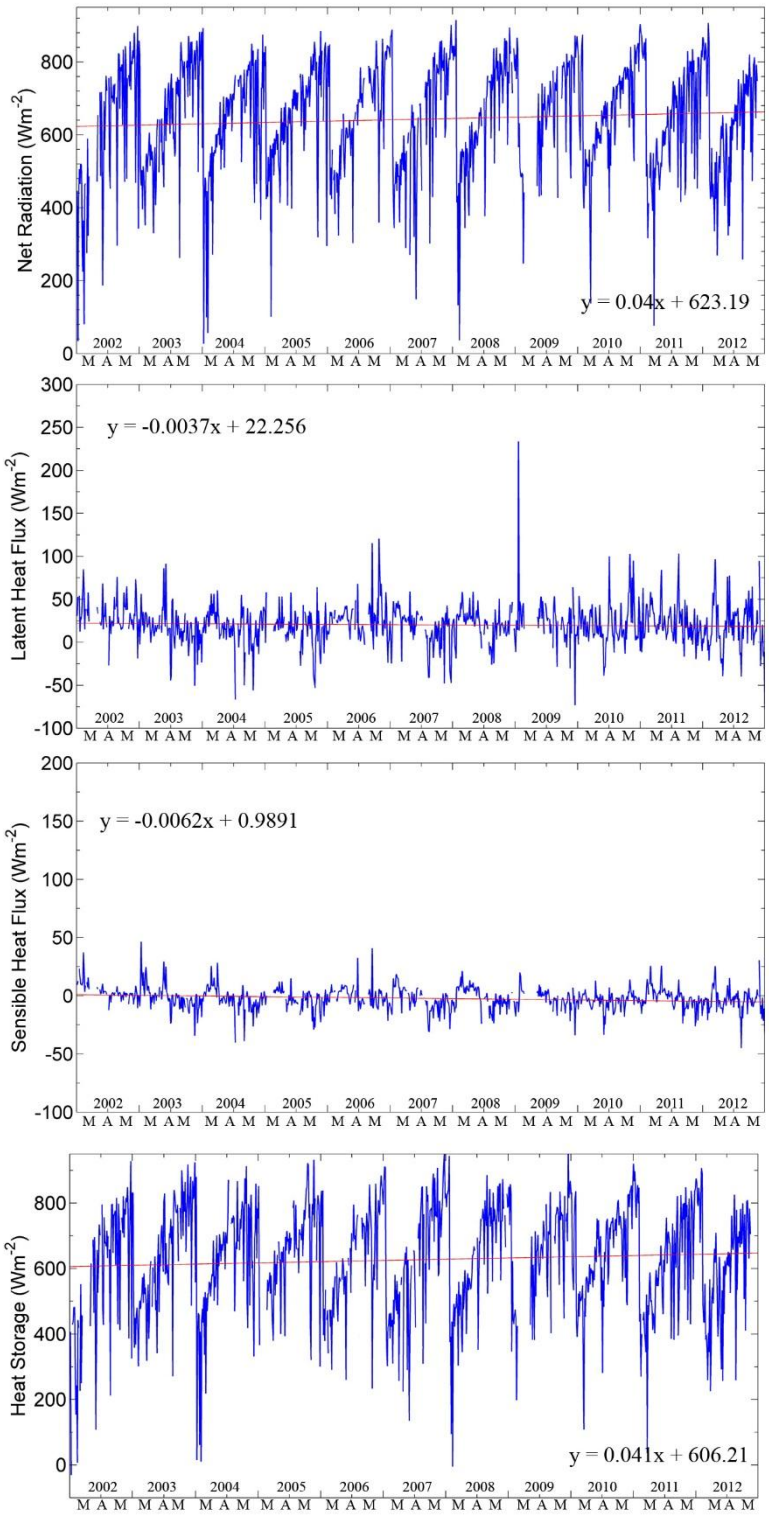

Figure 4.21 Time series for the daily surface energy balance components during the spring season (MAM) and the trend line for the 11-year period (2002-2012)

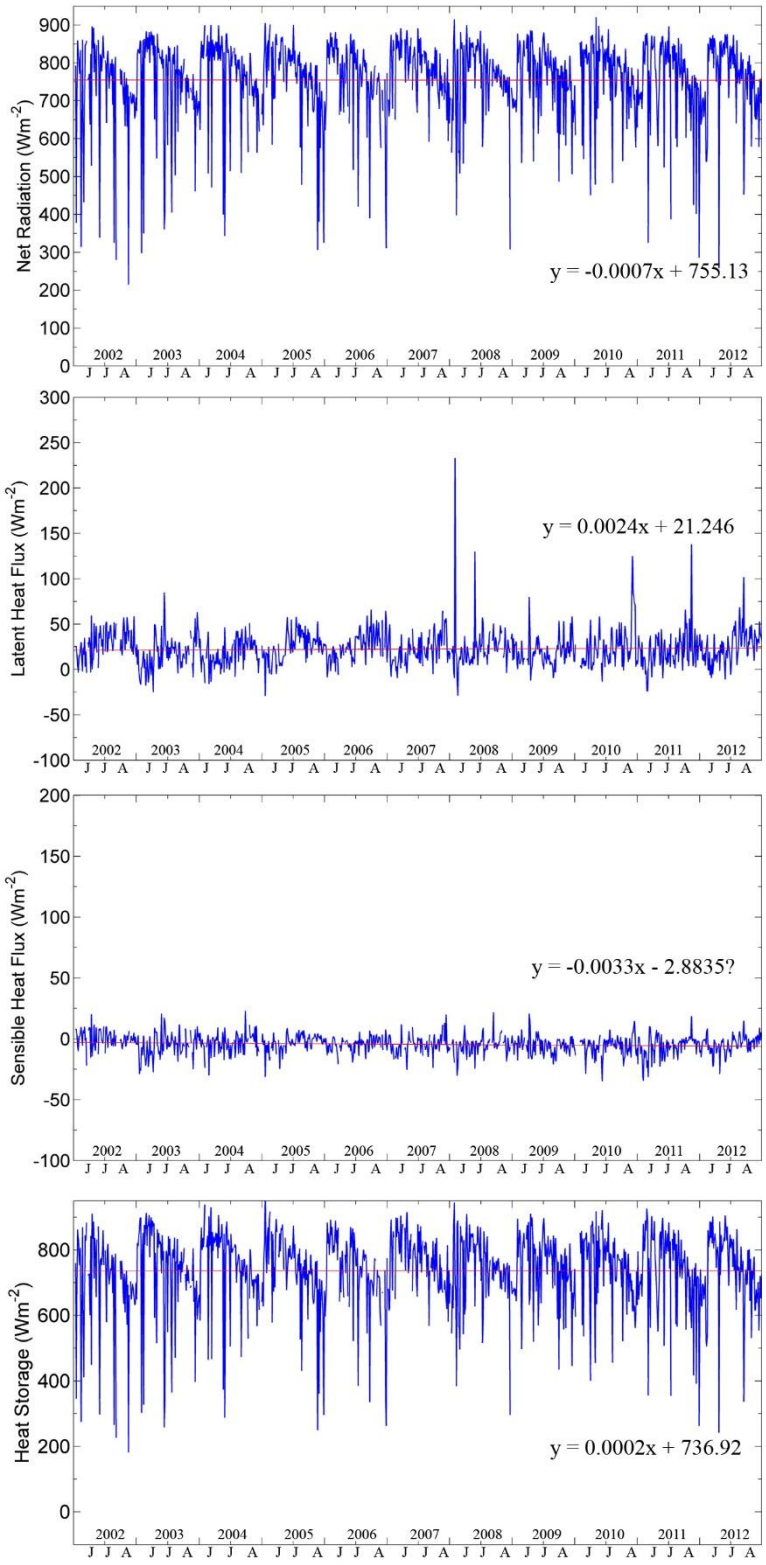

Figure 4.22 Time series for the daily surface energy balance components during the summer season (JJA) and the trend line for the 11-year period (2002-2012)

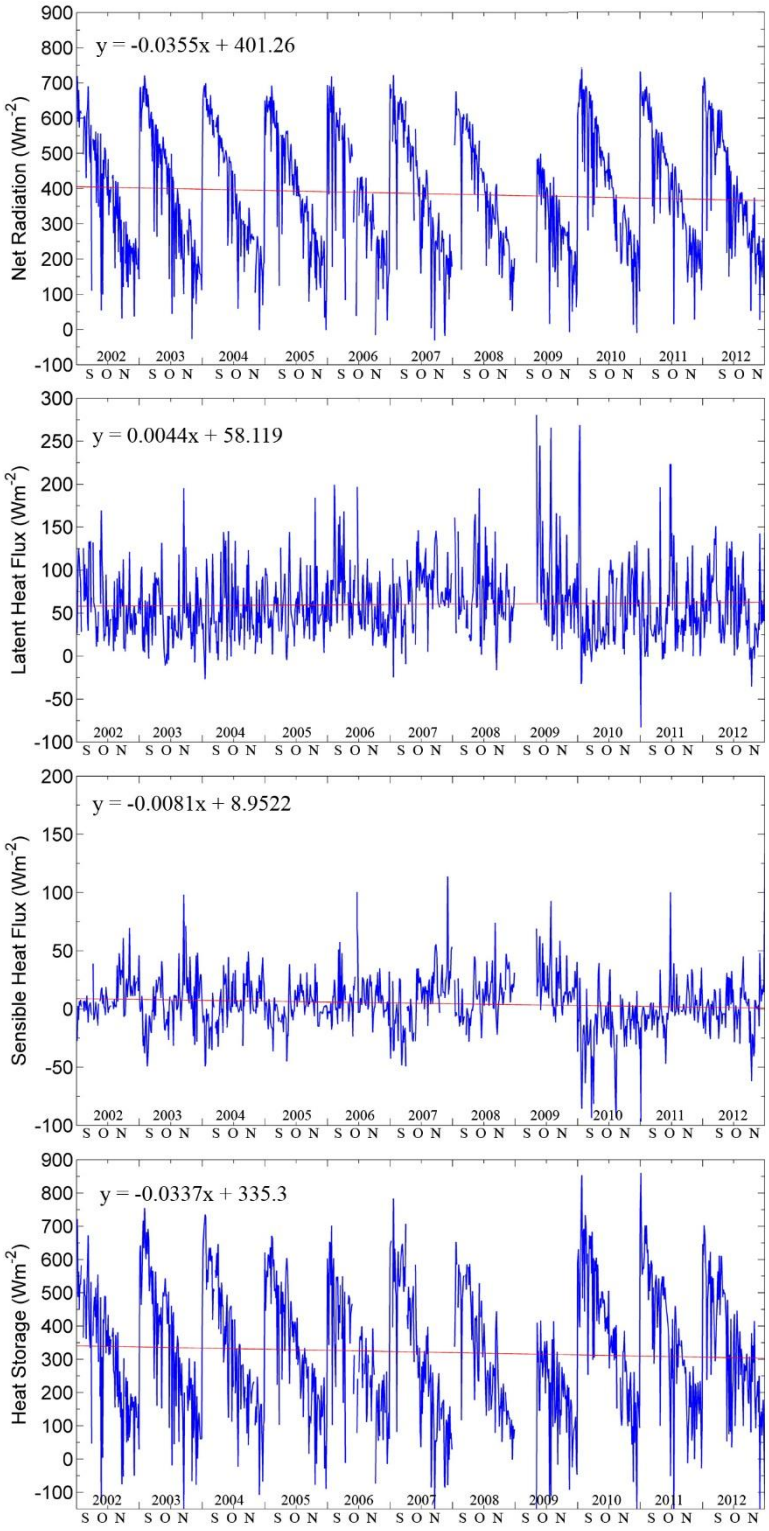

Figure 4.23 Time series for the daily surface energy balance components during the fall season (SON) and the trend line for the 11-year period (2002-2012)

4.6 Conclusion

The inter-annual and long-term variability of the surface energy balance components were estimated using the MODIS data together with field measurements. The bulk method was applied to derive the latent and sensible heat fluxes. the bulk transfer coefficients were estimated using the eddy correlation method and values between 0.54×10^{-3} to 2.71×10^{-3} were obtained for the latent heat and 1.83×10^{-3} to 0.21×10^{-3} were calculated for the sensible heat.

A correlation was found between the turbulent heat fluxes calculated from satellite data and those from the eddy covariance method. The correlation coefficient was 0.54 for the latent heat flux and 0.59 for the sensible heat fluxes. Both latent heat and sensible heat fluxes calculated from remotely-sensed data were underestimated by ~50%. However, the seasonal and annual values of the two methods were very close to the correlation coefficient of .95. The agreement between the seasonal satellite and in-situ data was good enough to suggest that these latent heat fluxes from the satellite sources were reliable. The major uncertainty occurred in the estimation of the sensible heat flux, which was underestimated in the mid-lake region due to the unusual high satellite air temperature during the winter season. This overestimation could not be confirmed or validated because there were no other ground measurements in the mid-lake region.

The spatial distribution of the surface energy balance components showed temporal and spatial heterogeneities. There was a strong seasonal pattern for all of the energy balance components, which was very high in summer and low in winter for net radiation and heat storage. In contrast, latent heat and sensible heat were very high in the winter and very low in the summer. The study found that there was no significant change in the energy balance components during the study period.

Validation is an essential component of most satellite data-based studies. This study validated the remote sensing data with in-situ data from the meteorological station at the Spectacle Reef Lighthouse located in the most north-western region of Lake Huron. Although the lake has a homogenous surface, the study results showed an unusual large difference in the satellite winter air temperature between various parts of the lake, particularly in the mid-lake region. Therefore, it is very important to have additional in-situ measurements for the mid-lake region.

Use of satellite data for computing the surface energy balance proved that better spatial distribution and spatial coverage can be obtained. To the best of author knowledge, this study is the first time that remotely-sensed data have been used to study most long-term surface energy balance under all sky conditions, and thus it has a potential to estimate most surface energy budget globally. Additionally, the information provided in this study can be an important parameter for exploring the cause of the recent water-level change phenomenon.

4.7 Bibliography

Alcantara E.H., Stech J.L., Lorenzzetti J.A., Bonnet M.P., Casamitjana X., Assireu A.T. 2010. Remote sensing of water surface temperature and heat flux over a tropical hydroelectric reservoir. *Remote Sensing of the Environment*, 114, 2651-2665

Assel A.R., Quinn F.H., Sellinger C.E. 2004. Hydroclimatic factors of the recent record drop in Laurentian Great Lakes water levels. *American Meteorological Society*, 85(8), 1143-1151

Blanken P.D., Rouse W.R., Culf A.D., Spence C., Boudreau L.D., Jasper J.N., Kochtubajda B., Scertzer W.M., Marsh P., Verseghy D., 2000. Eddy covariance measurements of evaporation from Great Slave Lake, Northwest Territories, Canada. *Water Resources Research*, 36(4), 1069–1077.

Blanken P.D., Spence. C, Hedstrom N, Lenters J.D. 2011. Evaporation from Lake Superior: 1. Physical controls and processes. *Journal of Great Lake Research*, 37, 707-716

Bolsenga S.J. 1975. Estimating energy budget components to determine Lake Huron evaporation. *Water Resources Research*, 11**,** 661 – 666

Changnon S.A. 2004. Temporal behavior of levels of the Great Lakesand climate variability. *Journal of Great Lakes Research*, 30, 184–200

Derecki J.A. 1981. Stability effects on Great Lakes evaporation. *Journal of Great Lake Research*, 7(4), 357-362

Gianniou S.K., Antonopoulos V.Z., 2007. Evaporation and energy budget in Lake Vegoritis, Greece. *Journal of Hydrology*, 345, 212-223

Granger R., Bussieres N. 2005. Evaporation/evapotranspiration estimates with remote sensing. *Remote Sensing in Northern Hydrology*. Dugua C.R., Pietroniro A. Eds. Washington, D C. American Geophysical Union

Hartmann H.C. 1990. Climate change impacts on laurentian great lake levels. *Climatic Change*, 17, 49-67

Koutsoyiannis D. 2012. Clausius–Clapeyron equation and saturation vapour pressure: simple theory reconciled with practice. *European Journal of Physics*, 33, 295-305

Large W.G., Danabasoglu G., Doney S.C., McWilliams J.C. 1997. Sensitivity to surface forcing and boundary layer mixing in a Global Ocean Model: Annual-mean climatology. *Journal of Physical Oceanography*, 27, 2418-2446

Lenters J.D., Kratz T.K., Bowser C.J. 2005. Effects of climate variability on lake evaporation: Results from a long-term energy budget study of Sparkling Lake, northern Wisconsin (USA). *Journal of Hydrology*, 308, 168-195.

Lofgren B.M., Zhu Y. 2000. Surface energy fluxes on the Great Lakes based on satellite-observed surface temperatures 1992 to 1995. *Journal of Great Lake Research*, 26(3), 305-314

MacDonagh-Dumler J., Pebbles V., Gannon J. 2005. Great Lakes (North American) – experience and lessons learned brief. *ILEC. 2005. Managing Lakes and their Basins for Sustainable Use: A Report for Lake Basin Managers and Stakeholders*. International Lake Environment Committee Foundation. Kusatsu, Japan

Oke T.R. 1996. *Boundary Layer Climates*, 2nd ed, Methuen, London. 464 p

Quinn F.H. 1979. An improved aerodynamic evaporation technique for large lakes with application to the international field year for the Great Lakes. *Water Resource Research*, 15(4), 935-940

Rouse W.R., Oswald C.J., Binyamin J., Spence C., Schertzer W.M., Blanken P.D., Bussieres N., Duguay C.R. 2005. The role of Northern Lakes in a regional energy balance. *American Meteorological Society*, 291-305

Schertzer W.M., Assel R.A., Beletsky ,D., Croley II, T.E., Lofgren B.M., Saylor J.H., Schwab D.J. 2008. Lake Huron climatology, inter-lake exchange and mean circulation. *Aquatic Ecosystem Health & Managemen*, 11, 144 -152

Schertzer W.M., Taylor B. 2009. Assessment of the capability to compute lake evaporation from Lake Okanagan and its Mainstem Lakes using the existing database. *Project Report to the Okanagan Water Supply and Demand Study on Lake Evaporation*, 105 p

Sellinger C.E., Stow C.A., Lamon E.C., Qian S.S. 2008. Recent water level declines in the lake Michigan-Huron system. *Environmental Science & Technology*, 42, 367-373

Smedman A.F., Hogstrom U., Sahlee E., Johnansson C., 2007. Critical re-evaluation of the bulk transfer coefficient for sensible heat over the ocean during unstable and neutral conditions. *Quarterly Journal of the Royal meteorological Society*, 133:227-250

Spence C., Blanken P.D., Hedstrom N., Fortin V., Wilson H., 2011. Evaporation from Lake Superior: 2Spatial distribution and variability. *Journal of Great Lake Research*, 37, 717-724

Spence C., Rouse W.R. 2002. The energy budget of Canadian Shieldsubarctic terrain and its impact on hillslope hydrological processes. *Journal of Hydrometeorology*, 3, 208 – 218

Swenson S., Wahr J. (2009). Monitoring the water balance of Lake Victoria, East Africa, from space. *Journal of Hydrology*, 370, 163–176

Winter T.C., Buso D.C., Rosenberry D.O., Likens G.E., Sturrock A.M., Mau D.P. 2003. Evaporation determined by the energy-budget method for Mirror Lake, New Hampshire. *Limnology and Oceanography*, 48(3), 995–1009.

Yao H. 2009. Long-term study of lake evaporation and evaluation of seven estimation methods: results from Dickie Lake, South-Central Ontario, Canada. *Journal of Water Resource and Protection,* 2, 59 - 77

Zimmermann K.A. 2013. *Great Facts about the Five Great Lakes.* Retrieved from http://www.livescience.com/32081-lake-huron.html

CHAPTER 5

EVAPORATION FROM LAKE HURON AND WATER LEVEL FLUCTUATION

5.1 Introduction

Lake Huron water levels peak during the summer and they are a function of the relative magnitude of precipitation, evaporation, and runoff from the previous fall, winter, and spring seasons (Brinkmann, 2000). The water levels of the Great Lakes have varied overtime, and their random extremes have been demonstrated to be problematic. Although the annual cycle of water level has been quite well recognized, the longer-term and most severe variations have revealed a high level of unpredictable, and clear relationships of these water level rise and fall to climate changeability have been deficient (Hanrahan *et al.*, 2010).

The current phenomenon of water level fluctuation is an issue because it is constant with many climate change predictions, raising worry that the water level decline may continue (Sellinger *et al.*, 2008). Lake Huron is not controlled for hydroelectric or business navigation and is minor influenced by the inflow and outflow of the other lakes (Changnon, 2004). Thus, the changes in water levels in Lake Huron are mainly responding to climatic or additional large-scale forces, including physical control of surface energy balance.

Evaporation, one of the surface energy balance components, is a vital component in both the water and energy balances of reservoirs and lakes (Duan and Bastiaanssen, 2014). It has a major impact on the water level (Lenters *et al*., 2005) and is also one of the largest parts of the lake water budget as a most important cause of water loss from the lake surface (Gianniou and Antonopoulos, 2007). The direct measurements of evaporation can be acquired from meteorological stations. In the Great Lakes region, there are few over lake meteorological stations that regularly observe evaporation. Thus, there will never be sufficient flux towers or

field measurements to adequately characterize the large area evaporation of the Great Lakes. Moreover, on a temporal scale, no such regular long-term instrumental observations exist on the Great Lakes' water surface because of winter severity and a lack of secure research instrument bases (Mckay *et al*., 2011; Oyserman *et al*., 2012).Therefore, with such too sparse a period of off-shore measurements, it is impossible to provide a realistic, thorough picture of large lake evaporation that meets the requirements of the climate research community.

Apart from the actual direct measurement of over lake evaporation, remote sensing satellites are the only technology that can efficiently and in a timely way provide over-lake direct observations or lake-representative data for critically required inputs for estimating evaporation. However, the remote sensing of evaporation from large lakes, particularly in the northern region, suffers from two main insufficiencies. First, there is rather little recognized about the evaporation system of the large lakes. There are only limited numbers of studies estimating the surface energy balance and evaporation over large lakes using highly-accurate direct measurements such as the eddy covariance method (e. g. Blanken *et al.*, 2000; Blanken *et al.*, 2011; Rouse *et al.*, 2005; Spence *et al*., 2011; Spence and Rouse, 2002). Second, in general, comparatively little attempt has been straight towards the development of remote sensing methods for the assessment of evaporation from large lakes (Granger and Bussieres, 2005). For example, most past studies of Great Lakes evaporation have used only thermal remote sensing data as support information for estimating evaporation (e.g. Lofgren and Zhu, 2000; Spence *et al.*, 2011) and all of these analyses were focused on a short-term period (1 or 3 years). This study is probably the first time that remotely-sensed data have been applied as the primary information to study long-term evaporation over a large lake.

The purpose of this chapter is to estimate the spatial and temporal distribution, as well as the long-term changes, in lake evaporation. The evaporation rate will be linked to the changes in water level and water storage, which can be discovered in observations of satellite altimetry and gravimetry. Radar altimetry system provides the ability in production of precise relative water level across the lake during all weather conditions (Cheng *et al.*, 2008). Changes in water storage are correlated with changes in the water mass, which is referred to as the change in total water storage and this can be recognized by monitoring the temporal variations of the Earth's gravity filed from space. The results of this study will be significant and useful in understanding the spatial and temporal distribution of large lake evaporation and will contribute to the climate research community both at regional and global scales.

This chapter is composed of the following sections: the first is description of the study site, followed by a description of the data and study methods. Next, the spatial and temporal variations (seasonally from 2006-2012) in the lake's evaporation is discussed. Next, the correspondences between evaporation and water level as well as total water storage are presented and discussed. In the final section are conclusions.

5.2 Study Area

Lake Huron is the second largest of the Great Lakes by surface area (59,600 km^2). It has the same water elevation as Lake Michigan. The water levels of Lake these lakes rise and fall simultaneously because they are linked through the Straits of Mackinaw. Figure 5.1 illustrates the long-term Great Lake water level fluctuation from 1969 to 2012. Lake Huron is one of the Great Lakes that have obviously experienced a decline in water levels (Sellinger *et al.*, 2008) and reached the lowest record in December 2012 (Gronewold *et al.*, 2013). The immediate and

prolonged water level drop since 1999 of Lake Huron (also the Great Lakes) has been mainly a response to climatic or other large-scale forces, including greater evaporative and increased lake surface temperature, as shown in Figure 5.2. (Gronewold and Stow, 2014).

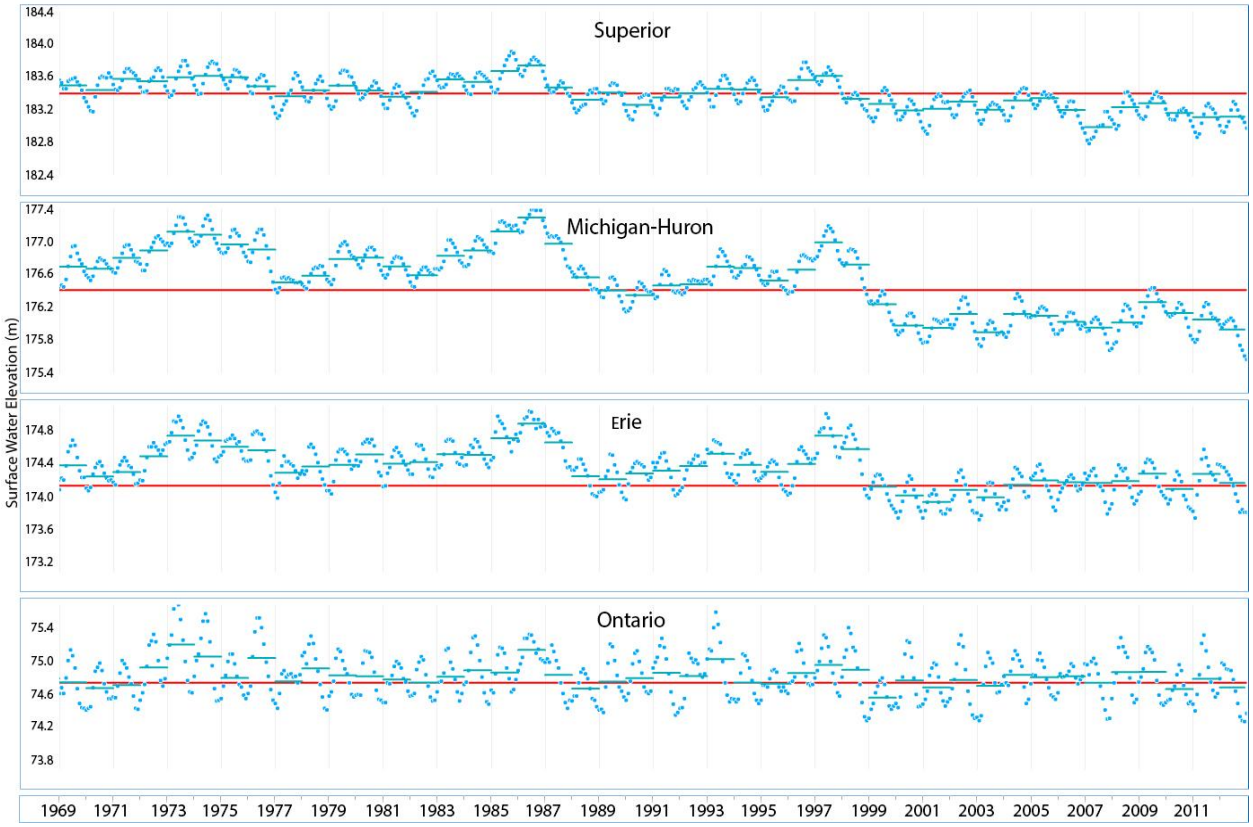

Figure 5.1 Monthly lake-wide average water levels (blue dots) of the Great Lakes from 1969 to 2012. The red and green lines present the average water level during the record period and annual average respectively (adapted from Gronewold *et al*., 2013)

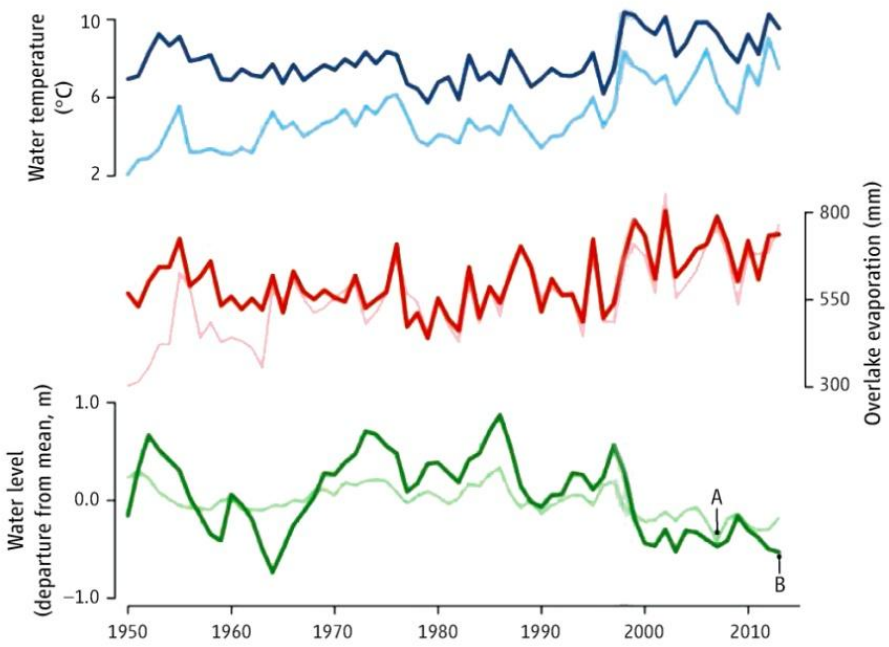

Figure 5.2 Annual water level (green lines), evaporation (red lines), and water temperature (blue lines) of Lake Huron (dark color) and Lake Superior (light color) during the period 1950-2012. Point A and B indicate the lowest water level record for Lake Superior and Lake Huron respectively. Adjusted from Gronewold and Stow (2014)

5.3 Objective

The objective of this chapter was to examine the connection between changes in evaporation rates and lake water fluctuations. The specific objectives of this study were to:

i) Examine the spatiotemporal interaction between lake-wide evaporation rates and ice cover.

ii) Examine the water level heights and total water storage in the Lake Huron region from multi-sensor remote sensing data.

iii) Examine the connection between changes in evaporation rate and lake water fluctuations over a period of 8 years (2005-2012).

5.4 Data and Methodology

This section presents the dataset applied for investigating the evaporation effect of the fluctuations of lake level, as well as the change in the gravities in the study region. Five datasets were used in this study: (i) latent heat fluxes derived from the previous chapter; (ii) ice cover (ice fraction) acquired during the period of 2005-2012 from the NOAA Great Lakes Environmental Research Laboratory (Wang *et al*., 2012); (iii) water height from Jason-1 and Jason-2 satellite altimetry; (iv) water storage from GRACE mission; and (v) water level from an in-situ gauge. All of the estimations of lake-wide evaporation, water level, and total water storage were calculated using ERDAS IMAGINE 9.2, MATLAB, ArcMap version 10.1 using the Python programming language.

5.4.1 Latent heat fluxes

The latent heat (W m^{-2}) calculated from satellite parameters together with the in-situ data discussed in the previous chapter were converted to a 30-minute evaporation rate (mm m^{-2} $30min^{-1}$) using the following equation:

$$E = \frac{Q_E}{\rho L_v} \tag{5.1}$$

where:

E is the evaporation rate (mm m^{-2} 30 min^{-1})

Q_E is the latent heat (W m^{-2})

L_v is the latent heat of vaporization (2.501×10^6 J kg^{-1})

ρ is the water density (kg m^{-3})

The water density (ρ) was estimated using the equation recommended by the National Institute of Standards and Technology (Harris, 2012):

$$\rho = a_5\left[1-\left(\frac{(t+a_1)^2(t+a_2)}{a_3(t+a_4)}\right)\right] \quad (5.2)$$

where:

a_1 = -3.983035

a_2 = 301.797

a_3 = 522528.9

a_4 = 69.34881

a_5 = 999.974950 (kg m^{-3})

t = the temperature of the water (°C)

Ice cover restrains direct lake-atmosphere interaction, which in turn influences the heat flux (Wang *et al.*, 2010). Recent observations of evaporation over Lake Erie (Gerbush *et al.*, 2008), Lake Michigan, and Lake Huron (Blanken, 2014) show a rapid decrease in evaporation magnitude as ice cover approaches 100%. Therefore, the evaporation rates of each pixel estimated from Eq. 5.1 will be multiplied by spatial ice cover using the following equation.

$$Ei = E(1-I_c) \quad (5.3)$$

where:

Ei is the evaporation rate under ice cover condition (mm m^{-2} 30 min^{-1})

I_c is the ice fraction (no units)

5.4.2 Jason-1 and 2 satellite altimetry data

Satellite altimetry is foundation on two primary techniques, radar altimetry and orbitography (Ponchaut and Cazenave, 1998). Radar altimetry is a non-imaging active remote sensing system which determines the distance between the spacecraft and the instantaneous target by sending out microwave or laser pulses and computing the time taken by the signal travel to and from the target. These altimeters have proven to be a valuable tool for measuring water level with high precision (Chelton *et al.*, 2001). However, this system is practical for comparatively flat surfaces such as oceans and large lakes, but is less effective over uneven continental topography as a result of large radar footprint of the sensor (CEOS, 2012). Satellite altimetry was originally planned to determine the water height of ocean surface (Singh *et al.*, 2012); however, previous works (e.g. Birkett, 1995; Morris and Gill, 1994) revealed that it is possible to observe lakes water level variations using satellite altimeters.

The satellite data used in this study consisted of Jason-1 data spanning the period January 2002 to August 2009 and Jason-2 from August 2009 to December 2012. The geophysical data record (GDR) series were downloaded from the Physical Oceanography Distributed Active Archive Center (DAAC) at the Jet Propulsion Laboratory.

The Jason-1 satellite was launched on 7 December 2001, with a 66^{o} inclination and an altitude of 1336 km, which corresponds to 110 min orbital time and 10 days for a revisit of the same location. Jason-2 was launched on 20 June 2008 in the identical orbit as Jason-1. These satellites measure the sea and lake level height to an accuracy of a few centimeters. The altimeter measures the surface height at 0.1 second intervals equal to every 7 km along the satellite orbital passes. Each of the Jason-1 and Jason-2 complete orbit cycles includes 254 passes, of which 127 are descending and 127 are ascending. In all of them, two ground tracks pass through Lake

Huron, Pass 076 ascending ground track and Pass 117 descending ground track. Figure 5.3 shows the Jason-1 and 2 descending ground tracks passing through the study area. Two hundred forty-seven tracks of Jason-1 and 100 tracks for Jason-2 were used for this study.

Figure 5.3 The exact ground tracks of Jason-1 and Jason-2 descending obit overpassing Lake Huron

Since Jason-1 and 2 altimetry missions have been designed to measure ocean topography at the centimeter level (Flohrer *et al.*, 2011), there is no automatic method for observing the Lake water level. The true lake surface height above the ellipsoid can be expressed as:

$$h = H - R + Corrected\ R \quad (5.4)$$

where:

h is lake surface height (m)

H is the satellite altitude (m)

R is an altimeter range (m)

Corrected R is range correction, which includes correction of wet and dry troposphere, ionosphere, pole tide, and solid earth tide.

In this study, the inland water surface was measured, and therefore the correction of the ocean tide and sea state bias could be neglected, and even if it occurred, the effect caused by both would also have been observed in the gauge measurements.

In order to measure the water level (h), The altimeter pass at all latitude and longitude locations along the lake ground track for each repeat cycle (10 days) was averaged. A buffer of 20 km from the shoreline was used to avoid the effects of seasons. Therefore, 44.0 - 46.0 N was the latitude range of the satellite pass through Lake Huron at which the data were used. These averaged data represented the average lake water level. Then lake water level variations with time were estimated by calculating the differences between instantaneous lake level height and the average of an 11-year (2002-2012) lake level height.

5.4.3 Gravity Recovery And Climate Experiment (GRACE) Data

GRACE is the satellite operation for mapping the gravity field of the globe with a spatial resolution of about 300-400 km to 40,000 km with a temporal resolution at monthly intervals. Grace consists of two co-orbiting identical satellites (GRACE-A and GRACE-B) at a 500 km altitude and flying apart from each other by roughly 220 km along-track (Tapley *et al.*, 2004). The spatial and temporal variations of the earth's gravity are mainly caused by the changes in water mass in the areas and these changes in the gravity field influence the orbits of the two identical satellites differently because they orbit at slightly different positions (approximately

220 km) in space. Over land, the GRACE data presents measurements of total terrestrial water storage, which includes surface water, soil moisture, groundwater, and snowpack (Becker *et al.*, 2010; Tapleyet *et al.*, 2004; Wahr *et al.*, 2004). The data are expressed in equivalent water thickness upon the hypothesis that detected changes of gravity are due to the redistribution of surface mass (Wahr *et al.*, 2004).

There are three levels of GRACE data, including Level-1A (the raw data), Level-1B, and Level-2 data. The raw data Level-1A are not distributed to the public, only level-1B and level-2 products are released to the research community. In this study, I used the most up to date GRACE data (RL05) of the CSR with a spatial resolution of 1×1 degree over land at a monthly temporal resolution. The data covered the time span from January 2004 through December 2012. Two months were missing (January and June 2011, June and October 2012). Thus a total of 95 months was used.

5.4.4 In-situ Data

The daily water level from the tide gauge measurements for 11 years (2002 – 2012) was acquired from the National Oceanic and Atmospheric Administration (NOAA) at Harbor Beach. This is the closest station that provides in-situ data located 10 km off the Jason-1/2 overpass descending ground tracks (Figure 5.3). The footprints, sited at least 20 km from the shoreline of Jason's scatter, were used for the validation and bias adjustment. The data were used to validate the satellite radar altimeter measurements from Jason-1/2.

5.4.4 Comparison of change in water level and total water storage to lake evaporation

Data from two satellite systems (Jason-1/2 and GRACE) were applied to examine the link between the variation in the spatial average lake surface height and total water storage in the Lake Huron region to the evaporation loss.

Finally, a linear regression model was also applied for the analysis of the trends in water level, total water storage, and evaporation rate time series. Statistical tests of the slope of the regression lines of the evaporation, water level, and total water storage were applied in order to determine if the temporal trend was significant using a student's t-test. The time series for evaporation, water level, and total water storage had lagged autocorrelations, requiring the estimation of effective degrees of freedom as suggested by Priestley (1981), Bretherton *et al*. (1999), Petchprayoon *et al*. (2010) and Santer *et al*. (2000).

5.5 Results and Discussion

5.5.1 Lake Evaporation

The average seasonal spatial variations in the evaporation of Lake Huron for the years 2005-2012 are illustrated in Figure 5.4. About 70% of the annual mean 30 min evaporation occurred during the fall (SON) and winter (DJF) seasons. This in part was a result of the very low overlying air humidity in the wintertime. In the fall, the lake tends to have the greatest surface water temperature, and at the same time the air temperature and vapor pressure decrease. These factors caused further increases in evaporation during this season. Although the water temperature dropped throughout the fall, the air temperature and humidity more rapidly decreased, resulting in a greater gradient in the water vapor ratio between the lake surfaces and overlying air. This study results were similar to the observation of Blanken *et al.* (2011), who

were conducted a direct measurement of the evaporation over Lake Superior from June 2008 through 2010. Their study found that 70-80% of the annual peak in evaporation of Lake Superior occurred between October and March. The spatial and temporal variations in lake evaporation are described in detail below.

In the wintertime, the highest evaporation rates tended to take place in the offshore regions of Lake Huron. This was a result in part of the low humidity of the cold overlying air, whereas the evaporation near the shore areas was greatly diminished by ice cover (Figure 5.5) because the evaporative fluxes could not be transferred between the water surface and atmosphere freely. The highest evaporation rate occurred in December with about 16% of the annual mean 30 min evaporation (Figure 5.6). In spring, the intensity of evaporation was noticeably weak during this season and continued through the summer. The lowest evaporation rate occurred in March, which was only 3% of the annual mean of 30 min evaporation (Figure 5.6). This was because the air started to warm and become humid while the lake water cooled, leading to weaker evaporation. During this season, the pattern of the spatial distribution of the evaporation switched to relatively higher rates in the shallow parts of the lake located near the shoreline regions and spread further toward the deeper region through the summer and fall season. This was because of the lower heat capacity of the shallow parts of the lake (they warmed more rapidly), and then active evaporation occurred earlier in these areas than in the deeper region.

In the summer, most of the areas in the lake had little evaporation; however, the evaporation appeared relatively stronger in the shallower regions (particularly in Saginaw Bay) and extended toward the deeper area at the mid-region of the lake. During the fall, most of the lake exhibited large latent heat fluxes, particularly in the southern portions. This was because of

the high volumetric heat capacity of the lake, resulting in continued high water temperatures (thus high saturation vapor pressures), and in the meantime the air temperature and humidity decreased and the rate of the decrease was greater than the decrease of the surface water temperature. This factor was reflected in a further increase in the magnitude of evaporation in the fall and continued through the winter season. However, this study found that during the month of November (Figure 5.6) the lowest evaporation rates in the fall season were observed, which was considered part of the high evaporation season. Weak evaporation rates in November were also observed in Lake Superior by the study of Blanken *et al.* (2011), who estimated over lake evaporation using highly-accurate eddy covariance direct measurements. These occurrences were possibly mainly due to the high evaporation in the month of September and October, for instance, which could cause lower water temperatures by the month of November, which then would limit the degree of evaporation during this part of the transition from the fall regime to the winter regime. After the month of November, the air temperature and humidity more rapidly decreased than the water temperature. These factors resumed a greater gradient between the lake surfaces and overlying air, and then the magnitude of in the fall season evaporation rapidly increased again.

The pattern of spatial distribution of lake-wide evaporation from this study was also similar to the study of Lofgren and Zhu (2000) and Spence *et al.* (2011). The former calculated the latent heat (under the assumption of ice-free surface) of Lake Huron using satellite water surface temperature and other meteorological data during the period 1992-1995. Similar to the results of the present study, they obtained high values of evaporation during the winter and smaller values in the summer. The latter study found a strong seasonal pattern of evaporation over Lake Superior, with a peak in December and January and very low evaporation in August

and March. Despite different study periods, datasets, and methods, all of the results of these studies were consistent in observing a spatial and temporal distribution in lake evaporation. However, Lofgren and Zhu (2000) found that the month of November had the highest heat of evaporation, which was different from this study and from the study of Blanken *et al.*, 2011. This is because the study of Lofgren and Zhu (2000) was based on a computer model using field measurement from a relatively sparse network of shore-line based stations, which might have introduced uncertainties due to a lack of over lake stations and the contamination of the signal from land.

Regarding long-term lake evaporation, the regression analysis of the mean entire lake evaporation revealed a positive trend of 0.017 mm m^{-2} per year (Figure 5.7), indicating that lake evaporation increased by 1.4 mm m^{-2} during the period 2005-2012; however, this was not statistically significant. The increase in the evaporation rate during this study period was possibly a result of a smaller amount of ice cover (Figure 5.8) and an increase in surface water temperature (chapter 2), leading to the overall higher evaporation rate. This result of a positive trend is in agreement with the study of Hanrahan *et al.* (2010), who stated that the evaporation rate of Lake Michigan and Lake Huron has begun to increase over the past few decades as a consequence of rising water surface temperatures, which are connected with declining ice cover in the wintertime.

Although these study results were in agreement with previous studies, the evaporations found in the present study were computed on the assumption of a homogeneous wind speed for the entire lake. Therefore, this could lead to uncertainty concerning the resulting evaporation because of the spatial heterogeneity of the wind speed over the entire lake.

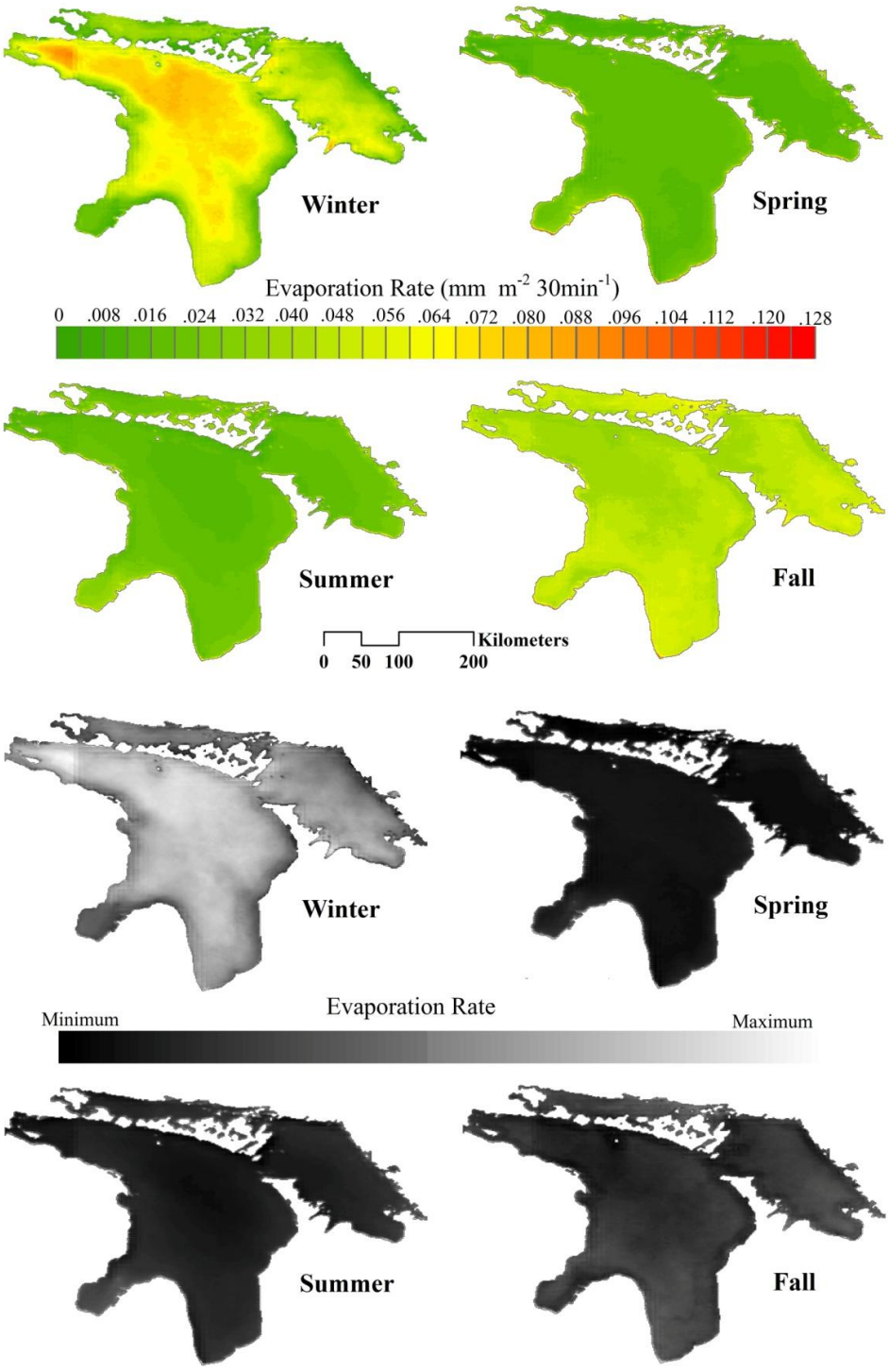

Figure 5.4 Seasonal average spatial distribution of evaporation rates (in mm m^{-2} 30 min^{-1}) for years 2005-2012. The gray scale in the lower part shows the radiation variability of each season

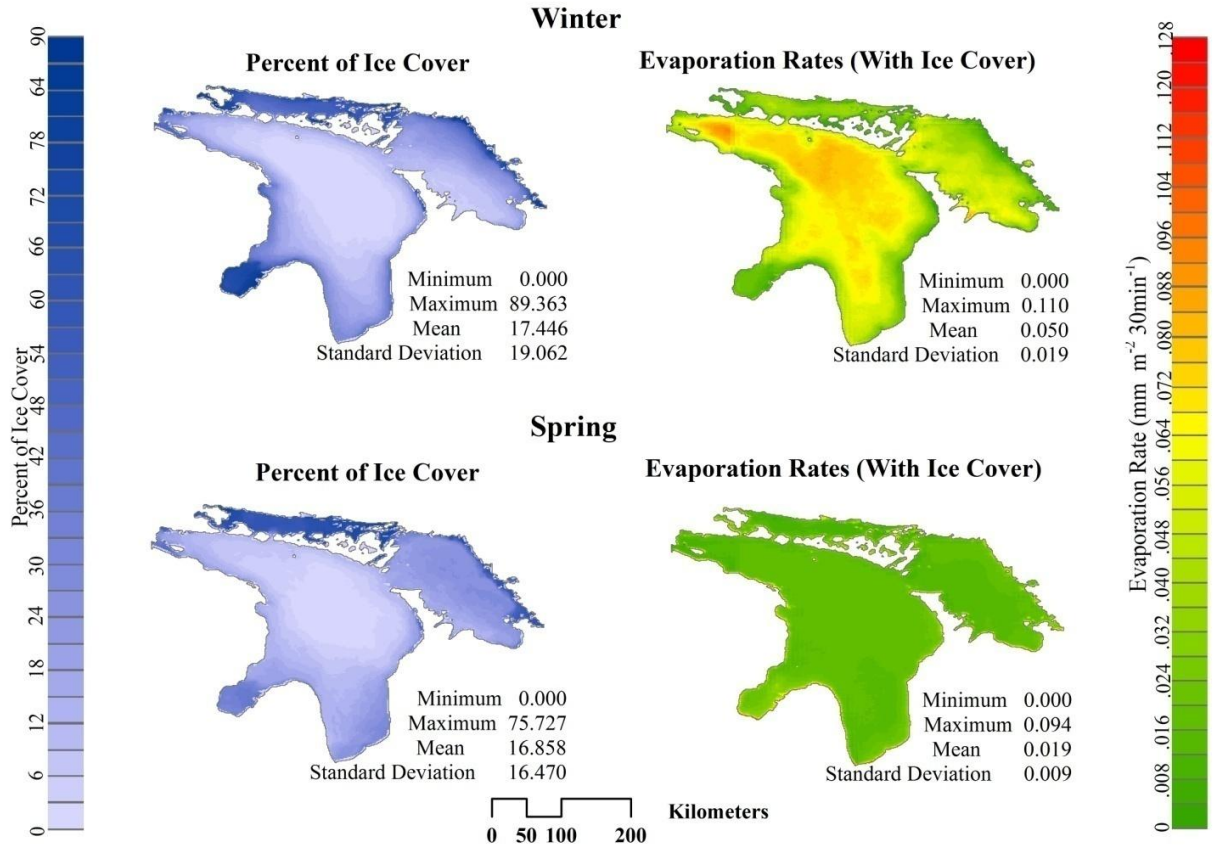

Figure 5.5 Spatial distribution of mean ice cover (in percent) and mean evaporation rate (in mm m^{-2} 30 min^{-1}) over Lake Huron in winter and spring seasons during the period of 2005-2012. Ice cover per pixel ranges from 0% (ice free) to 100% (complete ice cover)

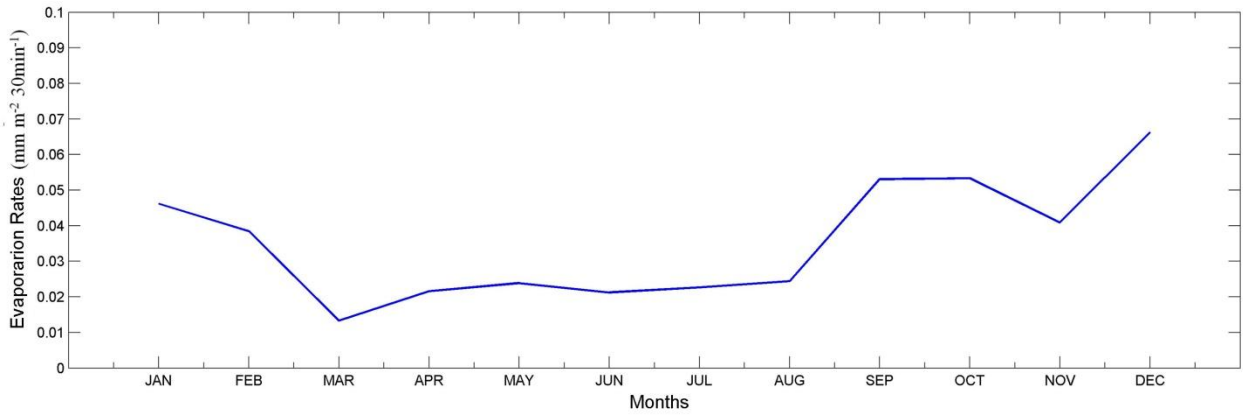

Figure 5.6 Monthly mean of 30 min evaporation rate (mm m^{-2} 30 min^{-1}) over Lake Huron during the period 2005-2006

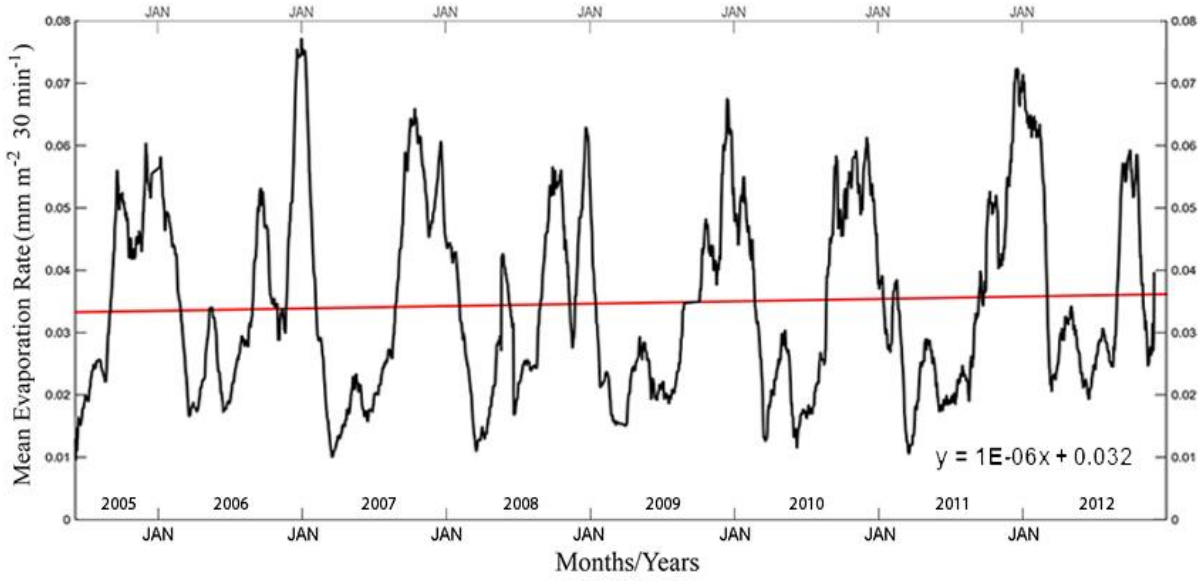

Figure 5.7 Time series of evaporation rate (mm m^{-2} 30 min^{-1}) and the trend line for the 8 years (2005-2012).

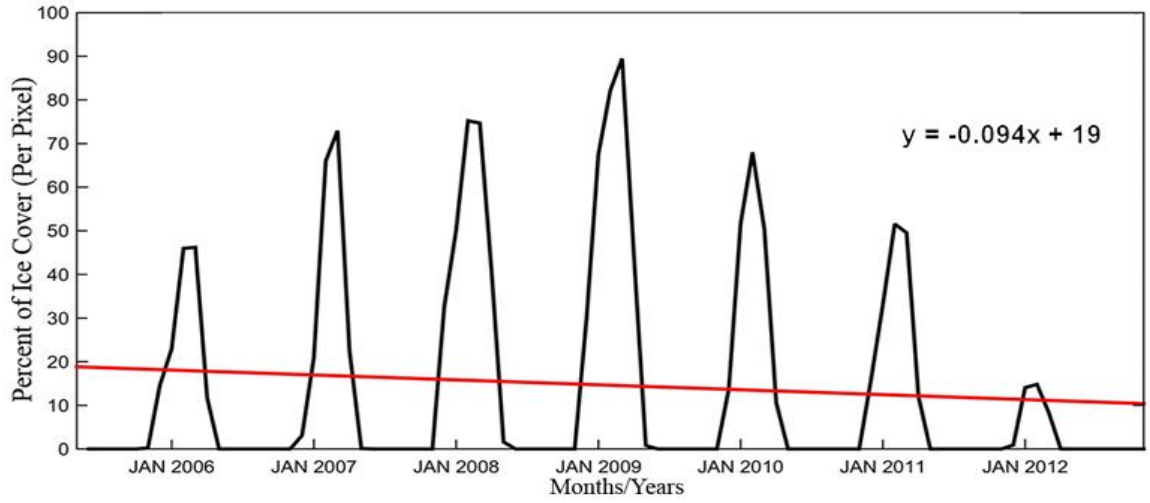

Figure 5.8 Time series of monthly mean ice cover per pixel (mm m^{-2} 30 min^{-1}) over Lake Huron and the trend line for the 8 years (2005-2012).

5.5.2 Lake Water Level

The water level time series derived from Jason1/2 for orbital pass 117 over Lake Huron and the daily water level data from the ground-based gauge at Harbor, MI were plotted against time (2002-2012) and are shown in Figure 5.9. These represented good consistency between satellite measurements and the in-situ data at 11.11 cm RMSE. This error might have been due to the limitations in the processing of the Jason radar footprint. It is also possible that some areas of the lake level spatial variability was caused by steric effects (the water getting hot and expanding, and then cold and contracting).

The observations of water level from the satellite altimetry showed that the lake water level was generally low during late winter to early spring season (DJF - MAM) and reached a maximum during the summer (JJA). These results were similar to the study of Brinkmann (2000), who stated that the Lake Michigan-Huron water level declines through autumn (SON) and winter (DJF) and reaches a maximum during the summer (JJA). The trend lines and regression analyses over study period 2002-2012 of the Lake Huron water level are shown in Figure 5.9. The regression coefficient (or slope indicating the long-term trend in the water level) was negative. The results demonstrated that the lake water level decreased by 0.04 m during the period 2002-2012; however, this was not statistically significant.

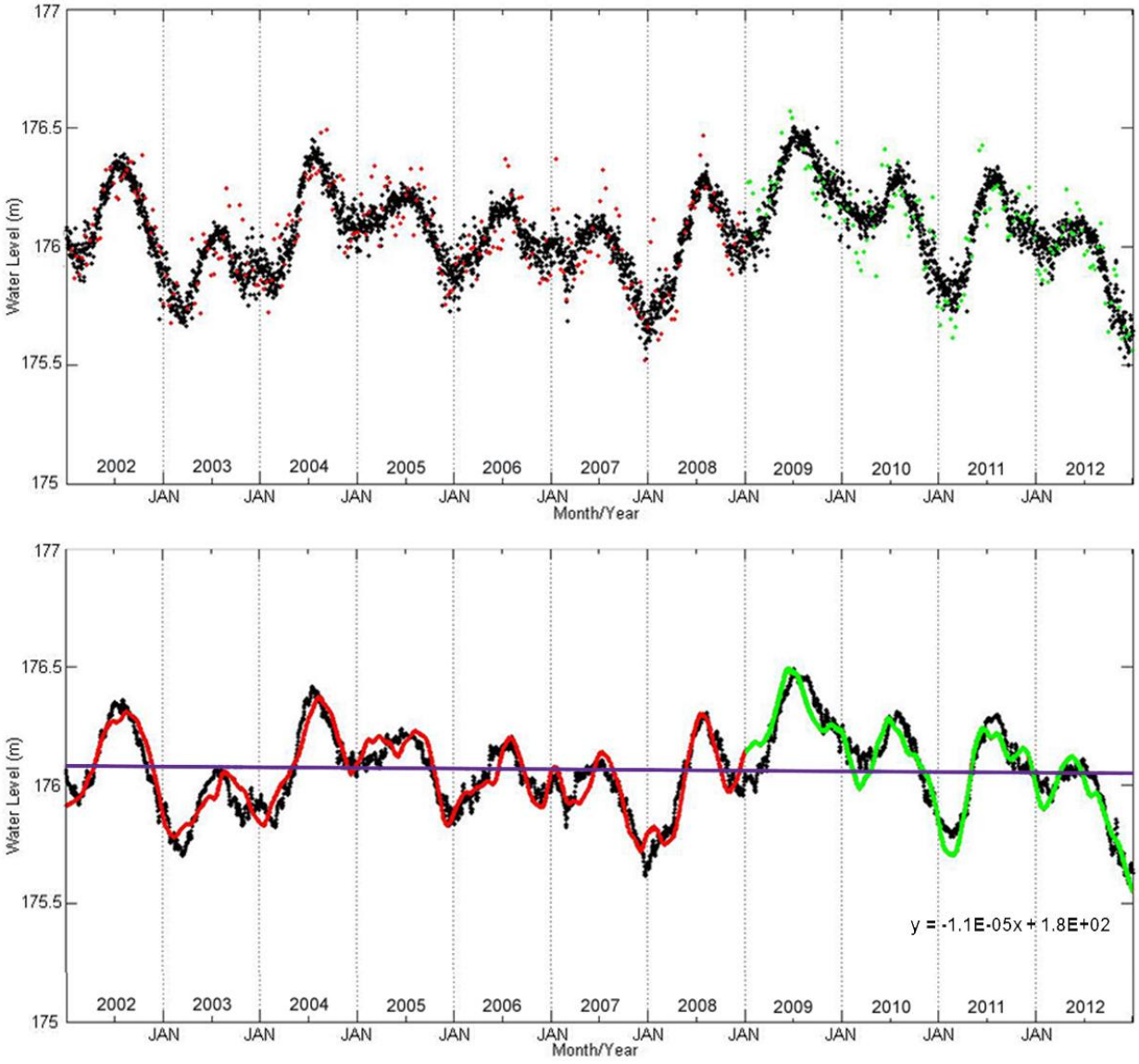

Figure 5.9 Plot of the combined Jason 1/2 for orbital pass 117 over Lake Huron and daily gauge data at Harbor Beach, MI against the study period (2002-2012). The Jason-1 and Jason-2 altimeter data are colored red and blue respectively, and the gauge data are presented in black. The top panel displays water level variations, while the water level variations time series in the lower panel has been smoothed with a median type filter. The purple line presents the regression line for the 11-year time period of 2002-2012

5.5.3 Total Water Storage Variation in the Lake Huron Region

Figure 5.10 shows the monthly estimates of the total water storage anomaly time series. The total water storage in the lake region was low during the late fall season and reached a maximum during spring (JJA). The Grace total water storage signal over the lake region had a downward trend of 0.13 cm per year, corresponding to 1.18 cm water thickness lost from the lake region for the entire study period; however, this was not statistically significant.

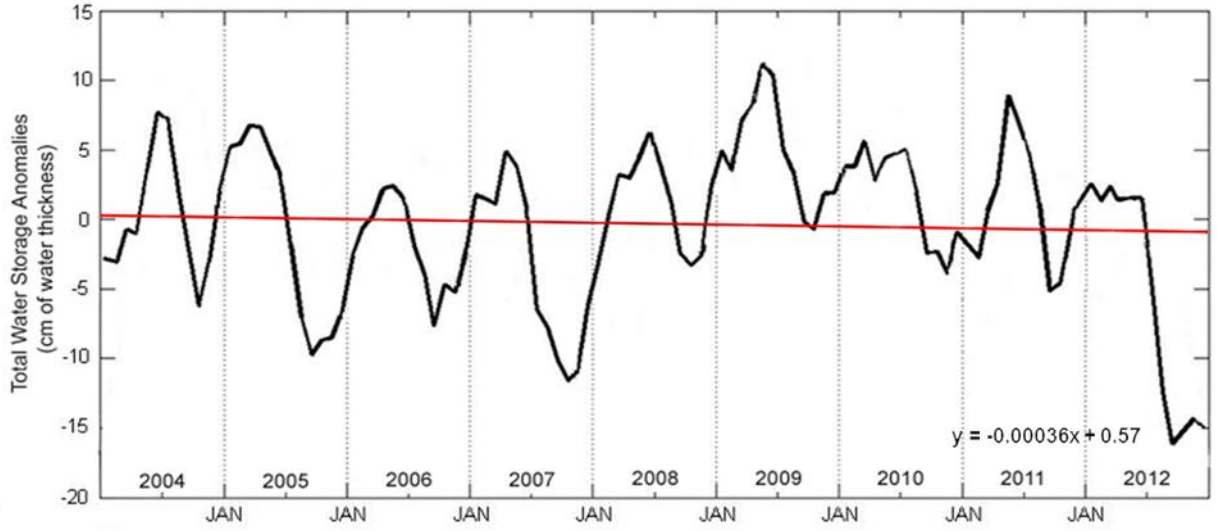

Figure 5.10 Time series of monthly GRACE total water starage anomalies (in cm of water thickness) over Lake Huron and the trend line for 9 years (2004-2012)

A comparison between the variation in the total water storage from GRACE and the water level change from the altimetry is shown in Figure 5.11. A time shift between the GRACE total water storage and Jason1/2 altimetry was explicitly present. The peak of total water storage was about 2 months earlier than the peak of the water level. This is because the surface area of Lake Huron itself (approximately 60,000 km^2) is relatively small compared to the resolution of the GRACE signal, which measures information on a larger area of about 100,000 km^2 (Zeng *et al*., 2007 and Yeh *et al*., 2012). Therefore, it was reasonably possible that the GRACE results

were receiving some additional signals caused by changes in the soil moisture, groundwater, and snow on the land surrounding the lake (Wahr, personal communication, April 25, 2013).

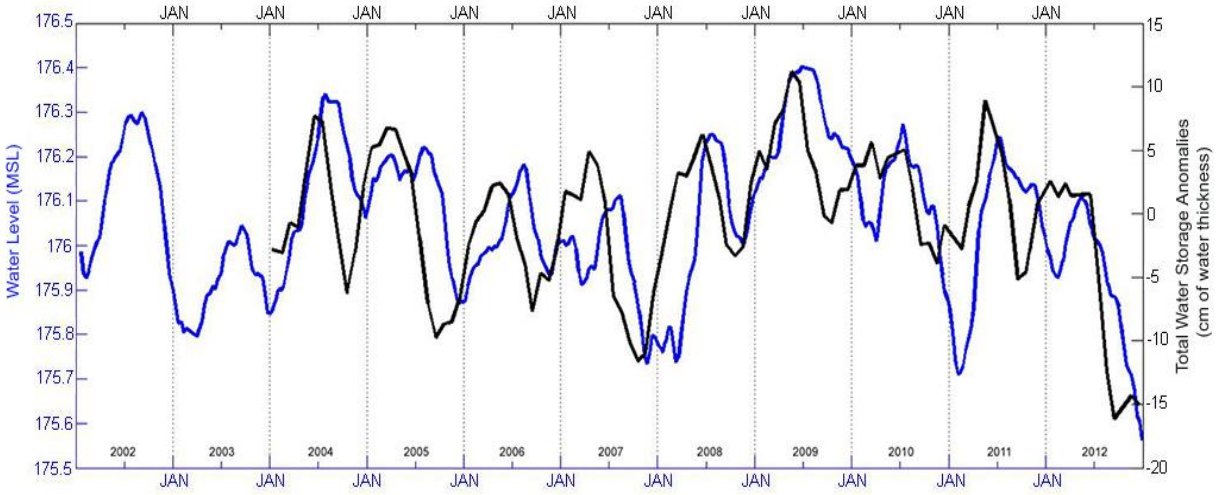

Figure 5.11 Comparison between the variation total water storage from GRACE (cm of water thickness) and water level change from satellite altimetry (m)

5.5.4 Relationship between Lake Evaporation, Water Level, and Total Water Storage

Figure 5.12 illustrates the time series of lake evaporation, the GRACE total water storage, and the Jason1/2 altimetry. The time series of evaporation and lake water level had the highest negative correlation coefficient at a temporal lag (or delay) of 66 days (Figure 5.13). Therefore, there was approximately a two-month delay between the time of maximum water loss from the lake by evaporation and the time of lowest water level. This was possibly because the water level of Lake Huron was not only controlled by the amount of evaporation but also was a function of other components of the hydrologic cycle in the lake such as precipitation and inflow from Lake Superior.

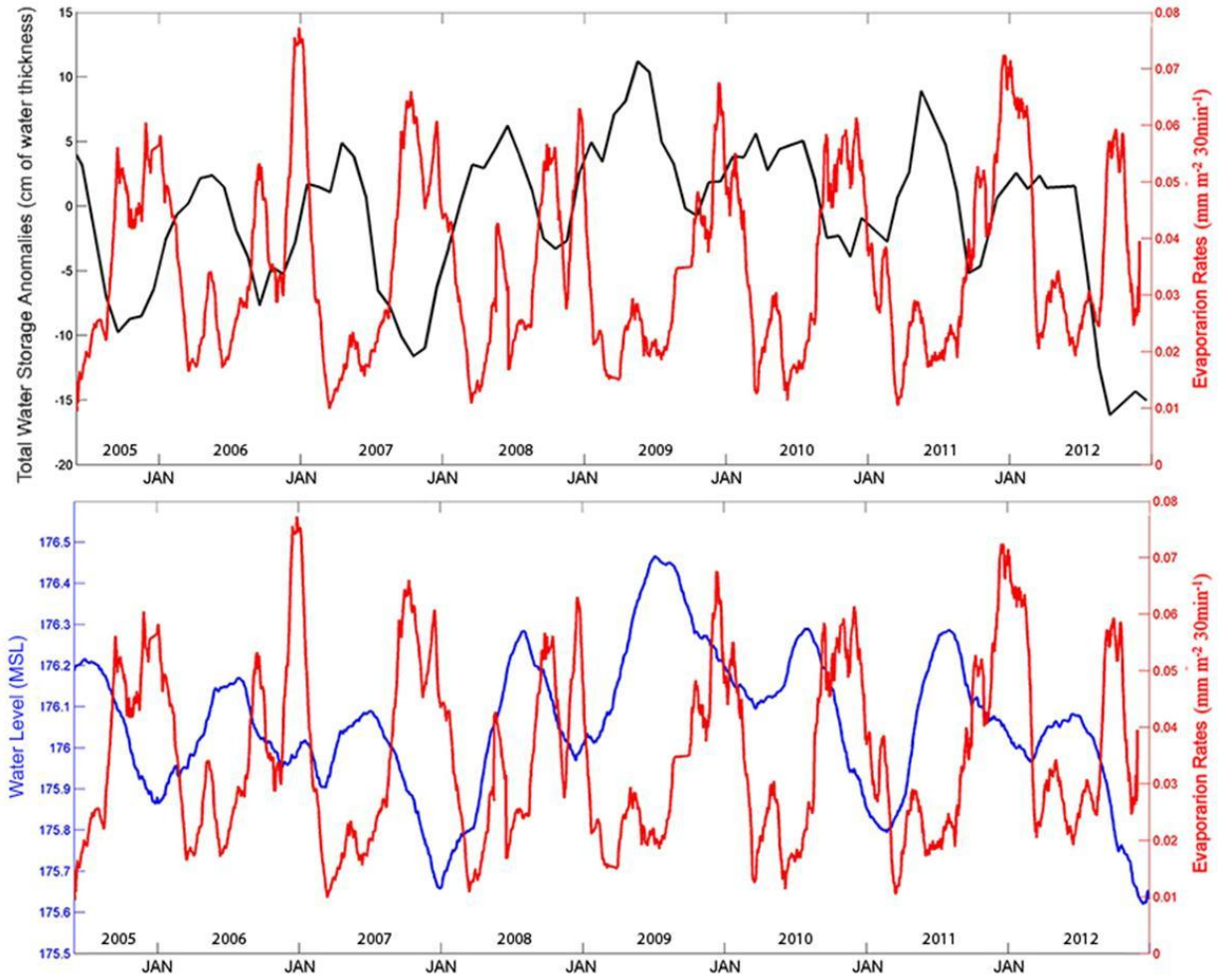

Figure 5.12 Upper panel shows the comparison between the time series of lake evaporation (red) and GRACE total water storage (black). The lower panel presents a comparison between lake evaporation and Jason1/2 altimetry (blue).

The time series of total water storage and evaporation had the highest negative correlation coefficient at a lag of 16 days (Figure 5.13). Thus, there was approximately a half-month delay between the time of lowest total water storage and the time of maximum water loss from the lake by evaporation. This was because the detected temporal mass variations of GRACE were not only influenced by the volume of water in the lake, but also controlled by all of the components of the hydrologic cycle in Lake Huron and the adjacent area, including snow pack, runoff, soil moisture, infiltration, and groundwater flow (Ahmed *et al*., 2011; Wahr *et al*., 2004), which is very low in October and begins to increase in November (Lofgren, 2004).

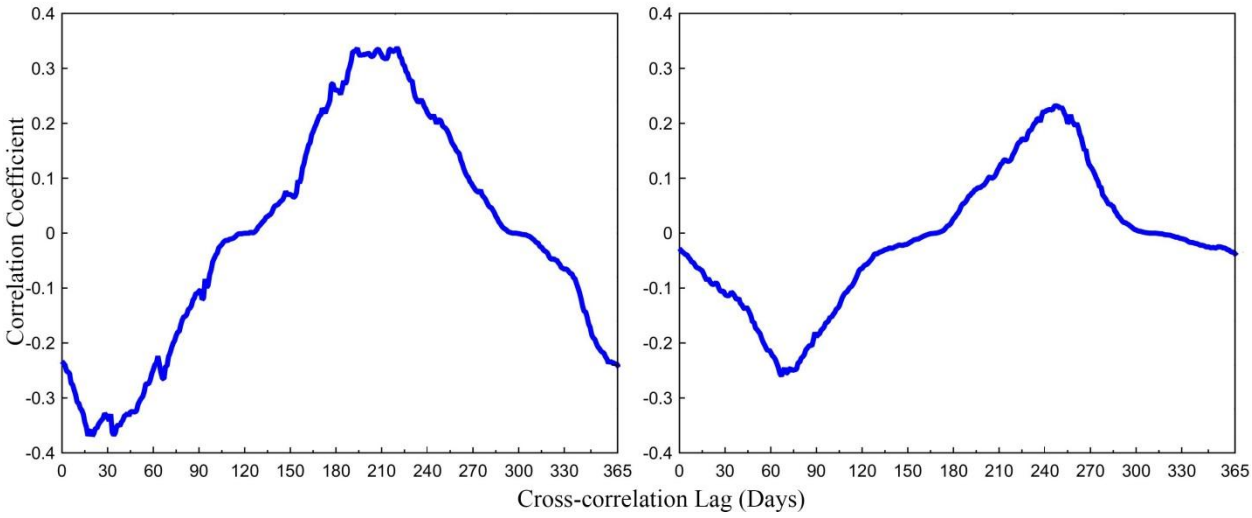

Figure 5.13 (left) Cross-correlation between GRACE total water storage and the 30 min evaporation; maximum negative correlation coefficients were found with a lag of 16 days. (right). Cross-correlation between the 30 min evaporation and lake water level, and maximum negative correlation coefficients were found with a lag of 66 days.

It was interesting that the time of high evaporation loss from the lake was cross-correlated (but was not statistically significant) with the lowest period of total water storage and then to the time of lowest lake water level. This was because GRACE captures the signal of the whole hydrologic cycle and would be more sensitive to lake evaporation (and also

evapotranspiration from the nearby land), which was high in late fall, whereas the precipitation was relatively low during this season. Another possible reason is the inflow from Lake Superior, which may have resulted in a delayed decline in the Lake Huron water level.

5.6 Conclusion

This chapter has estimated the spatial and temporal distribution, as well as the long-term changes, in the lake evaporation. The evaporation rate was linked to the changes in total water storage and water level by combining the observations of two complementary satellite systems: the gravimetry and altimetry satellites; namely, GRACE, Jason 1 and Jason 2, respectively.

The spatial distribution of the evaporation showed temporal and spatial heterogeneities. Approximately 70% of the annual mean 30 min evaporation occurred during the fall and winter seasons, whereas the lowest evaporation rate occurred in March, which was only 3% of the annual mean of 30 min evaporation. The study discovered that the month of November exhibited the lowest evaporation rates in the fall season, which was considered part of the high evaporation season. This was possibly due to the high evaporation in the month of September and October, which can cause lower water temperatures by the month of November, and then limits the amount of evaporation during this part of the transition from the fall regime to the winter regime.

There was an increase in the evaporation rate approximately of 1.4 mm m^{-2} over the 2005-2012 observation period, the water level decreased by 0.04 m. during the period 2002-2012, and there was a decrease in total water storage by 1.18 cm during the entire study period (2004-2012). However, none of these was statistically significant. There was obviously a negative correlation between lake evaporation and lake water level and also total lake water storage. There was approximately a two-month delay between the maximum evaporation rate

and the time of the lowest water level, whereas total water storage reached the lowest point a half-month earlier than the time of maximum evaporation. These time lags were mainly due to the water level being influent because of the inflow from Lake Superior, while the GRACE total water storage was affected by the signal from the land surrounding the Lake.

Use of satellite and in-situ data for computing the lake evaporation, water level, and total water storage proved that better spatial distribution and spatial coverage can be obtained. This study explored the relationship of recent increase in evaporation and total water storage, as well as the water level change phenomenon. If the present evaporation trend continues, it can be believed that the negative water level and total water storage trend will also continue. However, in terms of both natural climate changeability and the influence of human beings forced on nature, more study needs to be done to achieve an enhanced understanding of how the lakes react to climate changes.

5.7 Bibliography

Ahmed M., Sultan M., Wahr J., Yan E., Milewski A., Sauck W., Becker R., Welton B. 2011. Integration of GRACE (Gravity Recovery and Climate Experiment) data with traditional data sets for a better understanding of the time-dependent water partitioning in African watersheds. *Geology*, 39(5), 479-482

Becker M., Llovel W., Cazenave A., Guntner A., Cretaux J.F. 2010. Recent hydrological behavior of the East African great lakes region inferred from GRACE, satellite altimetry and rainfall observations. *Comptes Rendus Geoscience*, 342, 223-233

Birkett C.M. 1995. The contribution of TOPEX/POSEIDON to the global monitoring of climatically sensitive lakes. *Journal of Geophysical Research*, 100, 25179-25204

Blanken P.D., Rouse W.R., Culf A.D., Spence C., Boudreau L.D., Jasper J.N., Kochtubajda B., Scertzer W.M., Marsh P., Verseghy D., 2000. Eddy covariance measurements of evaporation from Great Slave Lake, Northwest Territories, Canada. *Water Resources Research*, 36(4), 1069–1077

Blanken P.D., Spence. C., Hedstrom N., Lenters J.D. 2011. Evaporation from Lake Superior: 1. Physical controls and processes. *Journal of Great Lake Research*, 37, 707-716

Blanken P.D., Spence C., Lenters J.D., Petchprayoon P., Gronewold A.D., 2014. Impacts of ice cover on Great Lakes evaporation: An analysis of simultaneous ice-covered and ice-free conditions on Lakes Michigan and Huron during the 2013-14 winter. *The 57th Annual Conference on Great Lakes Research*, May 2014. Ontario, Canada

Bretherton C.S., Widmann M., Dymnikov V.P., Wallace J.M., Blad´e I. 1999. The effective number of spatial degrees of freedom in a time varying field. *Journal of Climate,* 12, 1990–2009.

Brinkmann W.A.R. 2000. Causes of variability in monthly Great Lakes water supplies and lake levels. *Climate Research*, 15, 151–160

CEOS (Committee on Earth Observation Satellites). 2012. *The Earth Observation Handbook. Spaecial 2015 COPS 21 Editions*. Retrieved from http://www.eohandbook.com /cop21/capabilities/sat_earth_obs_radar_altimeters.html

Changnon S.A. 2004. Temporal behavior of levels of the Great Lakes and climate variability. *Journal of Great Lakes Research,* 30, 184 –200

Chelton D.B., Ries J.C., Haines B.J., Fu L.L., Callahan P.S. 2001. Satellite altimetry. *Satellite Altimetry and Earth Sciences: A Handbook for Techniques and Applications*. Fu L.L., Cazenave A. Eds. San Diego. Academic Press

Cheng K.C., Kuo CY., Shum C.K., Niu X., Li R., Bedford K.W. 2008. Accurate linking of Lake Erie water level with shoreline datum using GPS buoy and satellite altimetry. *Terrestrial Atmospheric and Oceanic Sciences,* 19, 53-62

Duan Z., Bastiaanssen W.G.M. 2014. A new empirical procedure for estimating intra-annual heat storage changes in lakes and reservoirs: Review and analysis of 22 lakes. *Remote Sensing of Environment*, 156, 143-156

Flohrer C., Otten M., Springer T., Dow J. 2011. Generation precise and homogeneous orbits for Jason-1 and Jason-2. *Advances in Space Research*, 48, 152-172

Gerbush M.R., Kristovich D.A.R., Laird N.F. 2008. Meso scale boundary layer and heat flux variations over pack ice–covered Lake Erie. *Journal of Applied Meteorology and Climatology,* 47, 668-682. doi: 10.1175/2007JAMC1479.1

Gianniou S.K., Antonopoulos V.Z. 2007. Evaporation and energy budget in Lake Vegoritis, Greece. *Journal of Hydrology*, 345, 212-223

Granger R., Bussieres N. 2005. Evaporation/evapotranspiration estimates with remote sensing: *Remote Sensing in Northern Hydrology*. Dugua C.R., Pietroniro A. Eds. Washington, D C. American Geophysical Union

Gronewold A.D., Clites A.H., Smith J.P., Hunter T.S. 2013. A dynamic graphical interface for visualizing projected, measured, and reconstructed surface water elevations on the earth's largest lakes. *Environmental Modelling & Software*, 49, 34–39

Gronewold A.D., Stow T.A., 2014. Water loss from the Great Lakes . *Science*, 343(6175), 1084-1085. doi*:* 10.1126/science.1249978

Hanrahan J.L., Kravtsov S.V., Roebber P.J. 2010. Connecting past and present climate variability to the water levels of Lakes Michigan and Huron. *Geophysical Research Letter,* 37, L01701. doi:10.1029/2009GL041707

Harris G.L. 2012. *Selected Procedures for Volumetric Calibrations (2012 ed)*. NISTIR 7383. National Institute of Standards and Technology. U.S. Department of Commerce. 104 p

Lenters J.D., Kratz T.K., Bowser C.J. 2005. Effects of climate variability on lake evaporation: Results from a long-term energy budget study of Sparkling Lake, northern Wisconsin (USA). *Journal of Hydrology*, 308, 168-195

Lofgren B.M. 2004. A model for simulation of the climate and hydrology of the Great Lakes basin. *Journal of Geophysical Research*, 109, D18108. doi:10.1029/2004JD004602

Lofgren B.M., Zhu Y. 2000. Surface energy fluxes on the Great Lakes based on satellite-observed surface temperatures 1992 to 1995. *Journal of Great Lake Research*, 26(3), 305-314

Mckay R.M.L., Beall B.F.N., Bullerjahn G.S., Woityra W.C. 2011. Winter limnology on the Great Lakes: The role of the U.S. Coast Guard. *Journal of Great lakes Research*, 37(1), 207-210

Morris C.S., Gill S.K. 1994. Evaluation of the TOPEX/POSEIDON altimeter system over the Great Lakes. *Journal of Geophysical Research*, 99(C12), 24527–24539. doi: 10.1029/94JC01642

Oyserman B.O., Woityra W.C., Bullerjahn G.S., Beall B.F.N., Mckay R.M.L. 2012. Collecting winter data on U.S. Coast Guard icebreakers. *EOS, Transactions American Geophysical Union*, 93(10), 105-106. doi: 10.1029/2012EO100002

Petchprayoon P., Blanken, P.D., Ekkawatpanit C., Hussein K. 2010. Hydrological impacts of land use/land cover change in a large river basin in central-northern Thailand. *International Journal of Climatology*, 30(13), 1917-1930

Ponchaut F., Cazenave A. 1998. Continental lake level variations from Topex/Poseidon (1993-1996). *Earth & Planetary Sciences*, 326, 13-20

Priestley M.B. 1981. *Spectral Analysis and Time Series, Volume 1 : Univariate Series. (Probability and Mathematical Statistics).* Academic Press, New York, 653 p

Rouse W.R., Oswald C.J., Binyamin J., Spence C., Schertzer W.M., Blanken P.D., Bussieres N., Duguay C.R. 2005. The role of Northern Lakes in a regional energy balance. *American Meteorological Society*, 291-305

Santer B.D., Wigley T.M.L., Boyle J.S., Gaffen D.J., Hnilo J.J., Nychka D., Parker D.E., Taylor K.E. 2000. Statistical significance of trends and trend differences in layer-average atmospheric temperature time series. *Journal of Geophysical Research*, 105: 7337–7356

Sellinger C.E., Stow C.A., Lamon E.C., Qian S.S. 2008. Recent water level declines in the lake Michigan-Huron system. *Environmental Science & Technology*, 42, 367-373

Singh A., Seitz F., Schwatke C. 2012. Inter-annual water storage changes in the Aral Sea from multi-mission satellite altimetry, optical remote sensing, and GRACE satellite gravimetry. *Remote Sensing of Environment*, 123, 187-195

Spence C., Blanken P.D., Hedstrom N., Fortin V., Wilson H., 2011. Evaporation from Lake Superior: 2Spatial distribution and variability. *Journal of Great Lake Research*, 37, 717-724

Spence C., Rouse W.R. 2002. The energy budget of Canadian Shield subarctic terrain and its impact on hill slope hydrological processes. *Journal of Hydrometeorology*, 3, 208 – 218

Tapley B.D., Bettadpur S., Watkins M., Reigber C. 2004. The gravity recovery and climate experiment: Mission overview and early results *Geophysical Research Letters,* 31, L09607. doi:10.1029/2004GL019920

Wahr J. 2013. Personal communication, April 25, 2013

Wahr J., Swenson S., Zlotnicki V., Velicogna I. 2004. Time-variable gravity from GRACE: First results. *Geophysical Research Letter,* 31, L11501. doi:10.1029/2004GL019779

Wang J., Assel R.A., Walterscheid S., Clites A.H., Bai X. 2012. Great Lakes ice climatology update: winter 2006 - 2011 description of the digital ice cover dataset. *NOAA technical Memoradum GLERL-155*. 37 p

Wang J., Hu H., Schwab D., Hawley N., Clites A., 2010. Development of the Great Lakes ice-circulation model (GLIM): application to Lake Erie in 2003 - 2004. *Journal of Great Lakes Research*, 36, 425-436

Yeh P.J., Tang Q., Kim Hyungjun. 2012. Validation of Gravity Recovery and Climate Experiment data for assessment of Terrestrial water storage variations. *Multi scale Hydrologic Remote Sensing Perspectives and Applications*. Chang N., Hong Y. Eds. New York. CRC Press

Zeng N., Yoon J., Mariotti A., Swenson S. 2007. Variability of Basin-Scale Terrestrial Water Storage from a PER Water Budget Method: The Amazon and the Mississippi. *Journal of Climate*, 21, 248-265

CHAPTER 6

CONCLUSIONS AND FUTURE RESEARCH

This research sought to investigate and describe the physical processes of energy exchange between water surface and atmosphere of Lake Huron using satellite remote sensing data integrated with spatially-constant surface meteorological parameters and GIS processes. The conclusions for this research will be discussed by each of the four chapter and then possible future research topics will be discussed.

6.1 Surface Water Temperature on Lake Huron

Chapter 2 examined the spatiotemporal distribution of the surface water temperature over Lake Huron, using remotely-sensed data. Eleven years of 1 km x 1 km surface temperature data were examined using images from MODIS on board the Terra satellite. Comparison of the MODIS surface temperature to in-situ observations from Lake Huron yielded satellite minus in-situ differences of 0.57 ^{o}C for clear-sky conditions, and -0.30 ^{o}C for cloudy-sky conditions. Water surface temperatures showed upward trends of 0.0039 ^{o}C per day during the summer period (June-July-August). The warming rate was greatest in the deepest areas of the lake; a statistically-significant correlation between the warming rate and depth was found. This phenomenon was due to the early summer stratification date which allowed a longer period of time for solar radiation to warm the water. To the best of author knowledge, this is the first study that the correlation between warming rate and lake depth was explored, and this was mainly due to the use of satellite data which provided continuous lake-wide data rather than data at one specific location.

6.2 Lake Huron Net Radiation

Chapter 3 used daily remotely-sensed data with a multi-spatial resolution of 1 km to 5 km to examine the spatiotemporal distribution of net radiation (Q*) and its four components: incoming shortwave (K↓), outgoing shortwave (K↑), incoming long-wave (L↓), and outgoing long-wave (L↑), under all sky conditions across the lake. Good agreement was found between the in-situ measurements of the net radiation components and the instantaneous estimates made from the satellite data with correlation coefficients between 0.95 and 0.60 for outgoing long-wave radiation and incoming shortwave radiation, respectively. The results showed that the Q* and none of its components showed any statistically-significant trends over the study period. Trend analysis revealed a slight decrease in the Q* at the rate of 0.003 Wm^{-2} day^{-1} with a decrease in shortwave (K↓ and K↑) and an increase in long-wave radiation (L↓ and L↑). The positive trend of outgoing long-wave radiation was a result of the increase in surface water temperature. A possible reason for the reduction in surface incoming shortwave radiation was mainly the increase of energy absorption by water vapor in the atmosphere.

This research is most likely the first time satellite data have been used to study long-term surface net radiation for all sky conditions, and therefore it has a potential to estimate the surface radiation budget worldwide. However, cloudy sky conditions make estimating incoming radiation (both short-wave and long-wave) from satellite data difficult compared to the in-situ data. The main uncertainly associated with the co-location of satellite and meteorological station measurement is temporal and spatial sampling errors.

6.3 Lake Huron Surface Energy Balance

Chapter 4 examined the inter-annual and long-term variability of the surface energy balance components estimated from the MODIS data together with field measurements. The bulk method was applied to derive the surface latent and sensible heat fluxes, with the bulk transfer coefficients estimated using the eddy correlation method. The spatial distribution of the surface energy balance components showed temporal and spatial heterogeneities. There was a strong seasonal pattern for all of the energy balance components. The net radiation and heat storage were very high in summer, with a very small net radiation and large release of the stored heat in winter. In contrast, the latent heat and sensible heat fluxes were very high in winter and very low in summer. This study found that there were no significant trends in the energy balance components during the study period. The seasonal and the annual values of the surface turbulent heat fluxes (latent heat and sensible heat) calculated-from remotely sensed data, and those from the eddy covariance method, were very close with a correlation coefficient of 0.95. The agreement between the seasonal satellite and in-situ data was good enough to suggest that the surface turbulent fluxes estimated from satellite sources were reliable.

The largest uncertainly occurred in the estimation of sensible heat flux, which was underestimated in the mid-lake region due to the unusually high satellite-estimated air temperature in the winter season. This overestimation could not be confirmed or validated because there were no other ground measurements in the mid-lake region. Moreover, comparison with other research was difficult because there are no reported errors for MODIS air temperature explicitly.

6.4 Lake Evaporation, Total Water Storage, and Water Level

Chapter 5 estimated the spatial and temporal distribution, as well as the long-term changes, in the lake evaporation. The changes in the evaporation rate were linked to the changes in total water storage and water level by combining the observations of two complementary GRACE and Jason satellites. The results showed that evaporation from the lake was variable in terms of both space and time. Approximately 70% of the annual mean 30-min evaporation occurred during the fall and winter seasons, whereas the lowest evaporation rate occurred in March, which was only 3% of the annual total. This study found that the month of November consistently had the lowest evaporation rates in the fall season, which was considered part of the high evaporation season. This was as a result of the high evaporation in the month of September and October, which can lower water temperatures by November, and then limit evaporation rates during this part of the transition from the fall regime to the winter regime.

The regression analysis of the 30-min mean lake-wide evaporation revealed a positive trend; however, it was not statistically significant. There was obviously an inverse relationship between lake evaporation and water level and also total water storage. If the current positive evaporation trend continues, it can be assumed that the decrease in water level and the decrease in total water storage trends will also continue.

6.5 Future Research

Based on a review of the completed research conducted in this thesis, three future research questions are suggested:

6.5.1 Study of the Great Lakes Surface Energy Balance

It would be interesting to apply the methods from this study to investigate the physical processes of energy exchange between the water surface and atmosphere in the other 4 lakes; Lake Superior, Lake Michigan, Lake Erie, and Lake Ontario. The findings from these additional new study sites would certainly help to improve our understanding of the processes behind such changes of long-term water levels in the Great Lakes region.

6.5.2 The November Exceptional Small Evaporation Rates

Although the lowest evaporation rates in the fall season in the month of November have already been discussed, it would be interested to investigate in detail of the physical processes behind this phenomenon, since it is contrary to the results from the NOAA Great Lakes Environmental Research Laboratory's computer model.

6.5.3 Calibration and Validation of Mid-Lake Air Temperature Retrieved from the MODIS Atmospheric Product

Air temperature is an important variable in a surface energy balance model because it modulates the surface sensible heat flux. Validation is an essential component of most satellite data-based studies. Although the lake has a homogenous surface, this study showed an unusually large difference in the satellite winter air temperature between various parts of the lake, particularly in the mid-lake region. Therefore, it is important to have additional in-situ measurements in the mid-lake region, which is a serious challenge for sensor placements in the remote off-shore locations that experience severe weather.

6.6 Conclusions

In conclusion, this research has shown that satellite data have a high potential for estimating changes in surface water temperature, net radiation, and the surface energy balance

components over a large body of water. This research demonstrated methods that provide better spatial distribution and improved spatial resolution over large areas that do not have surface-based measurements available. Also, the agreement between the remote sensing measurements integrated with GIS processes was sufficient to suggest that these surface estimates derived from satellite sources are reliable.

The research has revealed the physical processes of energy exchange between the lake water surface and the atmosphere. However, in terms of both natural climate inconsistency and the influence of human activity on nature, more study needs to be done to achieve an enhanced understanding of how the large lakes respond to climate change.

BIBLIOGRAPHY

Ackerman S.A., Heidinger A., Foster M.J., Maddux B. 2013. Satellite regional cloud climatology over the Great Lakes. *Remote Sensing*, 5, 6223-6240

Ahmed M., Sultan M., Wahr J., Yan E., Milewski A., Sauck W., Becker R., Welton B. 2011. Integration of GRACE (Gravity Recovery and Climate Experiment) data with traditional data sets for a better understanding of the time-dependent water partitioning in African watersheds. *Geology*, 39(5), 479-482

Alcantara E.H., Stech J.L., Lorenzzetti J.A., Bonnet M.P., Casamitjana X., Assireu A.T. 2010. Remote sensing of water surface temperature and heat flux over a tropical hydroelectric reservoir. *Remote Sensing of the Environment*, 114, 2651-2665

Arking A. 1996. Absorption of solar energy in the atmosphere: discrepancy between model and observations. *Science*. 273, 779-781

Assel R.A. 2005. Classification of annual Great Lakes ice cycles: Winters of 1973-2002. *Journal of Climate*, 18, 4895-4904

Assel R.A., Quinn F. H., Sellinger C.E. 2004. Hydroclimatic factors of the recent record drop in Laurentian Great Lakes water levels. *American Meteorological Society*, 85(8), 1143-1151

Austin J.A., Colman S.M. 2007. Lake Superior summer water temperatures are increasing more rapidly than regional air temperatures: A positive ice–albedo feedback. *Geophysical Research Letter*, 34, L06604, doi:10.1029/2006GL029021

Baum B., Platnick S. 2006. Introduction to MODIS cloud products. In: *Earth science satellite remote sensing.* Vol. 1: Science and Instruments. 74–91

Becker M., Llovel W., Cazenave A., Guntner A., Cretaux J.F. 2010. Recent hydrological behavior of the East African great lakes region inferred from GRACE, satellite altimetry and rainfall observations. *Comptes Rendus Geoscience*, 342, 223-233

Birkett C.M. 1995. The contribution of TOPEX/POSEIDON to the global monitoring of climatically sensitive lakes. *Journal of Geophysical Research*, 100, 25179-25204

Bisht G., Bras R.L. 2010. Estimation of net radiation from the MODIS data under all sky conditions: Southern Great Plains case study. *Remote Sensing of Environment*, 114, 1522-1534

Bisht G., Venturini V., Islam S., Jiang L. 2005. Estimation of the net radiation using MODIS (Moderate Resolution Imaging Spectroradiometer) data for clear sky days. *Remote Sensing of Environment*, 97, 52-67

Blanken P.D. 2014. *Footprint Analysis*. Unpublished manuscript

Blanken P.D. 2014. *The Value of Observations: The Great Lakes Evaporation Network*. Retrieved from http://www.ijc.org/en_/blog/2014/02/18/value_observations_great_ lakes_ evaporation network/

Blanken P.D., Rouse W.R., Culf A.D., Spence C., Boudreau L.D., Jasper J.N., Kochtubajda B., Scertzer W.M., Marsh P., Verseghy D. 2000. Eddy covariance measurements of evaporation from Great Slave Lake, Northwest Territories, Canada. *Water Resources Research*, 36(4), 1069-1077

Blanken P.D., Spence. C, Hedstrom N., Lenters J.D. 2011. Evaporation from Lake Superior: 1. Physical controls and processes. *Journal of Great Lake Research*, 37, 707-716

Blanken P.D., Spence C., Lenters J.D., Petchprayoon P., Gronewold A.D. 2014. Impacts of ice cover on Great Lakes evaporation: An analysis of simultaneous ice-covered and ice-free conditions on Lakes Michigan and Huron during the 2013-14 winter. *The 57th Annual Conference on Great Lakes Research*, May 2014. Ontario, Canada

Braswell W.D., Lindzen R.S. 1998. Anomalous short wave absorption and atmospheric tides. *Geophysical Research Letters*, 25, 1293-1296

Bretherton C.S., Widmann M., Dymnikov V.P., Wallace J.M., Blad´e I. 1999. The effective number of spatial degrees of freedom in a time varying field. *Journal of Climate*, 12, 1990–2009.

Brinkmann W.A.R. 2000. Causes of variability in monthly Great Lakes water supplies and lake levels. *Climate Research*, 15, 151–160

Bolsenga S.J. 1975. Estimating energy budget components to determine Lake Huron evaporation. *Water Resources Research,* 11**,** 661 – 666

Boyce F.M., Donelan M.A., Hamblin, P.F., Murthy C.R., Simons T.A. 1989. Thermal structure and circulation in the Great Lakes. *Atmosphere-Ocean*, 27(4), 607-642. doi: 10.1080/07055900.1989.9649358

CEOS (Committee on Earth Observation Satellites). 2012. *The Earth Observation Handbook. Spaecial 2015 COPS 21 Editions*. Retrieved from http://www.eohandbook.com /cop21/capabilities/sat_earth_obs_radar_altimeters.html

Changnon S.A. 2004. Temporal behavior of levels of the Great Lakes and climate variability. *Journal of Great Lakes Research*, 30, 184–200

Cheng K.C., Kuo CY., Shum C.K., Niu X., Li R., Bedford K.W. 2008. Accurate linking of Lake Erie water level with shoreline datum using GPS buoy and satellite altimetry. *Terrestrial Atmospheric and Oceanic Sciences*, 19, 53-62

Chelton D.B., Ries J.C., Haines B.J., Fu L.L., Callahan P.S. 2001. Satellite altimetry. *Satellite Altimetry and Earth Sciences: A Handbook for Techniques and Applications*. Fu L.L., Cazenave A. Eds. San Diego. Academic Press

Coll C., Caselles V., Galve J. M., Valor E., Niclòs R., Sanchez J.M., Viras R. 2005. Ground measurements for the validation of land surface temperatures derived from AATSR and MODIS data. *Remote Sensing of Environment*, 97, 288–300

Crosman E.T., Horel J.D. 2009. MODIS-derived surface temperature of the Great Salt Lake. *Remote Sensing of Environment*, 113, 73−81

Czajkowski K.P., Goward S.N., Stadler S., Walz A. 2000. Thermal remote sensing of near surface environmental variables: Application over the Oklahoma Mesonet. *The Professional Geographer*, 52(2), 345–357

Derecki J.A. 1981. Stability effects on Great Lakes evaporation. *Journal of Great Lake Research*, 7(4), 357-362

Dobiesz N.E., Lester N.P. 2009. Changes in mid-summer water temperature and clarity across the Great Lakes between 1968 and 2002. *Journal of Great Lakes Research*, 35, 371-384

Duan Z., Bastiaanssen W.G.M. 2014. A new empirical procedure for estimating intra-annual heat storage changes in lakes and reservoirs: Review and analysis of 22 lakes. *Remote Sensing of Environment*, 156, 143-156

Dugual C.R. 1994. An approach to the estimation of surface net radiation in mountain area using remote sensing and digital terrain data. *Theoretical and Applied Climatology*, 55, 55-68

Federer C.A. 1968. Spatial variation of net radiation, albedo and surface temperature of forests. *Journal of Applied Meteorology*, 7, 789-795

Flohrer C., Otten M., Springer T., Dow J. 2011. Generation precise and homogeneous orbits for Jason-1 and Jason-2. *Advances in Space Research*, 48, 152-172

Gerbush M.R., Kristovich D.A.R., Laird N.F. 2008. Meso scale boundary layer and heat flux variations over pack ice–covered Lake Erie. *Journal of Applied Meteorology and Climatology*, 47, 668-682. doi: 10.1175/2007JAMC1479.1

Gianniou S.K., Antonopoulos V.Z. 2007. Evaporation and energy budget in Lake Vegoritis, Greece. *Journal of Hydrology*, 345, 212-223.

Granger R., Bussieres N. 2005. Evaporation/evapotranspiration estimates with remote sensing. *Remote Sensing in Northern Hydrology*. Dugua C.R., Pietroniro A. Eds. Washington, D C. American Geophysical Union

Gronewold A.D., Clites A.H., Smith J.P., Hunter T.S. 2013. A dynamic graphical interface for visualizing projected, measured, and reconstructed surface water elevations on the earth's largest lakes. *Environmental Modelling & Software*, 49, 34–39

Gronewold A.D., Stow T.A., 2014. Water loss from the Great Lakes. *Science*, 343(6175), 1084-1085. doi*:* 10.1126/science.1249978

Hanrahan J.L., Kravtsov S.V., Roebber P.J. 2010. Connecting past and present climate variability to the water levels of Lakes Michigan and Huron. *Geophysical Research Letter,* 37, L01701. doi:10.1029/2009GL041707

Harris G.L. 2012. *Selected Procedures for Volumetric Calibrations (2012 ed)*. NISTIR 7383. National Institute of Standards and Technology. U.S. Department of Commerce. 104 p

Hartmann H.C. 1990. Climate change impacts on laurentian great lakes levels. *Climatic Change*, 17, 49-67

Hinkelman L.M., Stackhouse P.W., Wielicki B.A., Zhang T.P., Wilson S.R. 2009. Surface insolation trends from satellite and ground measurements: Comparisons and challenges. *Journal of Geophysical Research*, 114, D00D20. doi:10.1029/2008JD011004

Howell E.L., Brown, L.C., Kang K., Duguay C.R. 2009. Variability in ice phenology on Great Bear Lake and Great Slave Lake, Northwest Territories, Canada, from SeaWinds/QuikSCAT: 2000-2006. *Remote Sensing of Environment,*113, 816 – 834

Jensen J. R. 2007. *Remote Sensing of the Environment*. 2nd ed. Upper Saddle River, New Jersey Prentice Hall

Jin M. 2000. Interpolation of surface radiative temperature measured from polar orbiting satellites to a diurnal cycle 2. Cloudy-pixel treatment. *Journal of Geophysical Research*, 105, 4061-4076

Jin Y., Randerson J.T., Goulden M.L. 2011. Continental-scale net radiation and evapotranspiration estimated using MODIS satellite observation. *Remote Sensing of Environment,* 115 (9), 2302-2319. doi: 10.1016/j.rse.2011.04.031

Jones M.L., Shuter B.J., Zhao Y., Stockwell J.D. 2006. Forecasting effects of climate change on Great Lakes fisheries: Models that link habitat supply to population dynamic scan help. *Canadian Journal of Fisheries and Aquatic Sciences*, 63, 457-468

Justice C.O., Vermote E., Townshend J.R.G., DeFries R., Roy D.P., Hall D.P., Salomonson V.V., Privette J.L., Riggs G., Strahler A., Lucht W., Myneni R., Knyazikhin Y., Running, S.W., Nemani R.R., Wan Z., Huete A., Leeuwen W., Wolfe R.E., Giglio L., Muller J.P., Lewis P., Barnsley M.J. 1998. The moderate resolution imaging spectroradiometer (MODIS): land remote sensing for global change research. *IEEE Transactions on Geoscience and Remote Sensing,* 36, 1228-1249

Kaleita A.L., Kumar P. 2000. AVHRR estimates of surface temperature during the Southern Great Plains 1997 Experiment. *Journal of Geophysical Research,*105, 20791-20801

Kim H.Y., Liang S. 2010. Development of hybrid method for estimating land surface shortwave net radiation from MODIS. *Remote Sensing of Environment*, 114, 2393-2402

King N.J., Bower K.N., Crosier J., Crawford L. 2013. Evaluating MODIS cloud retrievals with in situ observations from VOCALS-Rex. *Atmospheric Chemistry and Physics*, 13, 191-209. doi:10.5194/acp-13-191-2013

Kondratyev K.V. 1969. *Radiation in the Atmosphere (International Geophysics Series, Volume 12)*. 1st ed. New York. Academic Press

Koutsoyiannis D. 2012. Clausius–Clapeyron equation and saturation vapour pressure: simple theory reconciled with practice. *European Journal of Physics*, 33, 295-305

Large W.G., Danabasoglu G., Doney S.C., McWilliams J.C. 1997. Sensitivity to surface forcing and boundary layer mixing in a Global Ocean Model: Annual-mean climatology. *Journal of Physical Oceanography*, 27, 2418-2446

Lenters J.D., Anderton J.B., Blanken P., Spence C., Suyker A. E., 2013 Assessing the Impacts of Climate Variability and Change on Great Lakes Evaporation. *2011 Project Reports.* Brown D., Bidwell D., Briley L. Eds. Available from the Great Lakes Integrated Sciences and Assessments (GLISA) Center. Retrieved from http://glisaclimate.org/media/GLISA_Lake_Evaporation.pdf

Lenters, J.D., Kratz T.K., Bowser C.J. 2005. Effects of climate variability on lake evaporation: Results from a long-term energy budget study of Sparkling Lake, northern Wisconsin (USA). *Journal of Hydrology*, 308, 168-195

Liang S., Li X., Wang J. 2012. *Advance Remote Sensing: Terrestrial Information and Application*. Academic Press is an imprint of Elsevier. ISBN: 978-0-12-385954-9. 800 p

Liepert B.G., 2002. Observed reductions of surface solar radiation at sites in the United States and world wide from 1961 to 1990. *Geophysical Research Letter*, 29, 1421, 10.1029/2002GL014910

Liou K.N. 2002. *An Introduction to Atmospheric Radiation*, *Vol 84*. 2nd ed. Academic Press. 583 p

Lishawa S.C., Albert D.A., Tuchman N.C. 2010. Water level decline promotes Typha X glauca establishment and vegetation change in Great Lakes coastal wetlands. *Wetlands*, 30, 1085–1096

Lofgren B.M. 2004. A model for simulation of the climate and hydrology of the Great Lakes basin. *Journal of Geophysical Research*, 109, D18108. doi:10.1029/2004JD004602

Lofgren B.M., Zhu, Y. 2000. Surface energy fluxes on the great lakes based on satellite observed surface temperatures 1992 to 1995. *Journal of Great Lakes Research,* 26, 305 – 314

Lu L., Venus V., Skidmore A., Wang T., Luo G. 2011. Estimating land-surface temperature under clouds using MSG/SEVIRI observations. *International Journal of Applied Earth Observation and Geoinformation,* 13, 265-276

MacDonagh-Dumler J., Pebbles V., Gannon J. 2005. Great Lakes (North American) – experience and lessons learned brief. *ILEC. 2005. Managing Lakes and their Basins for Sustainable Use: A Report for Lake Basin Managers and Stakeholders*. International Lake Environment Committee Foundation. Kusatsu, Japan

Magnuson J.J., Mortsch L.R., Schindler D.W., Quinn F.H., Webster K.E., Assel R.A., Bowser C.J., Dillon P.J., Eaton J.G., Evans H.E., Fee E.J., Hall R.I. 1997. Potential effects of climate changes on aquatic systems: Laurentian Great Lakes and precambrian shield region. *Hydrological Processes*, 11, 825-87

Mckay R.M.L., Beall B.F.N., Bullerjahn G.S., Woityra W.C. 2011. Winter limnology on the Great Lakes: The role of the U.S. Coast Guard. *Journal of Great lakes Research*, 37(1), 207-210

Monteith J.L., Unsworth M.H. 2008. Principles of Environmental Physics. 3rd ed. Amsterdam, Boston, Elsevier. 418 p

Morris C.S., Gill S.K. 1994. Evaluation of the TOPEX/POSEIDON altimeter system over the Great Lakes. *Journal of Geophysical Research*, 99(C12), 24527–24539. doi: 10.1029/94JC01642

MRT (MODIS Reprojection Tool). 2011. User's Manual. Release 4.1. Land Processes DAAC. USGS Earth Resources Observation and Science (EROS) Center. 69 p

Norris J.R., Wild M. 2007. Trends in aerosol radiative effects over Europe inferred from observed cloud cover, solar "dimming" and solar "brightening." *Journal of Geophycal Research*, 112, D08214, doi:10.1029/2006JD007794

Nunez M., Davies J.A., Robison P.J., 1972. Suface albedo at a tower site in Lake Ontario. *Boundary-Layer Meteorology*, 3,77-86

Oesch D., Jaquet J.M., Hauser A. Wunderle S. 2005. Lake surface water temperature retrieval using advanced very high resolution radiometer and moderate resolution imaging spectroradiometer data: Validation and feasibility study. *Journal of Geophysical Research*, 10(C12014), 1−17

Oesch D., Jaquet J.M., Klaus R., Schenker P. 2008. Multi-scale thermal pattern monitoring of a large lake (Lake Geneva) using a multi-sensor approach. *International Journal of Remote Sensing*. 29, 5785−5808

Oke T.R. 1996. *Boundary Layer Climates*, 2nd ed, Methuen, London. 464 p

Oyserman B.O., Woityra W.C., Bullerjahn G.S., Beall. B.F.N., Mckay R.M.L. 2012. Collecting winter data on U.S. Coast Guard ice breakers. *EOS, Transactions American Geophysical Union*, 93(10), 105-106, doi: 10.1029/2012EO100002

Painemal D., Zuidema P. 2011. Assessment of MODIS cloud effective radius and optical thickness retrievals over the Southeast Pacific with VOCALS-REx in situ measurements. *Journal of Geophycal Research*, 166, D24206, doi:10.1029/2011JD016155

Parlow E., 2000. Snow runoff models using remotely sensed data. *Remote Sensing for Environmental Data in Albania: A Strategy for Integrated Management*. Buchroithner M. F. Ed. Boston. Kluwer Academic Publishers

Petchprayoon P., Blanken P.D., Ekkawatpanit C., Hussein K. 2010. Hydrological impacts of land use/land cover change in a large river basin in central-northern Thailand. *International Journal of Climatology*, 30(13), 1917-1930

Ponchaut F., Cazenave A. 1998. Continental lake level variations from Topex/Poseidon (1993-1996). *Earth & Planetary Sciences*, 326, 13-20

Prata A.J. 1996. A new long-wave formula for estimating downward clear sky radiation at the surface. *Quarterly Journal Royal Meteorological Society*, 122, 1127-1151

Priestley M.B. 1981. *Spectral Analysis and Time Series, Volume 1 : Univariate Series. (Probability and Mathematical Statistics).* Academic Press, New York, 653 p

Prigent C., Aires F., Rossow W.R. 2003. Land surface skin temperatures from a combined analysis of microwave and infrared satellite observations for an all-weather evaluation of the differences between air and skin temperatures. *Journal of Geophysical Research*, 108, NO. D10, 4310. doi:10.1029/2002JD002301

Qian Y., Kaiser D.P., Leung L.R., Xu M. 2006. More frequent cloud-free sky and less surface solar radiation in China from 1955 to 2000. *Geophysical Research Letters*, 33, L01812, doi:10.1029/2005GL024586

Quinn F.H. 1979. An improved aerodynamic evaporation technique for large lakes with application to the international field year for the Great Lakes. *Water Resource Research*, 15(4), 935-940

Rao Y.R., 2012. Great Lake Processes: Thermal structure, circulation and turbulent diffusion processes. Encyclopedia of Lakes and Reservoirs. Bengtsson L., Herschy R.W. Fairbridge R.W. Eds. 298-303. doi: 10.1007/978-1-4020-4410-6_266

Reinart A., Reinhold M. 2008. Mapping surface temperature in large lakes with MODIS data. *Remote Sensing of Environment*. 112, 603−611

Richards J.A. 2013. *Remote Sensing Digital Image Analysis: An Introduction*. 5th ed. Springer, New York. 494 p

Richards J.A., Jia X. 2006. *Remote Sensing Digital Image Analysis: An Introduction*. 4th ed. Springer. 439 p

Rizzoli A., Neteler M., Rosà R., Versini W., Cristofolini A., Bregoli M., Buckley A., Gould E. A. 2007. Early detection of TBEv spatial distribution and activity in the Province of Trento assessed using serological and remotely-sensed climatic data. *Geospatial Health*, 1(2), 169–176

Roger R.R., Yau M.K. 1989. *A Short Course in Cloud Physics*. 3rd ed. New York. Pergamon Press. 227 p

Rouse W.R., Oswald C.J., Binyamin J., Spence C., Schertzer W.M., Blanken P.D., Bussieres N., Duguay C.R. 2005. The role of Northern Lakes in a regional energy balance. *American Meteorological Society*, 291-305

Santer B.D., Wigley T.M.L., Boyle J.S., Gaffen D.J., Hnilo J.J., Nychka D., Parker D.E., Taylor K.E. 2000. Statistical significance of trends and trend differences in layer-average atmospheric temperature time series. *Journal of Geophysical Research*, 105: 7337–7356

Santos C.A., Nascimento R.L., Rao T.V., Manzi A.O. 2011. Net radiation estimation under pasture and forest in Rondônia, Brazil, with TM Landsat 5 images. *Atmosfera*, 24(4), 234-446

Schaetzl R.J. 2005. Watershed *of Lake Huron: Geography of Michigan and the Great Lakes Region*. Course Material of GEO 333 Geography of Michigan and the Great Lakes Region, Department of Geography, Michigan State University. Retrieved from http://web2.geo.msu.edu/geogmich/lakehuron.html

Schertzer W.M., Assel R.A., Beletsky D., Croley II, T.E., Lofgren B.M., Saylor J.H., Schwab D.J. 2008. Lake Huron climatology, inter-lake exchange and mean circulation. *Aquatic Ecosystem Health & Managemen*, 11, 144 - 152

Schertzer W.M., Taylor B. 2009. Assessment of the capability to compute lake evaporation from Lake Okanagan and its Mainstem Lakes using the existing database. *Project Report to the Okanagan Water Supply and Demand Study on Lake Evaporation*, 105 p

Schmid H.P. 1994. Source areas for scalars and scalar fluxes. *Boundary Layer Meteorology*, 67(3), 293-318

Schneider P., Hook S. J. 2010. Space observations of inland water bodies show rapid surface warming since 1985. *Geophysical Research Letter*, 37, L22405

Schwab D.J., Leshkevich G.A., & Muhr, G.C. 1999. Automated mapping of surface water temperature in the Great Lakes. *Journal of Great Lakes Research*, 25, 468 - 481

Sellinger C.E., Stow C.A., Lamon E.C., Qian S.S. 2008. Recent water level declines in the lake Michigan-Huron system. *Environmental Science & Technology,* 42, 367-373

Sicart J.E., Hoch R., Ribstein P., Chazarin J.P. 2010. Sky longwave radiation on tropical Andean glaciers: Parameterization and sensitivity to atmospheric variable. *Journal of Glaciology*, 56(199), 854-860, doi:10.3189/002214310794457182

Singh A., Seitz F., Schwatke C. 2012. Inter-annual water storage changes in the Aral Sea from multi-mission satellite altimetry, optical remote sensing, and GRACE satellite gravimetry. *Remote Sensing of Environment, 123, 187-195*

Slingo A. 1989. A GCM parameterization for the shortwave radiative properties of water clouds. *Journal of Atmospheric Science*, 46, 1419-1427

Smedman A.F., Hogstrom U., Sahlee E., Johnansson C., 2007. Critical re-evaluation of the bulk transfer coefficient for sensible heat over the ocean during unstable and neutral conditions. *Quarterly Journal of the Royal meteorological Society*, 133:227-250

Solomon S., Qin D., Manning M., Chen Z., Marquis M., Averyt K. B., Tignor M., Miller H. L. Eds. 2007. *Climate Change 2007*: *The Physical Science Basis*. New York, Cambridge University Press

Spence C., Blanken P.D., Hedstrom N., Fortin V., Wilson H., 2011. Evaporation from Lake Superior: 2 Spatial distribution and variability. *Journal of Great Lake Research*, 37, 717-724

Spence C., Rouse W.R. 2002. The energy budget of Canadian Shieldsubarctic terrain and its impact on hillslope hydrological processes. *Journal of Hydrometeorology*, 3, 208 – 218

Steissberg T.E., Hook, S.J., Schladow S.G. 2005. Characterizing partial upwellings and surface circulation at Lake Tahoe, California–Nevada, USA with thermal infrared images. *Remote Sensing of Environment*, 99: 2−15

Sun Z., Gebremichael M., Wang Q., Wang J., Sammis T.W., Nickless A. 2013. Evaluation of clear-sky incoming radiation estimating equations typically used in remote sensing evapotranspiration algorithms. *Remote Sensing*, 5,4735-4752, doi:10.3390/rs5104735

Swenson S., Wahr J. 2009. Monitoring the water balance of Lake Victoria, East Africa, from space. *Journal of Hydrology*, 370, 163–176

Tang B., Li Z.L. 2008. Estimation of instantaneous net surface longwave radiation from MODIS cloud-free data. *Remote Sensing of Environment*, 112, 3482-3492

Tapley B.D., Bettadpur S., Watkins M., Reigber C. 2004. The gravity recovery and climate experiment: Mission overview and early results *Geophysical Research Letters*, 31, L09607. doi:10.1029/2004GL019920

Terjung W.T., Kickert R.K., Kochevar R.J., Mrowka J.P., Ojo S.O., Potter G.L., Tuller S.E. 1968. The annual March of the tropoclimatic spatial patterns of net radiation in Southern California. *Archives for Meteorology, Geophysics, and Bioclimatology, Series B*, 17, 21-50

Tian L., Curry J.A. 1989. Cloud overlap statistics. *Journal of Geophycal Research*, 94, 9925-9935

Trumpickas J., Shuter B.J., Minns C.K., 2009. Forecasting impacts of climate change on Great Lakes surface water temperatures. *Journal of Great Lakes Research*, 35, 454 - 463

USEPA (U.S. Environmental Protection Agency). 2005. *State of The Great Lake 2005, What Are The Current Pressures Impacting Lake Huron?* Retrieved from http://www.epa.gov/solec/indicator_sheets/huron.pdf

Van G.A., Meixner T. 2006. A global sensitivity analysis tool for the parameters of multi-variable catchment models. *Journal of Hydrology*, 324, 10-23

Wahr J. 2013. Personal communication, April 25, 2013

Wahr J., Swenson S., Zlotnicki V., Velicogna I. 2004. Time-variable gravity from GRACE: First results. *Geophysical Research Letter*, 31, L11501. doi:10.1029/2004GL019779

Wan Z. 1999. *MODIS Land Surface Temperature Algorithm Theoretical Basis Document.* Retrieve from http://modis.gsfc.nasa.gov/data/atbd/atbd_mod11.pdf

Wang J., Assel R.A., Walterscheid S., Clites A.H., Bai X. 2012. Great Lakes ice climatology update: winter 2006 - 2011 description of the digital ice cover dataset. *NOAA technical Memoradum GLERL-155*. 37 p

Wang J., Hu H., Schwab D., Hawley N., Clites A., 2010. Development of the Great Lakes ice-circulation model (GLIM): application to Lake Erie in 2003 - 2004. *Journal of Great Lakes Research*, 36, 425-436

Wang W., Liang S. 2009. Estimation of high-spatial resolution clear-sky longwave downward and net radiation over land surfaces from MODIS data. *Remote Sensing of Environment*. 113, 745-754

Winter T.C., Buso D.C., Rosenberry D.O., Likens G.E., Sturrock A.M., Mau D.P. 2003. Evaporation determined by the energy-budget method for Mirror Lake, New Hampshire. *Limnology and Oceanography*, 48(3), 995–1009

Yao H. 2009. Long-term study of lake evaporation and evaluation of seven estimation methods: results from Dickie Lake, South-Central Ontario, Canada. *Journal of Water Resource and Protection,* 2, 59 - 77

Yeh P.J., Tang Q., Kim Hyungjun. 2012. Validation of Gravity Recovery and Climate Experiment data for assessment of Terrestrial water storage variations. *Multi scale Hydrologic Remote Sensing Perspectives and Applications*. Chang N., Hong Y. Eds. New York. CRC Press

Yi Y., Minnis P., Huang J., Mack S., Chen Y., Ayers K. 2008. Validation of multi layered cloud properties using *A-Train Satellite measurements Geoscience and Remote Sensing Symposium, 2008*. *IGARSS 2008. IEEE International*. 574-577

Zeng N., Yoon J., Mariotti A., Swenson S. 2007. Variability of Basin-Scale Terrestrial Water Storage from a PER Water Budget Method: The Amazon and the Mississippi. *Journal of Climate*, 21, 248-265

Zimmermann K.A. 2013. *Great Facts about the Five Great Lakes.* Retrieved from http://www.livescience.com/32081-lake-huron.html